DEVELOPMENT OF NOVEL DEVICES FOR UPPER-EXTREMITY REHABILITATION

This work was supported by SenterNovem (grant TSGE2050) and the Institute for Biomedical Technology, Enschede.

This publication has also benefitted from the technical advice and financially support of the following companies. Their support is thankfully acknowledged.

Baat Medical	www.baatmedical.com
DL Rehab	www.dlrehab.com
Hankamp Gears BV	www.hankamp.nl
Hocoma AG (CH)	www.hocoma.com
Kunst & van Leerdam Medical Technology BV	www.kvlmt.nl
Moog FCS	www.haptist.com

The assessment committee consists of:

CHAIRMAN AND SECRETARY	
Prof.dr. F. Eising	University of Twente
PROMOTOR	
Prof.dr. F.C.T. van der Helm	University of Twente
ASSISTANT PROMOTOR	
Dr.ir H. van der Kooij	University of Twente
MEMBERS	
Prof.dr.ir. P.H. Veltink	University of Twente
Prof.ir. H.M.J.R. Soemers	University of Twente
Prof.dr. H. Nijmeijer	Eindhoven University of Technology
Prof.dr. J.P.A. Dewald	Northwestern University, Chicago (US)
Prof.dr.ir. J.L. Patton	University of Illinois, Chicago (US)
Dr. C.G.M. Meskers	Leiden University Medical Center

Paranymphs:

Edsko Hekman

Ewoud Vermeulen

Printed by:

Gildeprint Drukkerijen BV, Enschede www.gildeprint.nl

ISBN: 978-90-365-2784-2

DEVELOPMENT OF NOVEL DEVICES FOR UPPER-EXTREMITY REHABILITATION

PROEFSCHRIFT

ter verkrijging van
de graad van doctor aan de Universiteit Twente,
op gezag van de rector magnificus,
prof. dr. H. Brinksma,
volgens besluit van het College voor Promoties
in het openbaar te verdedigen
op donderdag 29 januari 2009 om 15.00 uur

door

Adrianus Hubertus Arno Stienen
geboren op 28 augustus 1976
te Delft

This dissertation has been approved by:

Prof.dr. F.C.T. van der Helm (promotor)

Dr.ir H. van der Kooij (assistant promotor)

ISBN: 978-90-365-2784-2

CONTENTS

SUMMARY

The goal of this dissertation was to improve rehabilitation robots by developing new patient-friendly devices which can assist therapists in the rehabilitation of neurological movement disorders of the upper extremities, such as hemiparetic stroke. In all, three novel rehabilitation devices were developed.

Given the changing demographics of developed nations, over the next two decades fewer therapists will be available to treat an increasing number of stroke patients. With patient-friendly robots assisting therapists, proven therapeutic exercises can be automated and new and better targeted interventions developed and tested. In addition to facilitating therapy sessions, robots can provide objective measurement of impairment. Overall, robots can make therapy more productive for patients and less labor-intensive for therapists, and provide physicians, therapists and the scientific community with more objective data.

To handle the wide range of impairments found in hemiparetic stroke patients, multiple devices are needed. Mildly impaired patients may have a near-normal range of motion, but have problems with fine motor control or moving heavier objects. Severely affected patients may not be able to even lift the weight of their own arm. Despite these differences, certain general strategies appear to work best. First and foremost, rehabilitation therapy works best when the patient is actively and intensively involved. Exercises should use repetitive movements that closely resemble those used in daily living for best results in reshaping the recovering brain.

Studying motor learning in healthy subjects supported the need for active patient involvement. Given the artificial motor relearning task of moving in a visuomotor-rotated field, the healthy subject fully adapted when he could freely make, and correct, errors in their movement execution. On the other hand, active delivery of a passive hand to the targets resulted in much less and much slower adaptation. In between lay the adaptation achieved with hard and soft guidance of the hand over virtual tracks. The conclusion is that both minimization of execution errors and control effort drive kinematical adaptation in a novel visuomotor task, but the latter occurs at a much slower rate.

Should the patient not be assisted at all? Perhaps the type of assistance is important. For instance, weight support of the arm facilitates movement, but movement initialization and control are left unchanged. Most rehabilitation devices for upper extremities include some form of weight support. An analysis of these devices concluded that weight support is most easily realized through a cable-suspension system that supports the arm via slings. However, the best possible solution for weight support depends on the primary design of the device. Careful upfront consideration of various design options will lead to better choices.

The first rehabilitation device was designed using this knowledge. The Freebal is a dedicated weight-support system that is less complex and has less movement inertia and a greater range of motion than other weight-support devices. This passive mechanical device uses ideal-spring mechanisms for constant-but-scalable forces to support the arm. It has a large workspace of roughly 1 m^3, low movement impedance, and independent support at the elbow and wrist of up to 5 kg. An explorative cross-sectional study with eight patients showed the Freebal instantly

extends the range of motion of the affected arm. Patient requirements are met by the Freebal, potentially enabling patients to advance sooner to more motivating, functional training.

Usage of the passive Freebal in a training experiment showed its potential to increase a patient's range of motion and to reduce the influence of abnormal multi-joint torque couplings. Four chronic stroke patients received three 30-minute weight-supported training sessions per week for six weeks. Baseline evaluations measured range of motion and determined angular movement patterns during circle drawing. General arm function was also measured. After training, arm function, active range of motion, and independence of simultaneous shoulder and elbow movements improved in all subjects.

However, the Freebal is less suitable for selectively enhancing the training intensity of moderate and mildly affected patients. It also cannot measure or control movements at the joint level. Exoskeletons are better suited for these goals. However, for exoskeletons to function correctly, their axes have to be closely aligned to the human axes to prevent painful interaction forces. We proposed to decouple the joint rotations from the joint translations, allowing the exoskeleton to align itself to the anatomical axes. In this model, the rotations are still controlled via applied torques, but the joint can freely translate when realignment is required. Decoupling reduces setup times and makes the exoskeleton responsible for solving any joint misalignment. The disadvantages are the need for an additional linkage mechanism between a global frame and the exoskeleton, increased complexity, and reduced interaction stiffness due to having two cuffs per limb segment. The decoupling was found to be an essential advantage for the shoulder joint, and useful for the elbow joint.

For the first exoskeleton, passive, energy-dissipating disk brakes were investigated for force-coordination training. These passive actuators are inherently safe and offer a high torque-to-weight ratio. Passive actuation with friction brakes does present direct implications for joint control. Braking is always opposite to the movement direction. During standstill, the measured torque is equal to the torque applied by the human. During rotations, it is equal to the brake torque. Actively assisting movements is not possible, nor are energy-consuming virtual environments. The evaluated disk brake has a 20 Nm bandwidth (flat-spectrum, multi-sine) of 10 Hz. This is sufficient for torques required for conventional therapy and simple passive virtual environments. The maximum static output torque is 120 Nm, which is sufficient for isometric training of the upper extremity. The minimal impedance is almost zero, as only inertia is felt. Therefore, these brakes are suitable for their intended goals.

Combining the self-aligning axes and the hydraulic disk brakes resulted in the first exoskeleton, the Dampace. It combines functional exercises resembling activities of daily living with impairment-targeted force-coordination training. In addition to offering control and measurements in joint space, the position and forces can also be recalculated for the hand. In the Dampace, the hand is free to interact with real-world objects. For future stroke therapy, selectively increase resistance for moving objects on a tabletop surface and to and from shelves is intended.

The Freebal and Dampace are well-suited passive therapy devices for patients with some functional control of movement. For more severely affected patients, carefully applied active assist-as-needed may be beneficial. Also, to measure some impairments such as spasticity, an active device is needed. For the final

but still uncompleted exoskeleton of this project—the Limpact—the disk brakes were replaced with rotation hydro-elastic actuators (rHEAs). The rHEA is a novel, custom-designed combination of a rotational hydraulic actuator and a symmetric torsion spring, and uses impedance control. With the innovative spring design, the maximum output torque is 50 Nm using a minimum of space and weight. Multi-sine identification showed the torque-tracking bandwidth restricted to 18 Hz for a constant spectral-density reference signal of 20 Nm. It was mostly restricted by the transport delays in the long flexible tubes. The measured torque resolution was better than 0.01 Nm and the delivered torque resolution below 1 Nm. Therefore, the rHEA is suitable for upper-extremity rehabilitation therapy because it can match the desired torque bandwidths, resolution, and amplitude ranges. rHEAs will be fitted on the upcoming Limpact, which also features an improved mechanical design based on the lessons learned with the Dampace.

In this dissertation, the following research questions were answered:

I **Which assistive forces improve motor learning in healthy subjects?**
In healthy subjects, unassisted movements resulted in the best adaptation. For stroke patients, we speculate that active assistance may be useful for severely affected patients, primarily when the assistance is used to support, and not complete, movements.

II **What is the optimal usage for each type of current rehabilitation devices?**
Cable suspension systems are the simplest to construct, and are primarily suitable for offering weight support to the arm. Endpoint manipulators are more complex and allow active and haptic interaction with the arm, but are restricted in their joint control and range of motion. Exoskeletons are the most complex of the three options and most difficult to use, but offer the best joint control and measurement possibilities.

III **How do the new devices improve upon existing designs?**
The Freebal demonstrates that a simple mechanical device may be all that is needed to offer weight support. The Dampace and Limpact exoskeletons use new self-aligning axes, reducing setup times and potentially painful interaction forces. The Dampace demonstrates the potential of passive and inherently safe braking in therapy. The Limpact uses a new compliant but powerful actuator, which is useful for both stroke therapy and impairment quantification. Endpoint manipulators were not investigated further.

IV **Does weight support enhance recovery after stroke?**
The Freebal showed both instant improvement of movements when using weight-support assistance, and long-term improvement without it when slowly decreasing weight-support over multiple sessions.

V **Is the full potential of rehabilitation robots used?**
Current endpoint manipulators show the potential for intelligent and novel interaction with patients, but are less useful for creating meaningful movements that resemble activities of daily living. With the greater control offered by the Dampace and Limpact exoskeletons—be it with limited stiffness and maximum torques—we hope to advance the field of robot-assisted therapy.

SAMENVATTING

Voor deze dissertatie zijn drie nieuwe revalidatieapparaten ontwikkeld waarmee therapeuten ondersteund worden in de revalidatie van patiënten met motorische aandoeningen van de bovenste extremiteiten, zoals hemi-paretische beroertes.

Gegeven de veranderingen in de leeftijdsopbouw in ontwikkelde landen, zullen in de komende twintig jaar minder therapeuten beschikbaar zijn om een toenemend aantal patiënten te behandelen. Met patiëntvriendelijke robots die therapeuten te assisteren, kunnen bewezen therapeutische oefeningen geautomatiseerd en nieuwe, gerichtere interventies ontwikkeld worden. Naast het faciliteren van therapiesessies kunnen robots ook objectieve metingen van de aandoeningen verrichten. In het algemeen maken robots de therapie productiever voor patiënten en minder arbeidsintensief voor therapeuten, en leveren ze objectievere data voor artsen, therapeuten en de wetenschappelijke gemeenschap.

Om de grote variatie van aandoeningen bij patiënten na een beroerte te behandelen, zijn meerdere apparaten nodig. De lichtst aangedane patiënten kunnen een bijna normaal bewegingsbereik hebben, maar hebben problemen met de fijne motorische taken of het verplaatsen van zware voorwerpen. De zwaarst aangedane patiënten kunnen soms niet eens in staat zijn om hun eigen arm omhoog te tillen. Ondanks deze verschillen lijken enkele algemene strategieen het beste te werken. Revalidatietherapie werkt het beste wanneer de patiënt actief en intens betrokken is. Oefeningen moeten bestaan uit herhaalde bewegingen uit het dagelijks leven.

Het bestuderen van motorisch leren in gezonden mensen ondersteunde de noodzaak van actieve patiëntbetrokkenheid. Gezonde proefpersonen pasten zich volledige aan aan de kunstmatige motorische leertaak van bewegen in visueel geroteerd veld wanneer ze vrij waren om foute bewegingsuitvoeringen te maken en te corrigeren. Het passief brengen van de hand naar het doel resulteerde in een veel mindere en langzamere aanpassing. Hiertussen lagen de resultaten met stijve en slappe begeleiding over virtuele paden. De conclusie is dat het minimaliseren van zowel de uitvoeringsfout als de uitvoeringsinspanning kinematische aanpassingen geven, maar dat bij deze laatste dat gebeurd op een veel lager tempo.

Moeten de patiënten misschien helemaal niet geassisteerd worden? Misschien is het assistentietype van belang. Gewichtsondersteuning van de arm faciliteert bijvoorbeeld bewegingen maar laat de bewegingsinitialisatie en -controle onveranderd. De meeste revalidatieapparaten voor de bovenste extremiteiten hebben een vorm van gewichtsondersteuning. Een analyse van deze apparaten concludeerde dat gewichtsondersteuning het simpelst te realiseren is met een kabelsuspensiesysteem. Maar de best mogelijke oplossing voor de ondersteuning hangt ook af van de het primaire apparaatontwerp. Zorgvuldige overwegingen van de mogelijkheden aan het begin van het ontwerpproces zullen leiden tot betere ontwerpen.

Het eerste revalidatieapparaat was ontworpen met deze kennis. De Freebal is een gespecialiseerd gewichtsondersteuningssysteem, welke minder complex is en minder inertia en een groter bewegingsbereik heeft dan andere soortgelijke apparaten. Dit passieve mechanische apparaat gebruikt ideale-veermechanismen voor constante-maar-schaalbare ondersteuning voor de arm. Het heeft een werkruimte van ongeveer 1 m^3, een lage bewegingsimpedantie, en onafhankelijke ondersteuning voor de elleboog en pols van tot 5 kg. Een exploratieve kruissectionele studie

met acht patiënten liet zien dat de Freebal de bewegingsruimte van de aangedane arm onmiddellijk vergroot. De Freebal voldoet aan de gestelde patiënteisen, en kan potentieel het mogelijk maken dat deze patiënten eerder overstappen op meer motiverende, functionelere training.

Het gebruik van de passieve Freebal in een trainingsexperiment liet zien dat deze het bewegingsbereik van een patiënt kan vergroten en de invloed van abnormale momentkoppelingen over meerdere gewrichtsassen kan verlagen. Vier chronische patiënten ondergingen drie 30-minuten durende trainingssessies per week, zes weken lang. Het bewegingsbereik, de gewrichtshoekpatronen bij cirkelbewegingen, en de algemene armfunctie werden gemeten. Na de training verbeterde de armfunctie, het actieve bewegingsbereik en het onafhankelijk bewegen van de schouder en elleboog in alle patiënten.

Maar de Freebal is minder geschikt om de trainingsintensiteit van matig en mild aangedane patiënten selectief zwaarder te maken. Ook het direct meten en controleren van de gewrichtshoeken is niet mogelijk. Exoskeletten zijn hiervoor beter geschikt. Om deze correct te kunnen laten functioneren, moeten hun assen dichtbij de mensenlijk assen geplaatst worden om pijnlijke interactie te voorkomen. We stellen voor om de gewrichtsrotaties los te koppelen van de -translaties, waardoor het exoskelet zichzelf kan uitlijnen. Rotaties worden nu geactueerd met momenten, niet met krachten, en het gewricht kan vrij transleren wanneer uitlijning nodig is. Ontkoppeling reduceert de insteltijd en geeft de verantwoordelijkheid van het uitlijnen van de gewrichten aan het exoskelet. De nadelen zijn de noodzaak voor extra koppelingsmechanismen tussen de globale wereld en het exoskelet, een toegenomen complexiteit, en een gereduceerde interactiestijfheid omdat twee koppelingen per armsegment nodig zijn. Voor het schoudergewricht lijkt de ontkoppeling een essentieel voordeel, en nuttig voor de elleboog.

Passieve, energie dissiperende schrijfremmen zijn onderzocht voor toepassing op een exoskelet voor kracht-coördinatietraining. Deze passieve actuatoren zijn inherent veilig en hebben een hoge moment-gewichtsverhouding. Passieve actuatie met wrijvingsremmen heeft directe gevolgen voor gewrichtscontrole. Remmen is altijd tegenovergesteld aan de bewegingsrichting. Bij stilstand is het gemeten moment gelijk aan het moment dat door de mens is aangebracht. Bij beweging is het gelijk aan het opgelegde remmoment. De geëvalueerde schrijfrem had een 20 Nm bandbreedte (vlak spectrum, multisinus) van 10 Hz. Dit is voldoende voor momenten die nodig zijn bij conventionele therapie en simpele, passieve virtuele omgevingen. Het maximum statische remmoment is 120 Nm, wat voldoende is voor isometrische training van de bovenste extremiteiten. De minimale impedantie is bijna nul, omdat alleen de inertia van het apparaat gevoeld wordt. Daarom zijn schrijfremmen geschikt gebleken voor de gestelde eisen voor revalidatie.

Het combineren van de zelfuitlijningsassen met de hydraulische schijfremmen resulteerde in het eerste exoskelet, de Dampace. Deze combineert functionele oefeningen van activiteiten uit het dagelijks leven met aandoeningsgerichte kracht-coördinatietraining. Naast de mogelijkheid van het direct controleren en meten van de gewrichten, kunnen ook de handpositie en -kracht berekend worden. In de Dampace is de hand vrij om echte objecten te manipuleren. Het selectief verhogen van de weerstand bij het verplaatsen van objecten op een tafel en van en naar muurrekken is hiermee een mogelijkheid voor toekomstige therapie.

De Freebal en Dampace zijn nuttige passieve therapieapparaten voor patiënten met nog minimaal enige functionele controle over hun bewegingen. Voor de zwaarst aangedane patiënten kan voorzichtig aangebrachte assistentie-waar-nodig

heilzaam zijn. Ook om aandoeningen zoals spasticiteit te meten is een actief apparaat nodig. Voor het laatste maar nog niet gereed zijnde exoskelet van dit project—de Limpact—worden de schrijfremmen vervangen door roterende hydroelastische actuatoren (rHEAs) De rHEA is een nieuw, zelfontworpen combinatie van een roterende hydraulische actuator en een symmetrische momentveer, welke gebruik maakt van een impedantie regelaar. Met het innovatieve veerontwerp is het maximale uitgangsmoment 50 Nm bij een minimaal gewicht en gebruik van ruimte. Multisinus identificatie liet zien dat de krachtsbandbreedte beperkt wordt tot 18 Hz voor een referentiesignaal met een constant spectrum van 20 Nm. Voornamelijk door de transportvertraging in de lange flexibele buizen. De meetmomentsresolutie was beter dan 0.01 Nm en de uitgangsmomentresolutie lager dan 1 Nm. Daarom is de rHEA geschikt voor revalidatietherapie van de bovenste extremiteiten met de toekomstig Limpact. De Limpact krijgt ook een verbeterd mechanisch ontwerp gebaseerd op de lessen geleerd met de Dampace.

In deze dissertatie werden de volgende onderzoeksvragen beantwoord:

I **Welke assistentie verbeterd motorisch leren bij proefpersonen?**
Bij gezonde proefpersonen geven niet-geassisteerde bewegingen de beste verbetering. Voor patiënten denken we dat actieve assistentie nuttig kan zijn voor zwaar aangedane patiënten, met name wanneer de assistentie gebruikt wordt om de bewegingen te ondersteunen en niet om ze af te maken.

II **Wat is het optimale gebruik van ieder type van revalidatieapparaten?**
Kabelsuspensiesystemen zijn het simpelst om te construeren and zijn primair geschikt voor gewichtsondersteuning van de arm. Eindpuntmanipulatoren zijn complexer en maken actieve en haptische interactie met de arm mogelijk, maar zijn relatief beperkt in de mogelijkheid om de gewrichtsassen direct te controleren en in hun bewegingsruimte. Exoskeletten zijn het meest complex van de drie en het meest moeilijk in gebruik, maar bieden de beste controle van de gewrichtsassen en meetmogelijkheden.

III **Hoe verbeteren de nieuwe apparaten bestaande ontwerpen?**
De Freebal laat zien dat een eenvoudig mechanisch apparaten voldoende kunnen zijn voor gewichtsondersteuning. De Dampace en Limpact exoskeletten gebruiken nieuwe zelfuitlijnende gewrichtsassen, welke de insteltijd en mogelijke interactiekrachten reduceren. De Dampace demonstreert het potentieel van passief, inherent veilig remmen voor therapiedoeleinden. De Limpact gebruikt een nieuwe compliante maar krachtige actuator, en is bruikbaar voor zowel revalidatie therapie als het kwantificeren van aandoeningen. Eindpuntmanipulatoren zijn niet verder onderzocht.

IV **Verbeterd gewichtsondersteuning het herstel na een beroerte?**
De Freebal geeft onmiddellijke bewegingsverbeteringen gedurende het gebruik van gewichtsondersteuning en lange termijn verbeteringen wanneer deze langzaam afgebouwd wordt over meerdere therapiesessies.

V **Wordt het volledige potentieel van revalidatierobots gebruikt?**
Huidige eindpuntmanipulatoren laten zien dat nieuwe, intelligente interactie met patiënten nieuwe mogelijkheden biedt. Deze zijn echter minder geschikt voor het oefenen van bewegingen uit het dagelijks leven. Met de grotere gewrichtscontrolemogelijkheden met de Dampace en Limpact—zei het met beperkte stijfheid en maximale momenten—willen we het onderzoeksveld van robot-geassisteerde therapie vooruit helpen.

Part I

GENERAL INTRODUCTION

1 GENERAL INTRODUCTION

1.1 INTRODUCTION

Given the changing demographics of developed nations, fewer physicians and therapists will be available to treat an increasing number of stroke patients over the next two decades. Baby Boomer retirements, including many health professionals, reduce the absolute number of available medical professionals. At the same time, an aging generation of health professionals and a general increase in life expectancy has increased the number of patients, since the incidence of neurological disorders (such as stroke) goes up with age. At the moment, stroke is the third leading cause of death, behind heart disease and cancer. Most survivors suffer from a wide range of motor impairments, making stroke the primary cause of permanent disabilities [176] and third in the ranking for the 'burden of disease' [232].

To ease the burden on health professionals, researchers initiated development of patient-friendly rehabilitation robots in the early 1990s. The first commercial versions of these devices are now available for both the upper [81] and lower extremities [30]. These robots assist in the recovery of motor function at many rehabilitation centers around the world. They make therapy more challenging for the patients, decrease the labor-intensity for therapists, and provide physicians, therapists, and the scientific community with more objectively gathered data.

1.2 STROKE AND REHABILITATION

A stroke results in a loss of neurological function due to a disturbance in the flow of blood in the vessels of the brain. The flow can get interrupted due to a hemorrhage (rupture), or, more frequently, an ischemia (blockage) caused by a thrombosis or embolism. The resulting lack of oxygen and build-up of blood pressure can severely damage brain tissue. The duration and extent of these processes determine the amount of neural damage. The location and volume of the damage also has a major influence on the impairment profile.

1.2.1 *Effects on arm function*

Each stroke incident is unique, but strokes predominantly occur in the irrigation of the middle cerebral artery, which includes the internal capsule between the thalamus and the basal ganglia (see Fig. 1.1) [197]. There, it damages the corticospinal pathways which originate in the motor cortices, travel through the internal capsule, and then project to the motoneurons in the spinal cord. It is thought that movement control in humans, as opposed to other animals, is highly dependent on these direct corticospinal projections [72, 52, 125, 91, 60, 126, 19, 116]. Their loss is difficult to compensate for, although alternative, less efficient routes exist [90]. For instance, the indirect connections via corticoreticular and reticulospinal pathways are both slower and less focused, because their axons are thinner, more widely branched, and often innervating over multiple spinal segments [128].

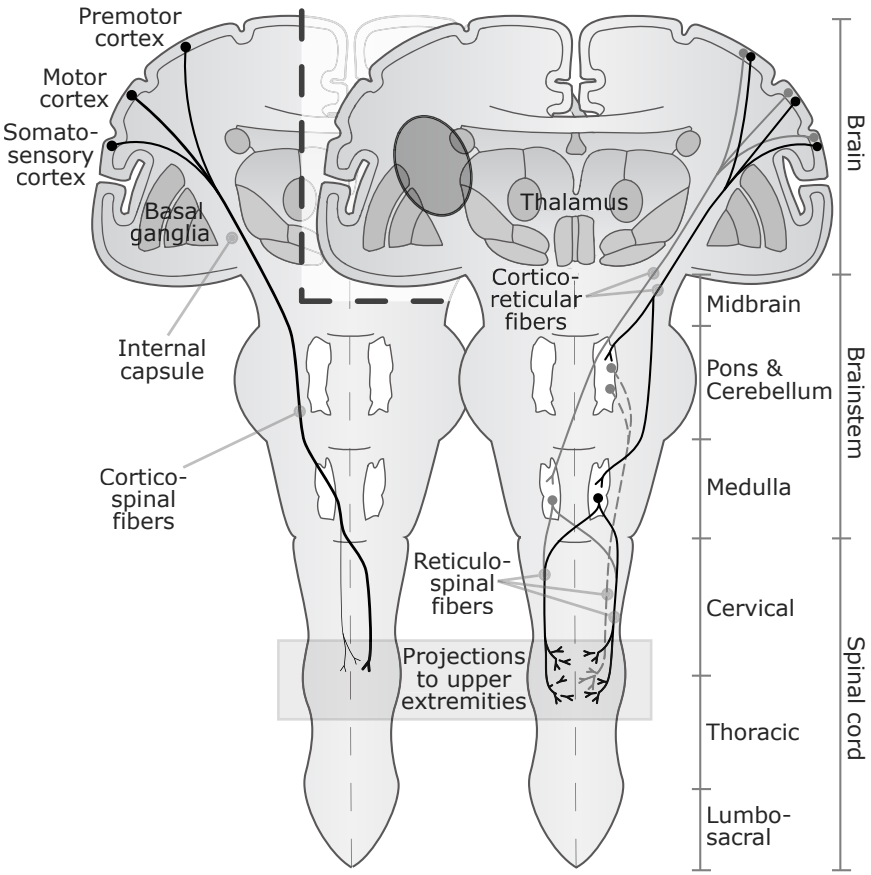

Figure 1.1: Coronal view of neural tracts important in motor control [71, 116]. (Not to scale). In healthy subjects (left image), the upper arm is predominantly controlled via contralateral corticospinal projections. After a stroke (right image), which often occurs in the internal capsule (black eclipse), control may be diverted via ipsilateral corticoreticular and reticulospinal pathways. The ellipse marks the common lesion location after an infarct in the middle cerebral artery.

About 80 percent of stroke survivors have a disturbed sensory feedback or motor control of the upper limb on the paretic side [115, 176]. Sensory distortion expresses itself through a reduction of tactile or afferent feedback, or as the opposite, through hypersensitivity. The loss of motor control is seen in typical neurological impairments, namely muscle weakness, hyperactive reflexes, and abnormal muscle synergies:

- *Muscle weakness* limits the maximum potential output force of a muscle [73]. It is caused by the damage to motor-cortex neurons or their corticospinal projections, diminishing the activation of spinal motoneurons controlling the muscles. The result of the diminished activation is the overall reduction in the motor unit firing frequencies as well as an reduction in the range of frequencies following stroke. Possible changes in motor unit recruitment order may also occur. The remaining operational projections now have limited

relief options. This hastens muscle fatigue, which further reduces output strength. Muscle weakness is initially almost solely caused by loss of neural activation, but after prolonged disuse, changes in muscle morphology can further reduce the output strength (see below).

- *Hyperactive reflexes* can resist or even temporarily reverse desired movements. The expression of hyperactive reflexes is felt as increased muscle tone or joint resistance when it depends on the muscle-length feedback (through Ia-static and II afferents) [160, 158, 135, 136]. When dependent on the muscle-speed feedback (through Ia-dynamic afferents), the effects are described as spasticity [113, 114, 3]. Hyperactive reflexes are thought to be caused by increased neural background activity of the motoneurons in the spinal cord, increasing both the motoneuron excitation and excitability. These changes may be due to modified network responses to afferent fibers, modified intrinsic properties of muscle fibers, and an increased reliance on the reticulospinal pathways [101, 203, 131]. The mono-aminergic inputs from these reticulospinal pathways greatly enhance motoneuron excitability by changing the resting membrane potential, thus reducing their activation thresholds.

- *Abnormal muscle synergies* express themselves through a loss of independent joint control, where involuntary co-activation of muscles occurs over multiple joints [35, 36, 206, 46]. For example, when attempting to reach up and out for an object on a shelf, the abduction torque in the shoulder causes an involuntary flexion of the elbow, reducing the achievable reaching distance of the hand [11, 206, 47]. These patterns are classified in stereotypical flexion and extension movement synergies [18] (see Tab. 1.1). Abnormal muscle synergies are thought to be caused by an increased reliance on the more widely branched reticulospinal pathways.

After prolonged disuse, this can result in muscle atrophy and increased joint stiffness:

- *Muscle atrophy* is a decrease in muscle mass and the results of muscle disuse over time [70]. The loss of neural activation leads to a slow wasting away of the affected muscle fibers, thereby contributing to long-term muscle weakness.

- *Increased joint stiffness* is due to changes in muscle and tendon properties. These changes are a result from permanent muscle activity due to continues muscle activity caused by abnormal muscle coactivation patterns or spasticity.

In publications and general use when dealing with patients, the levels of motor impairment are roughly classified as:

- *Severe*, with almost no useful muscle activation or limb movements.

- *Moderate*, with operational but clearly affected limb movements.

- *Mild*, with close to full functional control of arm, hand and fingers.

The immediate effects after a stroke can range from losing all voluntary muscle activation, to having no noticeable effects on limb movements. Spontaneous recovery can bring back some original motor function, but this takes many months to level out [134]. The spontaneous and rehabilitation-assisted recovery advances according to a generalized pattern of six stages [213, 18], although individual patients will have different initial and final stages:

I Patients are unable to perform voluntary movements. During passive motion, very little or no muscular resistance is felt.

II Along with small voluntary movements, components of synergetic patterns gradually appear. In most patients, the flexion synergy appears before the extension synergy. Spasticity may be present too, but is often nearly unnoticeable due to muscle weakness.

III Synergetic movement patterns can be called upon voluntarily. Spasticity increases and contractures can be formed, especially in the flexors of the wrist and fingers and in the forearm. For severe stroke patients, this is the final stage, reached months after the stroke incident.

IV Spasticity reduces and simple movements outside of the synergetic patterns become possible. The hand can now be placed behind the back and the arm elevated in the forward direction to shoulder level. When the elbow is flexed to 90°, the forearm can rotated around its central axis.

V Dependence on the basic synergies decreases and more complex movements are possible. The latter require high levels of concentration. The arm can now elevate sideways to shoulder level, and in the forward direction to above head level. Forearm rotation around its central axis are now also possible with an extended elbow. Spasticity is further reduced.

VI Most synergetic patterns have disappeared, and spasticity is almost completely gone. Complex movements may still appear clumsy.

1.2.2 *Stroke assessments*

Several stroke assessment scales are used to more precisely assess the need for medical treatment and assistance, and to monitor functional recovery. The following scales all capture some of the mental and motor impairments in stroke patients:

JOINT	FLEXION SYNERGY	EXTENSION SYNERGY
Shoulder girdle	retraction & elevation	protraction
Shoulder	abduction	adduction
Shoulder	external rotation	internal rotation
Elbow	flexion	extension
Forearm	supination	pronation

Table 1.1: Stereotypical flexion and extension synergy patterns [18].

- Barthel Index (BI): measures independent functioning and mobility in daily life.
- Functional Independence Measure (FIM): measures sensitivity and comprehensiveness in daily life.
- Chedoke-McMaster Stroke Assessment (CMSA): measures impairment and activities of daily life.
- Motor Activity Log (MAL): measures arm usage.
- Modified Ashworth Scale (MAS): measures muscle tone.
- Tone Assessment Scale (TAS): measures muscle tone.
- Modified Tardieu Scale (MTS): measures muscle tone
- Motor Assessment Scale (MAS): measures performance of functional tasks.
- Fugl-Meyer Assessment (FMA): measures motor and joint function and sensation.
- Action Research Arm Test (ARAT): measures ability to handle different objects.
- Nine Hole Peg Test (NHPT): measures fine manual dexterity.
- Wolf Motor Function Test (WMFT): measures time-based upper extremity performance.

These scores are placed in order of level of detail given. The top scales only yield an indication of the care and assistance needed. Scales measuring muscle tone are crude approximations of spasticity levels. The bottom scales measure the dexterity of the upper paretic limbs, and are most useful for upper-extremity research. Of these, the FMA [62] is a well-designed, feasible clinical examination based on the aforementioned general stages of recovery [213, 18]. It has been widely tested in the stroke population, but due to the amount of time it takes to administer, it is mostly used by scientists, not by therapists or physicians. The ARAT and NHPT have been suggested as faster and more accurate assessments to measure dexterity [112]. For measuring muscle tone, the MTS seems the most objective. It measures the stretch reflex induced catching angle when a joint is moved through its range of motion at different velocities [132].

A problem for most of these clinical scales is their non-linearity, lack of resolution, and inter-rater reliability. A one-point improvement can have different implications depending of the location on the scale. Some scales have only six possible levels, and when different examiners administer the test, the results may vary as well. Another problem is the inability to distinguish between compensation movements and restitution of function (see next section). Robots are now used in research environments to obtain more accurate measurements [37, 32, 38, 47].

1.2.3 *Patient strategies*

Presented with the loss of arm and hand function, patients develop different strategies. The choice of strategy differs based on the level of impairment, which includes cognitive changes, and can be directed through rehabilitation therapy. Based on current literature [216], the possible strategies for upper-extremities rehabilitation are:

- Ignoring the affected arm and performing all activities with the unaffected one.
- Compensating for diminished arm control by using other, less-affected body parts, such as flexing the trunk when reaching.
- Actively seeking restitution of normal motor control of the affected arm, without compensatory movements.

The first two strategies do not recover pre-stroke movement patterns in the affected limbs. They do offer a quick way to regain some functional ability, but may limit the patient's motivation to work at true recovery via restitution of normal movement patterns. Compensation is also inefficient, because it requires more segments to participate in the movement. It may also not always be possible, for instance, when less-affected body parts are otherwise simultaneously engaged performing their normal function. Finally, recovery via restitution always holds the possibility of maximizing performance by employing both the recovered function and compensatory movements.

Compensatory strategies are only possible when the musculoskeletal system has multiple options to combine different sets of joint movements to perform a desired task [216]. In other words, they are only possible when there are redundant degrees of freedom. But strategies to handle these redundant degrees depend on the tasks. For instance, restricting trunk movements during therapy prevents patients from using these compensatory movements [133]. However, restricting vertical displacements in reaching tasks with a virtual table [206], rewards patients for the erroneous motor pattern of pushing down while wanting to achieve horizontal movements. Rehabilitation devices should be designed to carefully handle these redundant degrees of freedom of the musculoskeletal system because rewarding patients for compensatory movement does not lead to restitution of normal control.

1.2.4 *Conventional therapy*

The treatment received by stroke patients differs from institution to institution. In the Netherlands, a modified version of the so called Bobath approach, also known as the Neurodevelopmental Technique (NDT), is the most popular [23]. The NDT now includes a focus on using repetitive, functional movements. In many other countries, Proprioceptive Neuromuscular Facilitation (PNF) or Motor Relearning Program (MRP) are more common. Patients require roughly six to 12 months of therapy before motor recovery levels out [134].

The amount and duration of spontaneous recovery is different for each patient, which makes it difficult to compare different stroke interventions. Systematic reviews of conventional therapy for upper extremities—where the results of a

large number of patients in clinical trials are compared—stress the importance of using intensive and task-specific exercises, such as active, repetitive movements, preferably as early as possible after onset [109, 8, 56, 222]. The improvements in most of the clinical studies were mainly restricted to tasks directly trained in the exercise programme. This closely follows the main principle of motor learning: the improvement in motor-control performance is directly linked to the amount of practice [187]. The deeper reasoning behind the therapeutic interventions seem less important, as long as the aforementioned intensive exercises are used.

In the last of the above systematic reviews [222], 151 randomized and controlled clinical trials were grouped into 10 intervention categories and evaluated on their effective functional outcomes. The intervention categories give an impression of the current approaches used in rehabilitation centers, for both the upper and lower extremities:

- Traditional neurological treatment approaches.
- Programs for training sensorimotor function or influencing muscle tone.
- Cardiovascular fitness and aerobic programmes.
- Methods for training mobility and mobility-related activities.
- Exercises for the upper limb.
- Biofeedback therapy for the upper and lower limb.
- Functional and neuromuscular electrical stimulation for both limbs.
- Orthotics and assistive devices for both limbs.
- Treatments for hemiplegic shoulder pain and hand oedema.
- Intensity of exercise therapy.

Most of these interventions target the neurological components of stroke. Some specific treatments also exist for non-neurological effects of prolonged disuse. Muscle atrophy can be partly prevented with repetitive electrical stimulation [193], contractures by passive stretching of the muscles [16], and finally, increased joint stiffness by continues passive motions that cyclically stretch the patient's limb [17, 124].

1.2.5 *Robot assisted therapy*

In an effort to assist therapists, patient-friendly robots are used as diagnostic and therapeutic aids. Rehabilitation robots differ from assistive robots. Assistive robots take over functions in daily living, such as picking up objects with a robot arm or helping a patient get in or out of bed. Conversely, rehabilitation robots help patients regain the original motor function of the limb. Many assistive robots become permanent aids, while rehabilitation robots are mostly used during therapy sessions in the clinic.

Current robots employ a number of different rehabilitation strategies (see Fig. 1.2). For example, the MIT-Manus [82] assists arm movements when needed during task execution, the MIME [22] mirrors the movement of the affected to the unaffected arm, the ACT-3D [206] tackles undesired abnormal muscle couplings,

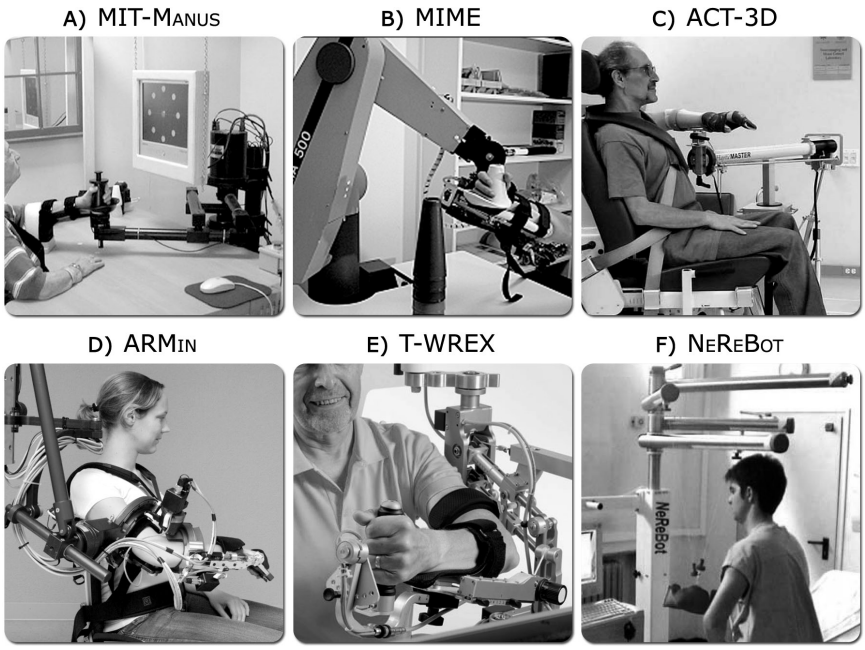

Figure 1.2: Current rehabilitation devices. The MIT-Manus, MIME and ACT-3D are endpoint manipulators, the ARMin and T-WREX are exoskeletons, and the NeReBot is a cable device.

the ARMin [143] motivates patients by interacting with virtual environments, the T-WREX [180, 85] compensate for the gravitational pull on the arm, and the NeReBot [127] combines peripheral manipulation with visual stimuli.

Upper-extremities devices can be grouped into three types: endpoint manipulators, exoskeletons, and cable suspensions. Endpoint manipulators have a single connection to the hand, wrist, or forearm. The single connection limits the control over individual joint axes. Patients often hold on to a handle while making movements in virtual environments. Exoskeletons are external skeletons placed over the arm and mostly powered by actuators on the joints. They control not only a single endpoint position, but also (a subset of) the joints of the shoulder, elbow, and wrist directly, at the cost of more complex mechanics. Cable suspensions link one or more cables to the arm, increasing both control options and complexity with every additional cable linkage. With overhanging cables and counterweights, these cable suspensions have been used by rehabilitation hospitals for decades. They are simplest to realize, but offer the least amount of control on the arm.

According to systematic reviews, new robot-assisted therapies are at least as good as regular therapy for stroke rehabilitation. Van der Lee et al. [219] tentatively concluded that the type of therapy matters less than its exercise intensity. Several approaches with and without robots resulted in roughly the same effect when the level of intensity was matched. They indicated that robots could be a useful way to increase exercise intensity.

Platz [157] found evidence for superior treatment efficacy of task-oriented, motor-relearning programs and giving different patient subgroups specific train-

ing strategies. They also found a higher intensity of motor rehabilitation resulted in an accelerated, although not necessarily better, motor recovery. A review from our project group [162] concluded that robot-assisted therapy of the shoulder and elbow improves motor control of these joints, and probably more than conventional therapy. Consistent influence on the functional abilities of the patients was not found. These conclusions are shared by Kwakkel et al. [112]. Measured on rough clinical scales, however, these significant improvements in motor control do not result in a higher functional score. This indicates both the potential for improvement over intensive conventional therapy, and an inability of the clinical scales to reflect recovery of the paretic upper limb [112].

With most rehabilitation robots, several components affect outcomes. Often, the therapy is simultaneously made more intensive, more supportive, and more motivating for the patients than is possible with regular therapy. More repetitions per session, movement assistance via external actuators, and an involving and stimulating virtual environment all influence the rehabilitation process. But in most efficacy studies, the effects of the individual components are not reported. This lumping of components may explain why the type of robot-assisted therapy has, so far, made little difference in systematic reviews. A common component like the increase in intensity is probably far more important than the type of rehabilitation therapy used.

The chosen rehabilitation strategies are mostly based on the experiences of therapists and physicians, general motor learning theories, and the results of stroke research. In conventional therapy, therapists interact with the patients by guiding or resisting their movements, in which the movement mimics activities of daily living. Motor learning theories state that active, repetitive movements, with the right type and amount of experienced error, result in the best performance. Finally, by quantifying impairments while controlling for some variables, therapists identify and subsequently target components limiting performance during therapy. Recent examples of this last process include decreasing the link between limb loading and workspace [11, 45, 206, 46] and reducing the number of submovements [173, 174, 80, 38]. Both of these stray from the recommended use of task-specific movements only, which perhaps is not as important as stated before [108].

Assist-as-needed is a popular strategy originating from the experiences of therapists. With it, the patient is presented a visual target and asked to move toward it. When a voluntary-EMG threshold has been exceeded, a certain amount of time has expired without sufficient progress, or when the desired movement goes outside a predefined region, the movement is guided or automatically completed [168, 107, 31, 24]. The goal is to increase muscle activity and thereby encourage neural reorganization. It also provides positive reinforcement to maintain the patient's motivation. However, when the assist-as-needed strategy is implemented incorrectly, patients can actually reduce their own efforts and let the robot take over [231]. Thus, when providing assistance, a difference should be made between completing a movement and enabling the completion [152]. The first takes over when the performance targets aren't met by the patient, but the second does not. This is most easily seen in as the difference between applying goal-directed assistance, and supporting the arm against gravity. No matter how much gravity support is provided, the robot never exerts forces in the direction of the movement target and the patient must always be active in completing the given assignment.

1.3 OBJECTIVES

In collaboration with Roessingh Rehabilitation & Research (RRD, Enschede, NL) and BAAT Medical (Hengelo, NL), we set out to develop, evaluate, and utilize new rehabilitation robots.[1] For the University of Twente, the primary role lies in the development process. To get the most out of the devices, development is interwoven with evaluations. That is, the experience gained while evaluating each device, should be used in the development of future devices.

Therefore, the goal of this dissertation is to improve rehabilitation robots by developing new patient-friendly devices to assist in stroke rehabilitation and research for the upper extremities.

For stroke rehabilitation therapy, the final set of devices must be usable for the entire range of patients suffering from mild, moderate, or severe impairments. The focus of the devices should be on the aforementioned working strategies to create intensive and task-specific exercises, consisting of active, repetitive movements that are performable.

For stroke research, the devices must help to understand the role of individual therapy components in the motor recovery mechanisms, such as task intensity, weight support, and compensatory strategies. By unraveling these different components in clinical trials, future device design can keep the components that work and disregard those that don't.

1.3.1 *Potential set of devices*

Starting development with the simpler devices can give a head start with patient experiments. These devices are quicker to design and construct, and safer to use. The experimental experiences gained from them can be used to iteratively design more complex devices. Therefore, the chosen approach is to have three different devices cover all the above requirements: a weight-support device which supports the arm against gravity, and two devices to passively resist and actively assist movements.

Weight-support device

The weight-support device should solely support the weight of the arm for severely to moderately affected patients. These patients often cannot lift their own arms against gravity, making most task-specific rehabilitation exercises impossible. By starting out with full weight support, patients can start earlier with these exercises, and perform them at a higher intensity and longer duration. This potentially helps them regain more arm function. Over the entire rehabilitation process, the amount of weight support should be reduced to keep the level of intensity high and slowly reacquaint the patient with the demands of gravity.

A simple, mechanical device has obvious advantages in cost, usage, and maintenance over more complicated mechatronic solutions. It should have scalable and independent support for the upper and forearm with maximum freedom of movement. Minimal impedance is required to not hinder the patients in any way. In use, a therapist should still have full access to feel and steer the arm as needed. Based on these requirements, the weight-support device, the Freebal, is developed and evaluated.

1 The collaboration has resulted in iMove Support (www.imovesupport.eu).

Passive-resistance device

In the training stages, active patient participation is essential. The resistance training device may be utilized for patients with more advanced requirements for high-intensity therapy. By offering interesting training environments and varying the levels of difficulty, patients stay motivated and challenged. These patients are primarily mildly and moderately affected, and have rough control of limb movements. With controlled application of resistance torques, the task-specific exercises can be made more intensive while ensuring active patient participation and safety. With control at joint level, such a device should also be able to assist in identifying causes behind stroke movement disorders.

The requirement of control in joint space with controlled resistance, suggests the use of an passive exoskeleton. Such an exoskeleton may have controlled disk brakes on each rotation axis of the shoulder and elbow. Disk brakes offer the advantage of a high torque-to-weight ratio and inherent safety. However, to use an exoskeleton without generating the misalignment forces and range of motion limitation normally associated with exoskeleton, its weight must be minimized and its joints closely aligned to the anatomical ones. This calls for an innovative self-aligning solution. Based on these requirements, the passive-resistance device, the Dampace, is developed and evaluated. The novel self-alignment mechanism and disk-brake usage must be evaluated separately.

Active-assistance device

For severely affected patients, full weight support might not be sufficient to generate movements. Intent and impairment-level-based assistance, also known as assist-as-needed, requires an active device. Mild and moderately affected patients could use this device for task-specific exercises in more realistic virtual environments. Such a device should also automate some of the impairment assessments that require involuntarily-driven movement of limbs, for instance to accurately measure the level of spasticity at each joint.

The requirement of control in joint space with active assistance, suggests the use of an active exoskeleton. This exoskeleton must use similar self-alignment mechanism as the Dampace, but must replace the passive disk brakes with active actuators. These actuators should not significantly add to the weight of the device, while still being able to generating high torques with fast performance. Series-elastic actuation has clear advantages in patient interaction. When combined with hydraulic actuators, it is powerful enough for the desired specifications. The hydro-elastic combination requires its own evaluation.

Due to the time consuming process of developing new robotics, the Limpact was not machined in time for a complete description and evaluation in this dissertation.

1.3.2 *Research questions*

This dissertation focuses on the new design aspects and technical verifications of the above devices. The most important objective—determining whether the devices are really suitable for all the described roles in stroke rehabilitation and research—can only be proven by multiple clinical trials with each device. Due to the time required to develop each device and a limited availability of stroke patients during our project, the device usage here has been limited to a cross-sectional and a training study with the weight support device.

This leads to the following specific research questions:

I *Which assistive forces improve motor learning in healthy subjects?*

II *What is the optimal usage for each type of current rehabilitation devices?*

III *How do new devices improve upon existing designs?*

IV *Does weight support enhance recovery after stroke?*

V *Is the full potential of rehabilitation robots used?*

1.4 DISSERTATION OUTLINE

Chapters 2 to 9 in this dissertation are written as full journal publications. This causes significant overlap between some chapters, but it also means that they can be read individually or out of order.

Chap. 2 identifies the influence of therapeutic force fields on visuomotor learning. We compare active participation and unassisted movements of healthy subjects in their ability to learn a motor task. The results may be helpful when designing assistive algorithms for stroke therapy.

Chap. 3 provides an analysis of weight-support mechanisms in upper-extremity rehabilitation devices. Weight support both facilitates movements of the patients and if applied externally, reduces stresses in the devices and on the actuators. Current robots are separated on the mechanisms to apply the intervention strategy, and the mechanisms that provide weight support.

Chap. 4 details the design of the Freebal, a minimal weight-support system for upper-extremity rehabilitation. The system uses ideal-spring mechanisms to support the wrist and elbow via an overhanging cabling system. The device was used in a cross-sectional experiment on stroke patients, and the results are presented here.

Chap. 5 describes the results of a six week therapy protocol, in which four chronic stroke patients received movement training with weight support. For these sessions, the Freebal was combined with a custom motivational computer game.

Chap. 6 establishes potential improvements for exoskeletons by using self-alignment mechanisms. Benefits and disadvantages are given. The mechanisms may overcome many of the objections against exoskeletons, such as long setup times, restricted shoulder movements, and high interaction forces.

Chap. 7 depicts the analysis of hydraulic disk brakes for suitability in upper-extremity force-coordination training. These passive but controllable actuators have high maximum torques and better-than-expected intrinsic properties, and may be suitable for use in rehabilitation robots.

Chap. 8 details the design and evaluation of the Dampace, an exoskeleton for force-coordination training in upper-extremity rehabilitation. The exoskeleton uses the self-aligning joints and hydraulic disk brakes as described in greater detail in the previous two chapters. The overall system performance is analyzed, and several options for integrating virtual reality in rehabilitation therapy shown.

Chap. 9 describes the performance of a new rotational hydro-elastic actuator for an active upper-extremity rehabilitation with exoskeletons. This novel actuator is designed for the upcoming active exoskeleton, the Limpact.

Chap. 10 concludes this dissertation, with a discussion section for each of the research question. A short summary of each device and future directions are given.

2

INFLUENCE OF HAPTIC GUIDANCE IN LEARNING A NOVEL VISUOMOTOR TASK

ABSTRACT In (re)learning of movements, haptic guidance can be used to direct the needed adaptations in motor control. However, guidance will decrease the magnitude of the execution errors, that are known to be a dominant clues for motor adaptations. During haptic guidance interactions occur that are considered not to be efficient. Minimizing the control effort will reduce these interaction forces and can this strategy indirectly contributes to learning a novel task. The aim of this study was to assess how different types of haptic guidance affects kinematical adaptation in a novel visuomotor task in which visual feedback of hand position was distorted. We hypothesized that adaptation was slower for those haptic force fields that reduced the execution errors more, and that even in the absence of execution error adaptation would occur but at a much smaller rate. We also predicted that in case execution errors were absent and control effort was not minimized adaptation would be absent. Five groups of subjects adapted to a visual rotation task, while being guided by per group different force fields. The force fields differed in magnitude and direction, in order to discern the adaptation based on execution errors and control effort. The execution error did indeed play a key role in adaptation; the more the guiding forces restricted the occurrence of execution errors, the smaller the amount and rate of adaptation. However, the force field that enlarged the execution errors did not result in an increased rate of adaptation. The presence of a small amount of adaptation in the groups who did not experience execution errors during training suggested that adaptation could be driven on a much slower rate and on the basis of minimization of control effort as was evidenced by a gradual decrease of the interaction forces during training. Surprisingly also in the condition in which no execution errors occurred and subjects were passive a small but significant adaptation occurred. The conclusion is that both minimization of execution errors and control effort drives kinematical adaptation in a novel visuomotor task, but the latter at a much slower rate. Other mechanisms that contribute to kinematical adaptation can not be excluded, but the possible contribution of these alternative mechanisms is smaller and has a longer time scale than minimization of control effort and execution errors.

2.1 INTRODUCTION

Haptic guidance of movements can be used to demonstrate a subject how fast and in which direction a movement should be performed. As such, haptic guidance is used for learning new skills in sports, but also for relearning motor control after having a stroke [100]. Haptic guidance of movements can be used to demonstrate a

Accepted pending minor revisions: Journal of Physiology, Paris (EHF van Asseldonk, M Wessels, AHA Stienen, FCT van der Helm, and H van der Kooij). EHF van Asseldonk and AHA Stienen shared the daily supervision of (then) master student M Wessels and contributed equally to this work.

subject how fast and in which direction a movement should be performed. As such, haptic guidance is used for learning new skills in sports, but also for relearning motor control after having a stroke [30, 122, 54, 80, 143] have been developed, which can provide unlimited guidance during the recommended highly repetitive practicing [109, 8, 56, 111, 207].

With these therapy robots different types of haptic guidance have been implemented. Soft guidance moves a limb through a pre specified trajectory where deviations from this trajectory result in forces towards this trajectory [2]. For hard guidance haptic tunnels are rendered; a subject can move within this tunnel [100] but not outside the stiff walls of the tunnel. When the robot is programmed in position control model the human subject can be fully passive since muscle activation will not (directly) change limb movements [77, 124]. To promote the subject to become active visual feedback of interaction forces have been implemented [123]. Interestingly the application of haptic force fields that increase instead of reduce errors in the execution of movement has shown that this principle effectively enhances motor learning [48, 229, 150].

Our interest is to understand the interactions between haptic guidance and the learning of a novel motor task. In the gross of computational motor control theories the underlying principle is the minimization of both control effort and task execution errors [218, 209, 191]. Also computational theories of motor learning exist in which both control and execution effort drives motor learning [205]. Experimental shows that minimization of both control effort and execution error characterizes learning dynamics [183, 51]. In these studies similar haptic devices as being used in neurorehabilitation were applied to study how people adapt when exposed to force fields applied to moving limbs while exposed to a novel dynamical environment. Scheidt and colleagues [182] used a rendered haptic channel that prevented the occurrence of kinematical after effects after removal of the previously learned viscous force field. They showed that subjects made movements while simultaneously exerting perpendicular forces to the haptic channel that were similar to the forces required to compensate for the viscous force field. Despite the absence of kinematical errors, subjects disadapted by decaying the forces exerted on the channel over the different movements. Still, the disadaptation occurred at a much slower rate than when kinematical errors were allowed to occur. Further evidence for a contribution of muscular effort in adaptation was recently provided by Emken and colleagues [51]. They examined the adaptation to an externally applied force field during the swing phase of walking and showed that a model describing the temporal evolution of error [208, 183] could be derived from minimization of a cost function that is a weighted sum of the execution error and control effort.

The aim of this study was to further study the interaction between haptic guidance and learning a novel visuomotor task. Do specific types of haptic guidance improve or limit the learning of a novel visuomotor task? The quality of learning in this study will be quantified by the completeness of learning, the generalization of learning and the learning rate. This is the first study to our knowledge that explicitly address the interaction of haptic guidance and learning a novel visuomotor task in which visual feedback of hand position is distorted. From previous work we expect that execution errors and control effort drive motor learning but we can not exclude at this stage that also other sources could drive visuomotor learning. For example the interaction forces or sensory conflicts between visual information and other sensory modalities could (in theory) be used to adapt internal models

and motor programs. As a model for a novel visuomotor task we used out of center reaching movements while the visual feedback of hand movement direction was rotated thirty degrees counter clockwise. Thus when moving your arm straightforward you will see your hand moving in a thirty degree counter clockwise direction. If a subject aims to a target in first instance (s)he will miss the target but after several trials humans will adapt to this visual rotational distortion. This task has been used to study several aspects of motor learning related to kinematical adaptations of visuomotor control [105, 64, 178, 210, 25, 226]. Force fields have extensively been used to study kinetic adaptations of visuomotor control [192, 66, 40, 184]. To our knowledge no studies investigated the interaction of kinematical and kinetic adaptations, which will occur when haptic guidance is used in combination with a visual rotation task. Different types of haptic guidance that are commonly used in therapy robots were applied to study the haptic interference with learning to deal with the visual distortion of hand movement. All but one of these force fields applied forces only in the direction perpendicular to the target direction, which necessitates the subjects to move in the target direction themselves. Subjects in the error enhanced group (EE) received hand forces that were proportional and in the same direction as the execution errors, defined as the deviations from the straight path towards the target. These forces effectively enlarged the execution errors. In the soft (SG) and hard guidance (HG) groups, error correcting forces were applied to the hand which were proportional but opposite to the execution errors. In the soft guidance group, the low stiffness of the force field still allowed considerable execution errors. However, in the hard guidance group, the high stiffness formed a haptic tunnel, denying all but very small deviations (<1.5 mm) from the optimal trajectory. In the passive group (P), the subjects were moved along the optimal trajectory by the robot and were instructed not to intervene. In this case execution errors are zero and the control effort does not influence task performance. In the control group (A) no force fields were applied and subject had to be active.

We hypothesized that adaptation to a novel visuomotor task with haptic guidance is mainly driven by minimization of execution errors and control effort. We hypothesize that when execution errors are increased (EE) or reduced (SG) by haptic guidance the rate of adaptation will be faster or slower respectively, and in both cases adaptation will be complete. In case execution errors are prevented (HG) but subjects had to actively move their hand towards the target we hypothesize that adaptation still occurs but at a most slower rate that in the A, EH, and SG groups. In this case adaptation is driven by minimization of control effort solely: directional errors will not occur but forces in the direction of the haptic tunnel are considered to be energy inefficient and thought to be minimized during adaptation. For the passive group we hypothesize that adaptation is absent since no executions errors occur and control effort is not related to task instruction and performance.

2.2 MATERIALS AND METHODS

2.2.1 *Subjects*

Fifty healthy subjects (ages 20-50 years, 16 females) were included, all giving their written informed consent prior to the experiment. The protocol was approved according to the institution's regulations. All subjects were right-handed, had no history of neurological impairments and had a normal or corrected vision. The subjects were randomly assigned to one of the following training programs,

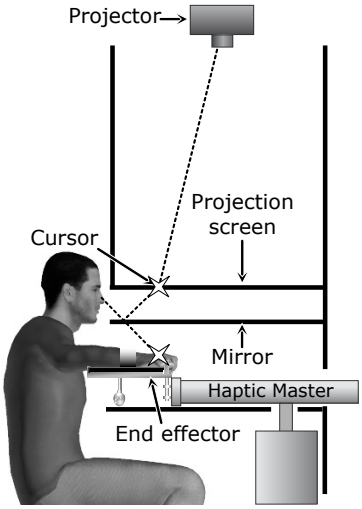

Figure 2.1: Schematic overview of experimental setup. Subjects sat behind a closet-like box and held with their right hand the end-effector of a haptic robot. Subjects looked into a mirror just below shoulder level to a projection of their (rotated) right hand position and the targets. The mirror prevented sight of their right arm. The arm was supported by a surface through a mechanism that allowed horizontal movements with low friction.

'Active' (A), 'Passive' (P), 'Hard Guidance' (HG), 'Soft Guidance' (SG) and 'Error Enhanced' (EE) training.

2.2.2 *Experimental apparatus and recordings*

The subjects were seated (see Fig. 2.1) and made reaching movements in the horizontal plane with their right arm while the right hand was holding the 'end-effector' of a 3D haptic robot, the Haptic Master (MOOG-FCS, Nieuw-Vennep, the Netherlands), which we restricted to functioning in the horizontal 2D plane just below the shoulder level. The force exerted by the Haptic Master on the hand was controlled at 2500 Hz to create the guiding forces described below in further detail. The arm robot was placed in a box to remove external light interference. The subjects were instructed to look into a mirror to see a projection of their right hand position on a screen located parallel and just above the mirror. The combination of a mirror and projection screen gave the illusion that the projected image was in the same horizontal plane as the hand, resulting in a veridical projection. The mirror also prevented direct sight of the arm. The right-hand position was indicated with a 6 mm blue sphere, in the following referred to as the cursor. The targets were presented as yellow spheres with a 10 mm diameter. The visual scene was updated with a frequency of 100 Hz. The arm was supported against gravity by a support mechanism which allowed low friction movements over an underlying surface (see Fig. 2.1). The arm support also prevented wrist movement. As a result, movements of the hand were restricted to the horizontal plane and solely the result of joint rotations around the vertical axes of elbow and shoulder. Velocity and position data of the end-effector of the Haptic Master were sampled at 200 Hz.

2.2.3 *Procedure*

Subjects made center-out reaching movements with their right hand to one of five different targets equally spaced (72° apart) about the perimeter of a circle of 10 cm radius. The center of movements was always in the midsagittal plane

10 cm beneath the right-shoulder position. The starting posture was obtained by a shoulder plane of elevation rotation of 45° and elbow flexion of 90° [233]. At the start of each trial, a target was presented and a short beep triggered movement. The order of the targets was randomized in each cycle, where a cycle consisted of one trial to each target, thus five movements. Subjects received feedback about the accuracy of the movement duration by means of target color and a sound. The end of the movement was defined as the moment at which the velocity decreased below 5 mm/s. The target color changed into green when the cursor was inside the target within the prescribed time interval (510-690 ms) and a normal tone was heard. Too fast or too slow movements were accompanied by a change of the color of the target into blue and red respectively, and a dropping and refuting sound. During all stages, the number of accurate reaches was shown on the visual display in the right upper corner. Between movements, the cursor was made invisible while the arm was returned to the starting position by the robot.

Visual distortion of hand position, during training and extended training, was a 30° CCW rotation about the starting location of movements. When exposed to the visual rotation, subjects received different force fields, depending on the group to which they were assigned (see Fig. 2.2). Besides the interacting forces, all groups except the passive also felt unintentional inertial forces of a 2 kg virtual floating mass in the virtual environment; a remnant of the employed admittance control in the haptic robot.

- Group A (active movements) did not receive any additional forces during training.
- Group P (passive movements) subjects were moved along the optimal trajectory to the target by stiff control (k = 5000 N/m) of the robot. This optimal trajectory was defined as a straight line from center to target position, with a bell-shaped velocity profile:

  $$v(t) = \frac{y_r}{T}(1 - \cos(2\pi\frac{t}{T})), \text{ for } 0 < t \leqslant T,$$

  where T is the movement duration (600 ms), t is time and y_r is the distance between center and target. Subjects in this group were specifically instructed not to intervene with the applied robot, so not to assist or resist the imposed movements.
- Group HG (hard guidance) movements were restrained to the desired path by a stiff force field perpendicular to the optimal trajectory acting on the right hand. Since the stiffness along this optimal trajectory was zero, the subjects were free to control the progress along the path. Force F is a function of deviation from a straight path from the start to the target:

  $$F(x) = kx,$$

  with k = 5000 N/m. Cursor trajectory error x'_c, same in magnitude as hand trajectory error x_c, was described as the distance between current cursor position and the y-axis, the optimal hand trajectory (see Fig. 2.2). The relation between force and deviation is visible as a high gradient surface V, shown in Fig. 2.3A.

- Group SG (soft guidance) experienced a similar force field as group HG but with a lower stiffness (k = 300 N/m). The low gradient gray surface in Fig. 2.3A illustrates the soft guidance force-error relation.
- Group EE (error enhanced) was exposed to an error enhancing force field. When subjects deviated from the optimal path, they experienced a force which pushed them even farther away. In this case, F was described as:

$$F(x,y) = \begin{cases} A(y)(\frac{1}{2} - \frac{1}{2}\cos(2\pi\frac{x}{B})) & \text{if } 0 \leqslant x \leqslant \frac{1}{2}B \text{ or } \frac{3}{2}B \leqslant x \leqslant 2B, \\ 0 & \text{if } x \geqslant 2B, \\ A(y) & \text{if } \frac{1}{2}B \leqslant x \leqslant \frac{3}{2}B, \end{cases}$$

  where B = 0.05 m is a quarter of the area in which forces are present (See Fig. 2.3B). Factor A(y), expressed as:

$$F(y_c) = -ky_c,$$

  was a maximum force, dependent with a stiffness k = 500 N/m on the current y-position y_c; the distance between center and the projection of hand position on the optimal path.

Each group attended a program that consisted of four different stages, in following order:

1. In the familiarization stage, the subject got familiar with the haptic and virtual environment. Participants executed 100 reaching movements, with every fifth movement a catch trial interspersed and the directions randomized per five movements. The last five trails were considered as baseline. During this stage, none of the groups had forces present.
2. During the training stage, participants performed the task in the visual rotated field. All subjects performed 60 cycles of five trials, thus 300 movements. Every tenth movement a catch trial was interspersed to monitor the adaptation of subjects to the visuomotor rotation. As subjects in the passive group were not supposed to generated movements themselves during the training, the catch trials were preceded by an additional tone to make the subjects aware of when they were required to reach on their own. Generally, the adaptation to the visuomotor rotation is determined from the movement trajectory error (see Fig. 2.2 for error definition) in subsequent training trials [210]. However, force fields influenced the magnitude of the error, which compromised error comparison of training trials in different groups. Therefore, we interspersed catch trials in which the group dependent force fields were turned off. Furthermore, during catch trials visual feedback was not presented to capture uncorrected movements and to rule out active learning moments, as reaching without additional forces with visual feedback would mimic the active learning condition.
3. The extended training stage deviated from the previous stage in that the catch trials occurred every fifth movement and that movements during these generalization catch trials were directed to generalization targets which deviated 36° from the trained directions, that is, located exactly between the original targets along the circle. Subjects performed 30 cycles of movement, thus 150 movements, which included 30 generalization catch trials.

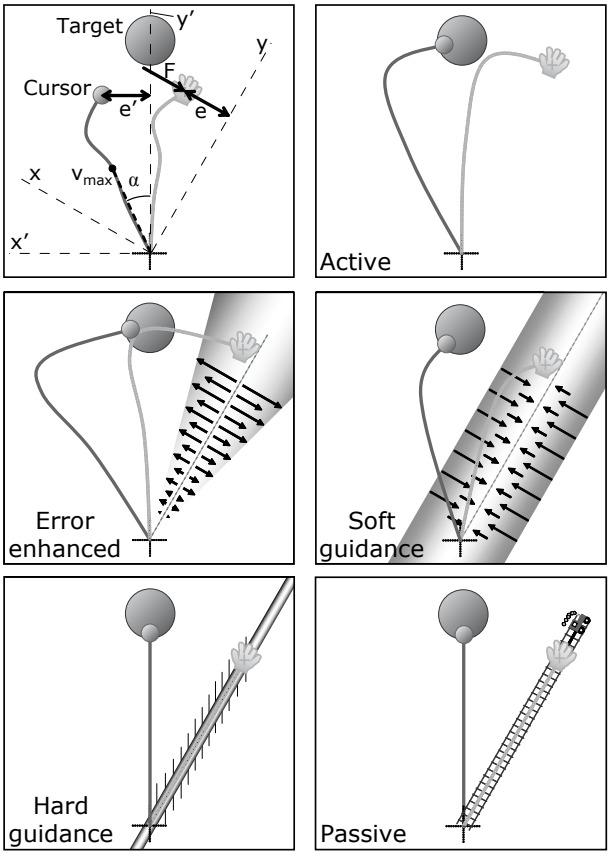

Figure 2.2: Definitions in the calculation of the guiding forces and the direction error, and the five types of therapeutic guiding forces used. In the top-left figure, error (e) is the distance x' from current cursor (small sphere) position to the y'-axis, which is also the optimal cursor trajectory from center to target (large sphere). Force F, dependent on hand position error ($e = e'$), acts on the arm and is perpendicular to the y-axis and parallel to the x-axis. The cursor path is 30° CCW rotated from the actual hand position. The angle α represents the angle between cursor position at maximum velocity (v_{max}) and optimal trajectory. In the other five figures, the 'active' condition had no guiding forces, the 'error enhanced' forces which increase any error made, 'soft guidance' forces which decrease these errors, 'hard guidance' forces which kept the hand from making any rotational errors, and finally in the 'Passive' condition, the hand was passively moved towards the target.

4. In the washout stage, visual feedback returned to normal. All visual distortions and force fields, if any, were turned off. This was the unlearning phase. Hand position was visible during all movements, with a total of 100 movements in 20 cycles.

In total, subjects performed 130 cycles of five movements. With short time-outs between every stage, subjects spend approximately 36 minutes to perform the experiment.

2.2.4 *Data analysis*

Movement position and velocity data of the hand were used to assess the reaching performance of the subjects in the different stages and conditions. We used the directional error as a measure of the execution error. Previous studies have shown that directional error is a sensitive and intuitive measure of adaptation to visuomotor rotations [106, 178]. The directional error is calculated as the angle between the vector from the starting position to the cursor position at maximum velocity and the vector from the starting position to the target (see Fig. 2.2). Fur-

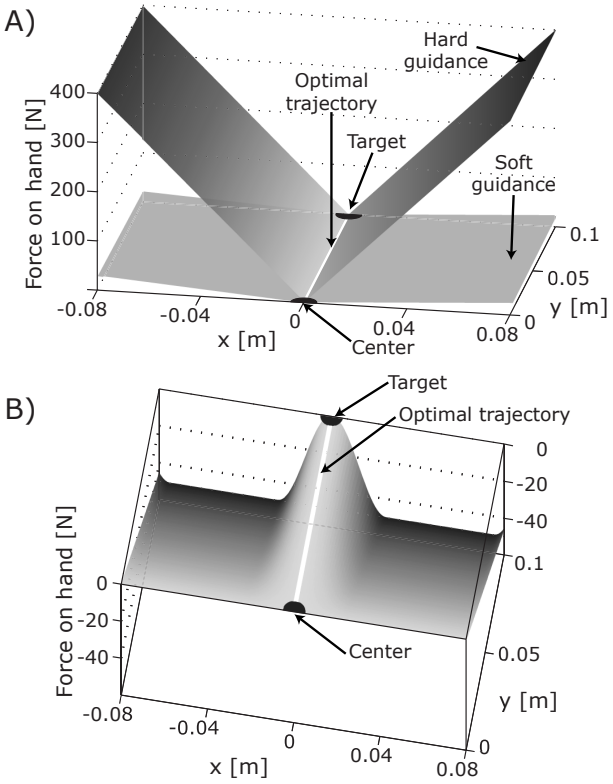

Figure 2.3: Forces exerted on the hand as a function of the deviation of the optimal trajectory (x) and the distance to the target (y). The forces are exerted in a direction perpendicular to the optimal trajectory. In A) the forces for the soft guidance stiffness (300 N/m) and hard guidance stiffness (5000 N/m) are depicted. These forces 'pushed' the hand of the subject towards the optimal trajectory in order to decrease the reaching errors. B) indicates the error enhancing forces, which were directed away from the optimal trajectory (indicated by the negative magnitude of the forces) to increase the reaching errors. In A) and B), the magnitude of the forces increases with the grayscale, though equal grayscale do not correspond with equal force magnitude in both figures.

thermore the directional error captures the learning in feedforward control and is insensitive for contributions of feedback mechanism to the final portion of the reaching movement. Baseline performance was quantified as the mean directional error of the last cycle of reaching movements during the familiarization stage. The catch trials and the generalization catch trials were each divided into six blocks of five trials and mean values of every block were calculated. The after effect was assessed by calculating the mean value of the directional errors of the first cycle in the washout phase.

As explained in the introduction, apart from using the execution errors in subsequent movements to adapt to the visuomotor rotation, subjects could also use the muscular effort. For group HG the haptic channel prevented the occurrence of execution errors. Subjects could push into the haptic wall, however as long as the force exerted on the end effector had a component in the direction of the target, the subject would reach the target. The force exerted in the direction perpendicular to the movement direction can be regarded as a waste of muscular effort. Minimizing the effort would be similar to minimizing these perpendicular interaction forces. We quantified the forces by averaging them from the moment the velocity in the direction of the target last exceeded the 10 cm/s before reaching the maximum velocity till the moment the velocity first dropped below zero, after having reached the maximum velocity. The average force was calculated for the subjects in the HG as well as the SG and EE group for every training movement during the training stage and the extended training stage, and were averaged over the non-catch trials in subsequent cycles of five movements.

Statistics

Baseline directional errors were compared by using an ANOVA with Group as between-subject factor. We tested whether the directional errors in the catch trails decreased in time and whether the groups differed in the amount of adaptation by using a repeated measures ANOVA with Group as between subject factor and Time (the repeated measure of the directional errors in the subsequent catch blocks) as within subject factor. A similar repeated measures ANOVA was used to assess differences in generalization by using the generalization catch blocks for the within subject factor Time. We performed a repeated measures ANOVA with group as between subject factor and the direction errors in catch block 6 and generalization catch block 1 as repeated measures to assess if the directional errors to the generalization targets deviated from the errors in the trained directions. Differences in after effects were assessed by using an ANOVA with Group as between-subject factor. For all significant main effects, post hoc tests (with Bonferroni adjustments for multiple comparisons) were performed to deduce which groups differed significantly from each other. To assess whether the interaction forces decreased significantly during training for the HG, SG and EE group, we performed a paired t-test for each separate group with the interaction forces in the first and last cycle as input. The level of significance was defined as $p<0.05$.

2.3 RESULTS

At the end of the familiarization stage, subjects of all groups were accustomed to the virtual environment and had learned to reach in the virtual environment (see Fig. 2.4). Last movement cycles were used as baseline movements. Baseline trajectories were straight lines and the baseline directional error did not significantly differ between the different training groups ($p=0.166$).

2.3.1 *Training trajectories*

The effect of the applied forces on the hand path during early (first 25 movements) and late (last 25 movements) training is illustrated in Fig. 2.4 for a representative subject of each group. The group A subjects did not experience any additional forces, so as expected these subjects showed hand paths that were initially directed roughly 30° counter clockwise to the target. During the course of the training the subjects adapted to the visuomotor rotation as evidenced by the approximately straight trajectories during late training. The error enhancing (group EE) and reducing (SG) forces led to larger and smaller curvatures of the initial hand paths, respectively. Also in these groups, the curvatures decreased during training. The aiming movements of group P and HG were forced along the optimal trajectory, resulting in absence of visible directional errors from the first training movement. The HG group had to generate the movement along the trajectory themselves, and consequently could show under and overshoot of the targets, as evidenced by hand paths passing the targets. On the contrary, group P never showed under or overshoot, as these subjects were moved by the robot along the optimal trajectory.

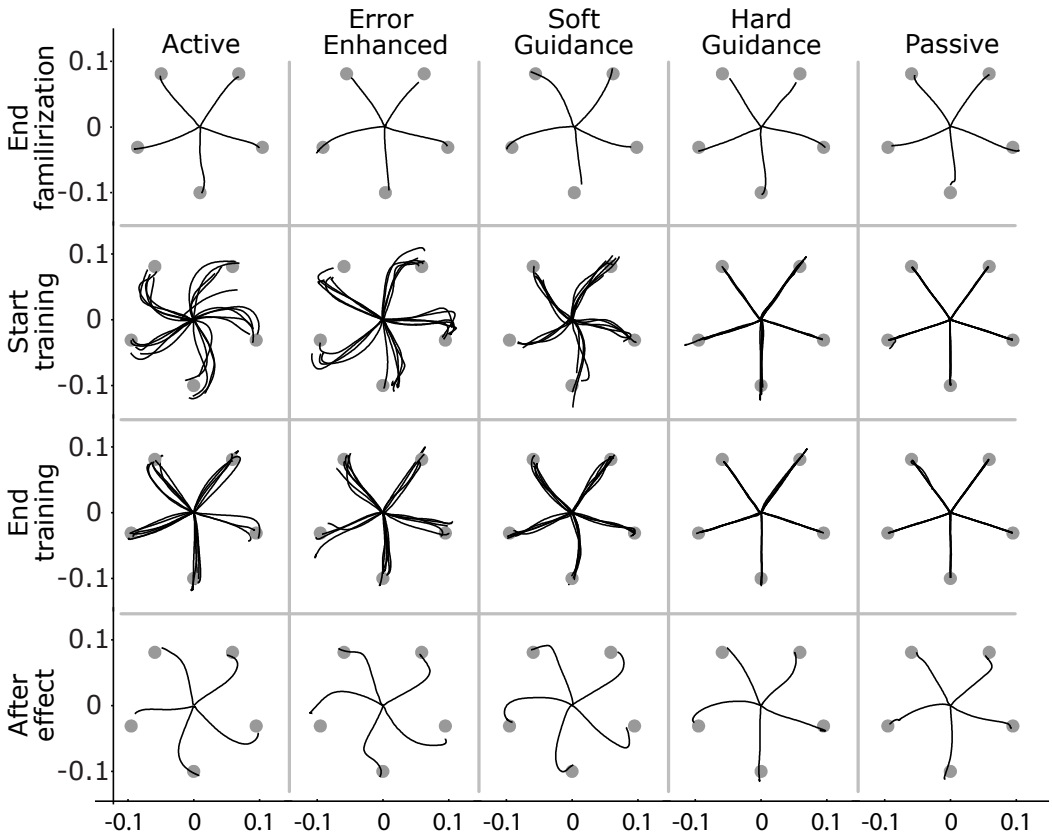

Figure 2.4: Representative hand-paths of a subject from each of the groups are compared to illustrate differences between hand paths during training (while they are exposed to the guiding forces) and wash out. The top row shows baseline hand paths, which are the last five movements during the familiarization stage. Hand paths of the first 25 movements (with the exception of the catch trials) performed during the training stage are shown along the second row, whereas the hand paths of the last 25 movements of the training stage are shown along the third row. The bottom row shows the after effects, which occur during the first cycle of movements during the wash out phase.

2.3.2 *Adaptation*

The presence of the force fields during the training movements made a direct comparison of the directional errors during these movements impossible. Therefore, directional errors made in the catch trials were used to assess the adaptation to the visuomotor rotation. Fig. 2.5 shows the group averages for the different catch blocks. The repeated measures ANOVA showed that there was a significant main effect of Time ($p<0.001$) and Group ($p<0.001$) and a significant interaction effect of Group and Time ($p=0.015$) on the directional errors in the catch blocks. These results indicated that the group as a whole adapted to the visuomotor rotation, that the directional errors in the different groups differed from each other and

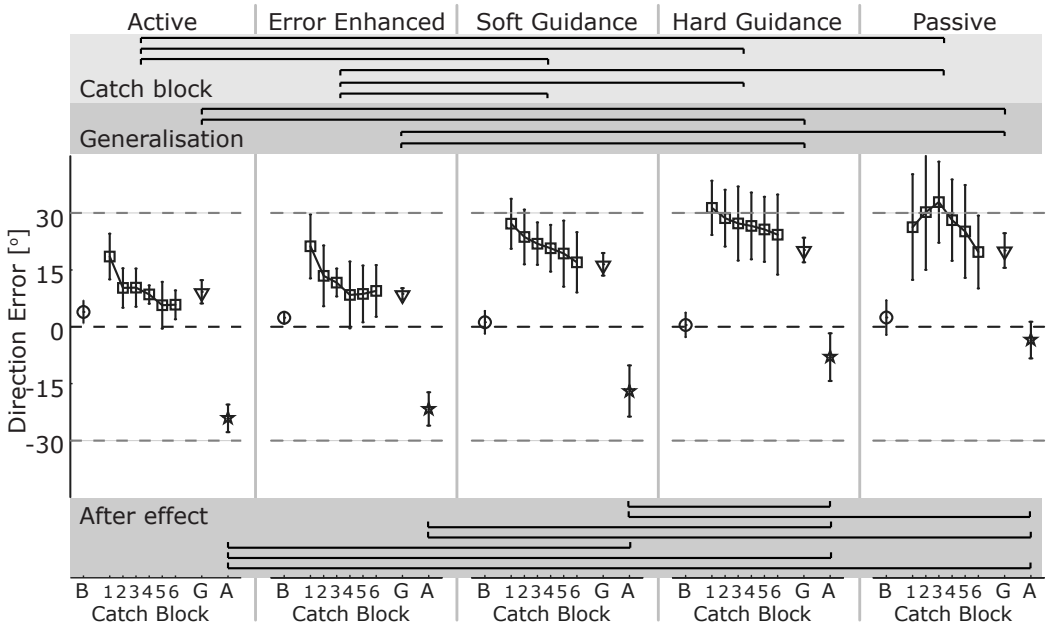

Figure 2.5: Mean directional errors for the different groups and for the different stages. The circles indicate the average directional errors over the last cycle of movement during the baseline. The squares show the average value of the subsequent blocks of catch trials during the training stage. For the generalization catch trials, the average value over all blocks is depicted (triangle) as the different generalization blocks did not differ significantly from each other. The stars show the average directional errors over the first cycle of movements during the wash out, the after effects. The error bars indicate the standard deviation. The horizontal brackets in the gray shading on the top and bottom indicate the significant differences (assessed with repeated measures ANOVA) between the groups in the overall average of the catch blocks, the generalization and after effect.

that the groups did not show similar changes over the different blocks of catch trials. Post hoc comparisons revealed that groups A and EE adapted the most to the visual rotation, expressed by directional errors that were significantly smaller than the errors of the SG ($p=0.002$ and $p=0.024$, respectively), HG ($p<0.001$ for A and EE) and P ($p<0.001$ for A and EE) group. The directional errors in the SG, HG, and P group did not differ significantly from each other.

In Fig. 2.5, it can be seen that all groups, except P, show a gradual decrease of directional errors in the catch blocks, though the rate of change differed among groups, which was also expressed in the significant Group times Time interaction effect. To explore the different rates of adaptation further, we assessed for each combination of groups from which catch block onwards the groups showed a significant difference (see Tab. 2.1). Group A and EE did not differ significantly in the rate of adaptation as for none of the catch blocks a significant difference was found. The adaptation rate for these groups was higher than for groups SG, HG, and P. Group SG showed an intermediate adaptation rate as on one side it took longer before A and EE showed a significantly smaller directional error for SG

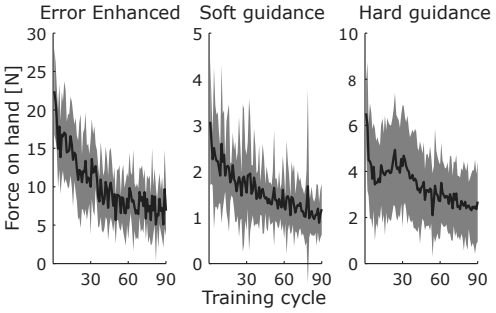

Figure 2.6: Average forces on the hand during the different training cycles for subjects in the Error Enhanced, Soft Guidance and Hard Guidance group. Each point on the curve represents the mean of subjects means, across the five movements within a cycle (excluding the catch trails and generalization trials). The shading around the solid line indicates the standard deviation across the subjects. The first 60 training cycles are part of the training stage, whereas the last 30 cycles are part of the extended training stage.

than for the HG and P group, whereas on the other side the SG, HG and P group did not show any lasting significant difference.

In addition to the execution errors during the catch trials, adaptation could also be derived from the average forces on the hand during the training trials. As the exerted forces on the hand were dependent on the deviation from the optimal path, a decrease of the forces would be indicative for adaptation. Fig. 2.6 shows the forces on the hand (averaged across subjects) as a function of the cycle. The average hand forces in group EE were larger as those in SG and HG; this could be mainly attributed to the instable character of the EE force field, in which forces were directed to further increase execution errors. The difference in magnitude between groups SG and HG could be attributed to the larger stiffness used in the latter. The gradual, significant ($p<0.001$) decrease of the forces in group SG and EE confirmed the results of the catch trials that subjects in these groups clearly adapted to the visuomotor rotation. Remarkably, group HG also showed a significant decrease ($p<0.001$) in the forces on the hand, which would point at the presence of adaptation. This adaptation is not likely to be driven by the execution errors, as the haptic channel in the HG prevented the occurrence of large execution errors. The average hand force in the first and last cycle were 6.5 and 2.7 N, which with the used stiffness of 5000 /m is equivalent to deviations of the optimal path of 1.3 mm and 0.54 mm, respectively.

2.3.3 *Generalization*

By using generalization catch trials we assessed how well subjects were able to use the learned visuomotor rotation in reaching to targets which were positioned exactly in between each pair of adjacent training targets. All groups performed equally well on reaching to the training targets as to the generalization targets, as there was neither a significant main effect of the repeated measure nor an

	A	EE	SG	HG
P	C2	C2	-	-
HG	C1	C2	-	
SG	C2	C3		
EE	-			

Table 2.1: Rate of adaptation. Number of catch block from which on the directional error of the group indicated on the top was significantly ($p<0.05$) smaller than the group indicated on the left side. A smaller directional error is an indication for a faster adaptation to the visuomotor rotation. A - indicates that there was no statistical significance between these groups for any of the catch blocks.

interaction effect. Therefore, it can be expected that the differences between groups found in the generalization catch blocks are similar to those of the catch blocks. A second repeated measures ANOVA (with the six generalization catch blocks as repeated measure) confirmed these expectations. There was a main effect of group ($p=0.001$) and post hoc tests showed directional errors for group A and EE were significantly smaller than HG ($p=0.023$ and $p=0.014$) and P ($p=0.027$ and $p=0.016$), and directional errors of SG, HG and P did not significantly differ from each other (see horizontal brackets in Fig. 2.5). Groups A and EE did not differ significantly from SG during generalization. Apart of these group effects, there was no main effect of Time or a Group times Time interaction effect. The absence of these effects indicated that none of the groups significantly increased their ability to reach to the alternative directions during the extended training stage.

2.3.4 *After effects*

The amount of adaptation in the preceding training stages was assessed by determining the after effects for the different groups when the visual rotation and any of the present force fields were turned off during the washout stage. The bottom row of graphs of Fig. 2.4 shows the hand paths of the first five movements for a representative subject of each group. Group A and EE showed clear after affects as their hand paths could be regarded as mirrored trajectories of those shown during initial training, as if they were learning a 30° clockwise rotation. The hand paths also show a late "hook" back towards the end of the motion, which are likely the result of feedback mechanisms. For group SG, the hand paths also showed a clear after effect and a "hook" back, though the effects were smaller. The hand paths of groups HG and P also showed slight clockwise curvature in some of the reaching directions.

The after effects were quantified by averaging the directional errors during the first five reaching movements in the wash out stage (see Fig. 2.5 for group averages). An after effect occurred when the directional errors during initial washout differed from the directional errors during baseline. We performed a repeated measures ANOVA with Group as between subject factor and baseline and average washout score as repeated measures to assess which groups showed an after effect. The test showed a significant Time ($p<0.001$) and Time times Group ($p<0.001$) effect, indicating that directional errors during washout were significantly different from directional errors during baseline and that this difference was not equally large for all groups. Yet, post hoc comparisons turned out that for all groups this difference was significant (P: $p=0.001$, other groups: $p<0.001$), and as a consequence all groups showed after effects.

To compare the magnitude of the after effects between groups, a one-way ANOVA was conducted. The ANOVA showed that there was a main effect of Group ($p<0.001$). The post hoc tests mainly confirmed the previously described differences in adaptation between the groups based on the catch trials. The effect between groups A, EE, P and HG were similar: groups A and EE ($p=1.00$) and groups P and HG ($p=0.643$) did not differ significantly from each other, whereas group A and group EE showed significantly larger after effects than groups P ($p<0.001$ for A and EE) and HG ($p<0.001$ for A and EE). The main deviation with the adaptation results from the catch trials lies in the comparisons between group SG and the other groups. The intermediate status of group SG between groups A and EE on one side and groups P and HG was now also supported by significant

differences and not merely from the absence of differences with groups on either of the sides. The after effect of SG was significantly larger than the after effect of the HG ($p=0.005$) and P($p<0.001$) group and was smaller compared to group A ($p=0.039$) and EE group ($p=0.528$), though the last effect was not significant.

2.4 DISCUSSION

In this study, we investigated the effect of providing haptic guidance during adaptation to a visuomotor rotation. The amount and direction of the provided guidance was manipulated through the use of force fields that differed in their dependency on the magnitude of the execution errors. Our data seem to provide support for the hypothesis that both the control effort and execution errors can be used for kinematical adaptation.

2.4.1 *Execution errors*

The hypothesis that learning rate decreases when execution errors are reduced by haptic guidance was supported by the found differences in the amount of adaptation and after effect between A group and the SG and HG groups. The hypothesis that learning rate increases by magnifying the execution error with haptic feedback could not be confirmed since significant differences were not found between the A and EE group. The hypothesis that in SG and HG condition the kinematical adaptation would be complete could not be confirmed nor refuted since although at the end of training the directional error in the catch trials were significant larger than for the A and EE groups this error still seemed to become smaller as training time progressed.

When the execution errors were enlarged by using error enhancing forces, the larger execution errors did not seem to lead to a faster or a larger adaptation as we hypothesized based on previous work [49, 229, 151]. There are two possible explanations for this absence of increased adaptation (rate). First, our assessment of adaptation might not have been sensitive for subtle changes in the rate of adaptation. We used catch trials every tenth movement to monitor adaptation and averaged the directional error of five subsequent catch trials. Consequently, the first data point during exposure reflected the average performance over the first 50 movements (10 cycles). Previous studies [106, 25] have shown that during the first 10 cycles adaptation occurs at its highest rate. To have a closer look at these cycles we omitted the averaging and compared the directional errors in the first 5 catch trials between the A and EE group by using repeated measures ANOVA. This analysis showed that the directional errors did not differ between the groups on any of the catch trials, further confirming that adaptation occurred at an equal rate for these groups.

Second, the error-enhanced forces might have changed the nature of the task. As the forces increased the reaching error, they made the task inherent unstable. Burdet and colleagues [21, 58] demonstrated that executing arm movements in an unstable dynamic environment resulted in an increase of the impedance in the direction of the instability. Therefore, subjects that attended the EE training program might have adapted their impedance during reaching, in addition to the adaptations in the pointing direction. The adaptations in impedance might have slowed down the adaptation to the visuomotor rotation per se. The negative

stiffness we used (-500 N/m) was even more unstable than the force field used by Burdet and colleagues (-300 N/m), so it is very likely that shaping of arm impedance did occur in the EH group.

Wei and colleagues [229] implemented error augmentation during learning of a visuomotor rotation by providing visual feedback in which the deviations from the optimal straight trajectory were amplified with a gain of two. They showed that a group of subjects receiving visual error augmentation during learning had a more than twice as large learning rate than a control group, which implies that magnification of execution errors without disturbing forces does have a positive effect on adaptation.

2.4.2 *Control effort*

For the HG group the execution errors were restrained to practically zero. This resulted in an absence of a significant adaptation in the catch trials, though the directional errors during the catch trials showed a slight gradual decrease. As the HG group showed a small but significant after effect, this slight decrease expresses a kinematical adaptation occurring at a very slow rate. As execution errors during training could not explain this adaptation, a different process drove this adaptation.

For the HG, SG and EE group a strategy minimizing the control effort as reflected by the reduction of interaction forces would have resulted in adaptation. These interaction forces indeed showed a small but gradual decrease during the course of training, showing that subjects little by little adapted their reaching direction, pushing less into the haptic wall and thus decreased the control effort even in the HG group. However, for the HG the adaptation of interaction forces group in the training phase occurred at a much slower rate than the reduction of execution errors in the A group.

This was the first study to show that minimization of control can also contribute to kinematical adaptation in a visuomotor task but at much slower rate than minimization of execution errors. This result is in agreement with studies that found that minimization of control effort plays a role in kinetic adaptation to novel dynamic environments, but is less effective than minimization of execution errors [182, 51].

2.4.3 *Possible other mechanisms underlying adaptation*

Our prediction that kinematical adaptation would be absent in the P condition was not in accordance with the significant after effect we found for the P condition. Neither minimizing execution errors nor minimizing control effort can explain the small amount of adaptation we found in the P group. This implies that another mechanism underlies this adaptation. Candidate mechanisms are based on resolving a conflict between or within the different sensory modalities.

The rotation of the visual feedback resulted in a conflict between the proprioceptively and visually perceived hand position. This mismatch could in theory be used to drive adaptation [6]. However, a major role of this mechanism is not likely as the magnitude of the inter-sensory discrepancy was equal for all groups (including the P group), whereas the groups showed different rates and levels of adaptation. Previous studies also provided support for the notion that this

mechanism could at best play a minor role. Jones and colleagues [96] showed that the muscle spindle activity was suppressed during visuomotor adaptation and therefore could not be used optimally. In addition, degrading of proprioceptive information by applying tendon vibration hardly affected the adaptation to a visual distortion [156]. Nevertheless, even when this inter-sensory discrepancy only plays a minor it could explain the small after effects for the P as well as the HG group.

Another possible driving force of adaptation is the mismatch between the proprioceptive feedback and the expected proprioceptive feedback, which is calculated based on the efference copy. This mismatch occurs when the force fields considerably influence the intended movement direction, as is the case for the HG group. However also for the P group, this mismatch can occur. When the subjects in this group actively plan their movement on appearance of the targets, an efference copy can be generated and the accompanying expected proprioception can be calculated. The mismatch between actual and expected proprioceptive information is generally believed to underlie adaptation to a new dynamic force field [210, 156]. In that case motor commands are adjusted such that the actual proprioception will gradually change towards the expected proprioception of a straight movement. However, in our study, this process would not be efficient, as the enforced actual proprioceptive feedback is the desired feedback. And consequently adaptation based on getting the actual feedback towards the expected feedback would reinforce moving in the baseline directions.

Another possibility is that subjects in the P group used a cognitive strategy during training. This could explain the large variation in the response in the catch trials of the subjects in the P as some of these subjects might have been aware of the rotation and used a cognitive strategy during catch trials, whereas others did not. The use of cognitive strategies can explain the large variation, however it is not likely that it can explain the small after effect. Recently, [130] studied the use of an explicit strategy in learning to adapt to a visuomotor rotation. The cognitive strategy resulted in an immediate increase of the performance. However, over time the directional errors increased again, which could be regarded as evidence for the implicit learning processes overriding the explicit strategy.

In short, the inter-sensory discrepancy could have been responsible for the slow adaptation in the P and HG group, whereas it is not likely that the proprioceptive intra-sensory discrepancy resulted in any adaptation. Although in the previous section we argued that the decrease of the forces in the HG group could be regarded as evidence in support for the minimization of effort in adaptation. This decrease could in fact also be a secondary effect of resolving the inter-sensory mismatch. Based on the results of this study we cannot discern whether minimizing the control effort and/or the inter-sensory discrepancy drives the small adaptation seen in HG.

2.4.4 *Generalization*

For all groups the kinematical adaptation generalized well to other reaching directions than those trained. The generalization catch trials showed that the direction error during reaching to untrained directions were not statistically significant from reaching to trained directions. So by only learning five directions, the subjects were able to interpolate the locally learned directions, to the intermediate directions without significant degradation of the performance. The difference in performance

on the generalization catch trials between the groups could be explained by the differences in performance on the catch trials. Therefore, it can be concluded that the difference between the groups in nature and extent of the error signals, only affected generalization through the amount of adaptation and did not affect generalization in a different way for example by inducing more locally learned directions.

2.4.5 *Limitations of study*

In this study we assumed that interaction forces are indicative for control effort. Control effort can be defined on various levels, like on joint torque, muscle tension or metabolic energy consumption level. In realistic musculo-skeletal models an energy-related cost function appeared to be a better measure for muscle energy consumption than muscle stress cost functions and led to more realistic predictions of muscle activation [161]. Such realistic models should be used to verify the assumption that minimization of control effort results in minimization of interaction forces when moving in haptic fields. A more direct measure of control effort should be the measurement of muscle activity of the major arm muscle groups.

In this study we did not investigate the condition in which the robot is positioned controlled as in the P condition but the subject is instructed to minimize the interaction forces instead of being passive. In a follow up study we implemented this condition. The results (not shown) of this study showed that biofeedback of interaction forces did not improve kinematical adaptation (rate) with respect to the P condition. One of our hypotheses was that minimization of control effort and execution errors would end in complete adaptation to a visual distortion. At the end of the training phase the directional errors were larger for the SG and HG than for the A group, but we can not exclude on basis of this study the possibility that these differences with the A group will disappear when training time will be increased. It would be interesting to investigate whether differences in the amount of adaptation between these groups will disappear when training time increased.

2.4.6 *Implications for motor relearning in neurological rehabilitation*

Robotic devices are increasingly popular to provide guiding forces, similar to the ones used in this study, to support the impaired movements during training of stroke patients [80]. The use of robotic devices has been promoted from the notion that relearning the control of movements in stroke patients is akin to motor learning [83, 103]. Systematic overviews of clinical effect studies have shown that the effect of training in stroke patients, like motor learning, is task specific and is largely depended on the intensity [109, 222]. These results are in concordance with studies showing that possibly similar neural correlates [227] underlie recovery [228] and motor learning [79]. The exact nature of neural plasticity is not yet known, yet it seems that repetitive time correlated motor and sensory stimulation of brain regions is required.

Different algorithms have been implemented to calculate the guiding forces to facilitate movements during training, including algorithms similar to 'soft guidance' [2], 'hard guidance' [100] and 'passive' [77, 124]. Based on the results of our study, we would suggest that for optimal relearning, patients can best

initiate and generate the movements themselves and in doing so are free to make execution errors. Still, guiding forces should be used to keep the execution errors of growing too large. Furthermore, the results of group SG in our study showed that subjects relied on the guiding forces in restraining the execution errors which slowed down further adaptation. Therefore, to prevent reliance on guiding forces, we suggest that the amount of support should be progressively lowered in the course of rehabilitation when patient increase their performance [24, 50]. It should also be minimized to stop the patient from reducing his effort and relying on the adaptive support of the robot [231], as they tend to do. In this light, an distinction should be made between assistance which enable movement, like gravity support, and which enhances it, for instance by completing movements [152]. With the first, the patient still has to complete the movement, but the second directly interferes with the task objectives of the patients, allowing the robot to take over.

Most effect studies of robot-aided training concentrated on comparing robotic therapy to conventional therapies [225, 122, 162] and although the different algorithms mostly showed favorable effects, none of them showed superior effects over the others. However, one study did [54], showing results in agreement with our suggestions. It used an algorithm that adapted the amount of assisting forces during the course of rehabilitation to the motor abilities of the patients. Patients trained with this performance-based progressive therapy showed larger decreases of impairments compared to stroke patients whose assisting forces were not adapted [83].

2.4.7 *Conclusions*

We conclude that applying guidance does not have a positive effect on adaptation to a visuomotor rotation. When guiding resulted in a decrease of the execution errors, the applied assistance cannot substitute for this decrease in driving adaptation. Restraining of the execution errors during either active of passive movements showed that minimization of muscular effort or the mismatch between visual and proprioceptive feedback could also be responsible for adaptation, however at a much lower rate. The less efficient use of muscular effort compared to execution errors, is in accordance with the minor role of minimizing muscular effort in adaptation to a new dynamic environment.

Part II

WEIGHT SUPPORT SYSTEMS

3

ANALYSIS OF WEIGHT-SUPPORT MECHANISMS IN UPPER-EXTREMITY REHABILITATION DEVICES

ABSTRACT In most upper-extremity rehabilitation devices, the arm is supported against gravity. This weight support assists the patient in making more meaningful movements earlier in the rehabilitation process. For devices, it reduces actuator strains and limits mechanical stresses. Weight support is often provided by separate mechanisms, indicating its importance. Current rehabilitation devices can be classified as endpoint manipulators, exoskeletons, and cable suspensions. The goal of this report is to evaluate their performance for providing weight support, based on the ease of use, construction and maintenance, best application per mechanism, and features like scalable compensation, range of motion and interaction impedance. The force-application and force-generation mechanisms are covered separately. In conclusion, the best possible solution of implementing weight support will depend on the primary design, but careful considerations at the start of the design process will lead to better design choices.

3.1 INTRODUCTION

Patient-friendly robots are used as diagnostic and therapeutic aids in upper-extremities rehabilitation, and almost none look alike. Through physical manipulation of the arm and assisted by virtual environments, innovative interaction schemes are explored in search of the best possible therapy. Overall, robot assisted therapy is considered to be as good or better than conventional therapy [219, 157, 162, 112].

Whether intended or not, in most devices the arm is supported against gravity. This weight support assists patients in making movements. For healthy humans, arm movements require two components of muscle activition; one 'phasic', steering the movement, the other, 'tonic', counteracting gravity [57, 163]. By reducing the latter without distorting the former [92], patients can perform more and more meaningful exercises earlier in the rehabilitation process. When applied as a stand-alone therapeutic means rather than being used as an addition to robot manipulation, dedicated devices like the T-WREX [180] show weight support to be effective in stroke rehabilitation [46, 85], or have similar results compared to full robot-mediated training [4]. For these studies, weight support systems were used which allow the amount of support to be scaled based on the need of the patient: full support in the early stages, reduced support as recovery progresses.

For assistive rehabilitation devices, weight support may reduce the power requirements of the actuators and can limit the stresses in the mechanical components. The support is either incorporated directly in the primary design of the device or provided by a completely separate mechanism (see Tab. 3.1). For instance, some exoskeletons use cable suspensions for the weight support [143, 202];

Submitted: IEEE Transactions on Neural Systems and Rehabilitation Engineering (AHA Stienen, EEG Hekman, FCT van der Helm, and H van der Kooij).

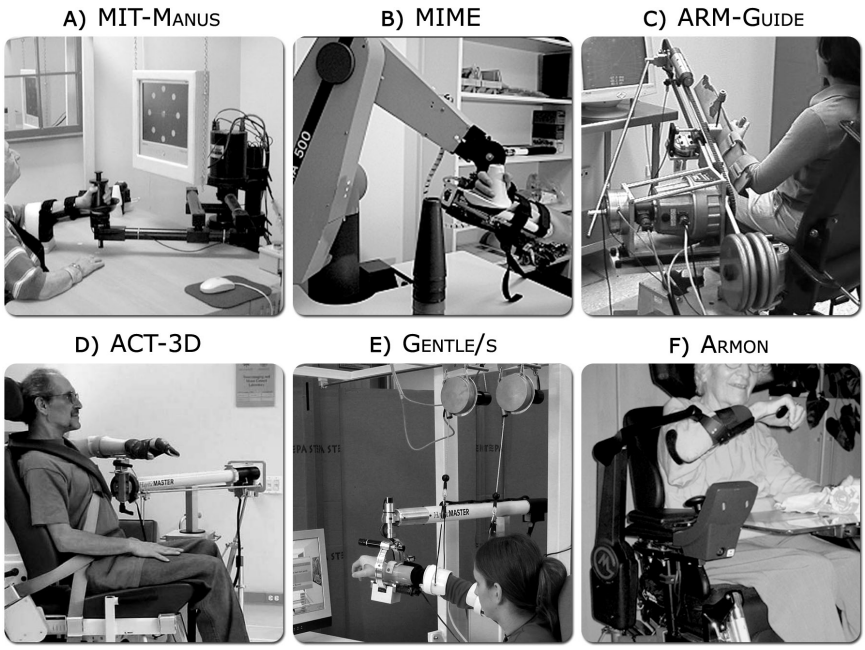

Figure 3.1: With endpoint manipulators, patients are connected to a single endpoint. They often hold a handle (MIT-Manus), or are strapped at the wrist (Gentle/s) or forearm (ACT-3D). Three positional degrees of freedom (DOFs) of an endpoint are not enough to influence the four DOFs of the shoulder and elbow. Therefore, most endpoint manipulators add one or more actuated (MIME), weight supported (Gentle/s), or fixed rotational DOFs. The additional DOF is often a stiff cast on which the forearm lays. The Gentle/s and the ACT-3D are build around a modified HapticMaster; a three-DOF haptic robot from MOOG-FCS Robotics. The Armon has no additional DOFs but support the arm exactly at the center of mass. It does not manipulate the arm in other ways.

others use powerful actuators in a mechatronic control loop [27]. Overall, weight-supporting forces can be generated and applied in many different ways, with some mechanisms more suitable than others.

The goal of this report is to evaluate the performance of different mechanisms for providing weight support, based on the ease of use, construction and maintenance, best application per mechanism, and features like scalable compensation, range of motion and interaction impedance.

3.2 ANALYSIS

3.2.1 *Classification of the primary design*

Although this report focuses on weight support systems, we start by grouping current rehabilitation robots based on their primary design: endpoint manipulators, exoskeletons, and cable suspensions (see Tab 3.1). Endpoint manipulators have a single connection to the hand, wrist or forearm. Often patients hold onto a handle

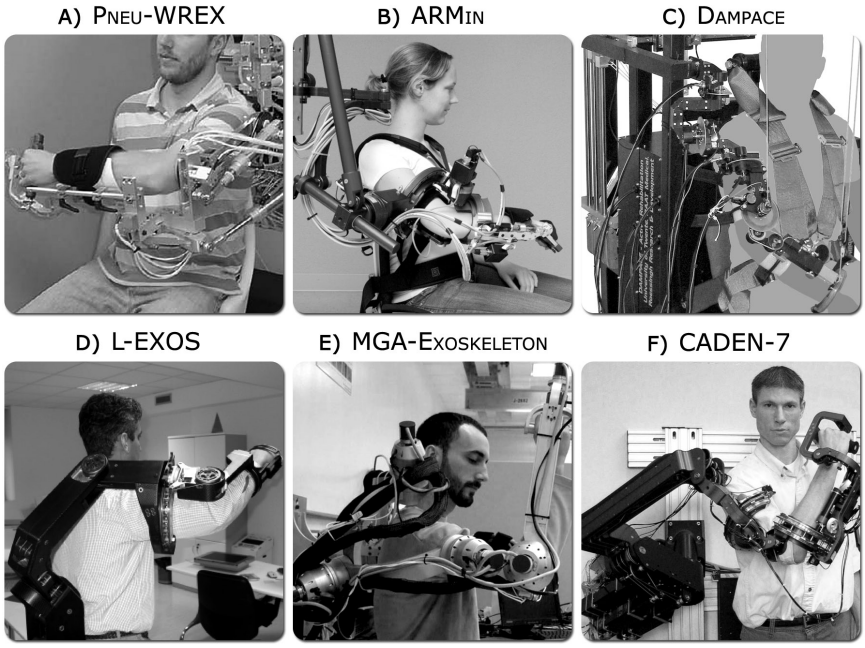

Figure 3.2: Exoskeletons are external skeletons on top of the arm, directly manipulating the shoulder and elbow joints. To prevent joint misalignments, the Pneu-WREX allows vertical translation of the shoulder, the ARMin and the MGA-Exoskeleton horizontal translation, and the Dampace translations in any direction. The L-EXOS and the CADEN-7 have a fix shoulder rotation center, forcing the whole body to deal with any misalignments. Unlike other exoskeletons, the Pneu-WREX does not follow axial rotations of the upper arm; its build in weight-support mechanism require an upright orientation. This has several implications for the controlled, free and fixed DOFs (see Tab. 3.1). The Dampace uses the same ideal-spring mechanism as the Pneu-WREX for weight-support, but applies the forces via an overhead cabling system to the elbow and wrist. The ARMin I has a similar cabling system, but uses a single counterweight to reduce the load on the electric motors.

while making movements in a virtual environment. Exoskeletons are external skeletons placed parallel to the arm and are generally powered by actuators on each of the joints. They control (a subset of) the joints of the shoulder, elbow, and wrist directly, at the cost of more complex mechanics. Cable suspensions link one or more cables to the arm, increasing both control options and complexity with every additional cable linkage. With overhanging cables and counterweights, these cable suspensions have been used by rehabilitation hospitals for decades. They are simplest to realize but offer the least amount of control on the motions of the arm.

Endpoint manipulators

Endpoint manipulators (see Fig. 3.1) have at most three positional degrees of freedom (DOFs) at the endpoint. This is not enough to control the four rotational DOFs of the shoulder and elbow. Therefore, one or more rotational DOFs are added

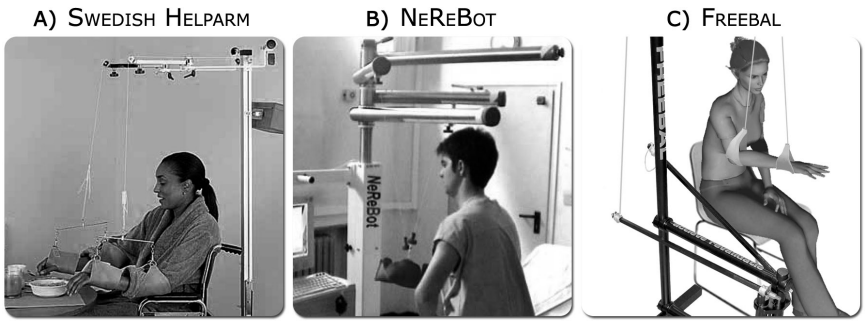

Figure 3.3: Cable devices are often dedicated weight support systems. Classic devices like the Swedish Helparm use counterweights or directly connected springs. By controlling the cable lengths and the overhanging system to guide the cables, the NeReBot is capable of manipulating the shoulder and elbow joints in any direction. The Freebal uses ideal spring mechanisms, with which the support force does not depend on the vertical deflection like with springs mounted directly inline.

at the endpoint, either actuated (MIME), cable supported (Gentle/s), or fixed (most others). These rotational DOFs need to bypass the wrist and be connected to the forearm to support the elbow, but often also fixe the pro-/supination angle of the forearm and most wrist rotations. The forearm is often supported by a stiff, vertically hinged cast or splint. A minimum of three translational and one rotational DOF fully define the shoulder and elbow rotations if the shoulder position is known. In general, active manipulation of the hand requires knowledge on the limb lengths and shoulder and trunk position to ensure comfort and safety during use.

Exoskeletons

External skeletons (see Fig. 3.2) positioned parallel to the arm control the shoulder and elbow directly in joint space, making precise measurements and manipulations possible. The main disadvantage is the need to align the exoskeleton axes with the anatomical axes, as misaligned axes can cause painful interaction forces [202]. Aligning axes can take from several to fifteen minutes, cutting into the time available for the therapy session. To overcome the alignment requirements, an exoskeleton may need additional mechanics [186, 202, 142]. Although the elbow is a relatively simple one-DOF joint, the shoulder isn't. It has at least five DOFs; three rotational DOFs from the spherical joint, and two translational in the sagittal plane, representing the shoulder girdle. The vertical translation is also coupled to the humerus elevation rotation [117, 233]. Some exoskeletons, like the ARMin and the MGA-Exoskeleton, therefore allow vertical and/or horizontal translations in their shoulder joint, or couple it to specific shoulder rotations. Others have to leave the trunk free to align the human shoulder axes to the robot. The mechanisms in the Dampace solve both the aligning and translation problem by allowing the shoulder joint to translate freely in three directions, with the device applying torques, not single forces, to the limbs [202].

Table 3.1: Overview of current rehabilitation robots.

I ENDPOINT MANIPULATORS		DOFS[a] AC	FX	FR	PRIMARY ACTUATORS	ADDITIONAL WEIGHT SUPPORT MECHANISMS
A) MIT-Manus	[81]	2	2	0	electric motors	vertical restriction
B) MIME	[22]	4	0	0	electric motors	-
C) ARM-Guide	[169]	3[b]	1	0	electric motors	-
D) ACT-3D	[206]	3	1	0	electric motors	-
E) Gentle/s	[120]	3	0	1[c]	electric motors	cables & springs
F) Armon	[75]	0	0	4[d]	-	spring mechanisms
II EXOSKELETONS						
A) Pneu-WREX[e,g]	[179]	3	1	0	pneumatic cylinders	spring mechanism
B) ARMin[e,f]	[143]	4	0	0	electric motors	cable & mass
C) Dampace[e,f,i]	[202]	4	0	0	hydraulic brakes	cables & spring mech.
D) L-EXOS	[61]	4	0	0	cables & elec. motors	-
E) MGA-Exoskeleton[f]	[27]	4	0	0	electric motors	-
F) CADEN-7	[154]	4	0	0	cables & elec. motors	-
III CABLE SUSPENSIONS						
A) Swedish Helparm	[h]	0	0	4	-	cables & mass | spring
B) NeReBot	[127]	4	0	0	cables & elec. motors	-
C) Freebal[j]	[201]	0	0	4	-	cables & spring mech.

[a] Degrees of freedom (DOFs). AC means actively controlled, FX fixed, and FR free. For endpoint manipulators, the DOFs are given as three translational DOFs at the endpoint, and one rotational for the orientation of the forearm; these four DOFs fully define the possible rotations of the shoulder and elbow when the shoulder is fixed against translation. For the exoskeletons and the cable suspensions, the DOFs are the three rotation DOFs of the shoulder, and one for the elbow.
[b] Two of the three actively controlled DOFs are slow due to the device inertia. When operated, the ARM-Guide is mostly used as a one DOF manipulator, but can be pointed in any direction.
[c] Although the last DOF is left free, it is supported by a separate gravity compensation mechanism.
[d] Armon is a dedicated gravity compensation devices, not capable of other active manipulation.
[e] Allows horizontal (forward) translation of the shoulder (for ARMin I: free, for III: forced).
[f] Allows vertical translation of the shoulder (for ARMin I: free, for II & III: forced).
[g] The DOFs for the passive T-WREX [180] (a Pneu-WREX without actuators) are [0 0 4].
[h] Kinsman Enterprises, Inc.
[j] Also see Chap. 4
[i] Also see Chap. 8

Cable suspensions

Cable suspensions (see Fig. 3.3) are often designed specifically for weight support. Single connections to the forearm from a sufficiently high mount point offer a large range of motion with simple mechanics. Similar to endpoint manipulators, multiple connections to the arm are needed to prevent a dangling elbow. By controlling multiple cables interacting with the arm, robots like the NeReBot are capable of manipulating the shoulder and elbow joints. In general, to control a single point in N DOFs, $N + 1$ cables are needed, although sometimes gravity is used as a virtual vertical cable. The lack of stiffness and stability in the cables and control make it a less accurate manipulator compared to endpoint manipulators or exoskeletons.

3.2.2 *Components of weight support systems*

The initial distinction between weight-support systems is between those restricting vertical displacement and those supporting the arm with constant vertical forces (see Fig. 3.4). Planar devices like the MIT-Manus support the weight of the arm by restricting all vertical displacement, which feels like forced sliding of the arm on a smooth horizontal surface. Although this fully supports an arm at rest, the amount of compensation is always equal to the normal force between the arm and the surface and cannot be scaled or externally controlled. Even when such planar mechanisms allow some upward displacements, patients need to fully support their arm themselves before any lift-off is achieved. Secondly, patients can actively press their arm downwards, potentially helping their achievements but hindering relearning normal movement control. For example, using a table-like support artificially increases the range of motion of stroke patients over a fully force-supported arm [206]. This rewards patients for the erroneous motor pattern of pushing down while wanting to achieve horizontal movements. As the support by restricted displacement is directly linked to the planar design and mechanically easy to realize, it will not be discussed further.

With the other endpoint manipulators and all the exoskeletons and cable suspensions in this paper, the patient is free to move in any directions. By definition, weight support for the arm in these devices has to be realized by applying essentially invariant, vertical forces. In the next sections, the force-based weight-support systems are evaluated separately for the mechanisms used to transfer the supporting forces to the arm, and the mechanisms to generate the forces.

Force application mechanisms

The choice of application mechanisms to transfer the supporting forces to the arm influences the variability of gravity compensation force in the workspace, the achievable range of motion, the movement impedance (mostly inertia and friction), the position and angle measurements, the ease of use, and finally, the ease of construction (including price and maintenance). In Tab. 3.2, each family of mechanisms is represented by a generic member to be able to compare relative strengths and weaknesses. Although within each family individual improvements can be made, these come at a cost. For instance, an exoskeleton can be made simpler in its construction than its generic model, but this would probably negatively influence the joint control (measurements) or ease of use. And an individual cable suspension can still be made even less complex than the simplest exoskeleton.

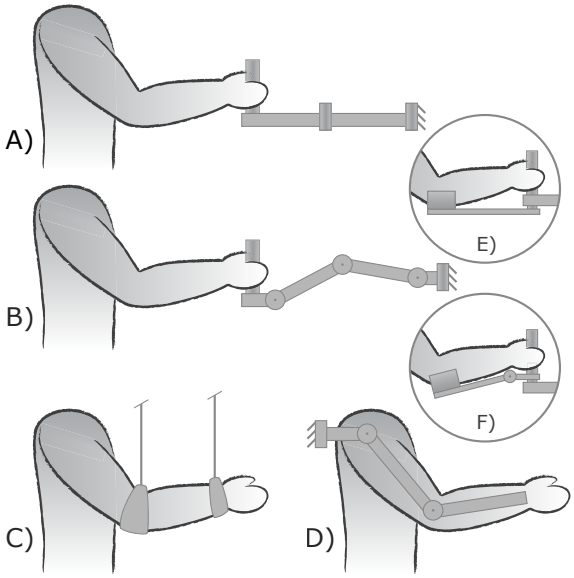

Figure 3.4: Application of weight support via: (A) restricted vertical displacement, (B-D) applied supportive forces. The first resembles sliding over a smooth flat surface, whereas with the others the arm moves freely in 3D. The weight support forces may be applied via: (B) an endpoint support at the hand, (C) one or more cable suspensions, (D) a full or partial arm exoskeleton. Endpoint devices (A,B) often include a stiff forearm cast, either (E) vertically hinged to the endpoint, or (F) also including a horizontal hinge, allowing control over the four DOFs of the shoulder and elbow. Examples include the MIT-Manus (A,E), MIME (B,F), ACT-3D (B,E), Freebal (C), and the ARMin (D).

In the table, the exoskeleton does not score high marks as a dedicated weight support system. The main problem for the exoskeleton is the need of mechanics for all joint rotations, and the alignment of the exoskeleton joints to the anatomical ones. As explained above, the misalignment of axes and the additional two translational DOFs in the human shoulder require additional mechanics, making the exoskeleton even more complex to construct and use. As an application mechanism, it has a relatively high impedance due to inertia, and a limited range of motion. Control of supporting forces depends on the joint orientation. Exoskeletons not directly linked to the limb movements (T-WREX) can use better force generating mechanisms with a larger range of movement.

The cable suspensions are mechanically the simplest to construct. They depend on an overhanging cable suspension, which is either fully fixed in space (Freebal, Swedish Helparm) or moves in a horizontal plane with the arm (Dampace, NeReBot). If it is fixed in space, the cable angle will reduce the vertical compensation and introduce unwanted horizontal forces [201]. If it moves with the arm, the

Table 3.2: Relative assessment of force application mechanisms.

	ENDPOINT MANIPULATORS	EXOSKELETONS	CABLE SUSPENSIONS
Constant force	+	+/-	+/-
Range of motion	+	+/-	+
Movement impedance	+/-	-	+
Measurements	+/-	+	-
Ease of use	+	+/-	+
Ease of construction	+/-	-	+

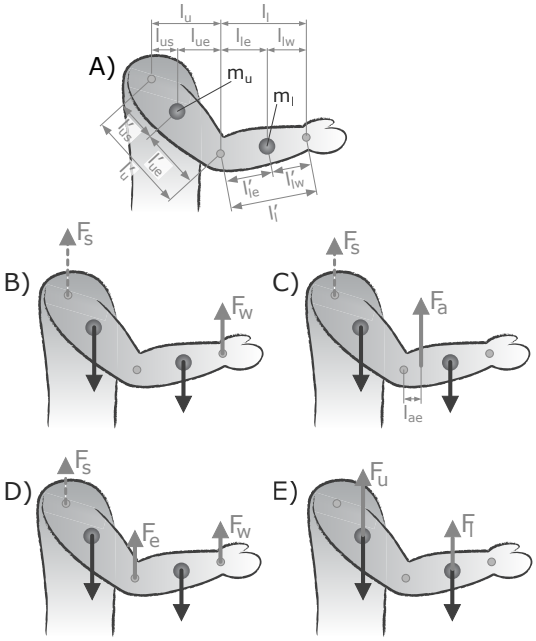

Figure 3.5: Point of force application on the arm. In (A), the masses of lower (m_l) and upper arm (m_u) are given together with the lower (l_l) and upper arm (l_u) lengths. The subscript s, e and w indicate lengths to shoulder, elbow and wrist, and the apostrophe the lengths parallel to the segment. In (B), the force is applied to the wrist only. This results in an unsupported elbow and the highest residual force in the shoulder. In (C), the support force connects at the mass center of the whole arm, resulting in a perfect balance. In (D), the connections to the wrist and at the elbow also fully support the arm, with a further reduced residual shoulder force. In (E), the connections at the mass centers remove any residual shoulder force, but support the arm at soft tissue locations. Examples include the MIME (B), Armon (C), and Freebal (D,E).

dynamics of the movable suspension may interfere with the arm movements. For most cable suspensions, separate measurement systems must be used to acquire the limb orientation.

The endpoint mechanisms are more complex to construct than cable suspensions, but easier than exoskeletons; the movement impedance is somewhere between the two. Having a mechanical system fully independent of the arm makes a constant force and a large range of motion easier to realize. Accurate position and angle measurements require recalculations from manipulator to arm coordinates and assumptions on the positions of trunk and/or shoulder.

Combination of the three application mechanisms have been used before. Many partial exoskeleton consist of endpoint mechanisms connection to a forearm cuff [139], often with reduced arm DOFs (ACT-3D). And the Gentle/s reduces the gravitational pull on their haptic endpoint device by lifting most of the weight of the arm by cable suspensions.

For the cable suspensions and the endpoint mechanics, the points of force application matters for the experienced comfort and the residual forces in the shoulder (see Fig. 3.5). Going from a single application point at the hand or wrist, to one just below the elbow, two at the wrist and elbow, and two at the mass centers, reduces the residual force on the shoulder with each step.

In our experience with the Freebal and Dampace, connecting the cables to the wrist and elbow was most comfortable, and cuffs do not slip from these bony points. Support of the upper arm at the elbow will keep some residual forces in the shoulder, which are beneficial according to the therapists we interviewed.

Force generation mechanisms

Counterweights, springs and actuators can all provide the forces needed for weight support (see Fig. 3.6). The choice of compensation mechanisms influences

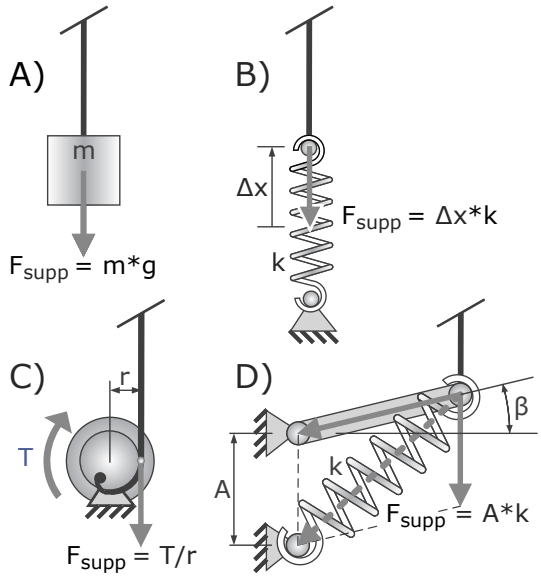

Figure 3.6: Force generation mechanisms resulting in the weight-support force (F_{supp}). Counterweights (A) double the vertical inertia and are difficult to fine tune (with mass m and gravity g). Springs (B) provide forces dependent on the deflection $\triangle x$ times the spring stiffness k. Mechatronics (C), consisting of an electric motor, controller, and force sensor, are complex and expensive, with the performance directly dependent on the achievable bandwidth of the system (with motor torque T and force-arm distance r). Ideal-spring mechanisms (D) require more complex mechanical components, but have low movement inertia, provide almost invariant forces despite the beam deflection angle β, and are easy to adjust by the spring base depth A. Examples include the Swedish Helparm (A,B), ARM-Guide (C), and Pneu-WREX (D).

the variability of the supportive force, the achievable range of motion, movement impedance (felt inertia and friction), scalability of forces, ease of use and ease of construction. In Tab. 3.3, each mechanisms is scored on these properties.

Counterweights (see Fig. 3.6A) are commonly used in weight-support systems (Swedish Helparm, ARMin). Compared to the other solutions, they have a high movement inertia, can be difficult to fine-tune when available weights are limited, and are heavy to handle.

Springs (see Fig. 3.6B) are regularly used as an alternative (Swedish Helparm). When connected directly to an application mechanism, the supportive force is dependent on the amount of spring deflection. This is a major disadvantage which can be partly overcome by using long, slack springs or so-called wound springs (Gentle/s). However, long slack springs require large default deflections and wound springs have significant amounts of friction. Changing the compensation

Table 3.3: Relative assessment of force generation mechanisms.

	WEIGHTS	SPRINGS	MECHA-TRONICS	SPRING MECHS
Constant force	+	-	+/-	+
Range of motion	+	+/-	+	+/-
Movement impedance	-	-	+/-	+
Scalable forces	+/-	+/-	+	+
Ease of use	+/-	+/-	+	+
Ease of construction	+	+	-	+/-

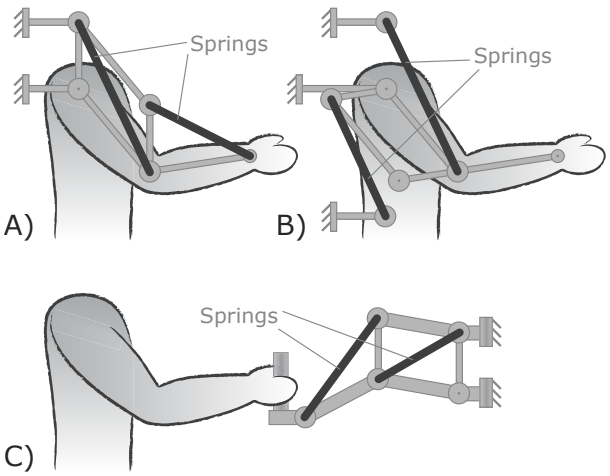

Figure 3.7: Suitable combinations of force application and generation mechanisms. In (A), a double ideal spring mechanism is connected to an exoskeleton with reduced DOFs in the shoulder. In (B), the springs of the ideal spring mechanisms are moved away from the exoskeleton towards the base, allowing full 3D shoulder DOFs with of ball and socket joint. In (C), ideal spring mechanisms are used in the endpoint mechanisms. Examples include the Pneu-WREX (A), the Anthropomorphic Robot Arm [212] (B), and the JAECO Mobile Arm Support (JAECO Orthopedic) (C).

force either requires a change of spring stiffness or a change in default deflection, both of which are not trivial to achieve.

With mechatronics, consisting of actuators, force sensors and a control loop [59] (see Fig. 3.6C), the amount of force can easily adjusted, at the cost of increased complexity in the controller and using complex and expensive electronic components (ARMin, MIME, ACT-3D). Achieving an exact constant-force for faster movement is strongly dependent on the force resolution and noise levels of the actuator and the sensor, and the backdrivability and bandwidth of the entire system.

Ideal-spring mechanisms (see Fig. 3.6D) generate a constant level of support throughout the range of motion. With the ideal-spring mechanisms, the amount of weight support is scaled with either the spring stiffness k or the spring base depth A. The amount of weight support F_{supp} is independent of the beam angle β, as the decomposition of the springs force results in a constant vertical force $F_{supp} = kA$ for all beam angles β. The theoretical ideal springs used in these mechanisms have constant spring stiffness over the entire range, no pretension and zero force at zero deflection. These mechanisms are more complex than counterweights or directly connected springs, but provide a constant vertical force at the end of the beam, independent of the beam angle (Freebal, Dampace, Pneu-WREX, Armon). Although stock springs do not normally satisfy the ideal spring requirements, using a specific amount of pretension based on the spring length, makes them functionally similar. Alternatively, additional mechanics can also be used to satisfy

Table 3.4: Relative assessment of suitable combination of mechanisms.

	WEIGHTS	SPRINGS	MECHA-TRONICS	SPRING MECHS
Endpoint manipulators	-	-	+	+
Exoskeletons	-	-	+	+/-
Cable suspensions	+	+	+	+

the ideal-spring requirements [74]. When the beam length and the distance from the rotation center where the spring connects to the beam are not the same, the ratio of this length and distance also scales the supportive force [74, 201].

Suitable combinations

All force generating mechanisms can be combined with a cable suspensions, and most indeed have been (see Tab. 3.4). For the other two force application mechanisms, the choice of force generation is generally limited to mechatronics and ideal-spring mechanisms. Counterweights or springs would require additional pivoting mechanics not present in these mechanisms. Mechatronics are suitable for both these application mechanisms, as the actuators can be directly mounted on the rotation axes. Ideal-spring mechanisms are best suited for endpoint mechanisms (see Fig. 3.7C), or exoskeletons with reduced DOFs in the shoulder (see Fig. 3.7A). By properly attaching the springs to the base of the mechanism and using ball-and-socket joints at the shoulder, ideal-spring mechanisms can also be used for full four-DOF exoskeletons (see Fig. 3.7B) [212]. Although getting the human arm in the mechanism while maintaining acceptable levels of range of motion is no trivial task.

3.3 DISCUSSION

To facilitate upper-extremity movements, most rehabilitation devices support the arm against gravity. With weight support, patients may do more and more meaningful exercises earlier in the rehabilitation process. For assistive rehabilitation devices, weight support reduces the stresses in the mechanics and loads on the actuators. The weight support is often provided by separate mechanisms, indicating its importance.

There is a fundamental difference between weight support by limiting vertical displacement or applying constant supportive forces which counteract the gravitational pull on the arm. Using constant supportive forces is the most natural way to facilitate arm movements as it allows full freedom of movement and the amount of weight support is scalable to the patients needs.

The weight support systems are divided in the mechanisms to apply the supporting forces to the arm, and mechanisms to generate them. Of the three application mechanisms, the cable suspension type is easiest to implement and has the widest range of potential force generation mechanisms. The other two types, endpoint mechanisms and exoskeleton, are increasingly more complex to develop and use, but they also offer increasingly better control of the arm for other manipulation purposes. For the generation of the supportive forces, they either require complex and expensive mechatronics, or ideal-spring mechanisms. They are especially suitable when combined with other therapeutic interventions as applying resistance torques to joints.

Ideal-spring mechanisms are well suited for providing compensation forces for both exoskeletons and cable suspensions. They introduce little movement inertia to the movement system and can be scaled by changing the spring stiffness, or more easily by changing the spring attachment point. Compared with counterweights, mechatronics or directly connected springs, they have the advantage of low inertia, not needing any external power, force sensors or active controllers and providing constant compensation forces over the entire range of movement. However, the

required construction space may be unavailable in exoskeletons, or the added weights of the springs undesirable. If these exoskeletons already have active actuators and force or position sensors, the gravity compensation can also be provided by the actuators if these are sufficiently powerful. For an average person, mechatronic weight support will increase the constant torque requirement on weight bearing motors by up to 20 Nm, which significantly reduces the motor potential for other goals.

3.3.1 *Conclusions*

In conclusion, the best possible solution of implementing weight support will depend on the primary design, but with the help of this study, the required weight support can either influence the choices made in the primary design, or better combine them. The ideal-spring mechanism generates near perfect weight support forces; constant over a large range with minimal impedance, without using complex and expensive electronic solutions.

4

FREEBAL: DESIGN OF A DEDICATED WEIGHT-SUPPORT SYSTEM FOR UPPER-EXTREMITY REHABILITATION

ABSTRACT Most rehabilitation devices for the upper extremities include a weight-support system. In recent publications, weight support is shown to be effective for stroke rehabilitation. But current devices are often complex, have significant movement inertia, and/or limit the movement range. The goal of this study is to improve on current designs by introducing a novel, dedicated weight-support device, the Freebal. This passive mechanical device uses ideal-spring mechanisms for constant-but-scalable forces to support the arm. It has a large workspace of roughly 1 m^3, low movement impedance, and independent support at the elbow and wrist of up to 5 kg. An explorative cross-sectional study with eight patients shows the Freebal to instantly extend the range of motion of the affected arm. In conclusion, the requirements are met for patients to benefit from therapy with the Freebal, potentially progressing earlier to more motivating, functional training.

4.1 INTRODUCTION

After a stroke, patients with affected motor control of the arm benefit from intensive and task-specific exercises, consisting of active, repetitive movements [109, 8, 56]. According to systematic reviews [219, 157, 162, 112], patient-friendly robot assisted therapy is at least as good as regular therapy for the movements exercised. Robot therapy is shown to improve motor control, although a significant improvement of control does not necessarily result in a higher functional ability when measured on clinical scales. Overall, robots make rehabilitation therapy more challenging for the patients and less labor intensive for the therapists, and they provide the physicians, therapists and scientific community with more objectively gathered data. They have been used as diagnostic and therapeutic aids for a wide range of disabilities and come in various designs [82, 95, 22, 120, 141, 179, 180, 127, 206, 121, 202].

In most rehabilitation robots, multiple therapeutic elements are combined. The therapy is simultaneously made more intensive, more supportive and more motivating for the patients than is possible with regular therapy. More repetitions per session, movement assistance via external actuators and involving and stimulating virtual environments also influences the rehabilitation process. But in most efficacy studies, the effects of the individual elements are not reported. The lumping may explain why the type of robot assisted therapy has so far made little difference in the above systematic reviews. A common element like the increase in intensity is suspected to be more important than the type of rehabilitation therapy used.

Another common element in rehabilitation robots is weight support, which facilitates upper-extremity movements [94]. The MIT-Manus [82] supports the forearm with a stiff, vertically-hinged plateau. The Gentle/s and /g [120, 121] link the wrist to a haptic robot, while the arm is supported by two suspension slings. The ACT-3D [206] uses a 3D haptic robot to support the weight of the arm.

Submitted: ASME Journal of Medical Devices (AHA Stienen, EEG Hekman, GB Prange, MJA Jannink, FCT van der Helm, and H van der Kooij).

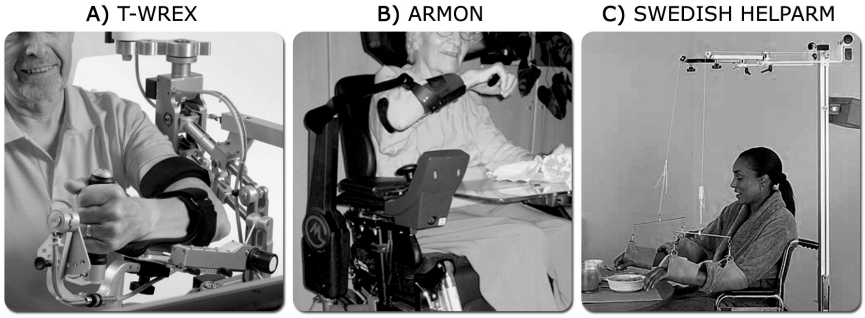

Figure 4.1: Current weight support devices. From left to right, the T-WREX exoskeleton, the Armon wheelchair mounted support, and the classic Swedish Helparm cable suspension.

The ARMin [143] uses both balancing counterweights and computer-controlled support via the actuators in the exoskeleton.

Recent training studies using weight support as a stand-alone therapeutic means show it to be effective in improving motor control [180, 85, 46], or have similar results compared to full robot-mediated training [4]. With the device detailed in this publication, we found muscle activity to decrease during short point-to-point movements with weight support, in cross-sectional experiments with both healthy elderly [163] and stroke patients [92], with the muscles maintaining arm posture against gravity alleviated the most.

Dedicated devices can provide the support needed without having additional robot manipulation schemes (see Fig. 4.1). The first, the T-WREX [180], was used in two of the above training studies. It uses ideal-spring mechanisms for scalable support independent of the vertical deflection (see Fig. 4.3). In this exoskeleton, two of these mechanisms are located parallel to the upper and forearm. The T-WREX may be more complex, costly, and, due to needing to align the human and exoskeleton joints, time consuming than required for conventional therapy, but it does have an integrated gaming interface to increase the motivation of the patient during therapy.

The second dedicated device, the Armon [75], also uses ideal-spring mechanisms. It is a permanent support for attachment to a fixed base like a wheelchair, but cannot scale the support for the lower and upper arm independently as it supports the arm with a single connection at the center of mass. The achievable range of motion with the Armon is limited to the range needed for activities of daily living, mostly directly in front of the user. Therefore, some therapeutic exercises exploring the outer limits of the range of motion of the shoulder and elbow joints of the patient cannot be done with Armon. As a permanent support for a single user, its adjustment controls were not designed to used in rehabilitation therapy by multiple patients in quick succession.

The last group of devices, like the classic Swedish Helparm[1], are still used by many rehabilitation centers. With these, the weight of the arms is supported by an overhanging cable suspension system and slings, and counterbalanced by either masses or springs. Both masses and springs have their disadvantages. Masses double the vertical movement inertia of the arm and are not always easy to handle.

1 Kinsman Enterprises, Inc

Directly connected springs make the amount of weight support strongly dependent on the vertical arm deflection, possibly leading to undesired oscillations.

We deduced we needed a device which would be easy to install and use in rehabilitation training, and which could also be used as a research tool to study the effects of weight support on motor control in patients. In therapy, its most important task is to facilitates movements for more severely affected patients so they can progress earlier to the more motivating, functional training. A simple, mechanical device has obvious advantages in cost, use and maintenance over more complicated mechatronic solutions. It should have scalable and independent support for the upper and forearm with maximum freedom of movement. Minimal impedance is required to not hinder the patients in any way. In use, a therapist should still have full access to feel and steer the arm as needed. Based on these requirements, we created the dedicated weight-support device, the Freebal.

The goal of this paper is to evaluate if the design requirements of scalable and independent weight support, full range of motion, minimal impedance, full access to the limb, and instant enhancement of the range of motion of stroke patients with weight support, are met with the Freebal design. This paper expands on prior conference proceedings [201, 200, 164].

4.2 REQUIREMENTS AND IMPLICATIONS

Current rehabilitation devices can be grouped as endpoint manipulators (for instance, the ACT-3D), exoskeletons (ARMin), and cable suspensions (Swedish Helparm). Endpoint manipulators have a single connection to the hand, wrist or forearm. Often patients hold onto a handle while making planar or 3D movements. Exoskeletons are external skeletons placed over the arm and mostly powered by actuators directly over the joints. They directly control (a subset of) the joints of the shoulder, elbow, and wrist. Cable suspensions use overhanging cables to link the arm to a mechanism providing the weight support; often counterweights or directly connected springs.

All three types of devices could potentially apply the needed supporting forces to the arm. To achieve the requirements of scalable and independent support with maximum freedom of movement in three dimensions and minimal impedance, while allowing the therapist access to the limb, some designs are more useful than others. In this section, the requirements and implications for each type of design are discussed.

4.2.1 *Scalable weight support*

Ideally, the amount of weight support is independent of joint angles, stays invariant over the entire workspace, but can be adjusted smoothly from no to full support of the limb. Early in the rehabilitation process, more support facilitates an increased usage of the arm, possibly with increased cortical reorganization [15, 29]. By later reducing the amount of weight support, the subjects also relearn to maintain their arm posture against gravity [180, 85, 46, 4]. Secondly, with scalable amounts of support, transitory effects can be examined. For instance, by gradually increasing the required shoulder-elevation torques by reducing the level of weight support, the effects on the achievable workspace can be studied [206].

The need for scalable support excludes horizontal planar devices like the MIT-Manus, which are part of the family of endpoint manipulators. These planar devices restrict the vertical displacement of the arm and support the arm similar to sliding it over a smooth horizontal surface. Although fully supporting the weight of an arm in rest, the amount of compensation is always equal to the normal force between the arm and the surface. The arm is not supported when it leaves the surface. This normal force cannot be controlled by the device, but only by the patient relying on either proprioceptive or external sensory feedback [123] to know how much of the weight of the arm they are lifting themselves. For stroke patients with reduced sensory and motor control, keeping the amount of support constant during movement is almost impossible. Planar devices also allow additional downward directed forces to artificially influence results. For example, using a table-like support artificially increases the range of motion of stroke patients over a fully force-supported arm [206]. This rewards patients for the erroneous motor pattern of pushing down while wanting to extend in the horizontal plane.

Three-dimensional endpoint manipulators, exoskeletons and cable suspensions all support the arm with vertical forces, kept invariant over a large range of motion. Contrary to the normal forces in the above planar devices, the applied forces can be scaled to the amount of support needed. Springs connected inline in cable suspensions result in deflection-dependent support and unwanted oscillations. However, spring mechanisms exist which generate deflection-independent constant forces [74], and have been used previously in the T-WREX and Armon.

4.2.2 *Independent weight support*

Independent weight support at both the wrist and elbow gives the therapist more control over the load distribution. Compared to a single connection at the wrist, the double connection also prevents the arm from dangling at the elbow and gives more influence over the residual weight still carried by the shoulder. Reducing the shoulder force is said to be important in reducing the occurrence of shoulder pain: a recent study claims that taping the shoulder, thus assisting the passive tissue and shoulder muscles, results in less painful shoulders [68]. With a requirement of 3.5 kg of support at the elbow and 2.5 kg at the wrist, the arms of most patients can be fully supported.

Endpoint manipulators, exoskeletons and cable suspension are all able to provide independent support. Exoskeletons have, by definition, independent control of the joints. Three dimensional endpoint manipulators connected need at minimum a fourth controlled or fixed degree of freedom to achieve it. Cable suspension will require a second, independently powered, cable going to the arm.

4.2.3 *Maximum range of motion*

In current stroke rehabilitation, many therapists ask the patients to perform a wide range of tasks. These task often mimic activities of daily living but also included reaching for the extremes in the patients' range of movement. The maximum reach for most patients from shoulder to elbow is less than 0.8 m. Within this movement range, the device should have little to no restrictions.

All three groups of device designs can achieve maximum range of motion, with some complications. A single endpoint manipulator with three degree of freedom connected to the hand doesn't support the arm at the elbow. Connected to the forearm just below the elbow, however, it can balance the entire arm [75]. For all other connections, the endpoint manipulator needs to control at least one additional rotation degree of freedom to give the forearm usable orientations. For exoskeletons, maximum range of motion for the shoulder and elbow require more complex mechanisms to account for voluntary and forced shoulder translation [117, 186, 202, 142]. Adding weight support to exoskeletons requires a trade off between the weight and the side effects of the support system. Endpoint manipulators and cable suspensions should be positioned such as not to limit the achievable range of motion.

4.2.4 *Minimal impedance*

The limited capabilities of severely affected stroke patients should not be impeded further by obstructing forces like inertia and friction. These forces slow the acceleration and deceleration of motions, possibly resulting in reduced movements and increased painful reaction forces in the shoulder.

Here, exoskeletons and endpoint mechanics introduce additional inertia and friction. Although these experienced impedance forces can be reduced by active mechatronic admittance controllers, these also make the system even more complicated. Balancing masses connected via cables and slings to the arm increase the vertical inertia and make the entire device heavier.

4.2.5 *Access to the limb*

Even during robot assisted therapy, therapist like to observe the movements and also to feel them. By interacting with the patient's arm, the therapist can feel the amount of spasticity or muscle tone and can steer movements in desired directions.

Both endpoint manipulators and cable suspensions allow reasonably good access to the limb. Exoskeletons add an external skeleton to the arm, making access more difficult and potentially dangerous due to the large amount of moving components.

4.2.6 *Overall implications*

Summarizing, the requirement for scalable support independent for upper and forearm, and maximum range of motion with minimal impedance in a simple mechanical device, while still granting therapist maximum access, led us to choose a cable suspension system with two independent mechanisms providing the supporting forces.

4.3 DESIGN AND VALIDATION

After evaluating several concepts, we created the Freebal (see Fig. 4.2). It uses two independent ideal-spring mechanisms for the supporting forces on the elbow and wrist, connected via overhanging cables to the suspension slings which support the arm. The ideal-spring mechanism has almost no impedance and is simple

Figure 4.2: The Freebal. The system generates the weight supporting forces with almost inertia-free ideal-spring mechanisms (see Fig. 4.3). The wrist and elbow are supported by two slings connected via cabling to these independent mechanisms. In the figure, the overhanging beam is shown lowered for display reasons. During normal use, it can extend up to 3.5 m above ground level dependent on available space and the work volume needed.

to realize, adapt and maintain. The supporting forces can be easily scaled by changing the spring attachment points. The cable construction does not inhibit arm movements, except for the straight upright orientation of the arm being unobtainable, as this would causing the slings to slide of the arm.

The construction is made of aluminum, thus is light and easy to move. The overhead beam can be lowered to below 2 m for storage or transportation. The device has a setup time of less than one minute to get a subject started with exercising with the right amount of weight support. The hand of the connected arm can still grab objects in functional exercises, and the therapist has full access to the arm to guide the movement.

4.3.1 *Ideal spring mechanism*

As opposed to directly connected springs, the supportive force generated by ideal-spring mechanisms [74] (see Fig. 4.3) are independent of the vertical deflection. Compared to counterweights, ideal-spring mechanisms do not double the vertical movement inertia. Over complex mechatronic systems [59], which would include several actuators, force-sensors and controllers, ideal-spring mechanisms have the advantage of being significantly less complex and costly.

The balancing forces come from two independent ideal spring mechanisms at the base of the Freebal (see Fig. 4.3). The mechanism gives a constant vertical

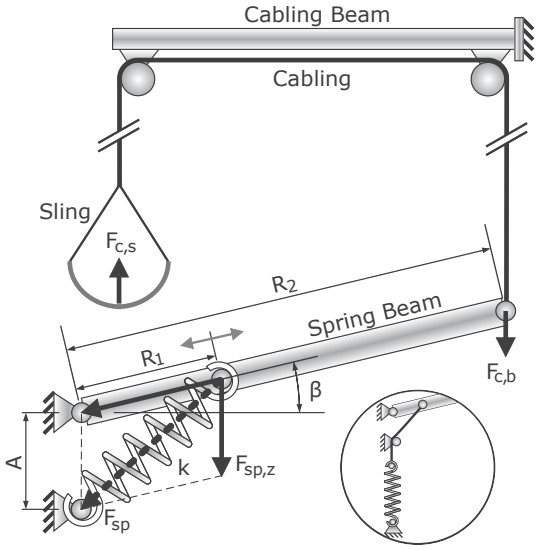

Figure 4.3: The ideal-spring mechanism. The Freebal has two of these mechanisms, connected to the wrist and elbow. The supporting force $F_{c,b}$ at the beam end is independent of the angle β, because the vertical component of the spring force $F_{sp,z}$) is always equal to distance A times spring-stiffness k (see Eq. 4.1). The support can be adjusted by changing the spring-attachment distance R_1. Cable angles and friction influence the effective weight support at the sling $F_{c,s}$ (see Fig. 4.5 and Fig. 4.4). To get the ideal-spring behavior with stock extension springs, the spring is placed in the vertical tube and connected via a cable (see inset).

force at the endpoint of the spring beam $F_{c,b}$—which is almost equivalent to the effective weight support at the sling $F_{c,s}$ (see Eq. 4.3)—according to:

$$F_{c,b} = F_{sp,z}\frac{R_1}{R_2} = kA\frac{R_1}{R_2}, \tag{4.1}$$

where $F_{sp,z}$ is the component of the spring force in the vertical direction, R_1 is distance from the spring beam rotation axis to the spring attachment point on the beam, and R_2 is the length of the spring beam. The vertical spring force $F_{sp,z}$ is equal to the spring stiffness k times the distance between the spring beam axis and the spring attachment point on the base, which must be located exactly underneath the beam axis. Furthermore, the spring must behave like an ideal-spring; that is, the spring force F_{sp} must change linear with the spring deflection Δx_{sp} and be zero at zero spring length [74]:

$$\begin{aligned} F_{sp} &= k_{sp}\Delta x_{sp}, \\ F_{sp} &= 0 \text{ when } x_{sp} = 0. \end{aligned} \tag{4.2}$$

Stock extension springs do not behave like this. Pretension and the length of the unloaded spring are not matched to get a virtual zero force at a virtual zero spring length. By hydraulically overstretching the spring, pretension is removed. The spring is placed in a vertical tube underneath the mechanism and connected to the spring beam via the short cable running over a cable pulley. The length of the short cable is adjusted to fulfill the ideal spring requirements (see Fig.4.3.

The endpoint force $F_{c,b}$ can be modified in multiple ways: changing the lengths A, R_1 or R_2, or changing the spring stiffness k. However, changing length A or the stiffness k also requires a change in the length of connecting spring cable, and changing length R_2 can extend or retract the mechanism beyond the needed boundaries (see next subsection). Thus the endpoint force is adjusted by changing the attachment point R_1 of the ideal spring on the spring beam via lead-screw slider in the spring. The needed amount of support is dependent on the measured weight of the arm. By locking the spring beams and weighing the load on the two

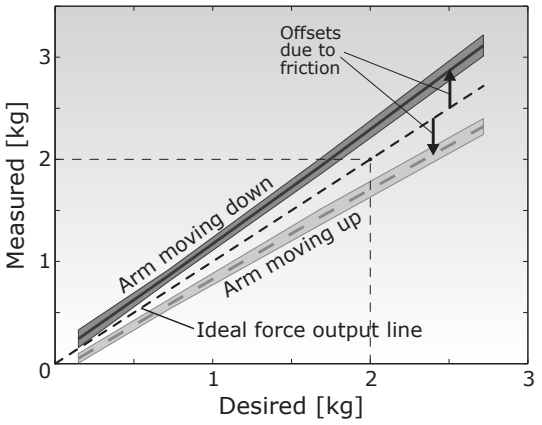

Figure 4.4: Effective weight support as measured in the ideal spring mechanism (see Fig. 4.3). With the arm moving down, and thus the beam end moving up, the mean effective amount of support is given by the dark, solid line (thin lines are the standard deviation). The light, stripped line gives the amount of support with the arm moving up. The effective support differs from the ideal force output line due to friction of the spring cable running over the small (10 mm diameter) guiding pulley (see Fig. 4.4). When measured, the friction was 12% of the weight support, although this was not felt manually.

cables with simple mechanical spring scales, the weight can be determined and later used to set the desired percentage of support.

Spring selection influences the resolution and range of the weight support. A stiffer spring increases the force change per revolution of the lead screw, and increases both the achievable minimum and maximum supporting force. The minimum force is reached when the slider cannot move further back in the tube. With a spring of stiffness 6 kN/m, length A at 40 mm, R_2 at 800 mm and R_1 varying between 1 mm and 160 mm, the minimum and maximum amounts of support per mechanism are respectively roughly 0.25 and 5 kg (see Eq. 4.1). An accurate value for the maximum spring deflection is calculated by using the maximum desired deflection angle of the spring beam, and solving the trigonometry problem for the maximum spring extension.

The construction impedance felt by the patients is dependent on the arm movement. When the arm moves in the horizontal plane, the spring beam stays almost stationary. When the arm moves vertically, the low reflected mass of the spring beam and spring (0.200 kg) and friction inside the ideal-spring mechanism may be felt. The short cable running between the spring and the beam is at high tension, and running over the guiding pulley causes significant friction. This friction was measured as 12% of the desired weight support by using an external motorized setup, but was also difficult to detect manually. The measurements were repeated for vertical translation speeds of 10 to 100 mm/s, but the speed had no measurable influence on the amount of friction, and the pooled results are presented here (see Fig. 4.4).

4.3.2 *Overhead cable construction*

Cable pulleys on a fixed overhead cabling beam guide the cable connecting the ideal spring mechanism to the cable suspensions (see Fig. 4.2). By positioning the overhead beam up to 3.5 m above ground level, the non-linearities of the angled vertical cables to the spring beam and the slings are minimized. This results in overall theoretical non-linearities of +/- 10% of the desired weight support in a work volume of a 1 m diameter ball (see Fig. 4.5), and keeps the occurring horizontal forces below 20% of the amount of weight support. The effective weight support $F_{c,s}$ and the undesired horizontal forces $F_{h,s}$ at the sling can be calculated

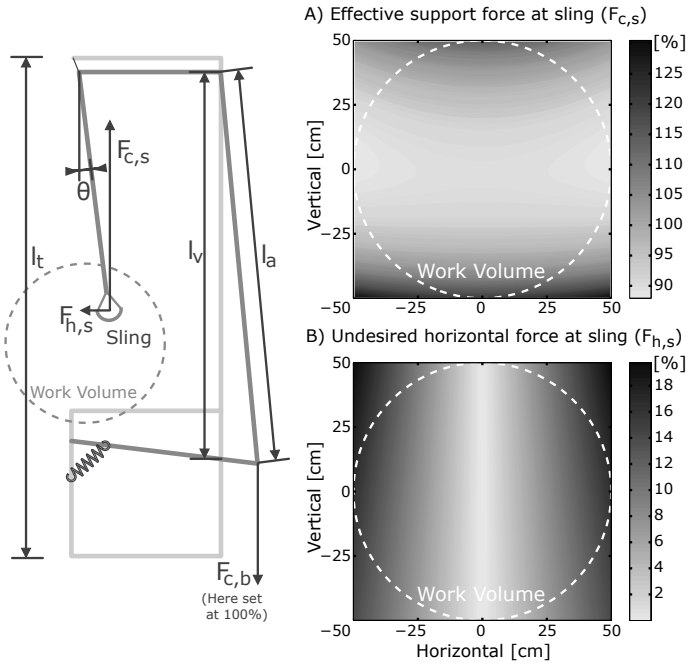

Figure 4.5: Cross-sectional view of the theoretical non-linearities caused by cable angles and spring mechanism. The work volume (1 m diameter) is 1 m above ground level beneath the foremost top pulley. The Freebal is extended to a height l_t of 3.5 m. For Eq. 4.3: cable length l_a, vertical length l_v, and sling-cable angle θ. In the top figure, the effective weight support $F_{c,s}$ is given as percentage of the vertical beam force $F_{c,b}$. In the bottom figure, the horizontal inward directed forces at the sling $F_{h,s}$ are given as percentage of $F_{c,b}$.

with the angled cable length l_a, the vertical length l_v, and the angle of the cuff cable θ, according to:

$$\begin{aligned} F_{c,s} &= \cos(\theta)\frac{l_a}{l_v}F_{c,b}, \\ F_{h,s} &= \sin(\theta)\frac{l_a}{l_v}F_{c,b}. \end{aligned} \tag{4.3}$$

Again, friction reduces the effective support and is minimized by careful selection of pulleys and cabling. Inexpensive, highly flexible, though not very stiff, 3 mm diameter cabling has almost no resistance in the pulleys. The lack of stiffness in the cable is not a problem, as it connects the sling with an almost constant force to the low-inertia ideal-spring mechanism.

4.4 PATIENT INTERACTION

To observe how weight support provided by the Freebal influences movement execution, we preformed an explorative cross-sectional study with eight stroke patients and ten healthy elderly. Both groups had to make large circular hand movements, enveloping an area as large as possible, and reach as far as possible in three horizontal forward directions.

4.4.1 *Methods*

The ten healthy elderly were over 50 years of age and had no known history of neuromuscular, orthopedic or rheumatological disorders of the upper extremity. Eight

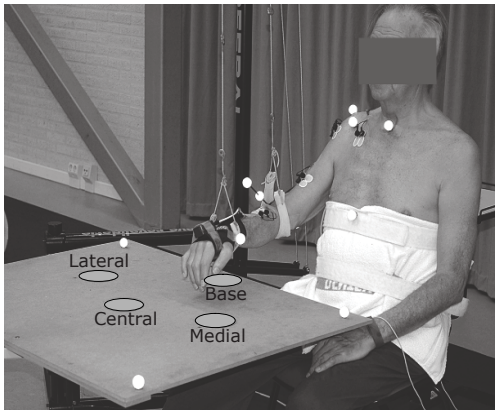

Figure 4.6: Experimental setup, with the Freebal connected to the wrist and elbow. On the arm the optical markers from the Vicon system are visible. Four circular dots of 0.1 m diameter on the table assist in the task execution; a base dot, from were all movements start, and the three target dots in medial, central and lateral direction. The base dot is located directly under the hand in front of the elbow when the subject has 90 deg shoulder plane of elevation, 0 deg of both shoulder elevation and humerus long axis rotation, and 90 deg of elbow flexion. The target dots are 0.35 m from the base dot, with the medial and lateral dots at 45 deg angles to the base to central dot axis.

stroke patients were recruited from the local rehabilitation center and included in this study after verifying that they were able to lift their arm at least partly against gravity and were not suffering from shoulder pain. All subjects provided written informed consent and the study was approved by the local medical-ethical committee. The mean (and standard deviation) age of the patients was 58 (14) years, and 66 (6.4) for healthy subjects. The patients' time post first stroke was 3.3 (3.0) months, ranging from 1 to 10 months. The upper extremity Fugl-Meyer score was assessed prior to the experiment as a clinical measure of the current arm function [62]. The FM-scores were on average 43 (9.1) out of 66, ranging from 33 to 60. The patients used their affected and the healthy subjects their dominant arm. For four patients, their affected arm was also their dominant one.

Task explanation and execution was assisted by four circular dots of 0.1 m diameter on a table (see Fig. 4.6). The base dot defined the general staring position for all movements, and was located directly underneath the hand when the elbow flexed 90 deg forward from the neutral anatomical position (90 deg shoulder plane of elevation, 0 deg of both shoulder elevation and humerus long axis rotation, and 90 deg of elbow flexion [233]). The three target dots in medial, central and lateral direction were located with their centers 0.35 m from the base dot center, with the medial and lateral dots rotated 45 deg around the base dot from the central dot. The top-front pulley of the Freebal was positioned directly above the base dot at 3.5 m from the ground, maximizing the usable work volume of the Freebal. Subjects were seated at an in height adjustable table and were secured to the chair by straps across the chest (see Fig. 4.6). The straps reduced compensatory movements of the trunk, but some voluntary translation of the shoulder was still possible.

Subjects performed two different series of movements; linear maximal reaching movements and circular range of motion movements. Both series were once performed with full and once without any weight support. To reduce the potential effect of learning or adaptation, the subjects were assigned randomly to one of two sequences, either performing the movements first with and subsequently without support, or in reversed order. The subjects were coached to do the reach and retrieve movements at a self selected speed, concentrating on the maximum

obtainable distance and performing the movements as close to shoulder level as possible.

During the series of linear maximum reaching movements, subjects had to horizontally reach over either the medial, central or lateral target dot, always starting and ending at the base dot. The different directions may reflect a difference between reaching inside the frontal working space and reaching out, where the latter is thought to be more difficult for stroke patients. Movements over a target were repeated five times before continuing to the next target. In total, two (support levels) times three (directions) times five repetitions were made.

During the series of circular range of motion movements, subjects had to make a horizontal circular motion over the table, starting at the base dot and encircling an as large an area as possible, either in clockwise or counter-clockwise direction (inverted when left hand was used), and ending at the base dot. Compared to the linear maximal reaching movements, these circular motions may reflect a difficulty in directly moving between the frontal working space and the outer reaches. Movements in a circular direction were repeated five times before continuing to the next. In total, two (support levels) times two (directions) times five repetitions were made.

Shoulder, elbow and wrist positions were recorded using an infrared 3D-motion analysis system (VICON 370: six cameras, sample rate 50 Hz; Oxford Metrics Ltd, Oxford, United Kingdom). The reflective markers were placed on the bony landmarks of the joints according to ISB recommendations [233]. The marker positions were low-pass filtered at 10 Hz with a second-order zero phase shift Butterworth filter.

Four remarks must be made. Due to measurement noise, the glenohumeral rotation center could not be estimated reliably via regression methods, and the marker on the most dorsal point on the acromioclavicular joint was used as a substitute. Because some shoulder translation was possible, the horizontal wrist position was corrected by subtracting the horizontal shoulder position. Full arm length was defined as the sum of the wrist to elbow and the elbow to shoulder distance. Finally, focussing on the performance of shoulder and elbow, the wrist, and not the hand, is used in the data analysis as the endpoint. The finger to wrist length is accounted for by repositioning the base dot underneath the wrist at the start of each trial.

For each of the five repetitions in the linear maximal reaching movements, the maximum wrist-to-shoulder distance was determined. The best three of these reaching movements were identified. On the exact occurrence of these furthest three reaches, the shoulder, elbow and wrist heights were sampled. All these sets of three were averaged to get the mean results per set of five repetitions.

For the circular range of motion movements, the results per repetitions are defined as the time-mean of the part of the movement with the wrist inside the triangle of dots (the gradient in Fig. 4.7). The three highest average wrist-shoulder distances are identified and stored together with the mean joint heights of wrist, elbow and shoulder of the movement component inside the triangle. Again, all sets of three are averaged to get the mean results per set of five repetitions.

For both types of movements, the maximum wrist-to-shoulder distance is normalized to the full arm lengths. The joint heights are normalized to table (0) to shoulder-at-rest (1) height.

Two-way Anova were used to test the significance of the change in reaching distance and execution heights of wrist, elbow and shoulder for healthy elderly

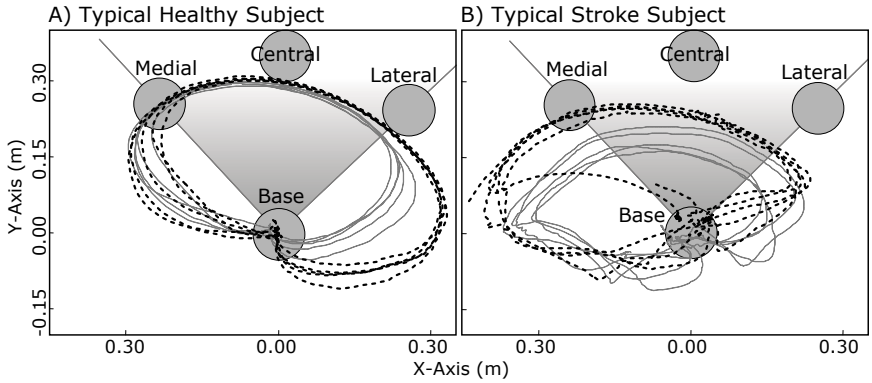

Figure 4.7: Typical circular range of motion wrist paths. In top figure A) the corrected wrist paths of a typical healthy subject are shown, and in the top figure B) of a typical stroke patient. The wrist paths are corrected for shoulder translation by subtracting the shoulder positions at each time step. The finger to wrist length is accounted for by repositioning the base dot underneath the wrist at the start of each trial. The gray solid lines are without weight support, each consisting of five repetitions, and the black stripped lines are with full weight support. In the latter analysis, only the wrist paths inside the dots triangle (shown with a gradient) are used.

and stroke patients separately. The two factors were the amount of weight support (two levels: full, none) and movement direction (five levels: medial, central, lateral, clockwise, counter clockwise). The significance level for all tests was set at $\alpha = 0.05$.

4.4.2 *Results*

Using weight support makes no difference for the elderly control subjects ($p = 0.52$, see Fig. 4.8A) as they were already able to reach to their maximum levels without any support. Stroke patients do instantly increase their range of motion by about 7% ($p < 0.001$). For both groups, the movement direction had no influence ($p > 0.3$).

As subjects were encouraged to perform the movements at shoulder level but not penalized for not doing so, Fig. 4.8B shows both elderly and patients to have their elbow and wrist below it. With weight support, patients can keep their elbow slightly higher ($p = 0.024$) and their wrist up to an average of 20% higher ($p < 0.001$). For elderly, the support has no significant influence on the average elbow heights ($p > 0.13$), although for the average wrist height, the movement direction does ($p = 0.014$).

4.4.3 *Discussion*

To observe how the Freebal and similar devices influence movement execution, the outcome measure most of interest is the change in kinematic performance with weight support. Thus how much further can stroke patients reach while using weight support. On average, our group of mild to moderately affected patients

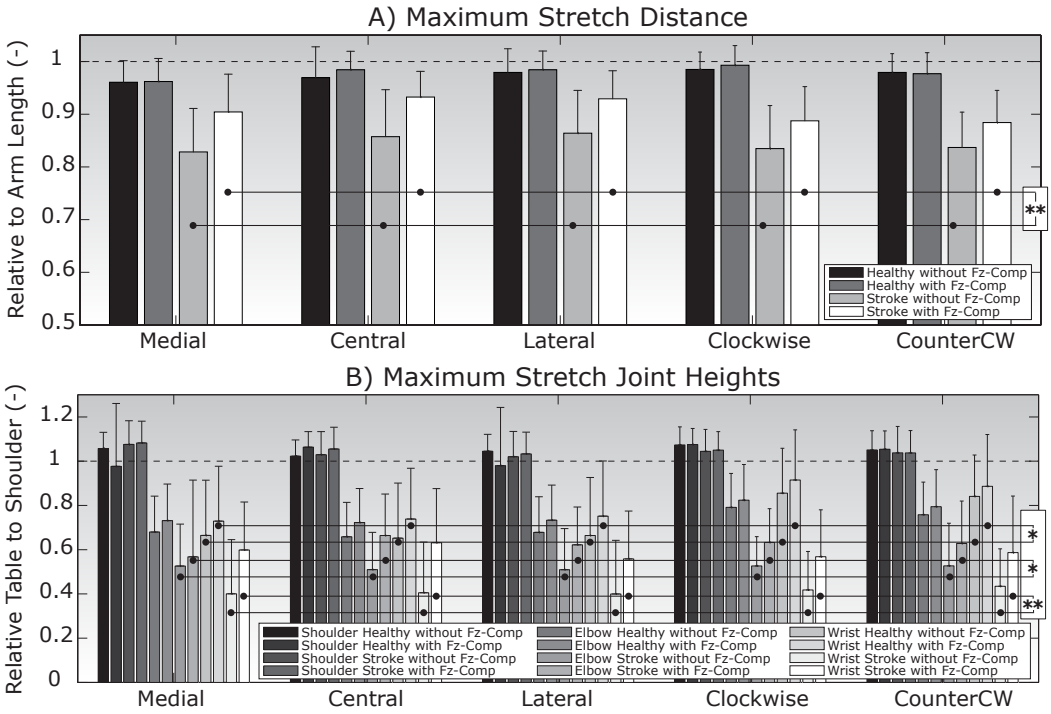

Figure 4.8: Maximum shoulder-wrist distance and joint heights. In the top figure A), the average normalized maximum shoulder-wrist distance is given for both the maximum stretch and the range of motion trials, respectively in the left three groups of bars in medial, central and lateral directions, and the right two in clockwise or counter-clockwise direction. In the bottom figure B), the average normalized shoulder, elbow and wrist heights are given as recorded at the occurrence of for the highest three maximum distance results. (* = $p < 0.05$, ** = $p < 0.001$.)

instantly reached 7% further with full support and could do this much closer to shoulder level.

The most likely explanation is that the more extended the elbow is, the more shoulder torque is required for elevation. Patients lacking the strength to do so have the movements of their affected arm facilitated by the weight support, instantly extending their range of motion. In doing so, more severely affected patients can progress earlier to more motivating, functional training, possibly with increased cortical reorganization [15, 29].

In a similar experiment, Dewald and colleagues [206] had stroke patients make range of motion movements in the horizontal plane just below shoulder level. They forced their patients to keep the arm at or above this level, and saw a great reduction in achievable work envelop which grew monotonic with increasing weight support. They attributed the linkage of weight support and work envelop to abnormal and involuntary coupling of the shoulder elevation to elbow flexion torque [18, 36, 11]; the shoulder elevation torque stimulates the elbow flexion muscles, hindering the elbow extension. Our results are not as clear as theirs because our patients reached almost to their maximums, even without weight

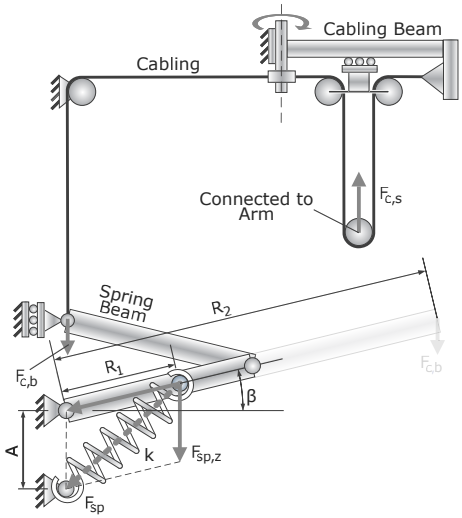

Figure 4.9: Alternative weight-support mechanism. Compare to the Freebal mechanism in Fig. 4.3. The spring beam is now split, eliminating the (small) non-linearities of the beam-endpoint horizontal translations. Furthermore, the cabling beam is vertically hinged roughly above the human shoulder and has a vertical slider underneath the cable beam. This can position the vertical cable exactly above the wrist and elbow and reduce the non-linearity due to the angles of the cable with the vertical. However, both changes make the mechanisms more complex and a more susceptible to friction and undesirable dynamics. For example, the hinged beam may swing with frequencies close to the eigenfrequencies.

support, and had less severe impairments. Our patients also had a greater freedom of choice in selecting how to make the extension movement. They did extend their elbow almost fully with the hand just above the table (see Fig. 4.8B) but subsequently couldn't lift it against gravity despite being verbally encouraged to do so. Keeping the hand close to the table level may be a way to reduce the amount of shoulder elevation torque needed. It keeps the coupled, involuntary elbow flexion as low as possible. It seems to us that patients thereby potentially negated the negative influence of the abnormal coupling. Still, the most likely explanation of the reduced range of motion in the unsupported condition is a general lack of strength to elevate a fully extended arm.

4.5 DISCUSSION AND CONCLUSION

The Freebal is designed for effective weight support with minimal undesirable side effects. The design meets most of the design requirements. Cable suspension systems are simpler to construct and use than endpoint manipulators or exoskeletons. With ideal-spring mechanisms, cable suspensions offer a large range of motion, low movement impedance and scalable support independently adjustable for wrist and elbow. The Freebal supports up to 5 kg at each sling with the current springs. This is higher than the desired 3.5 kg and 2.5 kg needed to support most patients at the elbow and wrist. It has an almost-linear workspace of 1 m^3 which accommodates most arm movements for most patients. The only orientation not achievable is the vertical forearm, which would cause sliding of the slings. At the edges of the workspace, the angle suspension cable will pull the arm inwards with a force up to 20% of the desired support force. For movements in the vertical directions, the impedance is a combination of the inertia of the ideal-spring mechanism at 0.20 kg and the friction of the spring cable (12% of support force). Finally, the therapist has full access to the limb during use, as the arm is supported using just two cables. Besides meeting these design requirements, the Freebal also requires no external power, force sensors or active controllers, nor complex mechanisms on

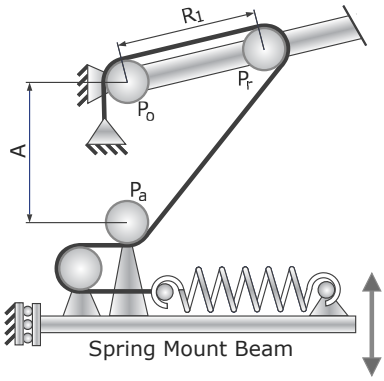

Figure 4.10: A possibly better spring cable guiding mechanism. By using three pulleys (P_o, P_r and P_a) of equal diameter, though larger (40 mm) as compared to the original P_a pulley (10 mm), the friction is removed. Lowering the spring cable tension by using a slacker spring and increasing the A and/or R_1 distances further reduces the friction, although this needs more space for spring deflection and longer springs. The amount of support cannot be adjusted by changing R_1 anymore, as the change in cable length between P_o and P_a negates the ideal spring mechanism. Instead, A now needs to be lowered or heightened, together with the spring and spring tube.

the arm. The device can be easily moved, serviced and used in arm rehabilitation with either sitting or standing subjects.

The increased performance as observed in our cross-sectional study can indicate why the training studies [180, 46, 85, 4] show weight support to be effective. For instance, being able to reach further more easily, knowing little can happen, may increase the stroke patient's confidence in using his full range of motion. With more regular movements, patients may also prevent stiffening of their muscles and joints, reducing the requiring physical therapy.

Experiences also learned that subjects had a preference for attaching the two slings to the wrist and elbow, and not at the mass centers of the lower and upper arm. This seems to be partly caused by the protruding bony structure at the wrist and elbow, which stop the slings from sliding. These points might also be less sensitive for applying the weight support. By connecting to the wrist and elbow, the weight of the upper arm is supported both by the force at the elbow and by a residual vertical force in the shoulder.

To record the joint rotation and muscle activation, additional systems are needed. As the Freebal is mostly made from aluminum, is painted black and hardly obstructs the view on the arm, both optical as magnetic based tracking systems can be used. In other studies, the Freebal was used with both visual tracking and EMG recording [163, 164, 92]. The Freebal can also be used to support the arm during interaction with virtual environments or playing games [165]. See Fig. 4.11 for an example of a setup currently used in out exploratory experiments.

Compared to other dedicated devices, the Freebal has advantages and disadvantages. Like the Freebal, the Armon [75] and the T-WREX [180] use ideal-spring mechanisms for scalable, vertical-position independent weight support. The Armon is designed as a permanent patient support for permanent attachment to a wheelchair and the T-WREX is used in stroke rehabilitation therapy. Contrary to the Freebal, neither requires a high ceiling or has horizontal forces pulling the sling to the center of the work volume. But the Freebal has lower impedance forces, a slightly larger range of motion, is easier to setup and use, while still giving the therapist full access to the limb. Specifically compared to the Armon, the Freebal can scale the weight support for the lower and upper arm independently, and thereby has better control over the forces in the shoulder.

The more conventional Swedish Helparm has been reported to cause shoulder pain in patients. Although speculative, this might be because the Helparm does not have independent support for the wrist and elbow. As most of the mass of the

Figure 4.11: Freebal supporting the arm during interactive sessions. Interacting with a virtual environment or playing games has been used by many rehabilitation devices as a way to increase the patient's motivation.

arm is located proximally, using the Helparm makes the shoulder bear most of the weight, but without the normal muscle forces around the shoulder keeping the humeral head stable in the glenoid. The arm is supported only by the passive tissue of the shoulder joint. A recent study shows that taping the shoulder, which assists the passive tissue and shoulder muscles, reduces the occurrence of shoulder pain [68]. Because the Freebal also supports the arm at the elbow, the weight the passive tissue of the shoulder carries is much lower. By connecting the sling to the middle of the upper arm, as discussed above, the load on the shoulder can even be completely removed.

Three improvements on the design may be desirable. Firstly, the friction in the ideal spring mechanism needs to be further minimized from the current 12% of desired weight support. It is possible to reduce the friction by using a better spring cable guiding mechanism, where the guiding pulleys can be constructed with larger radius [74] (see Fig. 4.10. Secondly, the spring beam can also be split in the middle, eliminating the (small) non-linearities of the beam-endpoint horizontal translations (see Fig. 4.9). This reduces the non-linearities in the work area due to smaller angles of the cables with the vertical. Finally, the overhanging cabling construction may be recreated to swivel along with the arm. However, all three changes increase the complexity of the mechanisms and can introduce some new and undesirable dynamic effects. For instance, the hinged beam tends to move with frequencies around the eigenfrequency, exciting unwanted oscillations.

4.5.1 *Conclusion*

The Freebal has a large workspace of roughly 1 m^3, low movement impedance, and independent support at the elbow and wrist of up to 5 kg, but the friction in the spring cable should be reduced. An explorative cross-sectional study with eight patients shows the Freebal to instantly extend the range of motion of the affected arm. In conclusion, the Freebal meets the requirements for patients to benefit from therapy with the Freebal, potentially progressing earlier to more motivating, functional training.

ACKNOWLEDGEMENT

The authors would like to thank Theo Krone for his work on the original design. The Freebal has recently been sold to Hocomo AG (Volketswil, Switzerland).

5

IMPROVING UPPER-EXTREMITY PERFORMANCE IN CHRONIC STROKE USING A PASSIVE WEIGHT-SUPPORT DEVICE

ABSTRACT Weight support for the arm can reduce the influence of abnormal multi-joint torque couplings on active range of motion after stroke. However, previous studies used complex, active rehabilitation devices to provide the weight support, which could be replaced with the simpler, passive Freebal. The objective of the this study is to examine 1) if the movement performance of chronic stroke patients improves after weight-supported training with the Freebal, and 2) if so, if the improvements are due to reduction of the influence of abnormal joint-torque couplings. Four chronic stroke patients received three 30 minute weight-supported training sessions per week for a period of six weeks. During baseline and evaluation measurements, range of motion and angular movement patterns were determined during circle drawing, in addition to measuring general arm function. After training, arm function, active range of motion and independence of simultaneous shoulder and elbow movements had improved in all subjects. Despite the small number of subjects, the present explorative study suggests that weight-supported training with the Freebal has the potential to decrease the influence of abnormal multi-joint torque couplings on arm movements after stroke.

5.1 INTRODUCTION

Stroke is the main causes of disability in Europe and North America. Due to hemorrhagic or ischemic damage to brain tissue, motor planning and the integration of sensorimotor information are degraded. This results in a disturbed control of muscle activity, seen as muscle weakness and spasticity. Coordination between muscles over one or more joints can also be impaired through abnormal multi-joint muscles-coactivation patterns, which reduce movement selectivity. In a majority of stroke patients, these limitations account for a reduced ability to use the arm. At most 20% of all patients regain complete arm function after 6 months [115, 110, 176].

In clinical practice, the stereotypical patterns of involuntary coupling of joint movements are often observed [213, 18]. Depending on the severity of the stroke, movements are restrained within either a flexion synergy (shoulder abduction, shoulder external rotation, elbow flexion and forearm supination) or an extension synergy (shoulder adduction, shoulder internal rotation, elbow extension and forearm pronation) [62].

It is thought that humans, as opposed to other animals, are almost fully dependent on the contralateral corticospinal projections from the primary motor cortex to the motoneurons in the spinal cord for their control of upper-extremity movement.

Submitted (in part): IEEE Transactions on Robotics (T Krabben, GB Prange, AHA Stienen, BI Molier, H van der Kooij, and MJA Jannink). The version here is significantly adapted by AHA Stienen to better support the development of the Freebal.

The loss of these projections is difficult to compensate for, although alternative, less efficient, routes exist to regain motor control [90]. For instance, the indirect connections between the motor cortex and the muscles via the corticoreticular and then reticulospinal pathways are both slower and less focussed, for their axons are thinner and more widely branched. They mainly project to proximal limb muscles and innervate motor neurons over multiple spinal segments [128].

Abnormal couplings between shoulder and elbow torques of stroke patients were identified during isometric contractions: high torques of shoulder abduction are related to simultaneous elbow flexion torques [9, 10]. Indications for coupling of these components are also observed in muscle activity during isometric contractions [35]. In the case of reaching movements, a certain amount of shoulder abduction is needed to lift the arm, provoking simultaneous elbow flexion torques and limiting elbow extension [36, 11].

The influence of these synergistic patterns can be instantaneously reduced by counterbalancing the weight of the arm. When the arm is supported, the required shoulder abduction torques during two-dimensional reaching movements at shoulder height are reduced and the range of elbow extension increases [36, 11, 206]. Using a weight-support device, the Freebal [201, also see Chap. 4], we found similar results in a study examining maximal reaching distance during supported and unsupported three-dimensional reaching movements of stroke patients [164]. Regarding muscle activity, our research in healthy persons showed that the application of weight support facilitates movements by reducing the amount of muscle activity needed for a reaching movement, particularly in muscles counteracting gravity [163]. This facilitating influence of weight support on muscle activity was also observed in chronic stroke patients with mild hemiparesis [92].

Besides the instantaneous reduction of torque couplings using weight support for the arm, the couplings can also be reduced via weight-supported exercises over multiple training sessions. A study investigating changes in circles drawn before and after training of robot-aided point-to-point arm movements showed that the shapes changed from ellipses towards circles, due to less strong abnormal synergistic movement patterns and a consequently more selective control of shoulder and elbow movements [37]. In this study, the weight support was present during both the evaluation measurements and the rehabilitation sessions. It is also possible to reducing the torque couplings and improved movement ability for the unsupported hemiparetic arm using weight support during the sessions, but preferably by reducing the amount of support over the sessions. Using a passive exoskeleton to support the arm, the motor control of the arm improved [180, 85], accompanied by an increased maximal reaching distance [180]. Using the weight-support capabilities of a 3D haptic robot, the abnormal torque couplings between shoulder and elbow were reduced [46]. A training period using only the sling suspension of another 3D haptic robot, also induced a modest improvement in motor control of the arm [5].

Nevertheless, the above studies used complex devices to provide the weight-supported rehabilitation. Our passive—and comparatively simple—device, the Freebal, may achieve the same results. Therefore, the objective of the this study is to examine 1) if the movement performance of chronic stroke patients improves after weight-supported training with the Freebal, and 2) if so, if the improvements are due to reduction of the influence of abnormal joint-torque couplings. Similar to some of the above studies, we used circle-drawing methods to look at training-induced changes of the abnormal couplings [37, 46].

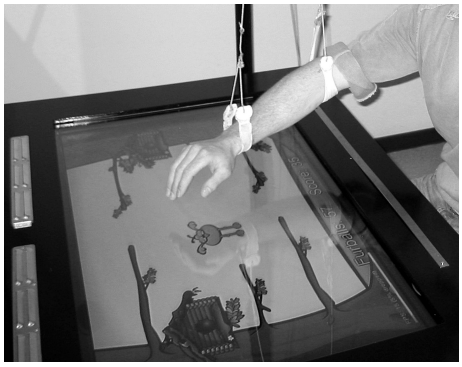

Figure 5.1: Training setup with FurballHunt game. In the game, the user has to chase away little birds called Furballs which fly from a birdhouse to one of the tree branches. The bird can be chased away by touching it with the hand, as detected by capturing software. The suspension slings from the Freebal (see Chap. 4) are visible at the wrist and elbow.

5.2 METHODS

5.2.1 *Subjects*

Subjects were recruited at a local rehabilitation center. Inclusion criteria were: 1) a history of a single unilateral stroke in the left hemisphere, resulting in right-sided hemiparesis (due to strictly right-sided Dampace, see Chap. 8), 2) the onset of the stroke was more than six months (chronic phase) before the start of the intervention period, 3) ability to move the shoulder and elbow joint against gravity but unable to hold the joints against a combination of moderate resistance and gravity, and 4) adequate cognitive function to understand the experiments, follow instructions, and give feedback to the researchers. Subjects were excluded from this study if: 1) a fixed contracture deformity in the affected upper limb was present, 2) pain was a limiting factor for the subjects' active range of motion, or 3) if they participated in other training experiments. All subjects provided written informed consent. The study was approved by the local medical ethics committee.

5.2.2 *Study design*

Subjects received three 30 minute weight-supported training sessions per week for a period of six weeks, making a total of 18 sessions. To study the effect of weight-supported rehabilitation training, three baseline measurements and an evaluation measurement were performed. Baseline measurements were performed three weeks prior to the start of the intervention period, spaced one week apart. After three and six weeks of training, subjects performed evaluation measurements.

5.2.3 *Weight-supported training*

In each training session, subjects practiced horizontal, goal-directed arm movements in a weight-supported, virtual-reality environment (see Fig. 5.1). The weight of the subject's arm is supported by the Freebal [201]. The Freebal consists of two overhead slings connected to ideal spring mechanisms via cables. One sling supports the subject's arm at the elbow and the other at the wrist. The Freebal allows easy and quick adjustment of the level of weight support by altering the force which is applied to the slings by the spring mechanisms. Use of the Freebal does not restrict movements to one plane, as reaching movements can be performed in

three dimensions keeping the exact same upward force throughout the workspace. If arm function improved over the training sessions, the level of weight support was decreased to ensure a challenging and motivating training environment. These adjustments were made based on the judgements of the therapists on patients' performance and motivation.

Virtual reality was delivered by a game named FurballHunt, in which the user has to chase away little birds called Furballs [165]. During the game, Furballs fly from a birdhouse to a tree branch where they sit down, while the user holds his/her hand on a start button. The bird can be chased away by moving the hand from the start button towards the bird and touch it. Motion capturing software detects arm movement as input to the game. Points are awarded to the user if a Furball is chased away within a certain time frame. Game difficulty is adjusted to the physical abilities of the user by varying the number and position of the tree branches (representing the targets to move to), the game speed, the number of Furballs, and the level of randomization in target sequence. The game was shown on a horizontally placed flat-screen television, which is mounted on an height-adjustable frame (see Fig. 5.1). All training sessions were assisted by the same physical therapist.

5.2.4 *Evaluation measurements*

Level of impairment of the arm function of stroke subjects has been evaluated and monitored with the upper extremity part of the Fugl-Meyer (FM) assessment. All measurements were performed by the same researcher, who was not involved in the training sessions.

Kinematic data during evaluation trials were recorded with a passive exoskeleton robot named Dampace [202, also see Chap. 8]. Although the Dampace can apply brake torques to the shoulder and elbow joint, it was strictly used as measurements device with disabled brakes. Weight support in the Dampace was either fully balancing the arm, or disabled, depending on the measurement requirements. For the slow evaluation movements used here, the weight support in the Dampace is as good as constant throughout the workspace. For the same reason, the inertial impedance is negligible, but a coulomb friction of about 6 N is always felt for any rotation of the shoulder.

Built-in potentiometers on three rotational axis of the shoulder joint allow measurements of upper arm elevation, transversal rotation, and axial rotation. Elbow flexion and extension were measured with a rotational optical encoder. Translations of the shoulder were measured with linear optical encoders. Signals from the potentiometers were converted from analog to digital (AD) values by a 16 bit AD-converter (PCI 6034, National Instruments, Austin, Texas). The rotational and linear optical quadrature encoders were sampled by a 32 bit counter card (PCI6602, National Instruments, Austin, Texas). Digital values were sampled with a sample frequency of 1000 Hz, low-pass filtered with a first-order Butterworth filter with a cut-off frequency of 40 Hz and stored on a computer with a sample frequency of 50 Hz.

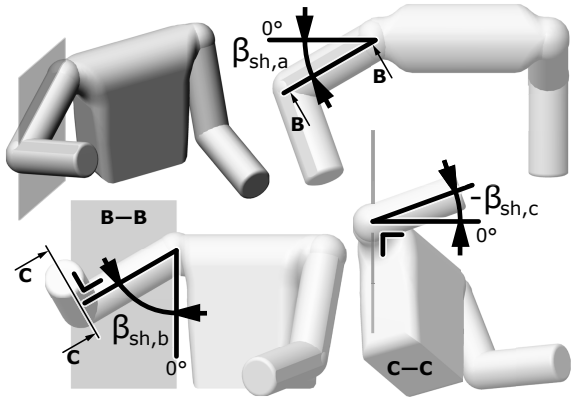

Figure 5.2: Shoulder rotations defined according to International Society of Biomechanics (ISB) [233]. Top-right: plane of elevation ($\beta_{sh,a}$). Bottom-left: negative elevation ($\beta_{sh,b}$). Bottom-right: axial rotation ($\beta_{sh,c}$). In this example, the shoulder is rotated by 30°, 60°, and -20° for the ISB-defined order of $\beta_{sh,a-c}$.

5.2.5 *Procedures*

Before movement execution, upper and forearm lengths were measured. Upper arm length was defined as the distance between acromion and the lateral epicondyle of the humerus. Forearm length was measured between the lateral epicondyle of the humerus and the third metacarpophalangeal joint. After measurement of the arm lengths, the exoskeleton was attached to the upper and forearm with soft straps and the wrist was immobilized with a splint. To minimize trunk and shoulder movement, subjects were strapped with a four point safety belt. The starting position of subjects in all movement tasks was with the upper arm aligned with the trunk and the forearm pointing straight forward, while the table was placed in such way that the hand rested on the table, with the wrist in the middle of the nearest edge of the table.

Subjects were asked to perform a circular motion in the transversal plane just above a tabletop, in a clockwise (CW) and counter-clockwise (CCW) direction. The order of direction has been randomized throughout the measurements. Subjects were instructed to draw five circles in each direction, as big as possible. For the latter purpose, template circles of different radii were shown on the tabletop. Movements were performed at a slow self-selected pace while verbal encouragement was provided to the subjects throughout the experiment.

5.2.6 *Data analysis*

Joint angles of the shoulder and elbow were measured according to the recommendations of the International Society of Biomechanics (ISB) [233]. The shoulder rotations are defined for the plane of elevation $\beta_{sh,a}$, the negative elevation $\beta_{sh,b}$, and the axial rotation $\beta_{sh,c}$ (see Fig. 5.2); these three euler angles can describe all rotations of the humerus. The elbow joint angle β_{el} is defined as the angle between the humerus and forearm (elbow fully stretched represents 0°).

Positions of the hand were calculated from the measured joint angles and arm lengths, relative to the shoulder position to exclude contributions of small shoulder and trunk movements to the size of the circles drawn by the subjects. The circle areas were calculated as the area enclosed by the horizontal projection of the hand trajectory onto the table surface. The three largest circles in each direction were selected for further analysis.

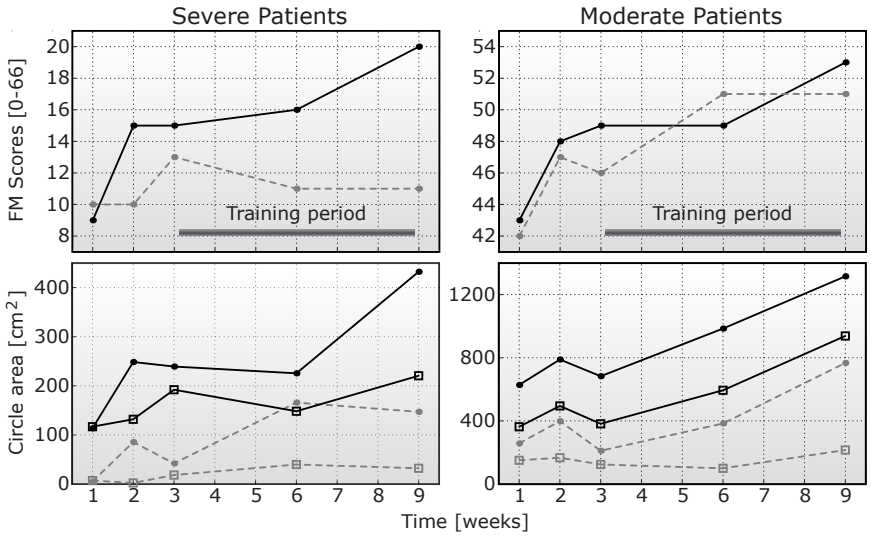

Figure 5.3: Fugl-Meyer (FM, top figures) and circle area (bottom figures) measurements for all subjects. The left figures give the results for the more severely affected subjects (P1: black solid line, P3: gray striped line), the right figures for the moderately affected subjects (P2: black solid line, P4: gray striped line). The separation was solely for figure readability: note the difference in scales. For the bottom figures: solid circles are with weight support, open squares are without.

To study the potential role of abnormal torque couplings over multiple joints, the shoulder plane of elevation $\beta_{sh,a}$ and the elbow β_{el} rotation angles of the circular movement are plotted against each other in angle-angle plots, for both the weight-supported and unsupported conditions.

5.2.7 *Descriptive analysis*

Initial analysis of the data obtained during baseline measurements revealed variations in motor performance but no clear trend was visible. Because of these variations the data of the baseline measurements were averaged per subject and compared with the data obtained during the evaluation measurement. Analysis of changes in outcome measures was performed descriptively rather than statistically because of the small sample size and the explorative character of the study.

5.3 RESULTS

5.3.1 *Subjects*

Initially, five subjects participated in this study. One withdrew after two weeks of training due to traveling and scheduling difficulties resulted in a too high physical burden. Data from this subject was excluded from further analysis. Demographic data at baseline of the remaining four subjects are displayed in Tab 5.1.

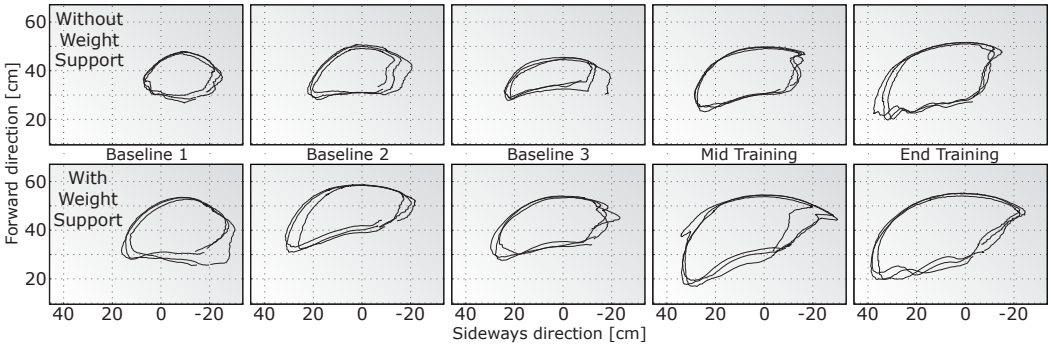

Figure 5.4: Single subject example of circle area changes over the baseline measurements (left three figures), and the measurements half-way true (3 weeks, fourth figure) and at the end of the training period (6 weeks, right figure), for both without (top figures) as without weight support (bottom figure) during measurements. The circle areas are for subject P2 and in the counter-clockwise direction

5.3.2 *Clinical evaluation*

Clinical evaluation of arm function is based on the upper extremity component of the Fugl-Meyer (FM) assessment (maximum score: 66 points). FM scores before the start of the training period in Fig. 5.3 (top figures) are three baseline measurements, during which some FM variability is seen. All subjects showed higher FM scores after the training compared to the initial score, indicating a decreased level of impairment. Individual changes from the mean of the baseline scores to the final FM score did not reach clinical relevance, defined as a 10% improved in scores [65].

5.3.3 *Circle area*

Although a slightly larger area of CCW circles at baseline was observed, we found no indications that CW and CCW movements were affected differently, and therefore the CW and CCW results are lumped together.

SUBJECT	AGE [YEARS]	SEX	DOMINANT SIDE	POST-STROKE [MONTHS]
P1	53	M	Right	59
P2	72	F	Right	14
P3	55	F	Right	28
P4	53	F	Right	24
GROUP MEAN	58	-	-	31

Table 5.1: Patient demographic characteristics at baseline.

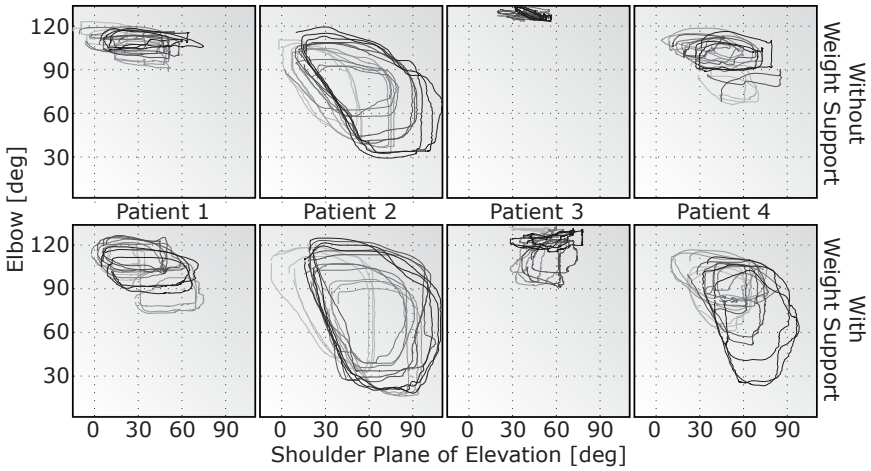

Figure 5.5: Angle-angle plots for the circle tasks of the shoulder plane of elevation $\beta_{sh,a}$ and elbow rotations β_{el} for all four subjects (left to right), with and without weight support, and with the development during time (in five steps from lightest gray for first baseline measurements to black for final evaluation).

In Fig. 5.4, the circle area over the baseline and evaluation measurements are plotted. Note the increase of area both over time and when changing the measurement condition from without to with weight support. In Fig. 5.3 (bottom half), these areas are averaged over all three CW and three CCW rotations, and plotted against time. Compared to the baseline values, all subjects increased their active range of motion.

5.3.4 *Joint couplings*

To study the potential role of abnormal couplings of joint torques during circle drawing tasks, the shoulder plane of elevation $\beta_{sh,a}$ and elbow rotations β_{el} are plotted against each other in an angle-angle plot (see Fig. 5.5) for both the supported and unsupported condition. All subjects have larger angular ranges for both the shoulder and the elbow with weight support compared to without. Subject P3 is unable to do voluntary elbow displacement without weight support, but able to do some with. During the intervention (from the light gray to the black lines), the angular ranges increase for all subjects.

5.4 DISCUSSION AND CONCLUSIONS

The objective of the present study was to examine if the movement performance of chronic stroke patients improves after weight-supported training in the Freebal in a virtually augmented gaming environment. The second objective was to determine if any improvement can be specifically accounted to the reduction of the influence of abnormal joint-torque couplings during unsupported arm movements. Our results indicate that arm function improved slightly, as observed by increased FM scores after training, but the improvement wasn't statistical significant over the four patients. This corresponded with increased areas of drawn circles. Both the

shoulder and elbow angular ranges also increased when no weight support was present, indicating a decoupling between shoulder elevation $\beta_{sh,b}$ torques and shoulder plane of elevation $\beta_{sh,a}$ and elbow β_{el} torques. Therefore, training with the passive Freebal has the potential to improve movement performance through reducing the abnormal multi-joint torque couplings.

5.4.1 *Influence of abnormal couplings on arm movements*

We observed that circles drawn by stroke patients were elliptical instead of round, which may indicate that the shape is influenced by abnormal torque couplings [37]. Indeed, when looking at the angle-angle plot of Fig. 5.5, many patients had lower angular ranges without weight support than with. This indicates that, although the patients were able to perform some voluntary rotations, they are unable to achieve the same amounts when they also need to maintain a lifted-arm posture. To maintain such an arm position without weight support, shoulder elevation $\beta_{sh,b}$ torque is required, which has been shown to reduce the voluntary elbow extension β_{el} torque and rotational range [36, 11, 206]. Fig. 5.5 indeed indicates that increasing the required shoulder elevation $\beta_{sh,b}$ torque reduces the elbow β_{el} rotation ranges for all patients. The shoulder plane of elevation $\beta_{sh,a}$ rotation seems less affected by a coupling to the shoulder elevation $\beta_{sh,b}$. The lesser affection of plane of elevation $\beta_{sh,a}$ rotation is in agreement with the study of Sukal et al. [206] (where $\beta_{sh,a}$ is reported as shoulder horizonal flex/extension), but contrary to Dipietro et al. [37] (where $\beta_{sh,a}$ is reported as shoulder horizonal ad/abduction). The latter could be due to the differences in required axial humerus rotations.

5.4.2 *Change in influence of abnormal couplings after training*

The present study indicates that the active range of motion can be enlarged by a training program applying weight support, as observed by the improvements in circle area after training. Comparable increases in range of motion have been found due to instantaneous application of weight support on circular and point-to-point reaching movements of stroke patients [11, 164, 206]. Due to support of the arm, the need to generate muscle activity for elevation of the arm is decreased and its involuntary coupling to elbow flexion is reduced, so that larger elbow extension excursions are possible. Again, this is seen in the angle-angle plots of Fig. 5.5.

Active range of motion is regarded as a robust measure to quantify the influence of abnormal joint torque coupling [47]. The observed improvement in active range of motion over the duration of the intervention in the present study suggests that the influence of abnormal torque coupling may be reduced after weight-supported training. When looking closer at the training-induced changes in angular movement patterns during unsupported arm movements, this impression is supported. After the training period, all subjects had a greater angular range for both the shoulder plane of elevation $\beta_{sh,a}$ and elbow β_{el} rotation in the unsupported condition.

Another intervention has also shown to have the ability to reduce the influence of abnormal torque couplings on unsupported arm movements. After training of simultaneous isometric shoulder and elbow torques outside of the typical synergistic patterns, the strength of the abnormal isometric coupling between

shoulder and elbow torques decreased [45]. Isometric strength training can reduce the influence of abnormal torque couplings, but it is not known whether this would translate to dynamic, unsupported conditions.

This raises a question about the role of muscle strength on the occurrence of abnormal torque couplings. Increased muscle strength of shoulder abductors or strengthening of elbow extensors relative to elbow flexors may be related to the reduction of abnormal torque couplings after isometric strength training. However, additional analysis showed no such correlation [45]. A recent study indicated that synergistic constraints on unsupported reaching movements of chronic stroke patients were unrelated to muscle weakness and imbalance of muscle strength between agonists and antagonists at the elbow [12]. This suggests that the synergistic movement patterns are more likely related to neural constraints, due to use of alternative neural pathways, such as via corticoreticular and then reticulospinal paths, in case of damage to the highly selective corticospinal tracts [36, 206, 46].

5.4.3 *Change in arm function after training*

The indicated improvements in independence and selectivity of unsupported shoulder and elbow movements after weight-supported training corresponded with increases in the maximal range of circular arm movements. Translation of these improvements on impairment level to more functional arm use is represented by a 7.5% increase in FM score in three out of our four patients. An improvement of 10% has been regarded as the minimal change needed for increased use of the limb in daily life [65]. This limit is approached in the present study, even though data of only four patients is available and the intensity of training is only moderate and its duration is comparatively short. Most of the other studies using weight-supported training are eight weeks, three days a week, for 45 minutes, compared to our six weeks, three days a week, for 30 minutes of ours. This suggests that weight-supported training might be able to stimulate functional recovery of the arm.

This indication is supported by a few studies. A study applying weight-supported training using a passive exoskeleton during virtual functional exercises showed comparable improvements in arm function and range of motion as found in the present study [180]. Another study with the same weight support device also showed improved arm movement ability [85]. In addition, reach training by de-weighting the arm via sling suspension resulted in improved motor status of proximal arm function [5]. Adequate hand function is required before full functional use of the arm can be achieved, which is an important addition to these interventions in future research.

In the present study, the FM assessment is regarded as the outcome measure indicating functional recovery of the arm. Other functional outcome measures, such as the Action Research Arm test, focus more on ADL-related tasks. Such measures put more emphasis on distal arm and hand function than the FM assessment. Since the current intervention was predominantly focused on the proximal function in shoulder and elbow, the FM assessment is regarded as the best impairment measure available. It is able to detect changes in patients with moderate to severe impairments after stroke, based on the stages of recovery with respect to movement synergies noted after stroke [62, 65]. These aspects correspond well with the focus of the involved interventions. In this light, the

outcome of the present explorative study is promising regarding the potential of weight-supported training to improve functional aspects of the arm.

5.4.4 *Passive versus active devices*

Compared to an active system, a passive weight-support device like the Freebal [201] has the advantage of being cheaper, easier and safer to use. The Freebal itself has no electronic components, although the FurballHunt game does require a computer, monitor and webcam. With a couple of mechanical scales in series with the cables, the arm weight is easy to measure. The spring attachment point in the ideal spring mechanisms can be quickly adjusted depending on the desired percentage of weight support before and during usage. As a passive device, its interaction with the human arm is inherently safe. Only a mechanical failure—broken spring mechanism or cable—could harm a patient via a sudden removal of the weight support.

The major disadvantage is the inability to automatically adjust the support force, run exactly scripted training sessions, or to add other virtual interaction elements. For example, some patients may benefit from a stabilizing, virtual damping field reducing painful tremors. Less severely affected patients may need negative weight support for optimal training levels. Although negative weight support could be realized by adding weights to the arm, an active system like the ACT-3D [206] could do this quicker, easier, and without adding movement inertia.

5.4.5 *Implications and recommendations*

When looking at common aspects between the three interventions that are able to reduce the influence of synergistic movement patterns, weight-supported training, robot-assisted point-to-point reach training and double-task isometric strength training, simultaneous activation of shoulder and elbow may be a key element. This enables natural, 3D movements as opposed to single joint training. Such functional and meaningful exercises are related to motor and functional recovery of the arm via normalization of cortical activity [55, 181, 144].

Furthermore, in two of those interventions, active generation of muscle forces is crucial (weight support and isometric strength training). Active initiation and execution of movements has also been shown to be very important to stimulate arm recovery [99]. Besides this, training exercises should commit to aspects that optimize motor (re)learning of a task, such as augmented feedback, motivation and adaptable levels of difficulty [39].

The intervention in the present study incorporated several of these key aspects. It required self-initiated 3D reaching movements during training, in a motivating and challenging virtual environment, providing feedback of results. This combination of aspects during only moderate intensity training showed promising results in the present study. Adaptation of the virtual environment to stimulate functional movements even more may enhance this potential of weight-supported training. Support for this is provided by other explorative studies where stroke patients improved arm function after training using weight support in combination with simulated functional tasks, which incorporated a hand grip pressure sensor, to accentuate the functional and meaningful character of the movements [180, 85].

Despite the small number of participants in this study, the present explorative study suggests that weight-supported training with a simple supportive device has the potential to decrease the influence of abnormal torque couplings on arm movements of chronic stroke patients. These results are achieved without specific exercises targeting abnormal couplings, although many of the movements did require movements outside of the synergetic patterns. Further research into the effect of weight-supported training with robots is warranted, to enhance insight into optimal application of this intervention in clinical practice.

Part III

REHABILITATION EXOSKELETONS

6

SELF-ALIGNING JOINT AXES FOR UPPER-EXTREMITY EXOSKELETONS

ABSTRACT Exoskeletons are well suited for direct joint manipulation and recording. For an exoskeleton to function correctly, its axes need to be closely aligned to the human axes to prevent painful interaction forces. We propose to decouple the joint rotations from the joint translations. The goal of this paper is to determine the suitability of the decoupling for use in upper-extremity rehabilitation robots. Decoupling allows the exoskeleton to align itself to the anatomical axes. The rotations are still controlled but the joint can freely translate when realignment is required. Decoupling reduces setup times and gives the responsibility of solving any joint misalignment to the exoskeleton and not to the human musculoskeletal system, to the trunk, or to the soft tissue between the arm and the exoskeleton. Any interaction force have to be passed to the arm as torque pairs, as any single force would be absorbed by the freedom of translation. The mechanism removes the reaction forces in the joint from the actuation, but also requires two cuff connections per segment, reducing interaction stiffness. Another disadvantage is the increased complexity. In conclusion, we found the decoupling to be an essential advantage for the shoulder joint, and useful for the elbow joint. We used the decoupling principle for two exoskeletons, the passive Dampace, for force-coordination training, and the upcoming hydraulically powered Limpact, for quantifying movement disorders and assist-as-needed training.

6.1 INTRODUCTION

Patient-friendly robots are used as diagnostic and therapeutic aids in upper-extremities rehabilitation. Through physical manipulation of the arm and assisted by virtual environments, innovative interaction schemes are explored in search of the best possible therapy. Overall, robot assisted therapy is considered to be as good or better than conventional therapy [219, 157, 162, 112]. It is more challenging for the patients and less labor intensive for the therapists, and has provided the physicians, therapists and scientific community with more reliable data.

Robot rehabilitation devices for the upper-extremities can be grouped into endpoint manipulators, exoskeletons and cable suspensions. Endpoint manipulators have a single connection to the hand, wrist or forearm [81, 22, 169, 120, 206]. For most of these, patients hold onto a handle while making movements in virtual environments. Exoskeletons are external skeletons placed over the arm and mostly powered by actuators on the joints [140, 179, 61, 143, 27, 154]. They control not only a single endpoint position, but also (a subset of) the joints of the shoulder, elbow, and wrist directly, at the cost of more complex mechanics. Cable suspensions [129, 127, 201] link one or more cables to the arm, increasing both control options and complexity with every additional cable linkage. In the simplest form with

Submitted: IEEE Transactions on Robotics (AHA Stienen, EEG Hekman, FCT van der Helm, and H van der Kooij).

overhanging cables and counterweights, cable suspensions have been used by rehabilitation hospitals for decades as weight-support devices.

Exoskeletons are well suited for direct manipulation and measuring of the joint angles and torques. The external skeleton runs parallel to the upper and forearm and has actuators and sensors directly on the joints. Unfortunately, for typical exoskeletons to function correctly, their axes need to be closely aligned to the axes of the human joints. Without correct alignment, the exoskeleton will feel uncomfortable in use [186], up to the point of becoming unusable. Aligning can take as much as five to fifteen minutes, cutting into the valuable rehabilitation time available for each patient.

Three reasons make alignment difficult to attain. First of all, human joints are seldom simple hinges. The shoulder girdle, for example, has not only three rotational degrees of freedom, but also two translational ones due to the rotation of the clavicula with respect to the thorax [175, 233]. Humans have some voluntary control over shoulder translations, but the vertical translation is also coupled with the shoulder elevation rotation [117]. This coupling is known as the scapulo-humeral rhythm. Secondly, the exact location of the human axes cannot be seen from the outside without the help of imaging devices. Bony landmarks only give a general approximation of the location of the rotation axes, which significant differences between people. Finally, the positioning of the exoskeleton on the arm may differ between therapy sessions, thus always requiring final adjustments even if device settings are stored for later recollection. But even when close alignment is achieved before therapy is started, the cuffs may slip during usage, requiring further adjustments [30].

Current exoskeletons solve the joint alignment and shoulder translation problems in different ways. The CADEN-7 [154] and the L-EXOS [61] use no additional mechanisms, but do not fix the trunk and thereby force the body to make any necessary translations relative to the exoskeleton shoulder position. The different variations of WREX exoskeletons [179, 180] have additional two-link mechanisms for horizontal shoulder translations with two degrees of freedom. The ARMin [143] uses an vertical four-link mechanisms which couples the shoulder elevation rotation of the exoskeleton to its vertical shoulder translation with a single degree of freedom. Finally, the MGA-Exoskeleton [27] adds a rotational degree of freedom to the shoulder, mimicking clavicula rotations to produce the vertical translations for the exoskeleton shoulder.

For all of the above exoskeletons, the elbow and shoulder joints need to be aligned as closely as possible to minimize any possible problems. By adding a large number of passive links to the actuated ones, the ESA exoskeleton [186] requires no joint alignment. But its actuators and linear-motion joints are optimized for low-force haptic interaction to control space robots, and are underpowered and unsuitable for many rehabilitation exercises.

We propose to decouple the joint rotations from the joint translations to create self-aligning axes. This lets the exoskeleton shoulder and elbow joints align themselves to anatomical joints. It should prevent painful interaction forces and prevent compensatory trunk movements. The larger allowable mounting variability could reduce setup times to less than a minute. A decoupled joint can only be powered by torques and not by single forces, which may or may not be an advantage.

The goal of this paper is to determine the suitability for use in upper-extremity robots. This paper describes the decoupling of the joint rotations and translations for the shoulder and elbow joints, the mechanical requirements, the advantages

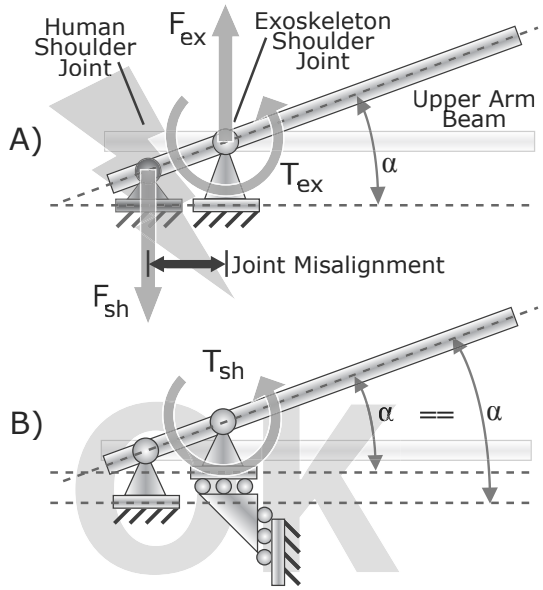

Figure 6.1: Self-alignment for exoskeletons axes in a planer view. A) The effects of a single misaligned axis at the shoulder. Due to exoskeleton torque T_{ex}, the arm and exoskeleton axes rotate an angle α. If these axes are misaligned, the human joint has to translate relative to the exoskeleton axis. If the axes are fixed, this movement creates a residual shoulder force F_{sh}, dependent on the stiffness of skin and bone, and an equal exoskeleton reaction force F_{ex}. B) Translating exoskeleton axes prevent these misalignment forces. If a misalignment causes a force F_{ex}, the exoskeleton translates until this force is gone. Torques can be applied to the limb from the rotational-stiff linkage mechanism. In 3D, the effects are the same, with adding the two other rotational axes requiring only one additional linear axis.

and disadvantages, and two implementation examples. With the decoupled design presented here, an alternative to the conventional design is established, which may overcoming many of the problems traditionally associated with exoskeletons.

6.2 ANALYSIS

6.2.1 *Decoupling of rotations and translations*

Most exoskeletons are firmly connected to the global world. When its axes are misaligned, any rotation forces relative translations on the human joint (see Fig. 6.1A). This translation is forced on the skin, the internal musculoskeletal system, and the trunk. Of these, the musculoskeletal system may not be able to translate in a required direction and the trunk can be practically unmovable when fixed to a chair or having a large movement inertia. In such a situations, the forced translation will result in large depressions of the soft tissue between the exoskeleton and the human skeleton. Depending on the amount of misalignment, the tissue depression can be from annoying to painfully limiting, especially for patients with skin-sensitivity problems. To prevent this situation from occurring, the axes need to be perfectly aligned, requiring long setup times.

By mounting the exoskeleton on a parallel linkage system instead of directly to the global world, the translations and rotations in the exoskeleton joints are decoupled (see Fig. 6.1B). The linkage system can freely translate in any direction, solving joint misalignments instead of requiring the human body to do so; whenever a misalignment generates a reaction force, the linkage will move until a new zero-force position is reached. The endpoint connector of the linkage needs to always maintain its original orientation and should have sufficient torsional stiffness to let the exoskeleton generate torques from it onto the human arm.

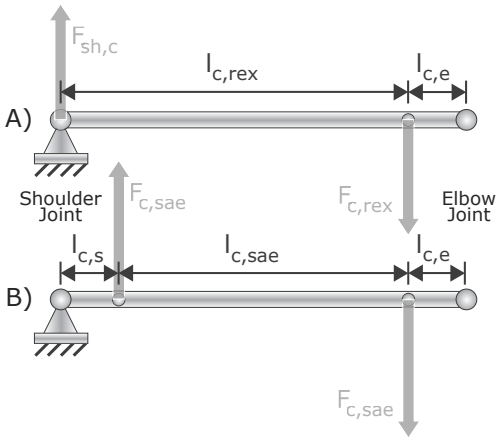

Figure 6.2: Isometric force interaction of the arm with a regular exoskeleton (A) or a self-aligning exoskeleton (B). The regular exoskeleton requires only one cuff where it exerts the interaction force $F_{c,rex}$, and thereby generates the shoulder reaction force $F_{sh,c}$. The self-aligning exoskeleton exerts pure torques to the limb, requiring two cuff connections with interaction forces $F_{c,sae}$. The resulting torque is the same, but the cuff distance $l_{c,sae}$ for the self-aligning exoskeleton is shorter than the distance $l_{c,rex}$ of the regular exoskeleton, requiring slightly greater forces. The shoulder cuff is positioned just below the arm pit at distance $l_{c,s}$ from the joint rotation center. The elbow cuff is positioned just above it at distance $l_{c,e}$.

The decoupling of translations and rotations influences the force interactions between the exoskeleton and human limb (see Fig. 6.2). Conventional exoskeletons apply single forces to the limb, generating a reaction force in the shoulder. The musculoskeletal system of the trunk needs to counteract this reaction force. With the decoupled mechanism, applying single forces to the limb becomes impossible, as the accompanying reaction force would simply translate the linkage. Instead, the forces must be applied pairwise as torques. The forces felt by the arm from the external mechanisms (linkage and exoskeleton) now consist of the impedance forces due to (rotational) inertia and friction. These reaction forces are generally much lower than the aforementioned misalignment forces and the reaction forces caused by the single-force interaction, especially for low-speed movements. The local forces caused by muscle activation around each joint are, of course, still present.

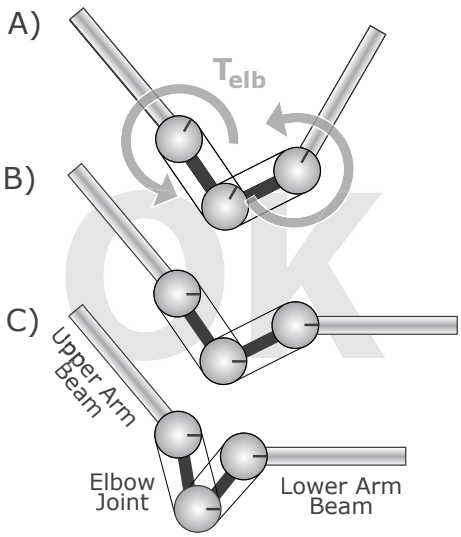

Figure 6.3: The implementation of the self-alignment of Fig. 6.1B for the elbow joint. The elbow joint has two extra links and two parallelograms transfer the forearm orientation to the upper arm. Translation of the joint is now independent of rotation (from C to B), and vice verse (B to A), removing the requirement for close elbow alignment. At the upper arm, the rotation can be controlled and measured; a torque applied here runs through the parallelogram and is applied to the forearm, without causing reaction forces in the elbow. The parallelogram can be created with cables and drums (as shown here), or with a push-pull design with rods.

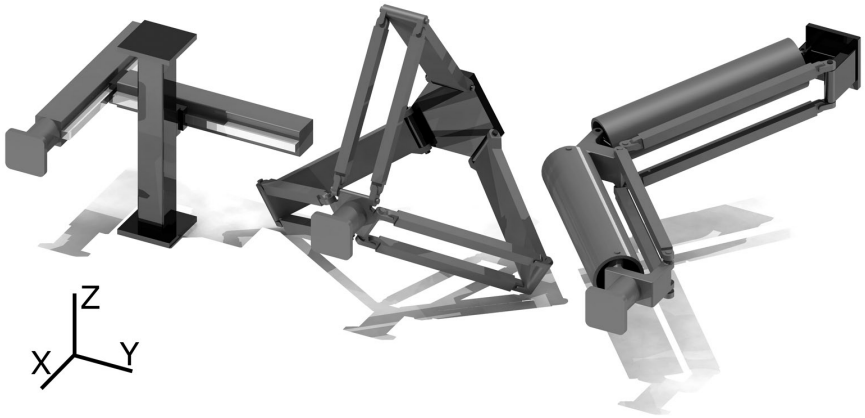

Figure 6.4: Three linkages which can translate freely in 3D space, but are rotational-stiff around any axis. From left to right: a linear guidance (LG) mechanism, based on linear-motion slider rails, a parallel hexapod (PH) as found in the Delta Robot [67], and a double 3D parallelogram (DP). The exoskeleton would be mounted to the front plate and the black base plate to the global reference frame.

The pairwise forces do require two connections of the exoskeleton to the limb per section. This additional cuff per section is a disadvantage, especially when it needs to be located over soft skin and muscle tissue. This significantly reduces the interaction stiffness between exoskeleton and arm.

An advantage of the pure-torque driven actuation is that it has now become independent of any positional misalignment, body supplied reaction forces, or torques applied to other joints. Also, for perpendicular limb orientations, torques applied around one joint will not cause the the exoskeleton to slide over the arm. For instance, when torques are applied to the elbow, the shoulder feels no forces other than due to inertia and friction, making selective training of muscles possible. Furthermore, any torques can be directly measured without interference from other joints. However, when endpoint forces are needed, the applied torques are less realistic than applied forces by conventional exoskeletons. Although those are also less realistic than endpoint forces generated with endpoint manipulators.

The decoupling at the human shoulder requires a full 3D linkage and three rotational degrees of freedom, but the elbow can make due with a 2D linkage and a single rotation degree of freedom (see Fig. 6.3).

6.2.2 *Comparison of linkages*

The design of the linkage influences the experience of the subject. As described in the section above, the impedance forces felt are due to friction and inertia in the linkage and exoskeleton. Therefore, three linkage designs were compared on their range of motion, stiffness and impedance forces hindering movement. The three designs are the linear guidance (LG) mechanism, the parallel hexapod (PH) and the double 3D parallelogram (DP), see Fig. 6.4. The linear guidance mechanism is based on linear-motion slider rails, which also have to provide the torsional stiffness. The parallel hexapod get its torsional stiffness from the parallel rods

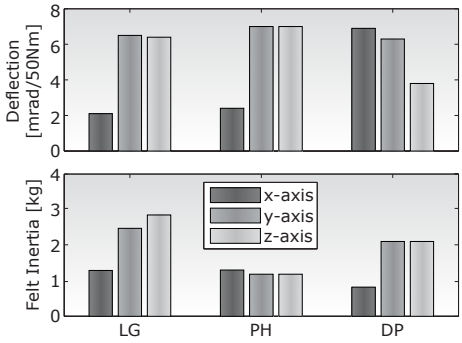

Figure 6.5: Comparison of the stiffnesses and felt inertia of the three linkages at the center of the workspace. The linkage dimensions were adjusted to have roughly equal deflection at 50 Nm of torque (top figure). The inertial matrixes are displayed in the bottom figure. For LG and PH, the eigenvectors are along the XYZ-axes as indicated in Fig 6.4; for DP, 'x-axis' indicates the eigenvector perpendicular to the lower parallelogram ([-0.7 0.7 0]), and 'y-axis' the eigenvector perpendicular to the upper parallelogram ([0.7 0.7 0]).

connected to the base plate. In the normal workspace, almost no segment receives significant torsional load, making it possible to use very thin-walled push-pull rods. The double 3D parallelogram uses one torsional-stiff thin- walled tube with a large diameter, and two push-pull rods per segment to handle the torsional loads around any axis.

All designs were created to have a cubic 300x300x300 mm workspace and a stiffness roughly equal to 6.5 mrad distortion when loaded with 50 Nm in a direction. A 6.5 mrad rotation equals a 7 mm translation at 1 m from the center of the linkage front plate. The workspace requirements defined the segment lengths: respectively 350, 275 and 375 mm, for the linear guidance, parallel hexapod and the double 3D parallelogram. The desired stiffness defined the segment strengths and the distance at which parallel members were placed from each other, with the dimensions and weights given in App. 6.3.1. Using COSMOSWorks (Dassault Systemes) to do the finite-elements calculations on the models, the beam and rod dimensions were adjusted until their stiffnesses roughly matched (see top half of Fig 6.5). These deflections were measured at the center of the work volume, representing the normal, ideal situation, when only small translation are necessary. The mechanisms were designed to have stiffnesses as independent from orientation as possible and none will get into an extreme configuration to reach the edges of the required workspace. Toward the edges of the work volume, the deflection per Nm of torque will increase exponentially with about 10% for all three designs (data not shown).

With the workspaces and stiffnesses closely matched, the inertial matrices were determined with Spacar [97], a multibody-dynamics analysis package (see Fig. 6.5). The linear-motion slider rails used in the linear guidance system has a load dependent friction of about 4 to 20 N. The rotational joints of the other two mechanisms have no significant friction. Coulomb friction is highly undesirable in these linkages, as it is felt at any movement speed and can be a significant force to overcome for all patients (also see Fig. 6.10).

From these simulations, the parallel hexapod has the least amount of inertia and friction, closely followed by the double 3D parallelogram. The impedance forces of the latter strongly depend on the direction of movement as it is a two link mechanism: for endpoint deflections perpendicular to the first stage, half the first stage and the full second stage will move, whereas for deflections perpendicular to the second, only halve the second stage will move. The average inertia for all three eigenvalues of the inertia matrices stay invariant over the work volume for the linear guidance, varying up to 10% for the parallel hexapod, and up to 20%

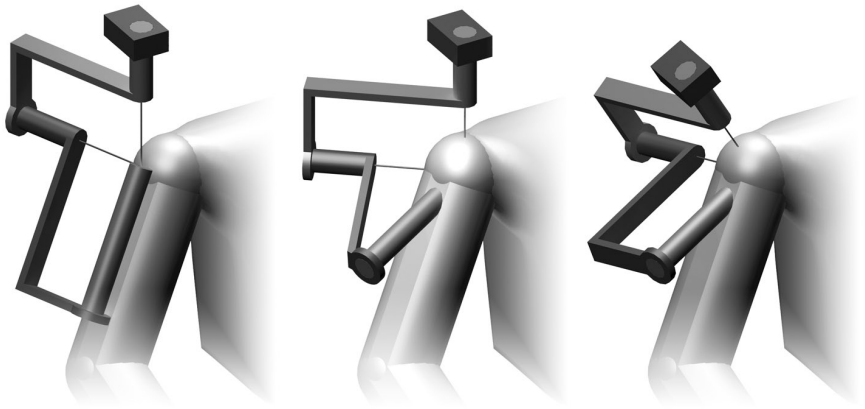

Figure 6.6: Possible configurations for the shoulder axes. Due to the decoupling of the rotations and translations, the third exoskeleton shoulder axis can be positioned parallel to the shoulder axial rotation axis (left figure). This configuration, as in the Dampace [202, also see Chap. 8], generates high levels of linkage movement and inertial forces. To reduce these and to stay away from gimbal-lock orientations, the third exoskeleton axis can be positioned at a 30 degree angle (middle and right figures). The axis now points to the glenohumeral rotation center. To optimize the shoulder range of motion, either the third exoskeleton axis is not perpendicular to the second axis (middle figure), or the first axis is positioned at an angle to the vertical (right figure). Both still restricts the shoulder negative elevation rotation to 90 degrees as verified with 3D modeling software.

for the double 3D parallelogram, again all exponentially increasing at the edges but more or less constant in the middle (data not shown).

Three other design considerations need to be made: the possibility to add a passive weight support mechanisms, the amount of space used by the segments in the linkage design, and possibility to add actuators to the linkage. The first, passive weight support, supports the weight of the mechanism without hindering the patient. It is most difficult to add to the parallel hexapod as it has multiple degrees of freedom resulting in vertical translation, with each requiring a separate weight support mechanism. Both the linear guidance system and the double 3D parallelogram only have one vertical degree of freedom, on the easily accessible first segment. The second, the amount of space used, may lead to the linkage interfering with the exoskeleton or body movements. Most space is used by the parallel hexapod as its three legs always point away from each other, whereas the other two use much less space. Finally, adding actuators can further reduce the impedance by employing an admittance control loop. This is easiest added to the parallel hexapod as all three actuators can be mounted on the base, working on the three single-axis segments there. Such actuation may also be used to provide active weight support but this would add a continues electrical load to the actuators. The other two system require either complex cabling systems or need to mount the heavy actuators directly on the segments.

Based on the ability to add passive weight support and its slender design and low space requirements, the double 3D parallelogram is considered best suited for

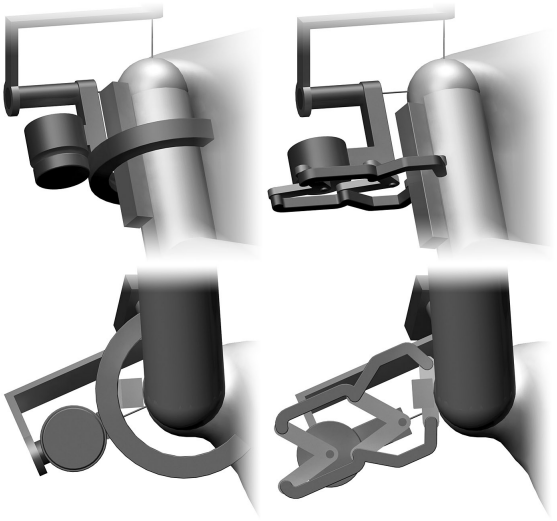

Figure 6.7: Alternative third exoskeleton axis configurations. In the left figures, the third axis is realized with a semi-circular guiding rail, powered by a motor directly attached to it. This configuration is often used in current exoskeletons [143, 154, 61], but requires the high-friction and heavy guiding rails. Alternatively, an external rotation center mechanism can also realize the rotation around the shoulder axial rotation axis (right figures). The mechanisms has to parallel bars, and centers around the main joint connection, with one side of the bars powered by an actuator, and the other connected to off-center connections to the arm. The bottom figures are the bottom views at the mechanisms of the upper figures.

a linkage system. When space requirements are less stringent, the parallel hexapod definitely warrants further investigations.

6.2.3 *Shoulder axes configurations*

The decoupling of translations and rotations loosens the requirements for exact axes orientation for the three shoulder rotations. As the linkage can take care of necessary exoskeleton realignments, the axes do not necessarily have to follow through the glenohumeral rotation center of the shoulder. However, any movement of the linkage will generate impeding forces and should be reduced as much as possible. The axes orientation is also a balance between staying away from singular configurations—when two axes are inline (gimbal lock) the accelerations and thus inertial forces are amplified—reducing potential movement and inertia of the linkage, and obtaining the desired range of motion possible.

Positioning the third exoskeleton axis parallel to the shoulder axial rotation axis (see Fig. 6.6, left) gives a misalignment of about 50 to 100 mm, depending on the thickness of the arm. This results in translations of the linkage of twice this amount for shoulder axial rotations, which is undesirable. The third exoskeleton axis can also be directed through the glenohumeral rotation center, but this requires additional changes to the axes orientation and reduces the shoulder negative elevation rotation to about 90 degrees (see Fig. 6.6, middle and right figures).

Alternatively, the third exoskeleton axis may be aligned closer to the shoulder axial rotation axis by using additional mechanics (see Fig. 6.7). Many exoskeletons [61, 143, 154] use the open, semi-circular slider rail, but this is has several disadvantages, mainly due to the weight of the steel rail, the friction in the bend-around linear bearings, and the lack of stiffness. Using an external rotation center mechanism, based on rotational bearings, is stiffer and lighter than the semi-circular

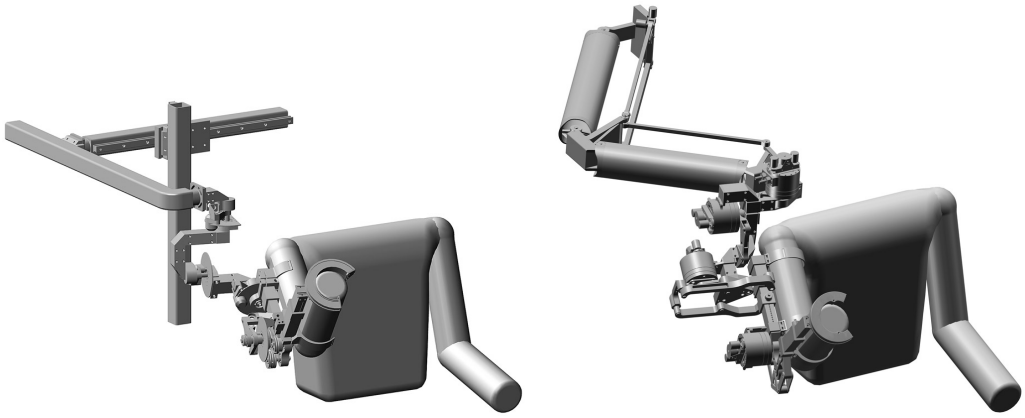

(a) Dampace (b) Limpact

Figure 6.8: (a) The Dampace exoskeleton [202, also see Chap. 8] has powered hydraulic disk brakes on the rotational axes of the shoulder and elbow. It uses the linear guidance linkage system and the parallel shoulder axial rotation axes. The friction of the first and the high movement amplitudes of the second result in significant impedance during rotation of the self-aligning joints. (b) The Limpact exoskeleton [204, also see Chap. 9] uses rotation hydro elastic actuators on its shoulder and elbow joints. With the lessons learned from the Dampace, it uses the double 3D parallelogram linkage mechanism and the external rotation center mechanisms at the shoulder axial rotation axis. The cabled design of the elbow joint of the Dampace has been replaced by a push-pull mechanism, which is stronger and requires less maintenance.

guiding rail. Any misalignment still present in either mechanism, for instance due to the varying thickness of the arm, will be handled by the linkage system.

6.2.4 *Example implementations*

The information presented in this paper is based on our experiences with the Dampace [202, also see Chap. 8] and Limpace [204, also see Chap. 9] exoskeletons (see Fig. 6.8a and Fig. 6.8b). The older Dampace uses the linear guidance linkage and its third shoulder axis runs parallel but with and offset to the upper arm. The already heavy and friction prone linkage thus has to move over large distances, especially for shoulder axial rotations. To improve on the performance, the new Limpact exoskeleton uses the double 3D parallelogram linkage and the external rotation center mechanisms for the axial rotations of the shoulder. For the elbow joint, the cables in the parallelogram have been replaced by a push-pull mechanism, which requires less maintenance.

With these two designs, the impedance of the three linkages were be compared. For each of the three shoulder axes, a 90° medium paced (0.5 Hz) sinusoidal rotation was simulated. The reaction force $F_{reaction}$ between a linkage and exoskeleton were calculated for forces caused by the inertia and friction of the linkage. Other forces, for instance caused by the inertia of the exoskeleton and arm, were ignored in this comparison of linkages.

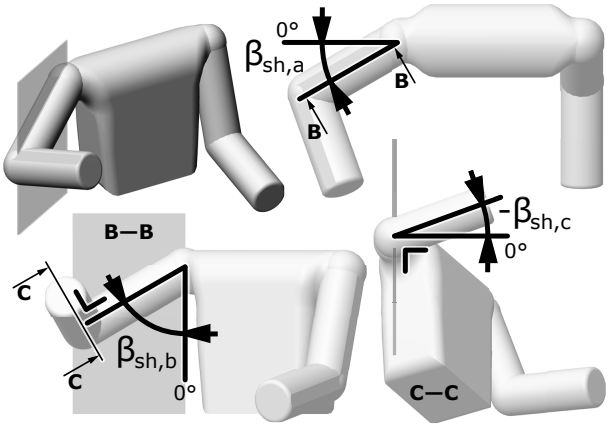

Figure 6.9: Shoulder rotations defined according to International Society of Biomechanics (ISB) [233]. Top-right: plane of elevation ($\beta_{sh,a}$). Bottom-left: negative elevation ($\beta_{sh,b}$). Bottom-right: axial rotation ($\beta_{sh,c}$). In this example, the shoulder is rotated by 30°, 60°, and -20° for the ISB-defined order of $\beta_{sh,a-c}$.

The shoulder axes were defined according to the ISB recommendations [233] for the thoracohumeral joint (see Fig. 6.9). The starting position of the exoskeleton was with the upper arm pointing forwards and the forearm pointing upwards. This results in shoulder plane of elevation ($\beta_{sh,a}$), negative elevation ($\beta_{sh,b}$), and axial rotations ($\beta_{sh,c}$) of respectively 90°, 90°, and -90°. From this initial orientation, three separate repetitive rotations ($\beta_{sh,a}$, $\beta_{sh,b}$, and $\beta_{sh,c}$) were performed to and from 0° for the axis under investigation.

The linear guidance used in the Dampace was compared against a theoretical linear guidance, parallel hexapod, and double 3D parallelogram for the Limpact. With the following equations, the reaction force $F_{reaction}$ was calculated as function of the angular position θ and its derivatives:

$$\begin{aligned} \theta &= \frac{pi}{4}(\cos(\pi t + \pi) + 1), \\ F_{reaction} &= -sgn(\ddot{\theta})\sqrt{(m_1 \sin(\theta)\ddot{\theta} r_m)^2 + (m_2 \cos(\theta)\ddot{\theta} r_m)^2} \ \ldots \\ &\quad -sgn(\dot{\theta})\sqrt{F_{fric,1}^2 + F_{fric,2}^2}, \end{aligned}$$

where F_{fric} the friction and m the inertia in a single direction, and r_m the misalignment for the axis. Numerical subscript '1' indicates the initial orientation, and '2' the orientation at 0° of the respective axis.

In the plot of Fig. 6.10, the large influence of the friction and the axis offsets in the Dampace are clear to see. By improving the orientation of the shoulder axes, the Limpact using the linear guidance has slightly less reaction forces. But only when the linkages with the rotational bearings are used do the reaction forces become almost insignificant.

6.3 DISCUSSION

Decoupling of the joint rotations and joint translations creates self-aligning exoskeleton joints. It removes the requirement of closely aligning the exoskeleton axes to the anatomical ones during setup. Decoupling gives the responsibility of solving joint misalignment to the exoskeleton, and not the human musculoskeletal system, the full body, or the soft tissue between the arm and the exoskeleton. By doing so, it prevents the interaction with the exoskeleton from becoming painful

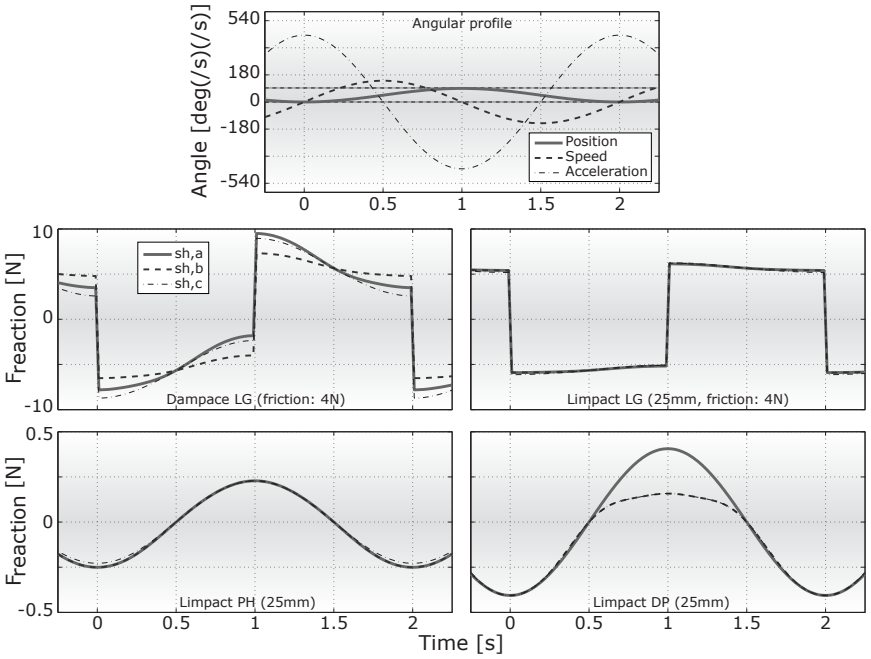

Figure 6.10: Reaction forces ($F_{reaction}$) at the linkage-exoskeleton connection caused by the impedance of the linkages. The top figure gives the angular sinusoidal profiles. The bottom four figures give the summed impedance forces caused by the friction and the inertia of the linkage. For the linear guidance of the Dampace, the misalignments were measured as 0.1, 0.04 and 0.08 m for the three shoulder axes (sh,a-c), and the inertia as 2.8, 5.0 and 5.3 kg for the x-, y- and z-axis. For the Limpact exoskeleton, a relatively large misalignment of 0.025 m was used for all axes, and the inertias from Fig. 6.5. The low friction of 4 N is only present in the linear guidance linkages. Note the difference in the scale of the bottom two and middle two figures.

[186, 185]. Decoupling also significantly reduces setup times, which is essential for use in stroke rehabilitation. The freely translating linkage gives the shoulder full freedom of translation, making voluntary and coupled translations [117] possible, independent of the rotations of the joint. Linkage translation also assist in adjusting the setup because of inter-patient differences in trunk height and width. Exoskeleton segment lengths still need to be adjusted when changing subjects. However, with decoupling, these adjustments do not need to be exact as they now have less influence on the joint alignment.

Several types of linkages can be used to decouple the rotations and translations. All of them significantly increase the device complexity. The three linkages in this study are all rotationally stiff, whiles allow translation in any direction. The parallel hexapod and double 3D parallelogram linkages require a large number of additional machined components and bearings. This makes the device heavier, more costly, and more likely to fail. Then again, the linkages aren't much more complex than the additional mechanics used for shoulder translations in the ARMin [143], the cable guiding mechanisms in the CADEN-7 [154], or the additional clavicula-limb in the MGA-Exoskeleton [27]. For reasons of minimal

space usage, low impedance and easy inclusion of weight support, the double 3D parallelogram is our preferred linkage.

An exoskeleton with decoupled joints can only transfer torques, which a possible second disadvantage. Single forces would just push the linkage away instead of being applied to the arm. Torque transfers requires two connections per segment. These can't always be located at bony parts of the arm and therefore reduce the overall interaction stiffness between the exoskeleton and limb. At the upper arm, one cuff can be positioned directly under the arm pit and the other just above the elbow, thus on either side of the biceps. For the forearm, the cuffs go just distal from the elbow and at the wrist. To allow pro/supination of the forearm, the wrist cuff needs to be able to rotate, possibly with an open, semi-circular guiding rail. The first three of these cuffs go on soft tissue, which is a problem for people with relatively slack tissue. For torques above 20 Nm, the cuffs will press on the skin and muscles, resulting in a mismatch between the elbow rotation of the exoskeleton and the arm.

For the shoulder joint, the decoupling also solves many of the misalignment problems caused by voluntary and forced translations. Conventional exoskeletons have less problems with aligning their elbow joints, but even there a self-aligning mechanism has the advantage of shorter setup times and less need for accurate positioning.

In this paper, the decoupling and the required linkages are described for the shoulder and elbow joint, but they could easily be adapted for the lower extremities. For the knee joint, the 2D self-aligning mechanisms could handle both the rotation and the coupled translation specific for this joint. For the hip joint, either several 2D mechanisms could be stacked, or one 3D mechanism used. A disadvantage specific for the lower extremities could be the mainly vertical orientation of the segments. As each exoskeleton segment is connected to each leg segment, without strong translational couplings to other exoskeleton segments, individual cuffs may slip due to gravity and cyclical inertial forces. It would not necessarily influence the self-alignment principle, but the cuff movement may irritate a subject.

6.3.1 *Conclusion*

Decoupling of joint rotations and translations creates self-aligning exoskeleton joints. This lowers potentially painful interaction forces and reduces setup times. The primary disadvantages are the increased complexity and the reduction in interaction stiffness. In conclusion, the decoupling is found to be an essential advantage for the shoulder joint, and useful for the elbow joint. The double 3D parallelogram is the preferred linkage mechanism.

The decoupling principle is used in two exoskeletons: the passive Dampace, for force-coordination training, and the upcoming hydraulically powered Limpact, for assist-as-needed training and quantifying movement disorders. So far, the reactions from therapists, patients and scientists have been almost exclusively positive.

APPENDIX

The main dimensions and weights of the three linkages from Fig. 6.4 are as follows.

The linear guidance (LG) linkage uses the 15 mm steel profile rail and carts from SKF. Its main tubes have a square 50x50 mm profile, 2 mm thick, and are 350 mm long, and are made from aluminium. On the end of the third tube, an endpoint spacer is located, which is needed to mount the exoskeletons at a safe distance from the mechanisms. The total weights for the x-, y- and z-axis and the endpoint spacer are, respectively, 991, 1180, 375, and 293 gr.

The parallel hexapod (PH) linkage uses at its base three rectangular 60x20 mm aluminium tubes, 1 mm thick and 275 mm from axis to axis. The second step is formed by six square 20x20 mm aluminium tubes, 1 mm thick and 275 mm from axis to axis. Each pair is spaced 70 mm apart, center to center. To endpoint spacer is identical to the one above. The weight of the bearings and helper constructions is summed at the three connection between base tube and thin tubes, totalling to 126 gram each. At the endpoint, the summed total is 778 gram. The base tube and thin tubes weigh 200 and 71 gram each. The starting position of the endpoint spacer is at its bottom 350 mm from the base.

The double 3D parallelogram (DP) linkage uses one thick and two thinner aluminium, 375 mm long, tubes at each stage. The thick tube is circular with a 90 mm diameter and 1.25 mm thickness, and has reenforced connection ends. The thin square 20x20 mm tube is 1.25 mm thick. The maximum parallel distance between the thick and thin tubes is 87 mm, and between the thin tubes 75 mm. The range of rotation for the vertical axis is always from 0 to 60°, centered around 30°, with the center angle used as offsets in the tube connectors to get the optimal working range. Rotation range around the single horizontal axis at the base is from -30 to 30°. The weight of each thick and thin tube is 494 and 102 gr respectively. In total, the moving parts in the first stage tubes, connector, second stage tubes and endpoint weight respectively 1090, 437, 698, and 582 gr.

7

HYDRAULIC DISK BRAKES FOR PASSIVE ACTUATION OF EXOSKELETONS

ABSTRACT Passive, energy-dissipating actuators are promising for force-coordination training in stroke rehabilitation, as they are inherently safe and have a high torque-to-weight ratio. The goal of this study is to determine if hydraulic disk brakes are suitable to actuate an upper-extremity exoskeleton, for application in rehabilitation settings. Passive actuation with friction brakes has direct implications for joint control. Braking is always opposite to the movement direction. During standstill, the measured torque is equal to the torque applied by the human. During rotations, it is equal to the brake torque. Actively assisting movements is not possible, nor energy-requiring virtual environments. The evaluated disk brake has a 20 Nm bandwidth (flat-spectrum, multi-sine) of 10 Hz; sufficient for torques required for conventional therapy and simple, passive virtual environments. The maximum static output torque is 120 Nm; sufficient for isometric training of the upper extremity. The minimal impedance is close zero, with only the inertia of the device felt. In conclusion, hydraulic disk brakes are suitable for rehabilitation devices.

7.1 INTRODUCTION

Patient-friendly robots are used as diagnostic and therapeutic aids in upper-extremities rehabilitation. Through physical manipulation of the arm and assisted by virtual environments, innovative interaction schemes are explored in search of the best possible therapy. Robot assisted therapy is more intensive and more challenging for the patients and less labor intensive for the therapists. It provides the physicians, therapists and the scientific community with more objectively gathered data.

For rehabilitation after stroke, robot assisted therapy is considered to be as good or better than conventional therapy [219, 157, 162, 112]. These reviews, and the systematic reviews on conventional therapy [187, 109, 8, 56, 119], indicate that intensive and task-specific exercises consisting of active, repetitive movements, give the best results. Interesting results are also achieved with exercises not directly resembling functional movements. Directly targeting the abnormal muscle-activation couplings over multiple joints [18, 11] improves the independent joint control and the achievable workspace [45, 37, 46, 47]. Training in which movement are made against resisting forces to improve muscle strength, potentially a bigger problem than the aforementioned loss of dexterity [146, 26], seem to regain both some quantity and control of muscle force [177, 84, 53, 199, 1, 100, 28]. The combination of functional exercises with dynamic, high-intensity resistance training looks particulary promising [147].

Our self-aligning exoskeleton for the upper extremities, the Dampace [202, also see Chap. 8], should be suitable for the task-specific, repetitive movements with

Submitted: Applied Bionics and Biomechanics (AHA Stienen, EEG Hekman, AC Schouten, FCT van der Helm, and H van der Kooij). *Patent pending:* Friction Control (EEG Hekman, AHA Stienen).

active patient participation. Active participation doesn't necessarily require active, energy supplying actuators. For movement- and force-coordination training, it may be sufficient to apply controlled resistance on the shoulder and elbow joints, as this still allows functional exercises with dynamic, high-intensity resistance. Overall, the selected actuators should be lightweight, powerful, and actively controllable.

Controlled resistance can be provided by strictly energy-dissipating, thus passive, actuators. Passive actuators are potentially lighter and inherently safe, both of which are very important in exoskeletons used in rehabilitation therapy. The disadvantages of passive actuators are that they can only apply resistance torques against movements, movements cannot be actively assisted [107, 168, 31, 24, 231], virtual environments are restricted to those which do not need external energy, and force exercises cannot be done eccentrically. It also requires a separate mechanism supporting the weight of the device and the limb.

Passive actuators can dissipate energy through dampers in conventional pneumatic, hydraulic and electric actuators, resisting respectively the flow of air, fluid or electricity, or through mechanical friction in conventional brakes. A recently developed damper uses electrical currents to control the damping in a magneto-rheological fluid [195, 198, 118, 196, 235]. These magneto-rheological dampers have been used in prosthetic knees [76] and resistance training devices [63, 41]. The resistive forces of all the above dampers are directly dependent on the magnitude of the speed of the actuator, making them difficult to control when combined with the highly variable movement patterns of stroke patients [38]. At almost zero speed and zero reference torque, most dampers will still have a residual friction torque present due to limited valve dimensions, fluid viscosity, or magnetic cogging. Mechanical brakes with pure coulomb friction are less dependent on the actuator speed and can be fully disabled, and are therefore chosen in the present design for further exploration.

Mechanical brakes, like hydraulic disk brakes used on mountain bikes, have a high torque-to-weight and torque-to-size ratio, but are untested for use in controlled rehabilitation robots. (Only very recently a similar bicycle disk brake was used in an elbow spasticity simulator [69].) Due to their commercially availability and lightweight and compact designs, the hydraulic disk brakes seem appropriate for providing the controlled resistance on the exoskeleton.

The goal of this paper is to determine if a hydraulic disk brakes are suitable to mount on an exoskeleton and to use for upper-extremity force-coordination training, by (1) designing an actuation and control system for the disk brakes, (2) analyzing the open-loop intrinsic and closed-loop system characteristics of the disk brakes, and (3) comparing the power- and torque-to-weight ratios to other passive actuators.

7.2 SYSTEM DESIGN

7.2.1 *Actuator requirements*

Structured conversations with several physicians, therapists and human movement scientists in the Netherlands resulted in a list of requirements for the exoskeleton and the actuators, including the torques needed for different force-coordination exercises as found in conventional therapy. The controlled disk brakes should be able to deliver 20 Nm of torque with a bandwidth of 5 Hz to dynamically resist arm movements of stroke patients during therapy [134]. These requirements

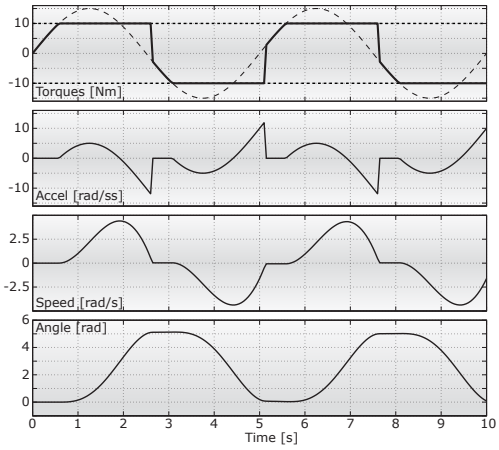

Figure 7.1: Theoretical effects of passive, energy-dissipating brakes on the control of joint angles. Top figure: the desired absolute braking torque $T_{br,des}$ at ± 10 Nm (short-stripped lines), the torque applied by the human on the joint T_{hum} as a 15 Nm sine (long-stripped lines), and the experienced brake torque $T_{br,exp}$ (solid line). Second figure: with unity inertia, this represents both the net-torque applied to the joint and its joint acceleration. The third and fourth figures: joint angular speed and angle. Note the complex dependency of the experienced brake torque $T_{br,exp}$ on the direction of the joint speed and the desired absolute braking torque $T_{br,des}$

should also be sufficient to generated simple virtual environments with which patients can interact. The minimal impedance, the torque felt when moving the arm while no torque is requested, is preferably as low as possible. For these patients, isometric-force measurements and training requires static torques up to 100 Nm. The disk brake construction should preferably weigh less than 1.0 kg to be directly mountable on an exoskeleton.

7.2.2 *Implications of passive actuation*

The use of the passive, energy-dissipating brakes which generate coulomb friction has three functional implications for the control of the joint angles, and therefore for the setup of the system. Firstly, the direction of the braking torque is always opposite to the direction of joint rotation and therefore cannot be manipulated by a control algorithm. Secondly, without movement, the experienced and measured braking torque is equal to the torque applied by the human and not to the potentially desired braking torque. Thirdly, with non-zero joint-rotation speeds the amount of experienced and measured braking torque is equal to the desired braking torque and not to the torque applied by the human. This is captured in the simulation of Fig 7.1 and the following equations, with $T_{br,des}$ the desired and $T_{br,exp}$ the experienced braking torque, T_{hum} the torque applied by the human on the joint, $\dot{\theta}$ the joint speed, and sgn the sign-function indicating direction:

$$T_{br,exp} = \begin{cases} -T_{hum} & \text{if } \dot{\theta} = 0, \\ -\text{sgn}(\dot{\theta}) T_{br,des} & \text{if } \dot{\theta} \neq 0. \end{cases} \tag{7.1}$$

7.2.3 *System setup*

The hydraulic disk brake needs to be powered by an active actuator to function. Therefore, a series elastic actuator (SEA) is connected to the hydraulic cylinder in the brake handle (see Fig. 7.2). The amount of joint resistance torque is regulated by controlling the internal hydraulic pressure with the output force of the actuator. A SEA has a better force output resolution than a directly connected electro motor and gearbox, at the cost of bandwidth performance [166, 171, 223, 214]. With a spring in series, the transferred force is measurable by the spring deflection and

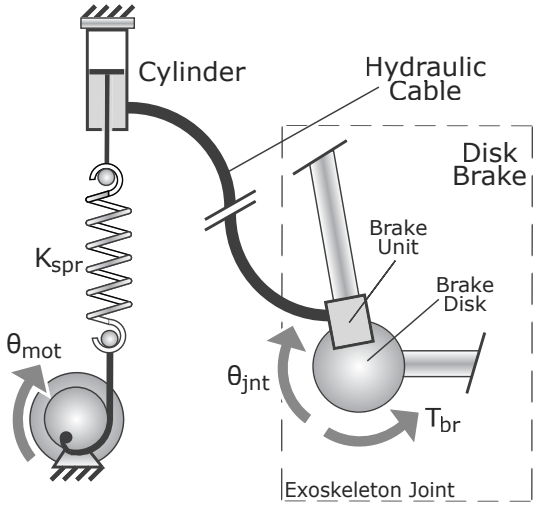

Figure 7.2: Disk brake as used on the exoskeleton joint, powered by a series elastic actuator (SEA) mounted on the base frame. The rotation of the motor θ_{mot} is converted by the spring with stiffness K_{spr} and the cylinder to a pressure in the hydraulic cable. This pressure is used to control the braking torque T_{br} on the exoskeleton joint. Note that the braking torque is always in the opposite direction of the joint velocity $theta_{jnt}$.

suffers less from torque output impurities of the motor due to gearbox friction or motor cogging. The series elastic configuration also makes it possible to use the motor angle in an inner control loop, and not depend on the conditional torque measurement at the joint (Eq. 7.1). Despite the active actuator, the braking torques in the actuator are still always opposite to the actuator rotation, ensuring passivity at the joint.

It is important to note that as soon as the brake pads in the brake unit engage the brake disk, the cylinder piston in the handle stops moving almost completely due to the high hydraulic stiffness. This simplifies the system analysis, as the spring deflection now only depends on the motor rotation. The lack of cylinder movement adds other reasons to using the elastic element. Without it, force control would depend on the low-fidelity force output of a stationary motor with gearbox [166]. The limited motor rotations could potentially wear out the internal motor wiring. Using a powerful direct-drive electric motor with a stiff force sensor instead of the SEA is an alternative, but these are far more expensive then SEA configurations.

For the single-axis experimental measurements in this study, the exoskeleton joint was positioned on an axis powered by an external electric motor. This motor generated simulated arm movements or kept the brake disk rotating continuously (see Fig. 7.3)

The electric motor and driver in the SEA are from LTI Drives, respectively the LSH050-4-60-320 (nominal torque: 0.7 Nm; maximum speed: 6000 RPM) and the CDD32.004C (operating voltage: 230 V; maximum current: 7,2 A). The motor is combined with a PLE60 gearbox (ratio 1:20) from Neugart. On the externally powered axis (resembling the exoskeleton joint), the hydraulic Mono Mini Disc Brake from Hope Technology (weight: 0.45 kg), is combined with a L1657 load sensor (capacity: 2224 N) from FUTEK Advanced Sensor Technology, mounted at 0.1 m from the central axis. The disk brake should be able to generate up to 200 Nm of braking torque on a custom steel brake disk (diameter: 0.12 m), although due to limited nominal torque of the electric motor in the SEA, it never gets above 120 Nm. The load sensors signals are conditioned by a SG-3016 isolated strain gauge input module from ICP DAS. The brake unit generated its brake forces at 0.055 m from the central axis, on a 0.12 m diameter brake disk. The rotations of

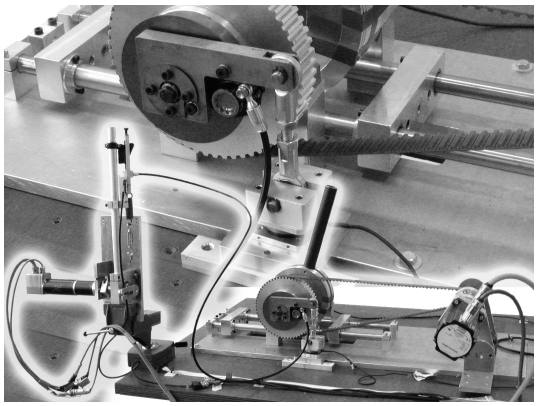

Figure 7.3: Experimental setup. The brake disk and brake unit are placed on the central axis at the bottom (enlarged as background). The axis is powered by an external electric motor (right) to simulate arm and joint movements. The disk brake is powered by the series elastic actuator (left), with the brake forces measured at a fixed distance from the rotation center of the axis by a force sensor (middle, beneath brake unit). The spring deflection is measured by the encoder in the brake motor. Note the images does not show the electric motor and force sensor used for the results in this paper, although the setup is exactly the same.

the externally powered axis was measured by a quadrature encoder (resolution: 2500 CPR) from US Digital, consisting of a transmissive rotary code wheel (outer dimension: 2 inch, inner dimension: 1 inch) and a separate encoder module (EM1).

7.2.4 *Controller design*

Based on the presumption of a linear relationship between the brake torque T_{act} and the motor angle θ_{mot} (to be verified in the next sections), the hydraulic disk brake is fully controlled by controlling the SEA (see Fig. 7.4). As the torque measurements depend strongly and non-linearly on the joint speed (see Eq. 7.1), the measured brake torque of the actuator T_{act} is not fed back via an outer control loop. A linear inverse model H_{inv} converts the reference torque T_{ref} to the reference motor angle θ_{ref}. All manually identified components outside the inner loop with PID controller are:

$$H_{inv} = K_{inv} = 0.0125[rad/Nm], \tag{7.2}$$

$$H_{ff} = K_{ff} = 0.5[Nm/rad], \tag{7.3}$$

$$r_{mot} = 0.025[m], \tag{7.4}$$

$$K_{spr} = 15.9 * 10^3[N/m], \tag{7.5}$$

$$r_{br} = 0.055[m], \tag{7.6}$$

$$H_{br} = \frac{K_{br}}{\tau_{br}s + 1} e^{-s\tau_t}, \tag{7.7}$$

where the hydraulic disk brake H_{br} is modeled by a first order system with gain K_{br}, time constant τ_{br}, and transport delay τ_t in the 2 m hydraulic cables. The above feed-forward gain K_{ff} was experimentally determined, but is also roughly equal to the analytical derivation:

$$K_{ff} \approx \frac{r_{mot}^2 K_{spr}}{i_{gb}}, \tag{7.8}$$

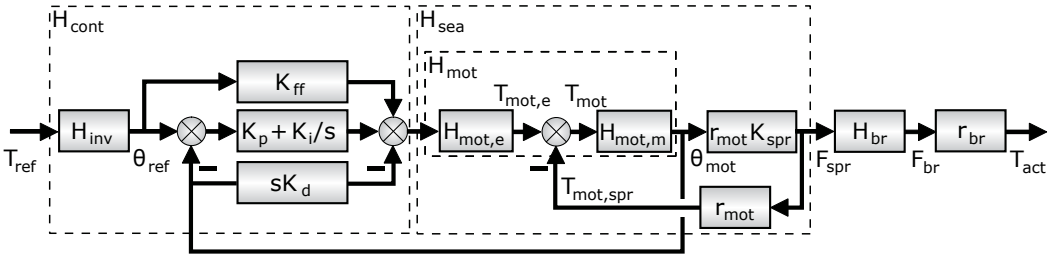

Figure 7.4: Control diagram of the SEA in combination with the hydraulic disk brake. The reference torque T_{ref} is converted to a reference motor angle θ_{ref} with inverse model H_{inv}. The motor angle is controlled (H_{cont}) with P- and I-actions on the error signal (with gains K_p and K_i), and a D-action K_d on the measured motor angle. The resulting control signal is fed through the electrical windings of the electric motor $H_{mot,e}$, which includes the gearing ratio, to get the generated motor torque $T_{mot,e}$. The second order model of the mechanical motor $H_{mot,m}$, including the gearbox inertia, converts the resulting motor torque T_{mot} to an motor angle displacement θ_{mot}. The motor angle times the motor radius r_{mot} and the spring stiffness K_{spr}, gives the springs force F_{spr}, which is the output of the SEA (H_{sea}). The torque on the motor due to the spring force $T_{mot,spr}$ is subtracted from the electrical motor torque $T_{mot,e}$ to get the resulting motor torque T_{mot} in the motor model H_{mot}. The controller has a feedforward gain K_{ff} to compensate for this subtraction. The SEA output goes through the hydraulic disk brake H_{br} to generate the brake force F_{br} at an distance r_{br} from the joint axis, resulting in the total brake torque of the actuator T_{act}.

with the gearbox ratio i_{gb} equal to 20. The theoretical nominal actuator output torque T_{act} can be calculated from the nominal motor torque $\overline{T}_{mot,e}$ (without the gearbox gain):

$$T_{act} = K_{br} i_{gb} \overline{T}_{mot,e} \frac{r_{br}}{r_{mot}}. \tag{7.9}$$

The controllers are programmed in Matlab Simulink (The MathWorks) and compiled to run in an open-source, real-time Linux environment (RTAI) [7, 20] with open-source hardware drivers (COMEDI) for the two National Instruments Corporation DAQ devices (analog in- and output: PCI-6025, encoder input: PCI-6602) and have real-time logging and graphical user interface possibilities. The controller ran at a minimum of 1000 Hz on a quad-core computer.

7.3 SYSTEM CHARACTERISTICS

7.3.1 *Intrinsic properties*

Before tuning of the SEA controller, the open-loop friction characteristic of the disk brake was analyzed. A ramped voltage step applied to the electric motor in the SEA in an open-loop control mode, gave an indication of the relationship between the motor control signal and the output torque T_{act}. From Fig 7.5 it is clear that the brake torque has almost no velocity dependency, thus closely resembling coulomb friction with a linear relationship to the normal force. During the constant voltage phases, the brake torque is independent of the angular velocity, closely resembling the normal force relationship seen in pure coulomb friction. The jumps during the

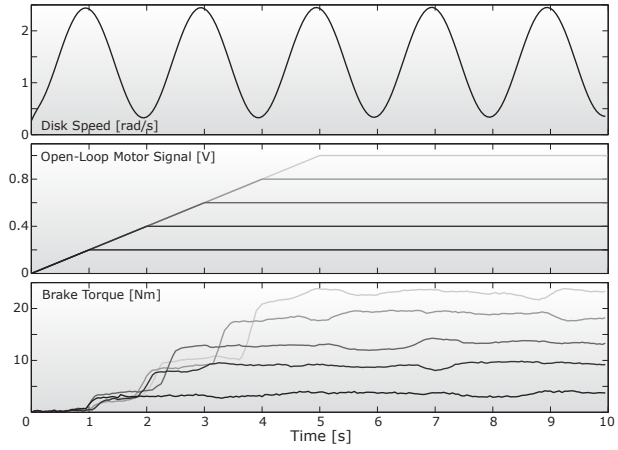

Figure 7.5: Open-loop intrinsic properties of the hydraulic disk brakes, using an uncontrolled, open-loop actuator. The angular speed of the joint was varied from almost zero to half a rotation per second (top figure), and the SEA powered by an open-loop ramp voltage signal (middle figure). The resulting brake torque is displayed in the bottom figure. The jumps in brake torque during the ramp phase are due to high levels of gearbox friction.

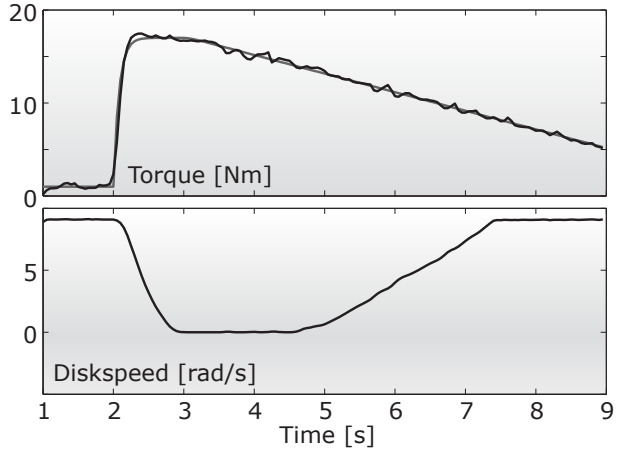

Figure 7.6: Absence of stick-slip effects during transitions around zero brake disk speed. In the top figure, the desired (gray) and measured (black) brake torques. In the bottom, the angular speed of the externally powered axis to which the brake disk was mounted.

voltage ramp phases were accounted for by jumps in the motor angle due to large amounts of gearbox friction.

Secondly, possible non-linearities due to stick-slip effects around zero joint speed may affect the performance. To investigate this, the brake disk was brought up to full speed, then to full stop by applying a brake torque step, followed by a slow, ramped release of the brake torque to observe the measured brake torques when disk rotations resumed. At the point of speed resumption in Fig. 7.6, no sudden jumps in the measured brake torque or disk speed can been seen, indicating the absence of stick-slip effects.

7.3.2 *System identification*

Method

For the open- and closed-loop identification, the system was perturbed with multi-sine input signals to estimate the frequency response function $C(s)$ and squared coherence function $\mathrm{Coh}(s)$. These functions are estimated with cross- and auto-

spectral densities $S(s)$ of input (i) and output (o) [93, 13, 217]. For a black-box system with single input and single output, the functions are:

$$C(s) = \frac{S_{io}(s)}{S_{ii}(s)}, \tag{7.10}$$

$$Coh(s)^2 = \frac{|S_{io}(s)|^2}{S_{ii}(s)S_{oo}(s)}. \tag{7.11}$$

The frequency response function $C(s)$ is an estimate for the dynamics of the black-box system, and the squared coherence function $Coh(S)$ a measure for the signal to noise ratio at each frequency. The squared coherence [155] ranges from zero to one, with zero meaning the lack of correlation between the input and output, and one the absence of noise or time-varying behavior. Higher harmonics in periodic signals may interfere with the interpretation of the coherence function.

The input perturbation signal consisted of 80 summed sines with a observation time of 256 s. The frequencies of the sines were spaced logarithmically from 0.1 to 100 Hz, were of constant power spectral density, and had random phase shifts to reduce amplitude peaks in the summed signal.

The minimum and maximum values of the amplitude of the total signal were scaled relative to three times the standard deviation in both directions. As the sign of the brake torques is directly dependent on the joint rotation direction and cannot be controlled by the actuator, the desired minimum values of the reference signals are always just above zero. The angular disk speed is kept constant at about 1 rad/s. Measurements are repeated four times with four uniquely generated multi-sine signals, differing on the random phases. The results are averaged in the frequency domain over four frequencies and the four repetitions to improve the coherence of the measurements and estimates.

The entire actuator system consists of the inner, closed-loop motor system followed by the open-loop hydraulic disk brake. These two sub-systems are identified separately, followed by the analysis of the complete system.

Results

The frequency response function of the tuned, inner- and closed-loop system of the electric motor $H_{mot,cl} = \theta_{mot}/\theta_{ref}$ (see Fig. 7.4) was identified by it tracking a multi-sine reference motor angle θ_{ref}. The reference angle had minimum and maximum values of 0.025 and 0.25 [rad]. The response function is plotted in Fig. 7.7 (left), and has a -3 dB gain bandwidth of 20 Hz and a 90° phase lag bandwidth of 14 Hz.

By using the output from the above closed-loop motor system as input for the open-loop hydraulic disk brake, the frequency response function $H_{br,ol} = F_{br}/F_{spr}$ of the latter was estimated. This response function is based on the forces exerted on the linear cylinder F_{spr} and by the disk brake F_{br}, not the input motor angle θ_{mot} and output actuator torque T_{act}, to keep the identification as close as possible to the unknown hydraulic disk brake properties. The response function for $H_{br,ol}$ is given in Fig. 7.7 (middle). By fitting the hydraulic brake model H_{br} (Eq. 7.7 on the response functions, parameters K_{br}, τ_{br} and τ_t are found to be 3.9, 0.0042 s and 0.0046 s, respectively. The hydraulic disk brake thus amplifies the force applied on the hydraulic cylinder at the handle almost four times. The time delay τ_{br} of the first order function is of few consequences, but the transport delay τ_t in the 2 m long tubes causes rapidly increasing phase lag. Note that the

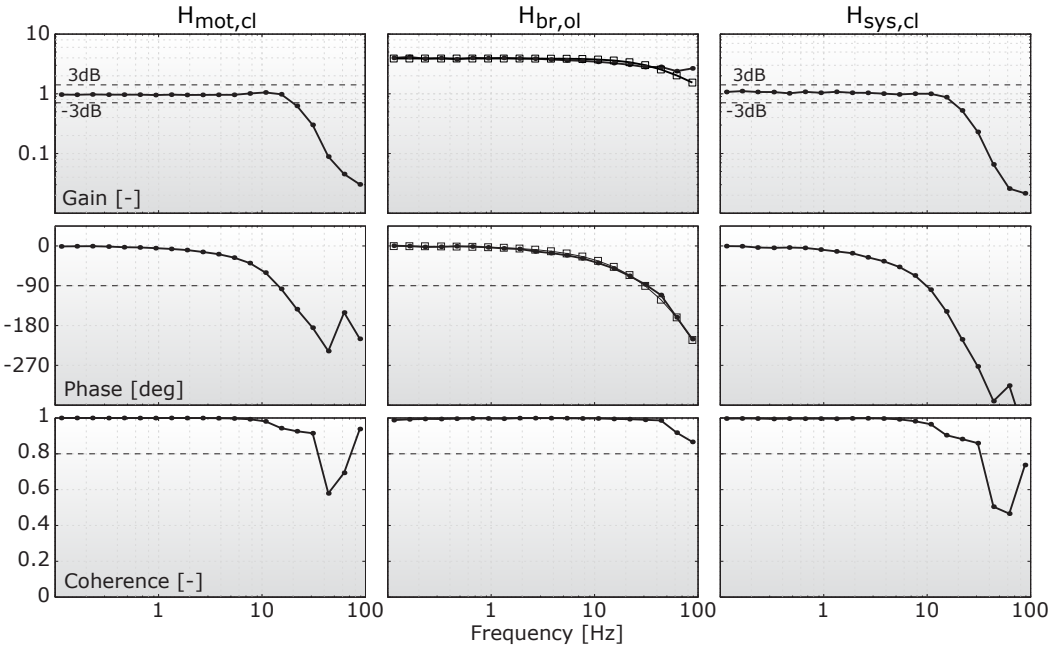

Figure 7.7: Bode plot of the frequency response functions of the closed-loop system around the electric motor $H_{mot,cl} = \theta_{mot}/\theta_{ref}$ (left), the open-loop hydraulic disk brake $H_{br,ol} = F_{br}/F_{spr}$ (middle), and the complete closed-loop system $H_{sys,cl} = T_{act}/T_{ref}$ (right) for the multi-sine reference torques (black lines with closed dots). The model for the disk brakes H_{br} (Eq. 7.7) was fitted to the open-loop response function $H_{br,ol}$ (black lines with open squares), giving a good fit.

experimentally determined K_{inv} is roughly equal to $1/(r_{mot}K_{spr}K_{br}r_{br})$, with the value for K_{br} as found above.

Finally, the frequency response functions of the complete system of closed-loop actuator and open-loop hydraulic disk brake $H_{sys,cl} = T_{act}/T_{ref}$ were estimated from the reference T_{ref} and measured output torques T_{act}. The reference torque T_{ref} had minimum and maximum values of 2 and 20 [Nm]. The response function is plotted in Fig. 7.7 (right), and has a -3 dB gain bandwidth of 18 Hz and a 90° phase lag bandwidth of 10 Hz. The major bandwidth limitation in the actuated hydraulic disk brakes is thus the phase lag caused by the length of the hydraulic tubes and the lag of the closed-loop actuator.

The above results show the frequency response functions of the bandwidth measurements. Another direct effect of the used disk brake on the interaction dynamics is the experienced minimal possible impedance. As the brake pads in the brake can fully disconnect from the brake disk, the minimal brake torque is equal to zero for all frequencies, with the only remaining impedance felt due to the acceleration forces of the brake components and the exoskeleton.

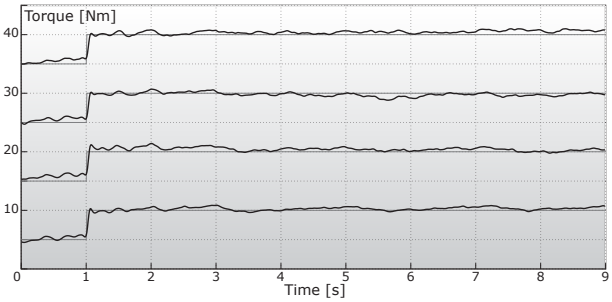

Figure 7.8: Time plots of step reference signals. In gray, the required torque T_{ref}. In black, the measured torques T_{act}.

7.3.3 *Control examples*

The performance of the complete closed-loop system of actuator and hydraulic disk brakes is illustrated by two tracking tasks for the actuator torque T_{act}.

The 5 Nm step responses at four different torque levels from 5 Nm to 35 Nm give an illustration of the overshoot and response times of the system. In the step responses of Fig. 7.8, overshoot and response are all acceptable for rehabilitation. Some output variation is seen, due to a slight unevenness of the brake disk surface and some heat development in test situation with continues rotations and high torques.

Tracking six sines of different amplitudes, varying in resolution of 5 Nm to 30 Nm, give a rough indication of the output resolution. For the sine tracking in Fig. 7.9, the controller has the most problems with the sines with the lowest amplitude, resulting in a torque output resolution of about 1 Nm. The present phase lag indicates the inverse model H_{inv} is not generating optimal results.

7.4 SYSTEM COMPARISON

Compared to the pneumatic, hydraulic, electric and magneto-rheological dampers (see Tab 7.1) [88, 235], the resistive power-to-weight ratio of the mechanical brake is virtually unlimited due to a constant resistance force and a speed only constrained by heat development. The torque-to-weight ratio of commercially available bicycle disk brake is in the middle of the table, with the torques for the dampers calculated by dividing the power-to-weight ratio by the average peak arm speed of stroke

PASSIVE ACTUATORS	POWER-TO-WEIGHT RATIO [W/KG]	TORQUE-TO-WEIGHT RATIO [NM/KG]
(Human muscle)	500	160
Pneumatic damper	2500	800
Hydraulic damper	250000	80000
Electric damper	300	100
Magneto-rheological damper	400	130
Mechanical brake	∞	400

Table 7.1: Resistive power-to-weight and torque-to-weight ratios (approximate).

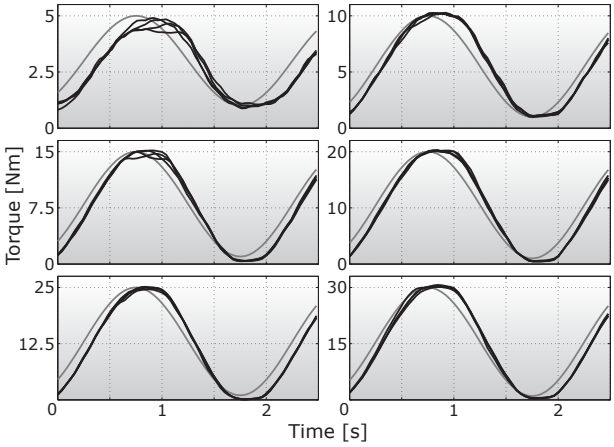

Figure 7.9: Tracking sine torques of different amplitude.

patients (180°/s) [134]. Although the torque-to-weight ratio of pneumatic dampers is higher, these dampers are also always highly compliant due to the compressibility of air, making them less suitable for applying resistive torques. The hydraulic damper has the highest torque-to-weight ratio, but no damper implementation currently exists with sufficiently high torques and with a weight, including valves, below 2 kg. Compared to brakes, dampers always have a minimal amount of friction present and the speed dependency makes their absolute torque levels more difficult to control. Therefore, in our opinion, the mechanical brake is better suited for energy-dissipating force-coordination training than any of the dampers.

7.5 DISCUSSION AND CONCLUSIONS

A series elastic actuator (SEA) was added to the hydraulic disk brake which was bought in a bicycle store. The SEA is better suited for force actuation than a directly connected electro motor and gearbox, at the cost of some bandwidth performance [166, 171, 223, 214]. It also made it possible to use the motor angle in an inner control loop, to overcome the particular dynamics of passive actuation with coulomb friction brakes. The SEA actively powers and controls the brake force, but when seen from the patient interaction the total actuator system is still passive. It can thus only dissipate energy, which makes it inherently safe. Still, the torque bandwidth and output levels make it suitable for functional exercises with dynamic, high-intensity resistance.

The passivity of the disk brakes with coulomb friction has three functional implications for the control of the joint angles. Firstly, the braking torque is always opposite to the direction of joint rotations. Secondly, with zero joint rotation speed, the experienced and measured braking torque is equal to the torque applied by the human, and not to the potentially desired braking torque. Thirdly, with non-zero joint rotation speeds, the amount of experienced and measured brake torque, is now equal to the desired braking torque, and not to the torque applied by the human. Passivity also implies that actively assisting movements is impossible and virtual environments are restricted to those which do not need external energy being added to the human arm.

The complete system of closed-loop series elastic actuation (SEA) and open-loop hydraulic disk brakes has a 20 Nm (flat-spectrum, multi-sine) bandwidth of 10 Hz.

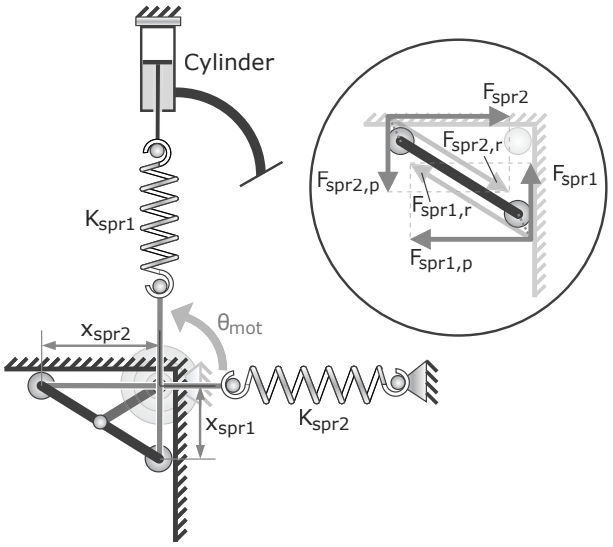

Figure 7.10: Modified SEA setup in a zero-energy configuration with second spring, reducing motor requirements. The runner-on-rails mechanism (lower left) is statically balanced for any motor angle θ_{mot}. K is the spring stiffness, x the spring deflection, and F the spring force, with $_{spr1}$ and $_{spr2}$ indicating spring 1 (directly connected to the hydraulic cylinder) and spring 2 (compensation spring). Inset: the spring forces with decomposition along the runner $_{,r}$ and perpendicular $_{,p}$. The forces are shown with a slight offset to improve readabilty.

The bandwidth is mainly restricted by the transport delays in the 2 m hydraulic tubes and the lag in the SEA responsiveness, probably due to internal friction in the gearbox. The performance should be sufficient to generate the torques required for force-coordination exercises as used in conventional therapy (20 Nm at 5 Hz), and for simple virtual environments. When higher bandwidths are required, these can likely be obtained by reducing the length of the hydraulic tubes. Including a higher order inverse model H_{inv}, in stead of the linear gain K_{inv} in Fig. 7.4, or addition of an outer control loop, may further improve the bandwidth of the system.

As the brake pads can be fully disengaged from the brake disk, the minimal impedance—the torque felt when moving the arm while no torque is requested—is close to zero. The minimal torques felt are dominated by the inertia of the brake on the joint. The disk brakes are rated for up to 200 Nm, and the electric motor could achieve 120 Nm of this, which is more than enough for isometric training of the upper extremity (100 Nm). At 450 gr, the disk brake construction was far below the 1 kg limit, and suitable to be mounted on an exoskeleton.

During testing, the disk brake occasionally suffered from overheating problems. With the external motor running the joint axis at π rad/s and while keeping the brake torque at 50 Nm, the brake disk would heat up after several minutes. Due to the heat, the brake torque slowly increased. Heating is not considered a problem in a rehabilitation exoskeleton, as humans cannot generate enough sustained output power on the brakes during therapeutic exercises.

The other source of brake torque variance was the use of brand new brake disks and brake pads. Each pair of pads needs a couple of minutes of constant wear and tear to get the optimal surface smoothness and constant braking torque. In the test setup, continual wear and tear eventually affected system performance. However, in a rehabilitation exoskeleton, wear and tear are minimal. The life span of a pair of pads is expected to be on the scale of years. Replacement of the inexpensive pads is straightforward.

7.5.1 *Zero energy implementation*

In the SEA setup of Fig. 7.2, the electric motor must apply constant power to keep the spring deflected during static brake torque generation. The output brake force is roughly four times the applied force at the handle, with the total relationship between the nominal motor torque and the output brake torque according to Eq. 7.9. Thus, to get a constant brake torque T_{br} of 20 Nm and 100 Nm, the nominal output torque of the motor $\overline{T}_{mot,e}$ should be respectively 0.12 Nm and 0.58 Nm. (The electric motor was with 0.7 Nm overpowered for the static tasks.)

To reduce the static loads on the electric motor, a statically balanced mechanism can be used with two ideal-springs. This reduces the function of the electric motor to generating change of equilibrium positions, making the use of smaller and cheaper electric motors possible.

Adding a second spring can reduce the torque requirement on the motor by counteracting the deflection (see Fig. 7.10). With both springs and ideal-springs, the mechanism is always in static equilibrium, only requiring motor torques to accelerate and decelerate the mechanism. (Theoretically, ideal springs deflect linearly with increasing force, and have zero spring length at zero applied force.) This mechanism can be used as the hydraulic cylinder in the handle has almost no further displacement when the brake pads are engaging the brake disk. Therefore, the connection between the spring and the hydraulic cylinder can be seen as a connection to the fixed world, maintaining ideal-spring properties in the statically balanced mechanism.

7.5.2 *Conclusion*

In conclusion, hydraulic disk brakes are suitable to actuate an upper-extremity exoskeleton for force-coordination training in stroke rehabilitation. The analysis of the open-loop intrinsic properties and closed-loop system performance of the disk brakes showed the brakes to be suitable for dynamic, high-intensity resistance exercises. Compared to other passive actuators, the hydraulic disk brakes have a descent power- and torque-to-weight ratio. Commercial designs are easily available from bicycle stores for the performance required for rehabilitation.

The hydraulic disk brakes were found to comply with the stated requirements, four of these disk brakes were mounted on the Dampace exoskeleton [202]. These disk brakes are powered by the original series elastic actuators, not the zero-energy implementation.

ACKNOWLEDGEMENTS

The authors would like to thank Gert-Jan Nevenzel for his assistance in design, construction and maintenance of the experimental setup.

8

DAMPACE: DESIGN OF AN EXOSKELETON FOR FORCE-COORDINATION TRAINING IN UPPER-EXTREMITY REHABILITATION

ABSTRACT The Dampace exoskeleton combines functional exercises resembling activities of daily living with impairment-targeted force-coordination training. The goal of this paper is to evaluate the performance of the Dampace. In the design, the joint rotations are decoupled from the joint translations; the robot axes align themselves to the anatomical axes, overcoming some of the traditional difficulties of exoskeletons. Setup times are reduced to mere minutes and static reaction forces kept to a minimum. The Dampace uses hydraulic disk brakes which can resist rotations with up to 50 Nm and have a torque bandwidth of 10 Hz for multi-sine torques of 20 Nm. The brakes provide passive control over movement; patients' movements can be selectively resisted, but active movement assistance is impossible and virtual environments restricted. However, passive actuators are inherently safe and force active patient participation. In conclusion, the Dampace is well suited to offer force-coordination training with functional exercises.

8.1 INTRODUCTION

Patient-friendly robots for upper-extremities rehabilitation are used as diagnostic and therapeutic aids for a wide range of disabilities. After a stroke, improving limited arm function is needed to regain functional abilities. Current rehabilitation robots try to accomplish this using a number of different rehabilitation strategies. For example, the MIT-Manus [82, 107] assists arm movements during task execution when deemed necessary, the MIME [22] mirrors the movement of the unaffected to the affected arm, the ACT-3D [206] tackles undesired abnormal muscle couplings and the ARMin [143] motivates patients by interacting with virtual environments. Overall, these robots make rehabilitation therapy more challenging for the patients and less labor intensive for the therapists, and supplied the physicians, therapists and scientific community with more objectively gathered data.

According to systematic reviews, the new robot assisted therapies are at least as good as regular therapy for stroke rehabilitation. Van der Lee et al. [219] tentatively concluded that the type of therapy matters less than the exercise intensity. Several approaches with and without robots resulted in roughly the same effect when the level of intensity was matched. They did indicate that using robots may be a useful way for increasing the intensity. Platz [157] found evidence for superior treatment efficacy of task oriented, motor-relearning programs and giving different patient subgroups specific training strategies. And a higher intensity of motor rehabilitation resulted in an accelerated, although not necessarily better, motor recovery. Finally, two recent reviews [162, 112], concluded that robot assisted

Submitted: ASME Journal of Medical Devices (AHA Stienen, EEG Hekman, GB Prange, MJA Jannink, AMM Aalsma, FCT van der Helm, and H van der Kooij). *Patent pending:* Orthesis (AHA Stienen, EEG Hekman).

therapy of the shoulder and elbow improves motor control of these joints, and probably more than conventional therapy. But consistent influence on the functional abilities of the patients was not found. These four systematic reviews agree with the main principle of motor learning; the improvement in motor-control performance is directly linked with the amount of practice done [187]. However, improved motor control is not necessarily the same as an increased functional ability.

The results with rehabilitation robots are in line with reviews on conventional upper-extremity therapy. The latter indicate that intensive and task-specific exercises, consisting of active, repetitive movements, give the best results [109, 8, 56]. Actively generating movements requires more brain activity and results in better motor learning than externally-powered arm movements [119]. For severely affected stroke patients, active participation can be facilitated by reducing the gravitational pull on the arm, as found in previous studies [163, 92, 164].

As an alternative to the strict functional and task-specific approach, Dewald and colleagues are using impairment targeted movements to achieve improved motor control in stroke rehabilitation [206, 18, 11, 45, 12, 44, 46, 47]. Their multi-degree-of-freedom force-coordination training tackles a commonly identified cause of stroke patients' movement disorders; the abnormal coupling between elbow and shoulder joint torques [213, 18].

Other groups of intervention with support in literature with less focus on activities of daily living are the targeted movement-coordination training [108], progressive resistance strength training, and force-coordination training [177, 230, 84, 53, 138, 145, 234, 1, 100]. Yet, on the latter two approaches, the evidence is not conclusive [14]. The combination of functional exercises with dynamic, high-intensity resistance training looks promising [147]. Additionally, training by actively resisting the patients' movements may also stimulate them to generate more appropriate movement patterns when emphasizing the movement error [170, 151]. General motor learning theories on which these theories are partly based, are thought to be useful for motor recovery after stroke [159, 39, 83].

Combining these approaches, a training device was needed which could help identify causes behind the movement disorders of stroke patients, tackle these causes with isolated force-coordination training over multiple joints, and integrate the isolated training into a functional, task-specific training protocol. In the training stages active patient participation is essential, and by offering interesting training environments and varying the levels of difficulty patients should stay motivated and challenged. Therefore, we created our dynamic force-coordination trainer for the upper extremities, the Dampace.

The goal of this paper is to evaluate the performance of the Dampace. The device should increase exercise intensity, stimulate active patient participation, allow most functional movements of daily living, offer selective control over joint rotations, and be practical for rehabilitation therapy. This study expands on an earlier conference publication [202]. For readability, this chapter contains summarized information from Chap. 6 and Chap. 7.

8.2 REQUIREMENTS AND IMPLICATIONS

Robot interaction with the upper-extremities is possible with endpoint manipulators, exoskeletons and cable suspensions. Endpoint manipulators have a single connection to the hand, wrist or forearm [81, 22, 169, 120, 206], thereby indirectly controlling joint rotations. Exoskeletons are external skeletons placed over the arm

and powered by actuators on the joints [140, 179, 61, 143, 27, 154], offering direct control possibilities on these joints, at the cost of more complex mechanics. Cable suspensions [129, 127, 201] link one or more cables to the arm, increasing both control options and complexity with every additional cable linkage. Due to the limited interaction possibilities, the cable suspensions are ignored in the remainder of this section.

Control over the limb movements with the above devices can be achieved via active actuators or passive brakes. If active assistance of movement is not necessary, than controlled passive brakes offer the advantage of a greater torque-to-weight ratio and inherent safety.

The choices between these devices and actuators are discussed in this section in relation to the device requirements. These requirements were refined with the help of several physicians, therapists and researchers in the Netherlands.

8.2.1 *Need for active assistance of movement*

Most of the current rehabilitation robots are actively powered and designed to assist arm movements when needed [168, 107, 31, 24]. However, when comparing training of unassisted reaching to reaching assisted by a rehabilitation robot, equal gains in range of motion were found [98]. Secondly, providing too much assistance may negatively influence the motor relearning as patients become less actively involved [231]. Thirdly, increasing the therapy intensity can be achieved without active assistance. And finally, even the evidence of a beneficial effects of passive stretching on spasticity in stroke is inconclusive [16]. All of this indicates that for motor relearning in stroke rehabilitation, active actuators may not always be necessary. For instance, force-coordination and error-enhanced training do not depend on active actuation. They can also be realized by brakes applying resistance torques on the joints. With such passive actuators, limb movements may still be facilitated by adding scalable weight support to the device [45, 44, 206, 163, 164, 92, 47]. Weight support only facilitates movements, but does not complete them, keeping the patients actively involved [231, 152].

Using controlled resistance has the advantages of inherent safety and a light-weight implementation. Disadvantages are the inability to actively complete movements and to create virtual environments which need external energy. A resistive device requires a separate weight support mechanism for itself and the human limb. But as the weight-supporting torques at the shoulder can easily exceed 10 Nm, even many actively powered devices use separate weight-support mechanisms; see for example the Gentle/s [120], the Pneu-WREX [179], and the ARMin [143]. Therefore, if active assistance is not necessary, passive brakes are preferred over active actuators. Both endpoint mechanisms and exoskeletons can be fitted with brakes or actuators.

8.2.2 *Control and range of limb movements*

To exercise most functional activities of daily living, the required ranges of motion for the shoulder and elbow joints are defined according to Tab. 8.1. In these activities, both the 3D position of the hand and the exact orientation of the limbs are important. For instance, for object grasping movements, the shoulder and elbow angles depend on the position and the type of object. The arm approaches

a cup of water differently than a small object like a coin. Thus for impairment assessments and targeted interventions, control over all degrees of freedom is preferred. Secondly, the shoulder joint does not only have the three rotational degrees of freedom, it also has two translational degrees. These five degrees of freedom form the shoulder girdle [233]. Humans have voluntary control over the shoulder position, but shoulder elevation rotation is also coupled with vertical shoulder translation [117, 142]. A rehabilitation device should at a minimum not restrict the coupled translations.

By definition, a three-dimensional endpoint device is not able to independently control all four axes of shoulder and elbow simultaneously. To do so, additional fixed (ACT-3D) or controlled rotational degrees of freedom (MIME) are needed. Exoskeletons can give full independent control of all four axes of the joints, but their axes need to be aligned closely to the anatomical axes. They do control joint axes directly. And as they closely follow the arm, their dimensions are less dependent on the desired workspace. Endpoint manipulators, by having no axis to align with the human, are less sensitive to (in)voluntary translation of the shoulder than exoskeletons. However, they apply all interaction forces via the hand, potentially creating high reaction forces in the joints. Finally, to match most of the range of motion of the human shoulder and elbow, endpoint manipulators need to cover a large workspace, resulting in a larger device. Overall, exoskeletons offer better control over and measurements of joint movements, have a greater range of motion, and have less joint reaction forces. But care must be taken to align their axes correctly to prevent painful human-robot interaction.

8.2.3 *Usability in rehabilitation therapy*

For the device to be useful in therapy, some usability issues need to be addressed. The device has to be safe, comfortable and easy to use and set up. An appealing design will help with patient acceptability. Patient motivation is enhanced by providing stimulating training environments.

JOINT AXIS	RANGE OF MOTION [DEG]	RESISTANCE TORQUE [NM]
Shoulder plane of elevation	0 - 135	25
Shoulder negative elevation	0 - 120	25
Shoulder axial rotation	-90 - 0	25
Elbow flexion/extension	0 - 135	50

Table 8.1: Desired range of motion and maximum resistance torques for shoulder and elbow axes. Defined according to ISB recommendations [233] for resp. thoracohumeral and humeroulnar joint. These values are the results of structured interviews with physicians, therapists and human movement scientists in the Netherlands. The values for range of motion are compatible with three of the four main categories of movements for activities in daily living [221, 215]: touching the contralateral shoulder, touching the mouth (drinking), and touching the head (combing hair); however, the fourth category—moving the hand to the back pocket—is just out of reach.

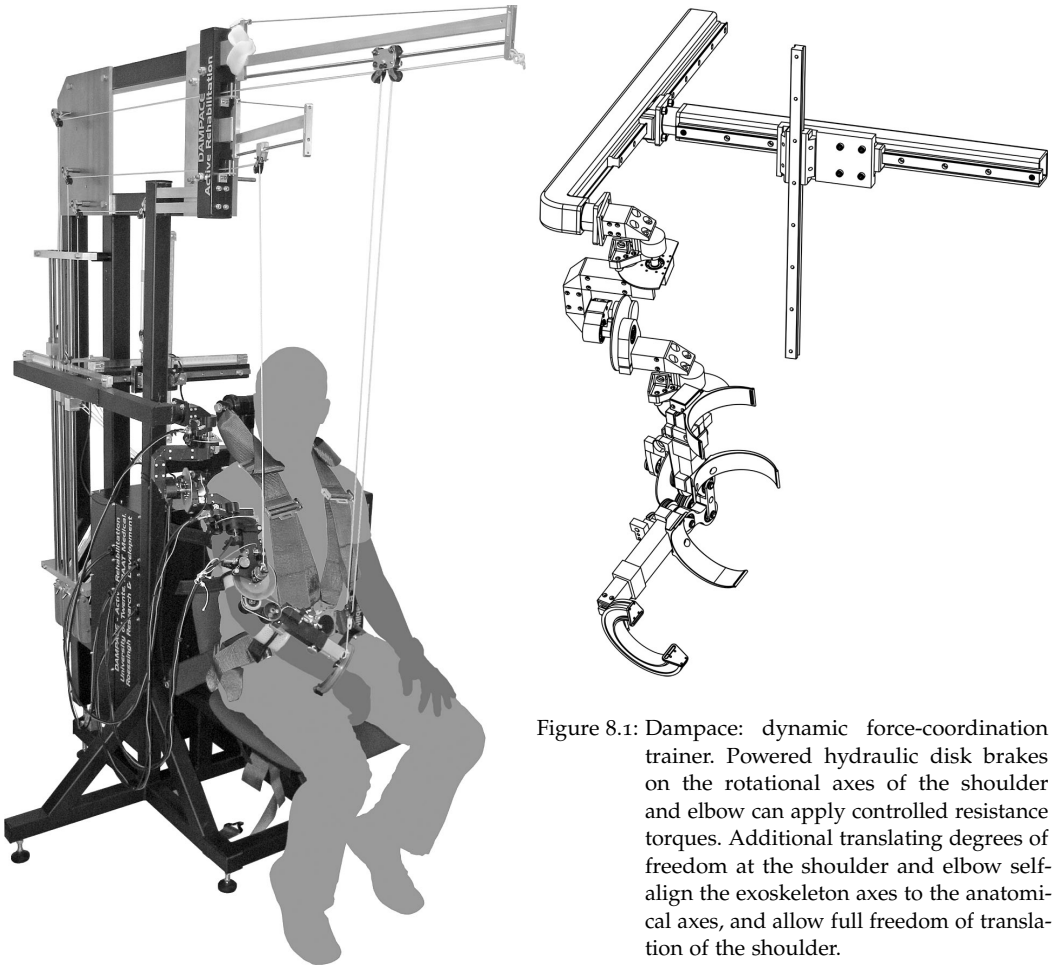

Figure 8.1: Dampace: dynamic force-coordination trainer. Powered hydraulic disk brakes on the rotational axes of the shoulder and elbow can apply controlled resistance torques. Additional translating degrees of freedom at the shoulder and elbow self-align the exoskeleton axes to the anatomical axes, and allow full freedom of translation of the shoulder.

Inherent safety is achieved by having controlled resistance instead of active assistance. Endpoint manipulators are comfortable when they don't move the endpoint out of the human range of motion. For exoskeletons, correct joint alignment and translations in the shoulder joint are important. For most of the current devices, the endpoint manipulators are easier in use compared to the exoskeletons, due to the longer setup times of the latter. Exoskeletons exist which do not require their axes to be aligned to the human axes [186]. This minimizes the difference in setup times and reduces some unwanted reaction forces in human joints. Stimulating gaming environments can be created with endpoint manipulators and exoskeletons. Overall, the usability of endpoint manipulators is slightly better.

8.2.4 *Overall implications*

Taken together, combining a self-aligning exoskeleton with controlled brakes at the joint axis results in an inherently safe force-coordination trainer. The combination

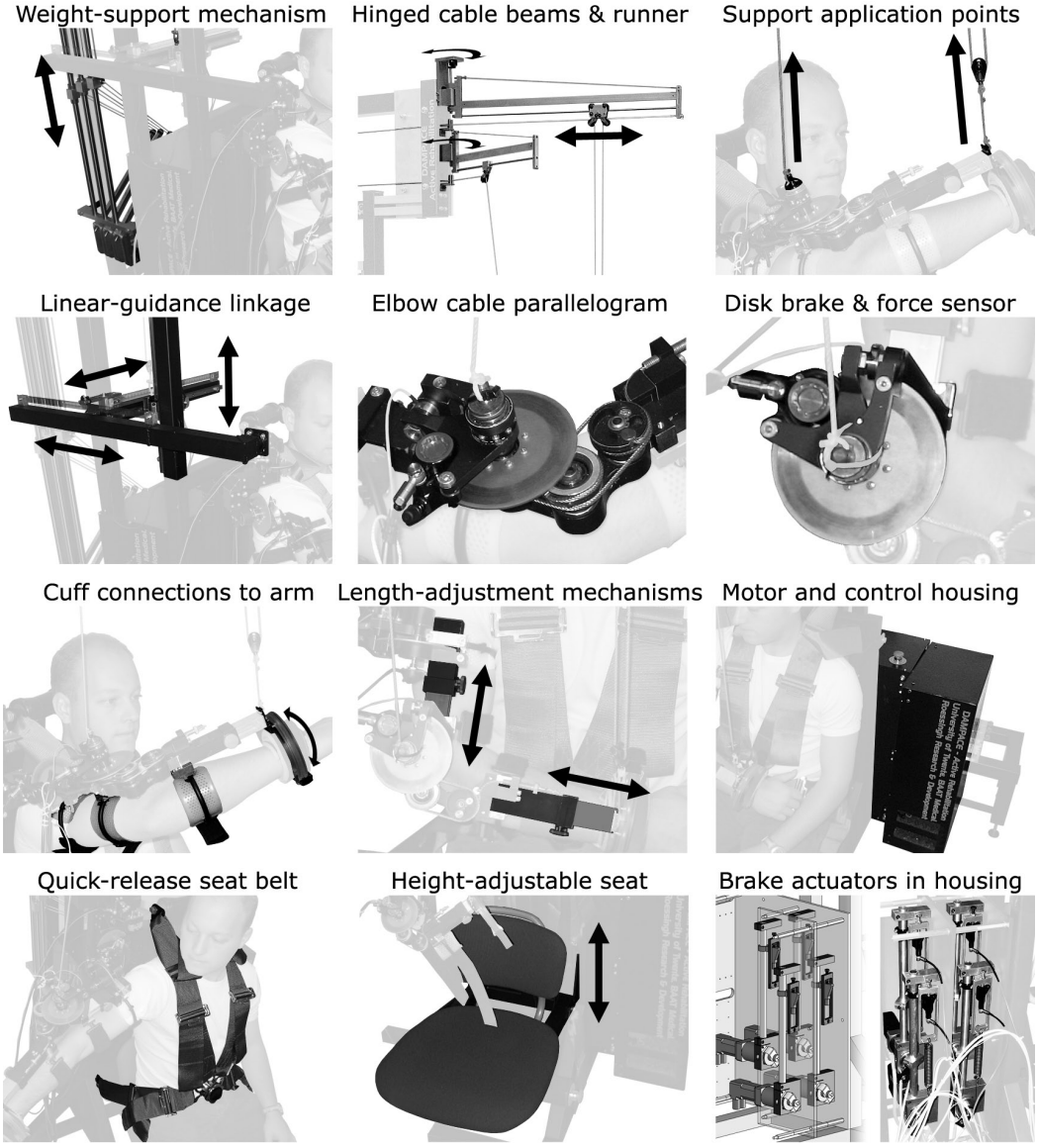

Figure 8.2: Collage of Dampace components.

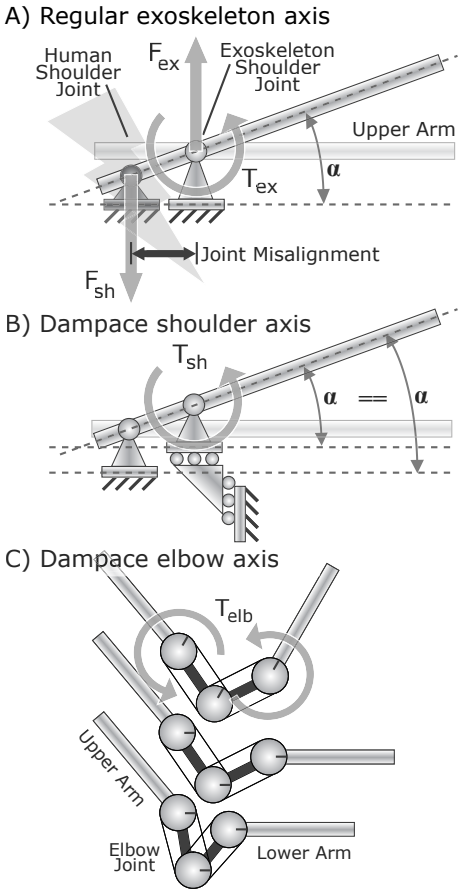

Figure 8.3: Axes alignment in exoskeletons. A) The effects of a single misaligned axis at the shoulder. Due to exoskeleton torque T_{ex}, the arm and exoskeleton axes rotate an angle α. If these axes are misaligned, the human joint has to translate relative to the exoskeleton axis. If the axes are fixed, this movement creates a residual shoulder force F_{sh}, dependent on the stiffness of skin and bone, and an equal exoskeleton reaction force F_{ex}. B) Translating exoskeleton axes prevent these misalignment forces. If a misalignment causes a force F_{ex}, the exoskeleton translates until this force is gone. Torques can be applied to the limb from the rotational-stiff linkage mechanism. In 3D, the effects are the same, with adding the two other rotational axes requiring only one additional linear axis. C) The Dampace elbow joint has two extra links, on top of which a parallelogram of cables transfer the forearm orientation to the upper arm. Translation of the joint is now independent of rotation, and vice verse, removing the requirement for elbow alignment. At the upper arm, the rotation can be controlled and measured; a torque applied here runs through the cables and drum mechanism and is applied to the forearm, without causing reaction forces.

can make therapeutic movements selectively more intensive and has good control over limb orientations with a large range of motion. To facilitate arm movements, a separate weight support system is needed. This should at a minimum supports the weight of the device, but preferably also a scalable amount of arm weight. Joint torques and rotations should be precisely measured for impairment assessments and use in active feedback control.

8.3 DESIGN AND VALIDATION

After evaluating several concepts, the Dampace was created (see Fig. 8.2.2 and Fig. 8.2). The rotations of the three joint axes of the shoulder and the one of the elbow can be actively resisted with the hydraulic disk brakes. Additional mechanisms in the exoskeleton auto-align the exoskeleton joints to the human joints. This also gives the shoulder full freedom of translation in any direction. The resistances are applied as pure torques, reducing reaction forces in the shoulder and elbow joint. The weight of the exoskeleton is compensated by an overhanging cabling system connected to an ideal-spring mechanism. Finally, feedback control is based on the state of the arm, determined via measurements of joint rotations and torques.

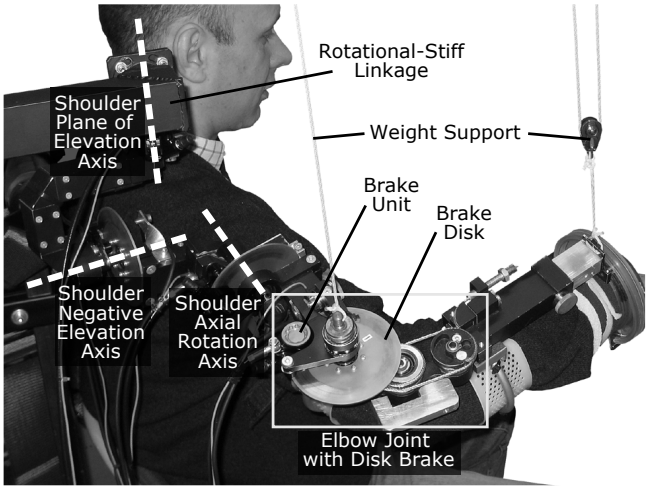

Figure 8.4: Shoulder and elbow axes of the Dampace. The three shoulder axes run parallel to the plane of elevation, negative elevation and axial axis of Tab. 8.1. The Dampace negative elevation is positioned at a 90° offset on the plane of elevation axes compared to the ISB axes. These axes do not necessarily run through the glenohumeral rotation center, but the movable, rotational-stiff linkage prevents the occurrence of shoulder reaction forces (see Fig. 8.3).

8.3.1 *Joint alignment*[1]

In most other exoskeletons, close alignment of exoskeleton and arm axes is a necessity and can be time-consuming to achieve. Rotation of misaligned axes is only possible by internal movements in the musculoskeletal system, full body and trunk movements, or by deforming the soft human tissue. The misalignments also creates potential painful reaction forces [185], especially for those with sensitive tissue or sensory problems.

The Dampace overcomes these problem by having the exoskeleton axes align themselves to the human shoulder and elbow axes (see Fig. 8.3 and Fig. 8.4). The translations and rotations of the joints are now decoupled. The exoskeleton is connected to the global reference frame via linear guidance system consisting of three perpendicular sliders, each of which can move freely over a range of 400 mm. As this linkage is rotational stiff, shoulder-joint torques can be still be applied onto the human limb. These torques do not generate the misalignment forces as seen in other exoskeletons. If these forces occur, the passive linkage would translate until they are reduced to zero. However, impedance forces due to inertia of the exoskeleton and friction of the linkage will still cause reaction forces. The inertia of the linkage and exoskeleton was measured to be 8 kg for vertical translations, 7 kg for sideways translations and 5 kg for forward/backward translations. Each of the three linear-motion rail and sliders (SKF, 15 mm profile rail) adds 4 to 20 N of static friction to the impedance, dependent on the torsional load on the slider. These values will be reduced in future versions by a redesign of the linkage, for instance with a linkage similar to the Delta Robot [67].

The Dampace elbow joint consists of a short two-beam linkage. On top of this, a parallelogram of cables and drums transfer the forearm orientation to the upper-arm (see Fig. 8.3C). Translation of the joint is now independent of rotation, and vice verse, removing the requirement for close alignment. At the drum on the upper arm, the rotation can be measured and controlled.

1 This subsection summarizes information from Chap. 6.

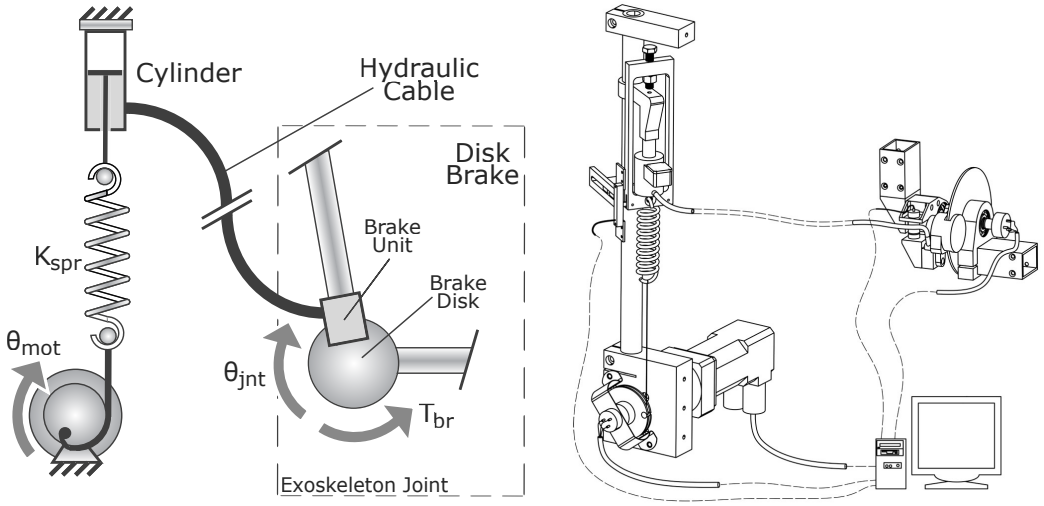

Figure 8.5: Disk brake as used on the exoskeleton joints, powered by a series elastic actuator (SEA) mounted on the base frame. The rotation of the motor θ_m is converted by the spring with stiffness K_{spr} and the cylinder to a pressure in the hydraulic cable. This pressure is used to control the braking torque T_{br} on the exoskeleton joint. Note that the braking torque is always in the opposite direction of the joint velocity $theta_{jnt}$. The sketch shows the disk brake as implemented on the negative elevation axis of the shoulder.

The decoupling of translations and rotations also influences the force interactions between the exoskeleton and human limb. Applying single forces to the limb is now impossible, as the accompanying reaction force would translate the linkage. Instead, the forces must be applied pairwise as torques, requiring two connections to the exoskeleton per limb segment. These additional cuffs are a disadvantage, as it is mounted on the soft outer tissue of the limb and thus reduces the interaction stiffness.

8.3.2 *Hydraulic disk brakes*[2]

Energy-dissipating resistance torques can be applied via pneumatic, hydraulic, (electro)magnetic and mechanical passive actuators. Of these, commercially available hydraulic disk brakes have the highest braking torque to weight and size ratio and were thus used in this study. By controlling the internal brake pressure with electro motors in a series elastic configuration [166, 171, 223, 43, 214], the amount of resistance can be regulated (see Fig. 8.3.2 and Fig. 8.6). The series elastic configuration makes it possible to use the motor angle in an inner control loop, after which the spring converts the motor angle to a force applied to the brake piston in the handle.

The electro motors and drivers used are from LTI Drives, respectively the LSH050-4-60-320 (nominal torque: 0.7 Nm; maximum speed: 6000 RPM) and the CDD32.004C (operating voltage: 230 V; maximum current: 7,2 A). Each motor is combined with a PLE60 gearbox (ratio 1:20) from Neugart. On the exoskeleton,

2 This subsection summarizes information from Chap. 7.

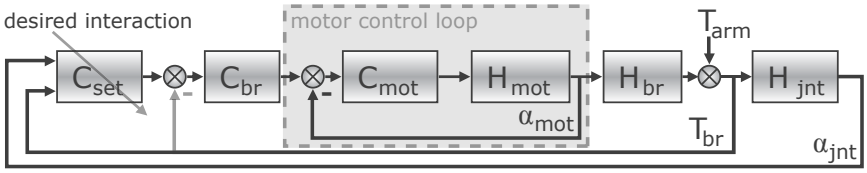

Figure 8.6: Control loop for a single disk brake (see Fig. 8.3.2), with controllers C, physical systems H, torques T and angles α. Subscripts denote the electro motor $\mathtt{mot}$, disk brake $\mathtt{br}$ and exoskeleton joint $\mathtt{jnt}$. C_{set} are the desired interaction settings, based on the measurements of brake torque and joint angle of all joints. The measured brake torque T_{br} is a complex function of the set brake torque (by the brake pressure) and the human interaction arm torque T_{arm}, and therefore difficult to use in a control loop.

each axis has a hydraulic Mono Mini Disc Brake from Hope Technology, combined with a L1657 load sensor (capacity: 2224 N) from FUTEK Advanced Sensor Technology. The load sensors signals are conditioned by a SG-3016 isolated strain gauge input module from ICP DAS. The rotation of the three shoulder axes are measured by three off-the-shelve potentiometers; the elbow axis by the quadrature encoder (resolution: 2500 CPR) from US Digital, consisting of a transmissive rotary code wheel (outer dimension: 2 inch, inner dimension: 1 inch) and a separate encoder module (EM1). The 3D position of the base of the exoskeleton is measured by linear quadrature encoders from US Digital (resolution: 250 CPI, consisting of a transmissive linear strip and a separate encoder module, EM1) over the full length of the three beams of the linkage. All analog and digital signals run through three shielded printer cables from the Dampace robot to a separate controller station with the computers.

Note that due to the passive brake mechanism, the measured brake torque T_{br} is a complex function of the internal brake pressure and the torque exerted by the human arm T_{arm}. When the arm is inactive, no torques are present in the system and thus none can be measured. With the arm active, the measure brake torque T_{br} is the minimum of the arm torque T_{arm} and the set brake torque. These nonlinearities of the measured brake torque T_{br} make closing of the middle torque control loop unstably variable.

In experiments with a constant brake pressure in a disk brake, varying the joint velocity from almost zero to the maximum arm velocity caused at most 10% variation on the braking torque. Because the braking torque is mostly hydraulic-pressure dependent and joint-speed independent, achieving a constant braking torque requires little effort. Based on these results, a feed-forward P-controller was implemented for the brake torque C_{br}, circumventing the inherent difficulties of using the measured brake torques F_{br} as mentioned above.

The torque-bandwidth was measured using multi-sine input signals to estimate the frequency response and squared coherence functions of the system of Fig. 8.6. The functions were estimated with cross- and auto-spectral densities $S(s)$ of input (i) and output (o) [93, 13]. The input signal consisted of 80 summed sines with a observation time of 256 s, spaced logarithmically from 0.1 to 100 Hz, and having a constant power spectral density and random phase shifts. Measurements were repeated four times with four different multi-sine signals and the results averaged in the frequency domain over four frequencies and the four repetitions. For a

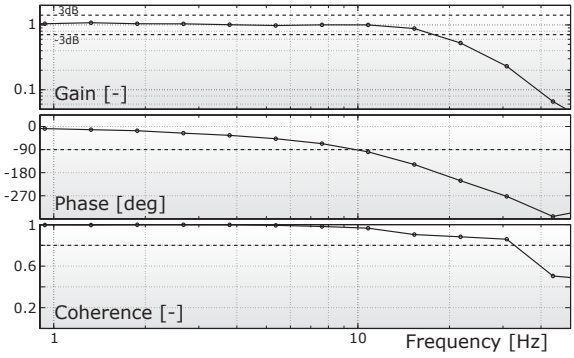

Figure 8.7: Torque bandwidth for a 20 Nm multisine reference signal, with the frequency response function from the reference torque T_{ref} to the measured torque T_{br}. The -3 dB gain bandwidths is 18 Hz, and the -90 ° phase bandwidths 10 Hz. The effects of the 2 m long hydraulic cable are seen by the rapidly increasing phase delay. The transport delay in the cable was found to be 5 ms.

black-box system with single in- and outputs, the estimated frequency response function $C(s)$ and squared coherence function $Coh(s)$ are:

$$C(s) = \frac{S_{io}(s)}{S_{ii}(s)} \tag{8.1}$$

$$Coh(s)^2 = \frac{|S_{io}(s)|^2}{(S_{ii}(s) * S_{oo}(s)} \tag{8.2}$$

The frequency response function $C(s)$ is an estimate for the dynamics of the black-box system. The squared coherence function $Coh(S)$ is a measure for the signal to noise ratio and thus the linearity of the system. The squared coherence ranges from zero to one, with one meaning no non-linearities or time-varying behavior are present.

Although the brakes are rated for up to 200 Nm, the dynamics of the chosen electro motors limit the actually braking torque to 50 Nm with a bandwidth of 10 Hz for multi-sine torques up to 20 Nm (see Fig. 8.7). These amplitude and bandwidth values allow for good positional and torque control of the exoskeleton axes. Speed-dependent resistance, for instance needed for isokinetic control, is more difficult to accurately achieve at high levels of torque and speed. Finally, contrary to the presence of residual resistance torques in other actuators like electro motors and magneto-rheological dampers [195, 198, 196], the achievable minimal impedance with disk brakes is zero. The only impedance torques exerted on the arm come from the inertia of the exoskeleton, not the brakes.

8.3.3 *Weight support*

The weight support forces come from three independent ideal-spring mechanisms at the base of the Dampace (see Fig. 8.8), similar to our earlier Freebal weight-support system [201, also see Chap. 4]. The three mechanisms deliver constant forces to the base of the exoskeleton, the elbow and the wrist. The cable beam is vertically hinged roughly above the human shoulder, which, together with the small slider underneath the cable beam, positions the weight support exactly over the wrist and elbow. To reduce swinging oscillations, a small damper was added to the hinge of the cable beam.

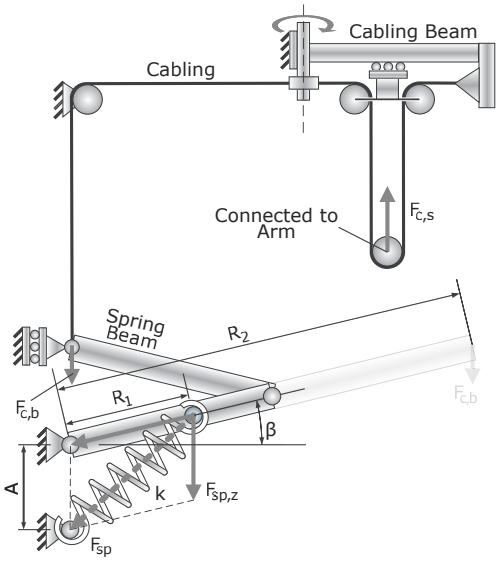

Figure 8.8: Weight support mechanism. The Dampace has three, operating independently of each other and connected to the exoskeleton linkage, the elbow and the wrist. The weight support force $F_{c,b}$ at the end of the split spring beam is independent of the spring-beam angle β for all angles, because the decompositioned ideal-spring force F_{sp} in the z-direction ($F_{sp,z}$) is always equal to distance A times spring-stiffness k. As $F_{c,b} = F_{sp,z}\frac{R_1}{R_2}$, the amount of weight support can be altered by changing the spring-attachment distance R_1. The weight support force on the sling, $F_{c,s}$, is here equal to $2F_{c,b}$ in a working volume as defined by Tab. 8.1. The cabling beam is vertically hinged roughly above the human shoulder, which, together with the small slider underneath the cabling beam, positions the weight support exactly over the wrist and elbow.

The worm-wheel slider in the spring beam alters the spring attachment point on the beam (see Fig. 8.8), length R_1), which linearly changes the compensation force $F_{c,b}$ according to [201]:

$$F_{c,b} = F_{sp,z}\frac{R_1}{R_2} = kA\frac{R_1}{R_2}, \tag{8.3}$$

where $F_{sp,z}$ is the component of the spring force in the vertical direction, R_1 is distance from the spring beam rotation axis to the spring attachment point on the beam and R_2 is the length of the projected spring beam. The vertical spring force $F_{sp,z}$ is equal to the spring stiffness k times the distance between the spring beam axis and the spring attachment point on the base. This attachment point must be located directly beneath the beam axis. Furthermore, the spring must behave like an ideal-spring; that is, the spring force must change linear with the spring deflection and be zero at zero spring length [74]:

$$\begin{aligned} F_{sp} &= k_{sp}\Delta x_{sp}, \\ F_{sp} &= 0 \text{ when } x_{sp} = 0. \end{aligned} \tag{8.4}$$

The needed amount of weight support is dependent of the measured weight of the arm. By locking the shoulder elevation and elbow axis (with a horizontal elbow axis orientation) and weighing the torques around these joints, the weight of the arm can be determined. The amount of support is indicated by the moving slider on the long axis of the spring beam.

8.3.4 *Interaction control*

The controllers are programmed in Matlab Simulink (The MathWorks) and compiled to run in an open-source, real-time Linux environment (RTAI [7, 20], [rtai.org]) with open-source hardware drivers (COMEDI, [comedi.org]) for the three National Instruments Corporation DAQ devices (analog input: PCI-6034, encoder input:

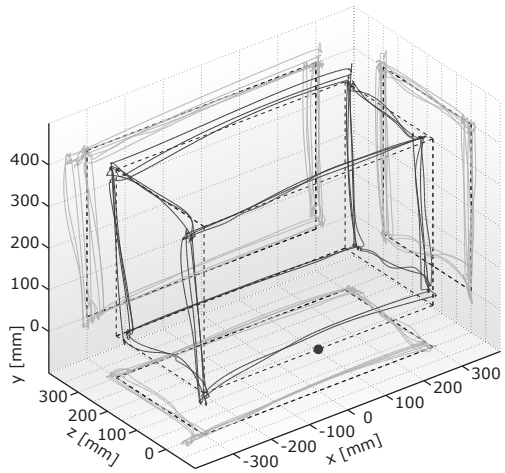

Figure 8.9: Measured accuracy of the reconstructed fingertip position. The healthy subject was seated in front of the long side of the 600 x 400 x 300 mm rectangular frame and asked to trace it with his fingertip. The black stripped lines represent the frame, the dark gray lines the actual trace, and the light gray lines the shadow projections of the trace. The starting position of the fingertip was at the solid black ball, with the upper arm pointing downward and the forearm forward. The lower front and right hand corners were difficult to trace due to the arm and exoskeleton being obstructed by the trunk of the subject and the ribs of the rectangular frame. In general, the fingertip was reconstructed within 20 mm of the actual position.

PCI-6602, analog output: PCI-6703) and have real-time logging and graphical user interface possibilities through Python scripts. The controller runs at a minimum of 1000 Hz on a single core Intel Pentium IV computer.

The feedback controller in the Dampace analyzes the measured rotation angles and joint torques of the four exoskeleton axes and the translation of the linkage. It applies resistance torques to the joints based on these measurements and/or the desired torques. Besides this control in joint-space, the Dampace can also calculate endpoint positions and forces in global coordinates. The accuracy of the calculated endpoint properties suffers slightly due to the large number of mechanical components between the global reference frame and wrist or finger.

To calculate the endpoint position, each component has its position and orientation information calculated relative to the previous component. This creates a cascading set of rotation and transformation matrices. The endpoint forces are calculated by measuring the torque at each axis, then dividing these by the perpendicular length of the axis vector to the endpoint, and summing the resulting four forces at the endpoint and accounting for movement inertia where needed.

To measure the endpoint positional accuracy, a healthy subject traced a 600 x 400 x 300 mm rectangular frame (see Fig. 8.9) with the tip of the index finger. The finger was kept stiff and inline with his forearm without using additional aids. Most of the time, the Dampace software reconstructed the tip of the finger within 20 mm of the actual position. The reconstruction was based on the know dimensions of the Dampace and the measurements of shoulder to elbow and elbow to fingertip lengths. Most problems, especially those in the lower right hand corner and the lower front bar, were due to the subject not being able to touch the frame due to the exoskeleton colliding with the frame or his own body. For control of rehabilitation exercises, this level of accuracy is more than sufficient. It represents the worst case scenario of a large volume to work in, with the finger as a non-stiff pointer.

Unfortunately, the calculated endpoint forces suffer from variable inter-joint interference. The measured elbow torque is affected by simultaneous movements against shoulder torques perpendicular to the elbow axis. The shoulder torque influences elbow measurements by up to 25%. In the final analysis, and after

trying several solutions to no avail, the elevated cabling at the elbow (see Fig. 8.4) seems to be the culprit. The shoulder torques cause some slight deformation of the elbow bearings, thereby increasing or decreasing the tension in the elevated cabling. To solve this problem, the cabling either has to be brought inline with the elbow joint—thus between the bearings instead of above them—or replaced by push-pull parallelograms. With no perpendicular loading on the elbow joint, the sensor measures the brake torques correctly and the above endpoint force calculation result in the correct endpoint force vector.

8.4 PATIENT INTERACTION

In the full set of identifying the limitations of a specific stroke patient, isolating the problem and combating these with functional or targeted force-coordination exercises, and integrating the achieved improvement back into activities of daily living, the Dampace can make an important contribution. Identification can be helped by determining the active, unrestricted range of motion, the maximum isometric and resisted forces and speeds, or any other combination of active forces and movements, all measured directly in joint space. In functional or targeted force-coordination exercises, the controller can apply resistance to specific parts of the movement. This can both restrict or guide the arm to stay inside a desired movement space or make a movement harder to do, thereby increasing the training intensity (see Fig. 8.10). Finally, at the end of the rehabilitation process, the isolated and targeted training exercises can be gradually integrated into fully functional movements. Thus a force-coordination training to increase the arm strength and control of, for example, an extended arm can be turned into manipulating real objects in a kitchen type of environment. The posture of the forearm also influences the sensory input to the motor cortex [137], increasing the importance of allowing the forearm to orientate itself correctly for the functional task at hand. In all stages, the hand can be an integral part of the exercises, as it is always left fully usable.

8.4.1 *Virtual environments*

Although an exoskeleton is probably not the best way to achieve perfect haptic feedback, it is possible to simulate some environments. Virtual movements in water requires damping, while static friction is needed for lifting a heavy object or movement over a rough surface. More elaborated environments [167, 43] with time-, position-, and directional-dependent resistance and damping have less clear real-world synonyms, but could be interesting for studying specific symptoms. Even so, the environments which can be simulated are limited to those which require no energy input to any part of the system. The resistance trainer can only disperse energy and the applied torques are always working against the rotational direction. Another restriction is the limited bandwidth of the brakes (10 Hz), which make it impossible to create hard surfaces at exact locations. These are not needed for most rehabilitation exercises. With all virtual environments, the haptic feedback is transferred from the exoskeleton to the human arm via cuffs to the upper and forearm, and not via the hand. The decomposition of hand forces to shoulder and elbow torques might be correct, but the 'erroneous' tactile connections of the cuffs do influence the haptic sensation.

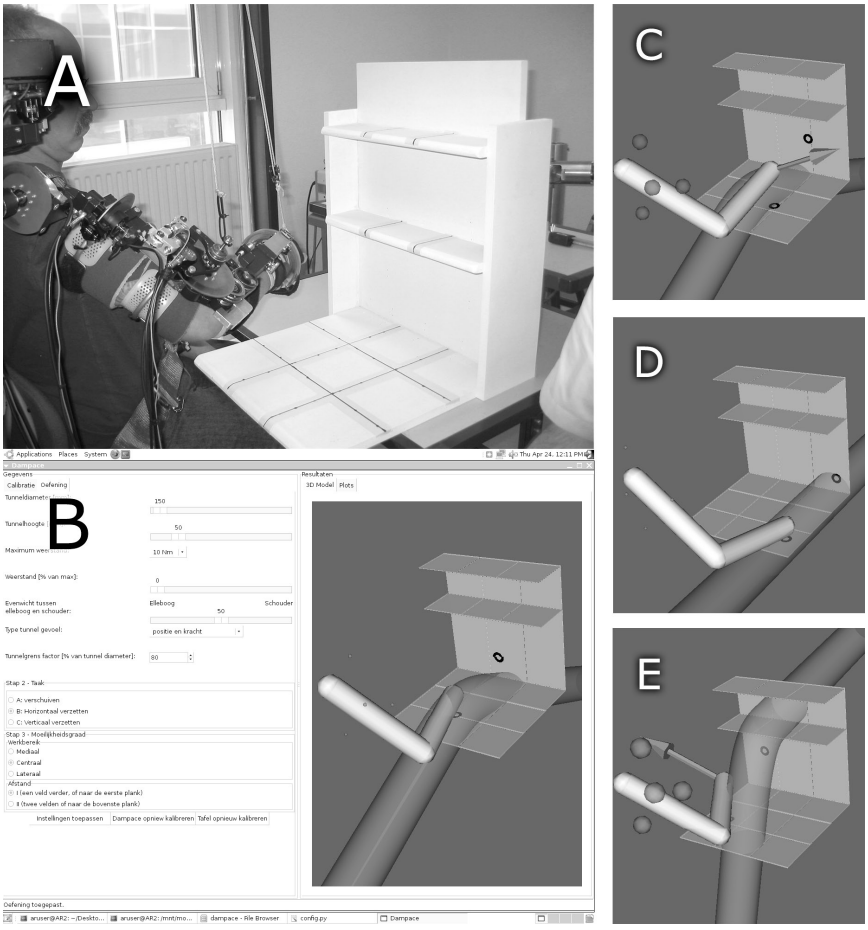

Figure 8.10: Resistance training setup (A) and user interface (B), where the table of the real world environment (A) is recreated in the computer to allow virtual control (B-E). Patients need to move real objects, sometimes just sliding, at other times lifting it to shelves at up to shoulder level. The movements can be made more difficult by increasing the resistance torque on the shoulder and elbow joint, which the therapist can adjust via the user interface. To guide the patient in making the movement, a virtual tunnel is created (B). When the hand moves out of the tunnel (C), all the disk brakes lock until the direction of the hand force (shown with an arrow) is again aimed toward the tunnel. The desired trajectory can be altered in direction and movement height (D), or desired vertical displacement (E). The amount of current brake force is indicated by the color and size of the four visible balls, representing the axes of shoulder and elbow.

8.4.2 *Gaming interface*

In another current example, specific training combats the effects of unwanted multi-joint muscle synergies [11, 45, 46], which is important for patients to regain more functional use in their affected side. To motivate subjects, the human movement

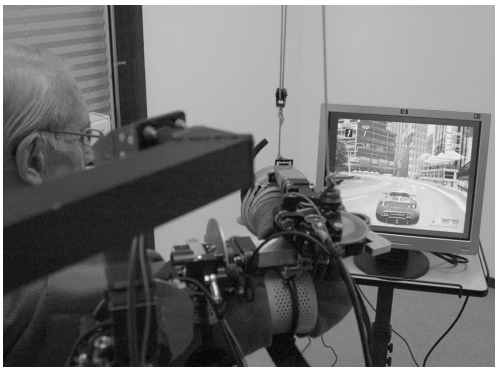

Figure 8.11: Integrated gaming environment connected to Dampace torques and movements. Either isometric thoracohumeral-elevation torques or isotone rotations are mapped to the gas paddle in the racing game, and either humeroulnar isometric torques or isotone rotations to the steering wheel. Good coordination of simultaneous shoulder and elbow torques is thus required for good driving control in the game and should motivate the subjects to keep exercising.

and force execution are linked to a gaming console (see Fig.8.11). Either isometric thoracohumeral-elevation torques or isotone rotations are mapped to the gas paddle in the racing game, and humeroulnar isometric torques or isotone rotations to the steering wheel. Good coordination of simultaneous shoulder and elbow torques is thus required for good driving control in the game and should motivate the subjects to keep exercising. Although this specific game is too demanding for most stroke patients, it gives an impression of possible alternative training environments with targeted impairment-reduction strategies.

8.5 DISCUSSION AND CONCLUSIONS

Not needing to align the Dampace axes to the human shoulder and elbow joints overcomes some of the difficulties traditionally associated with exoskeletons. Although it adds more complexity, the reduction of setup times to a few minutes and the absence of most reaction forces in the human joints are major advantages [186, 185]. These have been well received by therapists and physicians. Controlled braking instead of actively assisting actuators has the advantage of inherent safety and always actively participating patients, at the cost of not being able to assist movements or create some virtual environments. The inherent safety is an important aspect to ensure confidence in the device by patients, therapists and ethical commissions alike.

Early experiments with healthy subjects and stroke subjects showed that the attention paid to the self-alignment of the axes and reducing the friction in the linkage and weight support system was well spend. Still, the linkage is about four times heavier as desired, and the linear bearings have too much friction. Having the third shoulder axis of the exoskeleton run parallel but with an offset to the axial rotation axis of the human shoulder generates a lot of linkage movement. As these movements lead to large inertial forces, in future designs the orientation of this third axis needs to be reconsidered. Reducing the weight of and friction in the linkage, and also reducing the amplitude of the necessary linkage translations, should reduce the felt impedance forces fivefold. This should bring them close to 1 kg in any direction. Adding controlled actuators to the linkage in a zero-impedance mode [224], can further reduce these forces. For better measurements of joint angles during resisted movements, better arm cuffs are needed. These should potentially use more bony landmarks, as some elderly subjects had very soft arm tissue. The lack of interaction stiffness caused the exoskeleton to have

angle offsets with the the limb when subjected to torques above 25 Nm. Finally, with an static device it was determined that up to 120 Nm of static braking force may be needed for isometric measurements with healthy subjects. This is beyond the maximum strength of the Dampace exoskeleton, although the disk brakes could provide the these torques.

Although actively controlled resistance may be enough for motor relearning after a stroke, preliminary results of other, active robots seems to indicate that properly supplied assistance can help recovery times [168, 107, 31, 24]. Determining the proper kind of assistance is thus still a matter of current research in motor skill training and adaptive shared control contexts.

8.5.1 *Conclusion*

In conclusion, the Dampace is well suited to offer force-coordination training with functional exercises. It increase exercise intensity for patients by resisting movement. The passivity of the disk brakes forces active patient participation. The flexibility and range of motion of the exoskeleton allow most functional movements of daily living. Specific impairments can be targeted by the selective control over joint rotations. And finally, the decoupling of joint rotations and translations reduce setup times and minimize interaction forces, which improves the usability for rehabilitation therapy.

The Dampace can assist in quantifying movement impairments of stroke patients via unrestricted, isometric or isotonic torque measurements. After quantification, the impairments can be targeted with isolated force-coordination training, potentially over multiple joints. In the last step, the isolated training can be slowly transformed into functional, task-specific training protocols.

ACKNOWLEDGMENT

The authors would like to thank Gert-Jan Nevenzel, Huub ter Braak and Theo Krone for development assistance, and Thijs Rupert, Windel Bouwman and Thijs Krabben for their work on the Dampace software.

9

DESIGN OF A ROTATIONAL HYDRO-ELASTIC ACTUATOR FOR AN ACTIVE UPPER-EXTREMITY REHABILITATION EXOSKELETON

ABSTRACT The Limpact exoskeleton uses novel rotational hydro-elastic actuators (rHEAs) consisting of rotation hydraulic actuators and symmetric torsion springs. The goal of this paper is to validate the suitability of the new actuator for its intended use in stroke rehabilitation. The desired control modes include regular impedance and springless admittance control of up to 50 Nm at 5 Hz and 5 Nm at 20 Hz. Static forces should be measurable up to 100 Nm. The long flexible tubes between the valve and cylinder required changes to the existing theoretical models, resulting in a better model fit of the frequency response functions. Finding the best design for the symmetric torsion spring was an iterative process, and the spring used here had a maximum torque (22 Nm) below requirements. For current springs actually in use in the Limpact, the maximum output torque is 50 Nm. Identification showed the torque bandwidth at 18 Hz for a desired 20 Nm (multi sine, constant spectrum) signal, mostly due the transport delays in the long flexible tubes. The measured torque resolution was better than 0.01 Nm. The delivered torque resolution was below 1 Nm. In conclusion, rHEA is suitable for upper-extremity rehabilitation therapy, as it matches the desired torque bandwidths, resolutions and amplitudes.

9.1 INTRODUCTION

Patient-friendly robots are used as diagnostic and therapeutic aids in upper-extremities rehabilitation, and almost none look alike. Through physical manipulation of the arm and assisted by virtual environments, innovative interaction schemes are explored in search of the best possible therapy. Overall, robot assisted therapy is considered to be as good or better than conventional therapy [219, 157, 162, 112]. Robot assisted therapy is more challenging for the patients and less labor intensive for the therapists, and provides the physicians, therapists and scientific community with more objectively gathered data.

Systematic reviews on non-robot assisted therapy for the upper-extremities also indicate that intensive and task-specific exercises consisting of active, repetitive movements, give the best results [187, 109, 8, 56]. Actively generated movements requires more brain activity and results in better motor learning, when compared to externally-powered arm movements without active patient participation [119]. But for all this, it is important to remember that improved motor control is not necessarily enough to restore lacking functional ability.

With the Freebal [201, also see Chap. 4] and Dampace [202, also see Chap. 8], we created two passive devices for rehabilitation therapy. The Freebal supports the arm against gravity via a passive cable-pulley system, and facilitates shoulder and elbow movements without disturbing normal motor control [92, 163, 164]. The

Accepted pending minor revisions: IEEE Transactions on Biomedical Engineering (AHA Stienen, EEG Hekman, H ter Braak, AMM Aalsma, FCT van der Helm, and H van der Kooij).

Figure 9.1: The design of the upcoming torque-driven exoskeleton, the Limpact. It has self-aligning joints in the exoskeleton, made possible by a freely translating but rotational stiff linkage behind it. The four rHEAs are positioned such on the joints that the flexible tubes (not displayed) do not interfere with each other.

Dampace is a passive, self-aligning exoskeleton, which actively controls resistance torques on the shoulder and elbow joints.

As passive devices, both the Freebal and the Dampace force the patients to actively participate. In a three step process of identification, isolation, and integration—that is, identifying causes behind the movement disorder, tackling these with isolated, impairment-directed training, possibly over multiple joints, and integrating the improvements via functional, task-specific training back into activities of daily living—they are well suited for the last two stages. But passive devices are not always appropriate for impairment quantification. For example, for separating intrinsic and reflexive components of human arm dynamics [217], active devices are needed to trigger the human system. With an active device, it is also possible to provide assist as needed [231] and create more realistic virtual environments [143].

In the LOPES project for the lower extremities [224], we have had good experiences with series elastic actuation (SEA) [166, 171]. The SEA makes highly-compliant impedance control for the LOPES joints possible [223, 43, 214], despite high and highly variable friction forces in the Bowden cables. More in general, a SEA has low output impedance and good back-drivability, force output resolution and force control, as compared to directly connected electro motors with gearboxes. SEA does not require a perfect model of the entire actuator to operate, as the actuator is controlled on the direct measurement of the spring deflection. This spring deflection measures the applied forces at the point of application at the end of the force chain, allowing the SEA controller to reject most of the system noise, non-linearities and interfering dynamics which entered the chain at any previous point. These properties make SEA a good choice for a powered exoskeleton for the arm.

Therefore, for active assistance during therapy and more possibilities for impairment quantification, an additional active device is needed which stays close to the mechanical design of the Dampace and uses SEA as its power source. For the SEA, space and weight requirements on an exoskeleton lead to a low-volume rotational design. The goal of this paper is to validate the suitability of the new actuator for

powering the new Limpact rehabilitation exoskeleton (see Fig.9.1) for use in stroke therapy.

A preliminary version of this work has appeared at IEEE Biorob 2008 [204].

9.2 REQUIREMENTS

The SEA should be able to deliver 50 Nm of torque with a bandwidth of 5 Hz. This is needed for weight support of exoskeleton and arm, measuring spasticity in stroke, and triggering the internal human systems for identification. For more conventional therapy exercises and simple virtual environments, 5 Nm at about 20 Hz is sufficient. The delivered torque resolution should be below 1 Nm, and the measured torque resolution below 0.1 Nm. The minimal impedance, the torque felt when moving the arm while no torque is requested, is preferably as low as possible. Isometric torques need to be measured at up to 100 Nm, but additional mechanisms may be used to make this possible. The final design should weigh less than 1.5 kg, to be directly mountable on an exoskeleton.

Most other requirements for the SEA result from the overall design of the Limpact exoskeleton. Like in the LOPES project [224], electric motors and gearboxes which can deliver the required power are too heavy to directly mount on the exoskeleton. LOPES uses Bowden cables to connect the motors on the base frame to the series elastic elements on the joints. The required cable pretension results in large amounts of non-linear friction which fluctuates strongly with cable orientation changes due to exoskeleton movements, up to 40% of maximum torque, and a lot of wear and tear. The SEA can compensate for most of the friction, but not all. An arm exoskeleton has much larger joint rotations than one for the legs, resulting in more cable bending and thus more unpredictable friction.

For the Limpact, the Bowden cables were replaced with hydraulic actuation, while keeping the series-elastic element. The rotational hydraulic actuators are mounted directly on the joints, but the large servo valves are not. These are placed on the base frame, connected to the actuators via 2 m long flexible tubes. Tube dynamics, and other effects like piston friction, are better predictable and much less variable with movement than the friction forces in Bowden cables, and any remaining unknown dynamic effects are account for by the aforementioned principle of SEA. The resulting rotational hydro-elastic actuator (rHEA) is a rotational variant of the linear HEA [172].

9.3 DESIGN

The rHEA design (see Fig.9.2) is a combination of a symmetric torsion spring, an hydraulic actuator, and high precision quadrature encoders. The overall design weighs less than 1.5 kg, including oil, but excluding the weight of the flexible tubes. At 70x100mm, it is very compact (see Fig.9.3). The springs is at 0.150 kg the heaviest component and is located at the bottom of the rHEA; the lightest elements, the sensors, are positioned on top, resulting in the best possible weight distribution.

The design has three rings at the bottom. The upper ring is connected to the base of the hydraulic actuator, the middle spring ring to the output of the hydraulic actuator and the base of the spring, and the lower ring to the output of the spring and total rHEA. At the elbow, for instance, the upper ring is fixed to the upper arm

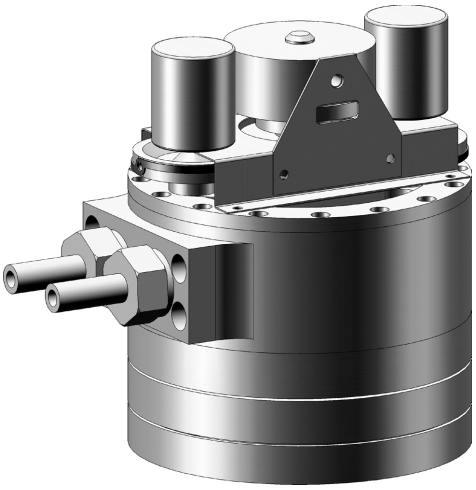

Figure 9.2: Rotational hydro-elastic actuator (rHEA), a rotational variant of the linear HEA [172], in a compact design [189, 190], for use on the Limpact exoskeleton.

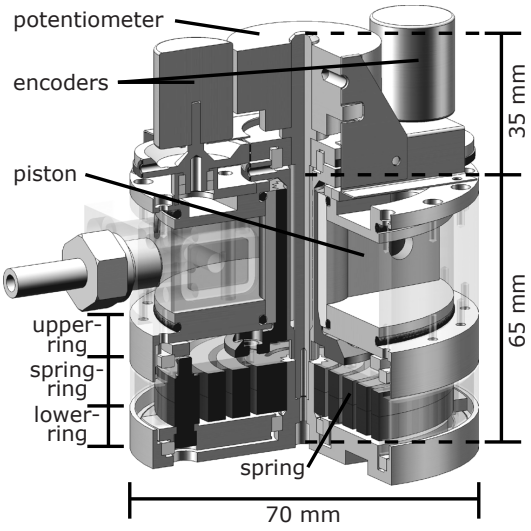

Figure 9.3: Open view of the rHEA. From top to bottom: the angular sensors, the hydraulic actuator, and the spring.

and the lower ring to the forearm. The difference between the lower ring and the spring ring, times the spring stiffness, is the actuator torque. The spring deflection is limited to the maximum desired torque by a chamber in the lower ring. By manually locking the lower and spring ring together, the spring is bypassed and the rHEA can be used as a regular spring-less hydraulic actuator. Locking all three rings together sets up the actuator for isometric measurements up to 100 Nm, with the torque measured by strain gauges in the lower ring.

9.3.1 *Symmetric torsion spring*

The most important element in a SEA design is the elastic element. The spring stiffness should be chosen carefully; too low and it reduces the torque bandwidth, too high and it increases the impedance and worsens the torque output resolution [166]. With recommendations from literature [172] and based on the experience with LOPES, a desirable stiffness of about 150 Nm/rad was selected.

In another compact SEA design [189, 190], they used a spandrel-shape torsional spring with a stiffness of 327 Nm/rad. This long torsional spring runs through the center of their frameless motor and gearbox, but the hydraulic actuator has no room for such a solution. Besides this, for the desired torque output resolution, their spring stiffness is too high and their maximum permissible torque too low. Lowering the spring stiffness with equal or higher maximum strength and equal dimensions, is not trivial.

To fit in a compact design, the torsion spring has to be flat like a clock spring. Wrapping or unwrapping a clock spring offsets the middle of the spring, resulting in large loads on the bearings and deformations in the construction. Using two

Figure 9.4: Symmetric torsion spring from strong-yet-malleable maraging steel, were the reaction forces of both windings are canceled out, keeping spring center always in the middle.

symmetric windings cancels their offsetting forces (see Fig. 9.4), at the cost of needing more material to achieve the same maximum strength and spring stiffness. By using maraging steel (type 18Ni, alloy 350), which has a high yield stress of 2400 MPa and is very tough, resilient and malleable, the dimensions of the spring need only to be 10 mm high, 60 mm in diameter and with 4.5 mm thick windings for a maximum strength of 50 Nm and an expected spring stiffness of 150 Nm/rad. The springs are made by electrical discharge machining.

The used finite element program (COSMOSWorks, Dassault Systemes) could not handle the large deformations in the original spring design. This first spring, used in the validation experiments below, was 50 mm in diameter, with 3.5 mm thick windings, and was a lot less stiff (88 Nm/rad) than the intended 125 Nm/rad. The windings touched each other at 22 Nm, long before the intended maximum torque of 50 Nm. Overall, the oval shape deformation of the windings was much flatter in the real spring than predicted. Therefore, the spring for the final rHEA design for the Limpact has been scaled to the aforementioned dimensions.

As a rule of thumb, the thicker the winding or the overall spring, the higher the allowable torque and the stiffer the spring. Longer windings reduce the spring stiffness, but need more room to wrap and unwrap. Best results are achieved when the windings just touch when the maximum torque is reached, as this acts as an integrated safety mechanism to reduce overstretching of the outside of the windings.

9.3.2 *Sensors*

In the rHEA, two ultra miniature, high resolution quadrature kit encoders (Avago AEDA-3300 Series, $N_{ppr} = 80000$ pulses per revolution) measure the angle between the upper and lower ring, and between the upper and spring ring. The difference between the two encoders is equal to the deflection of the spring. By multiplying the deflection with the spring stiffness, the encoders function as torque sensor with a resolution equal to $2\pi K_{spr}/N_{ppr} \approx 0.01$ Nm, with K_{spr} the spring stiffness.

The angle between the upper and lower ring is also measured by a potentiometer to initialize one of the encoders and signal any sensor malfunctions. Strain gauges at the lower ring have the same function for the other encoder, and will also measure the torque on the actuator during isometric measurements.

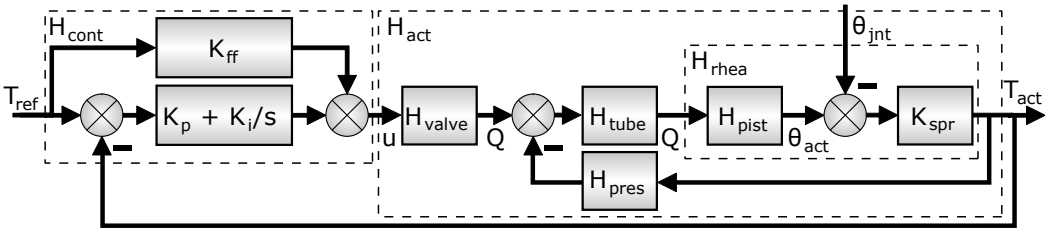

Figure 9.5: rHEA control diagram, with the feedforward gain K_{ff}, and proportional and integrator gain settings K_p and K_i [172] as the controller H_{cont}. H_{valve} represents the hydraulic valve, H_{tube} the tube dynamics of the 2 m long flexible tubes, H_{pist} the rotational piston in the rHEA H_{rhea}, and K_{spr} the rotational spring stiffness, which together form the complete actuator H_{act}. The actuator torque T_{act} is measured by multiplying the deflection of the spring ($\theta_{act} - \theta jnt$) with K_{spr}.

9.3.3 *Control model*

One of the advantages of using an elastic element at the final end of the actuation chain is the use of straightforward control schemes. No complex hydraulic modeling of the rHEA is required, as just the relative displacement of the spring is controlled. On the linear hydro-elastic actuator (HEA) [172], they used a standard PI controller. The control diagram for the rHEA is similar (see Fig. 9.5), but has an additional feedforward gain K_{ff} parallel to the PI controller $(K_p + K_i/s)$. The feedforward gain sets the opening of the hydraulic valve to get a known displacement of the spring. This prior knowledge results in less tracking error, enabling higher feedback gains of the PI controller, improving overall performance.

Almost no modeling is needed to control a rHEA and the PI-controller was tuned based on generic tuning rules. But to better analyze the performance of the rHEA in open en closed-loop situations, several models based on the generic control diagram in Fig. 9.5 were fitted on the measured results. The following analysis is based on the HEA of Robinson and Pratt (2000, denoted below by 'rp') [172]. To get from their linear, force controlled HEA to the rotation, torque controlled rHEA, some changes were made. Each force F is replaced by torque T, displacement x by angle θ, and piston area A by piston area times the radius to the piston area center Ar ($A = 420\ mm^2, r = 16\ mm$). Tube dynamics H_{tube} and pressure feedback H_{pres} were added.

The original components of the generic control diagram [172], converted to the rotation actuator, are:

$$\begin{aligned} H_{valve,rp}(s) &= \frac{K_{v,rp}}{(\tau_1 s + 1)} \text{ or} \\ &= \frac{K_{v,rp}}{(\tau_1 s + 1)(\tau_2 s + 1)(\tau_3 s + 1)}, \\ H_{tube,rp}(s) &= 1, \\ H_{pist,rp}(s) &= \frac{1}{Ars}, \\ H_{pres,rp}(s) &= 0, \end{aligned} \tag{9.1}$$

in which the H_{valve} is a first or third order approximation of the highly-complex valve dynamics, converting a control signal opening the hydraulic valve u to a hydraulic flow Q, based on the valve gain $K_{v,rp}$ and the time constants τ_{1-3}. The rotational piston H_{pist} in the rHEA displaces the spring by an angle θ_{act} based on the delayed incoming flow Q. After subtracting the joint displacement angle θ_{jnt}, the spring displacement is multiplied with the rotational spring stiffness K_{spr}.

The actuator model H_{act} was changed to account for some of the valve-flow dependency on the pressure drop caused by the increase of pressure feedback due to the deflected spring [172]:

$$Q_{max} = K\sqrt{P_s - \frac{T_{act}}{Ar}}, \tag{9.2}$$

by reducing the valve flow Q with a rough linearized gain approximation K_{pf} in the pressure feedback H_{pres}. As these effects were originally captured in the valve model $H_{valve,rp}$, this model was simplified to a direct gain. A transport delay H_{tube} was added which mimics the effects of the long tubes by delaying flow Q through the tubes by τ_2. The components of the control diagram now become:

$$\begin{aligned} H_{valve}(s) &= K_v, \\ H_{tube}(s) &= e^{-s\tau_2}, \\ H_{pist}(s) &= \frac{1}{Ars}, \\ H_{pres}(s) &= \frac{K_{pf}}{Ar}. \end{aligned} \tag{9.3}$$

The complete power chain H_{act} of valve, tube and rHEA and the frequency response function of the entire controlled system H_{sys}, are given by:

$$\begin{aligned} H_{act}(s) &= \frac{H_{valve}H_{tube}H_{pist}K_{spr}}{1 + (H_{tube}H_{pist}K_{spr}H_{pres})}, \\ H_{sys}(s) &= \frac{(K_{ff} + K_p + \frac{K_i}{s})H_{act}}{1 + (K_p + \frac{K_i}{s})H_{act}}. \end{aligned} \tag{9.4}$$

9.4 VALIDATION

The open-loop and closed-loop performance of the rHEA was measured by output torque tracking with fixed angular output θ_{jnt} to get the torque bandwidths, and maintaining zero output torque during angular disturbances to get the minimal impedance. Step responses and virtual springs show some general uses of the rHEA.

For these measurements, the test setup in Fig. 9.6 was used. The generic hydraulic pump and external accumulator delivered a close to constant source pressure P_s of 8 MPa throughout the tests. The servo valve used was the Parker D1FP-E50M-9NS00, connected to flexible tubes rated for a maximum of 120 MPa and with a 6 mm inner diameter.

9.4.1 *Multi-sine identification*

For the open- and closed-loop identification, the system was perturbed with multi-sine input signals to estimate the frequency response $C(s)$ and squared coherence

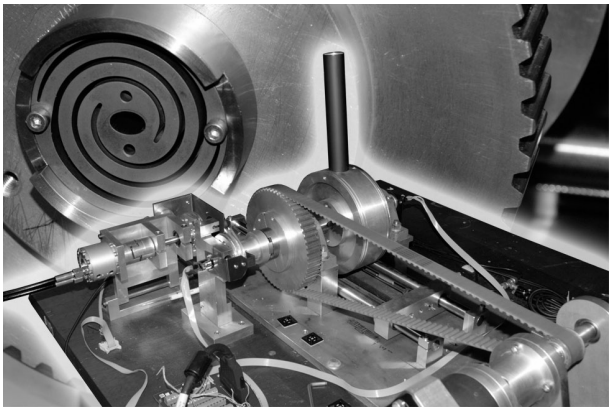

Figure 9.6: Experimental setup. The hydraulic actuator (left mid), spring (mid and background) and sensors were mounted separately for easy access. The actuator drives the spring center and the outer spring ring is mounted to the gear wheel. Fixing the gear wheel gives a static base for bandwidth experiments. The impedance is measured by powering the gear wheel with an external electro motor (bottom right). Freeing the gear wheel and using the top handlebar allows manual interaction.

$\mathrm{Coh}(s)$ functions. These functions were estimated with cross- and auto-spectral densities $S(s)$ of input (i) and output (o) [93, 13, 217]. For a black-box system with single input and single output, the functions are:

$$C(s) = \frac{S_{io}(s)}{S_{ii}(s)},$$
$$\mathrm{Coh}(s)^2 = \frac{|S_{io}(s)|^2}{S_{ii}(s)S_{oo}(s)}. \tag{9.5}$$

The frequency response function $C(s)$ is an estimate for the dynamics of the black-box system, and the squared coherence function $\mathrm{Coh}(S)$ a measure for the signal to noise ratio at each frequency. The squared coherence [155] ranges from zero to one, with zero meaning the lack of correlation between the input and output, and one the absence of noise or time-varying behavior. Higher harmonics in periodic signals may interfere with the interpretation of the coherence function.

For all but the minimal-impedance measurements, the input perturbation signal consisted of 80 summed sines with a observation time of 256 s. The frequencies of the sines were spaced logarithmical from 0.1 to 100 Hz, were of constant power spectral density, and had random phase shifts to reduce amplitude peaks in the summed signal. Due to the lack of motor power for external disturbance in the minimal-impedance measurements, this multi-sine input signal was limited to 64 sines, spaced from 0.1 to 25 Hz.

The logarithmical spacing of the sine frequencies prevented the use of crest optimization on the total signal. Therefore, the amplitude of the total signal was scaled on two or three times the standard deviation and not the peak-to-peak values, with the mean of the signal always at zero. Measurements were repeated four times with four uniquely generated multi-sine signals, differing on the used random phases. The results were averaged in the frequency domain over four frequencies and the four repetitions to improve the coherence of the measurements and estimates.

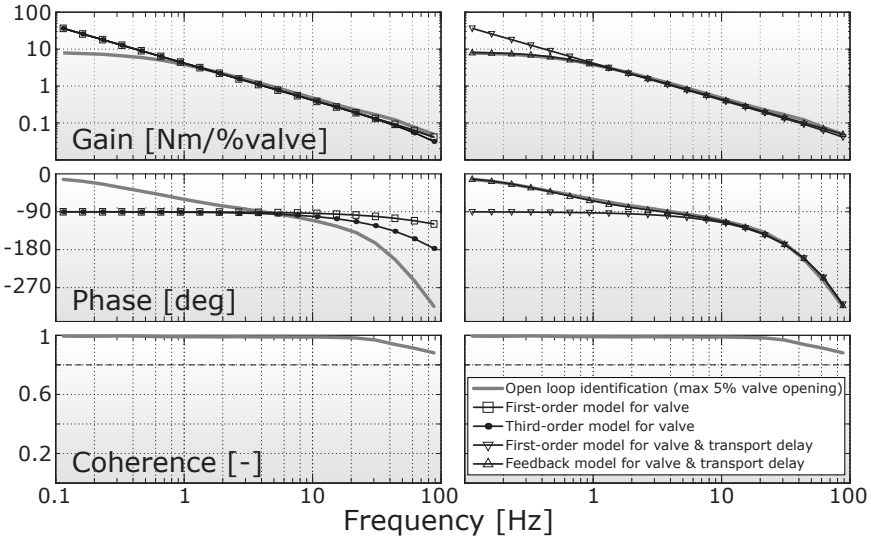

Figure 9.7: Bode plot of the open-loop identification of the complete actuator $H_{act,ol} = T_{act}/u$. The open-loop results were fitted with actuator models $H_{act,ol1-4}$ consisting of the valve, tube, piston and spring components. $H_{act,ol1}$: line with open squares, $H_{act,ol2}$: line with closed circles, $H_{act,ol3}$: line with downwards pointing triangles, $H_{act,ol4}$: line with triangles pointing up. $H_{act,ol4}$ clearly results in the best fit.

9.4.2 *Open-loop actuator*

For the open-loop identification of the actuator $H_{act,ol} = T_{act}/u$, the controller H_{cont} was disabled, the output position $theta_{jnt}$ fixed, and the valve opening signal u fed with a 0.1-100 Hz multi-sine, with three times the standard deviation equal to 5% valve opening. At 5% the spring would already be rotated to generate its maximum torque output of 22 Nm and restricted from rotating further. More valve opening contributing to increasing the rotational piston speed when the spring was not already at the maximum torque output.

The identified frequency response function of the complete actuator $H_{act,ol}$ was fitted with the following models:

$$H_{act,ol1}(s) = \frac{K_{v,rp}}{(\tau_1 s+1)s}\frac{K_{spr}}{Ar}, \tag{9.6}$$

$$H_{act,ol2}(s) = \frac{K_{v,rp}}{(\tau_1 s+1)(\tau_2 s+1)(\tau_3 s+1)s}\frac{K_{spr}}{Ar}, \tag{9.7}$$

$$H_{act,ol3}(s) = \frac{K_{v,rp}}{(\tau_1 s+1)s}\frac{K_{spr}}{Ar}e^{-s\tau_2}, \tag{9.8}$$

$$H_{act,ol4}(s) = \frac{K_v/K_{pf}}{(Ar/(K_{spr}K_{pf}e^{-s\tau_2}))s+1}. \tag{9.9}$$

$H_{act,ol1}$ is the direct adaptation of the HEA actuator model [172], with a first-order valve model and without any additional tube dynamics. $H_{act,ol2}$ is the same, except it uses a third-order valve, also from the HEA [172]. $H_{act,ol3}$ follows

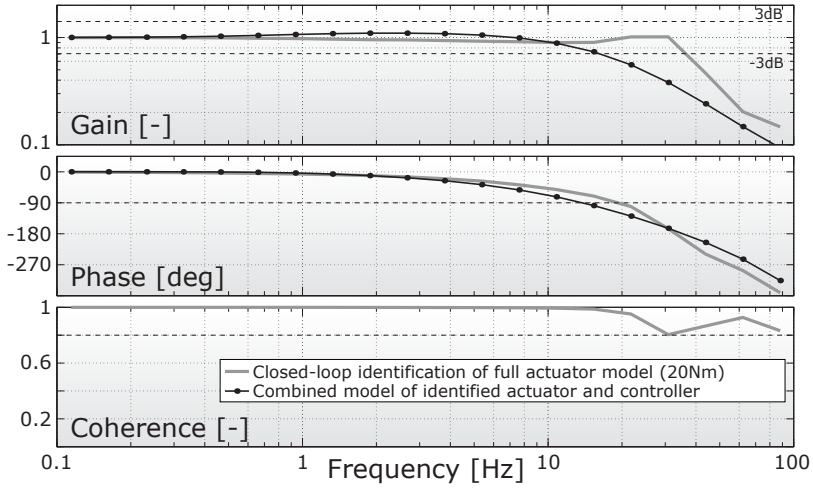

Figure 9.8: Bode plot of the closed-loop frequency response function $H_{sys,cl} = T_{act}/T_{ref}$ for the 20 Nm multi-sine reference torque (the gray line). The best fitting actuator model ($H_{act,ol4}$) was combined with the system model H_{sys}. With the closed-loop control gains, the fit was far from perfect (line with filled circles).

directly from Eq. 9.4 and 9.4, and now include a transport delay as model for the tube dynamics H_{tube}. $H_{act,ol4}$ is an adapted actuator model which uses the pressure feedback. In effect, it is the same as $H_{act,ol3}$ but with the pure integrator from the piston model H_{pist} converted into a first-order system due to the pressure feedback.

The identified open-loop actuator and the four model fits are given in Fig. 9.7. The first two models ($H_{act,ol1-2}$) fit the data badly. Not only does the low-frequency gain not match, the pure integrator in the model keeps the low-frequency phase lag at 90°, while the identified actuator approaches 0°. They also do not match the high-frequency phase, at least not without significant distortion to the high-frequency gain. Adding a transport delay as the model for the tube dynamics H_{tube} does improve the fit on the high-frequency phase for $H_{act,ol3}$, but still doesn't give a match the low-frequency gain and phase. As the pressure feedback model $H_{act,ol4}$ has lost the pure integrator, it fits perfectly on the identified open-loop actuator. The parameters for the fits of Fig. 9.7 are found in Tab. 9.1, were K_{sys} is the system gain of each model. For $H_{act,ol4}$, τ_1 is the time-constant of the equivalent first order system.

9.4.3 *Torque bandwidth*

The frequency response function of the close-loop system $H_{sys,cl} = T_{act}/T_{ref}$ was identified by letting it track a 0.1-100 Hz multi-sine reference torque T_{ref}, with three-times the standard deviation equal to 20 Nm (see Fig. 9.8), with the output position $theta_{jnt}$ fixed. The identified frequency response function has a -3 dB gain bandwidth of 35 Hz, and a 90° phase lag bandwidth of 18 Hz. The effects of the 2 m long tubes between the hydraulic valve and the hydraulic actuator are clearly seen by the rapidly increasing phase lag.

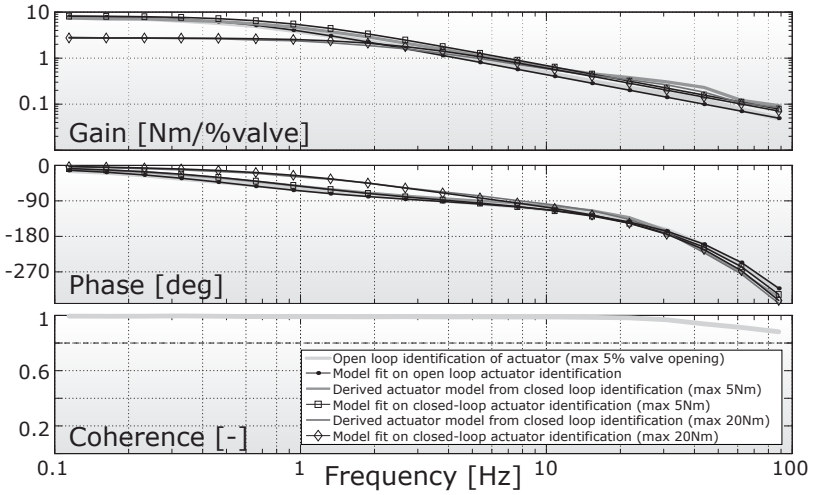

Figure 9.9: Bode plot of the open-loop identified $H_{act,ol}$ and closed-loop estimated actuators $H_{act,cl05}$ and $H_{act,cl20}$. The behavior of the identified actuator (light-gray line) and the closed-loop estimated for the 5 Nm amplitude (gray line with closed circles) closely resembles each other. For the 20 Nm amplitude, the closed-loop actuator (dark-gray line with open squares) is significantly shifted in the gain and phase lag plots. For all identified actuators, the best fitting actuator model $H_{act,ol4}$ fitted the data close to perfect.

The best fitting actuator model ($H_{act,ol4}$) was combined with the system model H_{sys}. With the closed-loop control gains ($K_{ff} = 0.15$, $K_p = 1.85$, $K_i = 10$), the fit of the complete system $H_{sys,cl}$ was far from perfect, indicating the presence of non-linearities as saturation in the actuator. The reduced coherence at the resonant peak is due to the spectral averaging over four frequencies, which is no reason for concern.

With the used control gains known, the actuator can be reverse estimated from the closed-loop identification $H_{sys,cl}$ by rewriting (Eq. 9.4):

$$H_{act,cl}(s) = \frac{H_{sys,cl}}{(K_{ff} + K_p + \frac{K_i}{s}) - (K_p + \frac{K_i}{s})H_{sys,cl}}. \tag{9.10}$$

The frequency response function of these actuator estimations $H_{act,cl05}$ and $H_{act,cl20}$, estimated from the closed-loop frequency response functions at respectively 5 Nm and 20 Nm (three times standard deviation) desired torque amplitudes,

	K_{sys}	τ_1	τ_2	τ_3
$H_{act,ol1}$	26	0.001	-	-
$H_{act,ol2}$	26	0.001	>0.001	>0.001
$H_{act,ol3}$	26	0.001	0.006	-
$H_{act,ol4}$	8.3	0.300	0.007	-

Table 9.1: Parameters to fit models $H_{act,ol1-4}$ to identified $H_{act,ol}$ (Fig. 9.7).

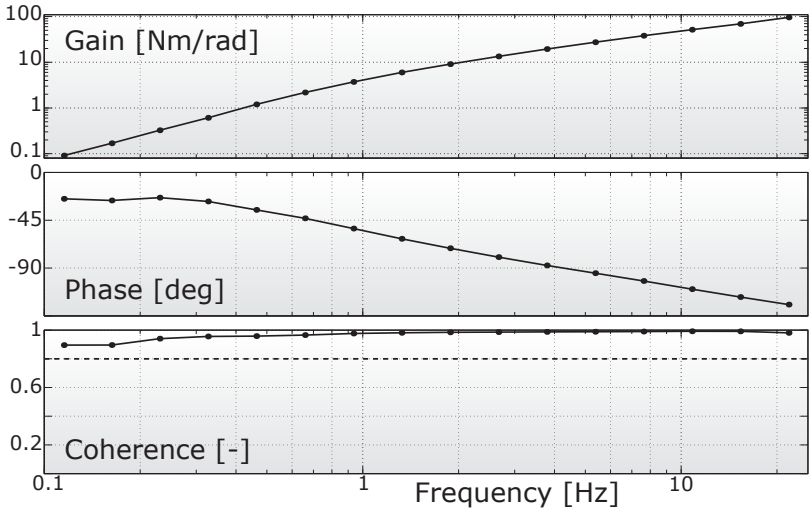

Figure 9.10: Bode plot of the minimal impedance measurements, with impedance $H_{img} = T_{act}/\theta_{jnt}$. For these measurements, the references torque T_{ref} is 0 Nm, while the angular position θ_{jnt} was perturbed by a 0.1-25 Hz multi-sine with two times the standard deviation equal to 0.1 rad.

are compared to the actuator $H_{act,ol}$ from the the open-loop identification in Fig. 9.9. The previously best-fitting model ($H_{act,ol4}$) was fitted to each estimation (see Tab. 9.2). The behavior of the identified open-loop actuator and the closed-loop actuator at 5 Nm closely resembles each other, but at 20 Nm amplitude, the closed-loop actuator is significantly shifted in the gain and phase lag plots, indicating the saturation and other non-linearities of the valve-flow modeling in the actuator. Again, the simplest first-order actuator model $H_{act,ol4}$ closely fitted all actuator frequency response functions, except for the measured gain and phase-lag bumps at 30 Hz.

9.4.4 *Minimal impedance*

For the minimal impedance measurements (see Fig. 9.10), the references torque T_{ref} is 0 Nm, while the angular position θ_{jnt} provided by an external electro motor became the input to the system. The angular position θ_{jnt} was perturbed with a 0.1-25 Hz multi-sine with two times the standard deviation equal to 0.1 rad.

	K_{system}	τ_1	τ_2
$H_{act,ol}$	8.3	0.30	0.0070
$H_{act,cl05}$	8.3	0.19	0.0075
$H_{act,cl20}$	2.6	0.07	0.0080

Table 9.2: Parameters to fit model $H_{act,ol4}$ to identified $H_{act,ol}$, $H_{act,cl05}$ and $H_{act,cl20}$ (Fig. 9.9).

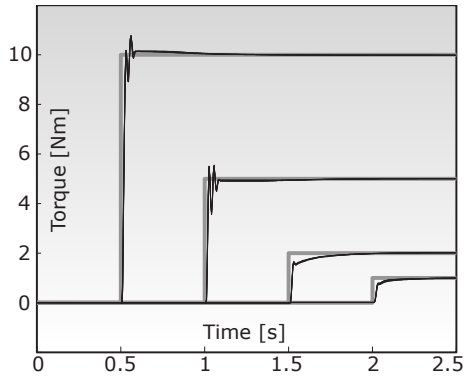

Figure 9.11: Time plots of step reference signals. In gray, the required torque T_{ref}. In black, the measured torques T_{act}.

Above 5 Hz, the external electric motor was not capable of maintaining the constant power spectral density and decayed slightly, but this should not be a problem in Eq 9.5. The expected leveling of the gain at the spring stiffness (88 Nm/rad for the measured spring) at high frequencies was not achieved, as the external motor could not reach these. Extrapolating, it should start at about 25 Hz, above which only the physical spring characteristics of SEA are felt.

9.4.5 *Step response*

In the step responses of Fig. 9.11, four different torque steps responses are plotted for eight repetitions per step size. Overshoot and response time are all acceptable for rehabilitation purposes, although using an better inverse model for the feedforward control H_{ff}, as opposed to the current linear gain K_{ff} in Fig. 9.5, may further improve the results. The variability of the response overshoot and settling-time indicates non-linearities are present in the physical rHEA.

9.4.6 *Virtual spring*

To illustrating the power of impedance control, virtual springs of different stiffness were created. The rHEA had to respond to an angular displacement θ_{nnt} as if it was a spring with a stiffness ranging from 5 to 200 Nm/rad. The angular displacement was realized by the external electro motor, and consisted of a 1 Hz sine with a 0.1 rad amplitude. Based on these results and experimental experience, the minimal stiffness was limited by the minimal output torque required and not necessarily the lowness of the virtual stiffness. Below 1 Nm, even though the controller could realize the required output torque resolution, it also generates phase-lead, probably because of unaccounted valve and tube dynamics and piston friction. The 200 Nm/rad upper limit of the virtual spring stiffness was the result of the maximum actuator torque T_{act} of 22 Nm and the 0.1 rad reference amplitude. Increasing the first or lowering the second makes higher virtual spring stiffness possible, although a system with high virtual stiffness might need an input filter to ensure stable operations at every frequency [214].

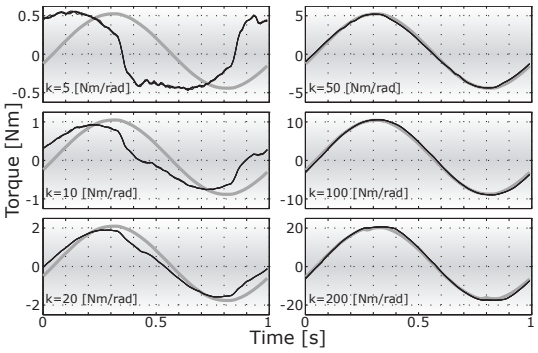

Figure 9.12: Time plots of virtual springs. The external motor maintained a 1 Hz sine with a 0.1 rad amplitude on the angular position θ_{jnt}, while the virtual spring stiffness was increased from 5 to 200 Nm/rad. (Note the real spring stiffness of 88 Nm/rad.) The gray lines are the measured joint angles θ_{jnt} multiplied by the virtual spring stiffness, resulting in the desired torque signal T_{ref}. The recorded actuator torques and plotted in black.

9.5 DISCUSSION AND CONCLUSIONS

The modified theoretical model of the actuator, based on the work of Robinson and Pratt [172], had a good fit to the measured open-loop frequency response of the actuator. To recreate the time lags as observed in the response function, a transport delay was added to the original actuator model, which improved the high-frequency fit. But only when a rough approximation of pressure feedback was added to the actuator model, in effect removing the pure integrator, did we reach an almost perfect fit to the gain and phase lag at high and low frequencies. Comparison to the original study [172] is difficult, as the fit they showed of the open-loop actuator did not include frequency responses below 2 Hz. Based on what can be seen, the adapted model may better fit their actuator measurements too, as (1), their low-frequency phase response seems to start with less than 90° phase lag, and (2), their phase lag at high-frequency keeps on dropping, where their third-order valve model and pure integrator should level out at 360°. We speculate that more realistic and non-linear valve-flow functions based on both pressure drop over the valve and the valve opening (see Eq. 9.2), might result in better future models.

After the validation measurements, the results are mixed. The torsion spring did not reach the desired maximum torque of 50 Nm and was weaker than expected. The multi-sine torque bandwidth of at least 18 Nm, measured torque resolution of 0.01 Nm, and the torque output resolution of less than 1 Nm are more than acceptable. The weight of the rHEA is at 1.3 kg below the maximum of 1.5 kg. When the minimal impedance and modeled virtual springs were felt by manually rotating the actuator output via a stick, almost no torque distortion was felt, even when manipulating with forefinger and thumb. By manually locking of the outer rings, the rHEA can also operate as a stiff hydraulic actuator, when disabling the spring ring, or as an isometric measurement device, when locking all three rings together. A stiff hydraulic actuator in admittance control can achieve more precise and faster position perturbations, as compared to impedance control of SEA.

In conclusion, the rHEA was found to be suitable for upper extremity rehabilitation therapy, as it can match the desired torque bandwidths, resolution and amplitude ranges, but still has a very limited build-in volume and low weight. Using an iterative approach to achieve the optimal spring characteristics, the latest rHEA has the desired 50 Nm of maximum output torque and is to be mounted on the new exoskeleton, the Limpact (see Fig.9.1).

Part IV

GENERAL CONCLUSIONS

10 GENERAL CONCLUSIONS

10.1 INTRODUCTION

From the early 1990s, patient-friendly robots have assisted therapists in recovering motor function in patients suffering from neurological impairments. Stroke is the most frequent of these impairments. Rehabilitation robots are well-suited for intensive and task-specific exercises that involve active, repetitive movements. These exercises are reported to give the best results in both conventional [109, 8, 56, 222] and robot-assisted rehabilitation therapy [219, 157, 162, 112] for the upper-extremities.

The goal of this dissertation was to improve rehabilitation robots by developing a series of new patient-friendly devices to assist in stroke rehabilitation and research for upper extremities. With the new robots, the entire range of mildly to severely affected patients should be able to perform the aforementioned intensive, task-specific exercises with active, repetitive movements. They also had to help analyze the influence of individual therapy components in the motor recovery mechanisms.

The following research questions were answered during the development process and technical evaluation:

I *Which assistive forces improve motor learning in healthy subjects?*

II *What is the optimal usage for each type of current rehabilitation devices?*

III *How do the new devices improve upon existing designs?*

IV *Does weight support enhance recovery after stroke?*

V *Is the full potential of rehabilitation robots used?*

10.2 MOTOR LEARNING IN HEALTHY SUBJECTS

I - Which assistive forces improve motor learning in healthy subjects?

Motor relearning after a neurological incident bears a similarity to motor learning in healthy individuals [100]. When learning new skills in sports, the instructor often uses physical guidance to demonstrate how a movement should be performed. In stroke rehabilitation, the guidance forces are traditionally manually applied by a therapist to the limb. The manual labor of the instructor or therapists can be replicated and improved upon through rehabilitation robots [30, 122, 54, 80, 143].

In Chap. 2, external guidance forces commonly used in neuromotor rehabilitation were used to direct the adaptations that occur between motor learning attempts. The guidance forces that directly improve the execution of the movement also decrease the magnitude of the execution errors. This execution error is considered the main driving force in adaptation [208, 183, 156]. Therefore, an instantaneous improvement of performance due to the external assistance, may reduce motor learning.

As predicted, Chap. 2 showed that healthy subjects adapted best when not assisted by the robot. The more the guidance forces restricted the occurrence of execution errors, the smaller the amount and rate of adaptation. Some statistically-significant adaptation was observed in the groups with the most restrictive guidance forces, suggesting learning also took place based on minimization of the muscular effort. This adaptation was both slower and to a lesser extent, but was indeed accompanied by a slight gradual decrease of the interaction forces. In other studies, guidance forces that enhanced the error increased the adaptation and adaptation speed [229, 151]. However, in our study, these error-enhancing guidance forces were not statistically different from the non-assisted trials.

If visuomotor learning in healthy subjects can be used as a model for motor relearning after neurological incidents, these results further support the importance of active patient participation. When giving assistance, it may be best to only enable voluntary movements, not to complete them [231, 152].

10.3 COMPARING CURRENT ROBOTS

II - What is the optimal usage for each type of current rehabilitation devices?

Upper-extremity rehabilitation robots can be grouped into three types: endpoint manipulators, exoskeletons and cable suspensions. These types are evaluated based on therapy performance, ability to handle different levels of impairment in different stadia of rehabilitation, and the technical aspects of the designs (see Tab 10.1). The scores are explained in the following paragraphs. Although individual improvements can be made within each family of devices, these come at a cost. For instance, an exoskeleton can definitely be made simpler in its construction than its generic model, but this would probably negatively influence the joint control (measurements) or ease of use. And an individual cable suspension can still be made even less complex than the simplest exoskeleton.

It is important to distinguish between 2D (planar) and 3D endpoint manipulators. The MIT-Manus [82] is an example of the first, the MIME [22] and ACT-3D [206] are examples of the second. Horizontal planar manipulators [54, 149, 108] are relatively simple to design and use, but they cannot make vertical movements or scale the amount of weight support. Vertical movement is important as many task-specific movements of daily living are three dimensional, such as moving a cup to a shelf. Aforementioned systematic reviews show the functional gains achieved to be limited to those movements practiced. In Chap. 3, it was explained that planar devices support the weight of the arm by restricting vertical displacements, not by applying compensation forces. In such an environment, the patient can learn inappropriate muscle activation patterns. For instance, restricting vertical displacements in reaching tasks with a virtual table [206] rewards patients for the erroneous accompanying motor pattern of pushing down. Additionally, scaling of weight support by vertical restrictions, is not possible. Without scaling, patients cannot gradually readjust to the gravitational pull. Thus for the reasons of resembling functional movements, learning correct motor patterns, and slowly readjusting to gravity, rehabilitation robots should allow full 3D movements. The generic endpoint manipulators in Tab 10.1 are of the 3D type.

The relative therapy performance (Tab 10.1-I) is scored based on the systematic reviews of randomized clinical trials [219, 157, 162, 112]. Most trials were performed with endpoint manipulators. The reviews showed a general usefulness of robot-assisted rehabilitation, although results were similar to high-intensity

conventional therapy. The available clinical studies with exoskeletons [180, 85] or a cable suspensions [127] show a similar effectiveness. Since the type of device does not strongly influence the functional outcomes, they all earn an average score.

Suitability for different levels of impairment (Tab 10.1-II) is coupled with the types of therapy possible with the device. Weight support is essential for severely affected patients, because otherwise they cannot perform voluntary movements. Moderate to severely affected patients with spasticity or movement discoordination may need both weight support and intelligent active assistance. Mild to moderately affected patients more likely benefit chiefly from resistance training to keep intensity levels high. The scores in Tab 10.1-II-A are directly taken from the analysis of weight-support systems in Chap. 3. Cable devices have difficulty providing active-assisted and passive-resisted therapy, due to the slackness and space requirements. Using eight steel cables connected to a single handlebar, the MACARM [129] has overcome the slackness problem. But this multitude of cables has transformed the device into an endpoint manipulator. Both exoskeletons and endpoint manipulators are suitable for active-assisted and passive-resisted training since they offer good control of movements and interaction forces. For these types of training, the type of actuator is more important than the mechanical design. Active assistance requires an active, energy-supplying actuator. For passive resis-

		ENDPOINT MANIPULATORS	EXOSKELETONS	CABLE SUSPENSIONS
I	THERAPY PERFORMANCE	+/-	+/-	+/-
II	IMPAIRMENT LEVELS	+	+/-	-
A	Weight supported	+/-	-	+
B	Active assisted	+	+	-
C	Passive resisted	+	+	-
III	REHABILITATION STADIUM	+/-	+	-
A	Quantification	+/-	+	-
B	Isolated training	+	+/-	+/-
C	Integrated training	+/-	+	+/-
IV	TECHNICAL ASPECTS	+/-	-	+
A	Control of movement	+/-	+	-
B	Range of motion	+	+/-	+
C	Movement impedance	+/-	-	+
D	Accurate measurements	+/-	+	-
E	Simple construction	+/-	-	+
F	Ease of use	+	+/-	+

Table 10.1: Relative scoring of generic endpoint manipulators, exoskeletons, and cable suspensions.

tance, a passive, energy-dissipating brake may suffice. The latter has the advantage of inherent safety and light weight. Collectively, endpoint manipulators outscore the exoskeletons and cable devices.

The stadium of the patient's recovery process (Tab 10.1-III) determines the protocol used. Initially, the impairment must be identified. This impairment is then targeted with isolated training. Finally, the isolated exercises are gradually transformed into functional movements of daily living. Cable suspensions have the lowest movement control, resulting in the lowest score. Exoskeletons outscore endpoint manipulators due to direct control and measurements of joint axes. For simple isolated exercises, the endpoint manipulators offer better endpoint interaction than is possible with exoskeletons, along with the simplicity of cable suspensions. To integrate these simple exercises in functional movements, the endpoint manipulators now score the least amount of points. They often restrict degrees of freedom of the arm when combined movements are performed. They also do not allow the patient to interact with real objects as the hand is often already holding the handle. Cable suspension devices get an average score on reintegration. They are useful for functional movements earlier in the rehabilitation process, but they do not have the flexibility of exoskeletons in applying guidance forces to the movements. In total, exoskeletons outscore the endpoint manipulators.

Finally, the technical aspects (Tab 10.1-IV) are again taken directly from Chap. 3. The only change is the replacement of the constant-force requirement with the suitability to control movement. For the control of movement, the score is the same as for the quantification in Tab 10.1-III above, for the same reasons. Overall, cable devices are simplest to construct and use, and the exoskeletons are the most complex, cumbersome, and expensive. This is expressed in the total score.

10.3.1 *Optimal usage per device type*

For weight support, the simplicity and effectiveness of a dedicated cable suspension system are unmatched by the other two. But simple cable suspensions are far less suitable for controlled-force interaction. Endpoint manipulators and exoskeletons can both provide active-assisted and passive-resisted training. Of these, exoskeletons have better control over joint torques and rotations, at the cost of more complex mechanisms and usage. Another problem of exoskeletons is their need for close alignment to human joints [186, 185, 142]. Without alignment, interaction forces can become too painful to continue the therapy [185], especially for patients with sensitivity problems. Thus, when optimal control over movement is needed, an exoskeleton is the best option. But for many isolated exercises, a 3D endpoint manipulator offers the same effectiveness with an ease of use and construction.

Considerable importance is placed on the ability to distinguish between restitution and compensation (see Chap. 1). Restitution is the relearning of original functions, and compensation is the usage of compensatory movements of more proximal body parts to work around the impairment. Distinguishing between these requires measurements and control of the redundant degrees of freedom in the musculoskeletal system. Together with the ability to better control functional movement, the need for control over the redundant degrees led us to prefer exoskeletons over endpoint manipulators for active-assisted and passive-resisted training.

10.4 IMPROVING DEVICE DESIGNS

III - How do the new devices improve upon existing designs?

To take care of the needs of each patient in each stadium of rehabilitation, the use of multiple devices seems the best option. A dedicated cable suspension is best for the weight-support training. Two separate exoskeletons can handle the passive-resistance and active-assistance therapies.

For the exoskeletons, novel actuators were implemented. Passive, energy-dissipating actuators have the advantages of inherent safety while still providing powerful force-coordination training [177, 230, 84, 53, 138, 145, 234, 1, 100, 108]. With active, energy-providing actuators, assist-as-needed can be given [168, 107, 31, 24, 231], movement disorders quantified [217, 47, 153], and more realistic virtual environments created [86, 143, 194].

The first device, the Freebal, was designed using the analysis of weight support systems in current rehabilitation devices. Analysis of potential self-aligning exoskeleton joints and hydraulic disk brakes led to the design of the passive exoskeleton, the Dampace. For the active exoskeleton, the Limpact, the disk brakes of the Dampace were replaced with rotational hydro-elastic actuation. The Limpact also has significantly improved self-aligning mechanisms for the shoulder and elbow.

10.4.1 *Freebal for weight-supported training*

Current weight support systems were analyzed (see Chap. 3) for their design and usability. Of the four possible means to generate the necessary forces in a weight-support systems, ideal-spring mechanisms were deemed to be the best. They generate a constant upward force throughout the work space, but do not double the vertical movement inertia as counterweights do, nor does their support force depend on the spring deflection as with directly connected springs. Compared to mechatronics, they have the advantage of being less complex and less costly to build. The forces for the weight support are most easily transferred by connecting the powering mechanisms to an overhanging cable construction.

These findings led to the design of the dedicated weight-support device, the Freebal (see Fig. 10.1 and Chap. 4). The purely passive, mechanical device uses ideal spring mechanisms to provide constant, smoothly adjustable forces to support the arm. The device has a large range of motion, small movement impedance, and independent control over the support of the lower and upper arm.

Several other dedicated weight-support devices exist. Compared to the Swedish Helparm[1], the Freebal uses the ideal-spring mechanism. This mechanism has less movement inertia than counterweights and no deflection-dependent support as with directly connected springs, both of which have been used in the Helparm. Compared to the Armon [75], the Freebal has a greater range of motion and independent scalable support for the lower and upper arm. Compared to the T-WREX [180], the Freebal has less inertia and is easier to set up. Compared to both, the Freebal needs more height and tends to pull the arm slightly to the center of the workspace, but it also gives the therapist full access to the limb.

1 Kinsman Enterprises, Inc

Figure 10.1: Freebal: dedicated weight-support.

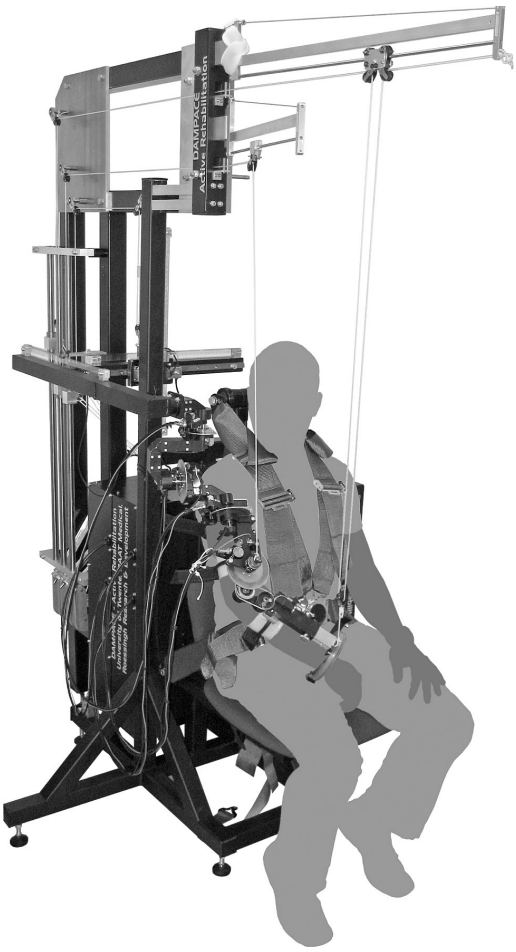

Figure 10.2: Dampace: force-coordination trainer.

10.4.2 *Dampace for passive-resistance training*

To better align exoskeleton axes to human axes, we propose the decoupling of exoskeleton joint rotations and joint translations (see Chap. 6). The decoupling is achieved by mounting the exoskeleton on a linkage system. The linkage must translate freely in any direction, yet be rotationally stiff. When misaligned joints are rotated, the linkage translates until a new zero-force equilibrium is reached. As single forces from the exoskeleton would directly result in a translation of the linkage, joint control must be realized with torques as pairwise forces. The decoupling removes the misalignment forces and isometric reaction forces, but does increase the reaction forces due to exoskeleton accelerations. Torque transfer needs two connections per segment, which reduces interaction stiffness between the exoskeleton and human arm.

The best linkage is the one with the least amount of inertia, the greatest stiffness, and the least amount of space needed. Of the linear guidance system, parallel hexapod, and the double 3D parallelogram (see Chap. 6), the latter best matches those requirements. The felt inertia is further reduced by directing the shoulder axes through the glenohumeral joint, although exact alignment is not required.

Hydraulic disk brakes were found to be suitable as the passive resistance actuators on the Dampace exoskeleton (see Chap. 7). These disk brakes are normally found on mountain bikes and have the highest torque-to-weight ratio compared to other actuators. They have a 20 Nm multi-sine bandwidth of 10 Hz and a maximum torque of up to 200 Nm, yet weigh less than 500 gr. This is sufficient for force-coordination training in stroke rehabilitation. The passivity of the disk brakes does have functional implications for joint control. First, the braking torque is always opposite to the direction of joint rotations. Second, with zero joint-rotation speed, the experienced and measured braking torque is equal to the torque applied by the human. Third, with non-zero joint-rotation speeds, the amount of experienced and measured braking torque is now equal to the desired braking torque. Passivity also implies that actively assisting movements is impossible and virtual environments are restricted to those that do not need additional external energy .

In the Dampace (see Fig. 10.2 and Chap. 8), the usage of the self-aligning axes and hydraulic disk brakes sets it apart from other exoskeletons. The Dampace can do some of the initial impairment quantification, but its real strength is in the use for force-coordination exercises that target specific impairments. Later, these targeted exercises can be integrated back into daily living activities. The Dampace has angle and torque sensors on all its axes and can use these in real-time control loops. The resistance torques may be applied to single or multiple axes, or made dependent on the movement direction. For instance, resisting the elbow extension but not flexion, exercises the triceps but not the biceps. In stroke, where the biceps is often overpowering the triceps due to spasticity and the abnormal coupling between the shoulder abductors and the elbow flexors, training the biceps sometimes must be avoided.

The Dampace can have its torques and joint rotations recalculated to 3D endpoint forces and positions. In this mode, patients complete tasks in the real world while the Dampace tracks their performance in the virtual one. At the same time, the arm is prevented from deflecting too far from the desired trajectory. In the device, the forearm pronation and supination and the hand are left free. Therefore, the hand can interact with real objects while the controller applies targeted resistance to the shoulder and elbow. In planer 2D devices, interaction with real objects made little difference [108], but in the 3D world, with performance of stroke patients also depending on the loading of the limb [206, 47], it may make the training more realistic.

10.4.3 *Limpact for active-assistance training*

Finally, a novel design of a rotation hydro-elastic actuator was deemed suitable for providing the new Limpact exoskeleton (see Fig.10.3 and Chap. 9) with active force actuation. The hydro-elastic actuator has a 20 Nm multisine bandwidth of about 18 Hz, mostly restricted by the transport delays in the 2 m long hydraulic cables. The spring element in the actuator can be disabled, making it more suitable for stiff positional control. Many other exoskeletons use pure position control or

Figure 10.3: Dampace: force-coordination trainer.

low-compliant force control, potentially imposing a positional trajectory on the arm and thereby reducing the amount of motor learning (see Chap. 2).

Besides using the active actuator, the self-aligning mechanism of the Limpact is an improvement over the one used in the Dampace. Instead of the friction-sensitive linear guidance, the Limpact uses the double 3D parallelogram. The shoulder axes of the Limpact are also more closely aligned to the human shoulder. Less misalignment leads to fewer inertial forces due to fewer linkage movements. The lighter double 3D parallelogram with almost no friction in its rotational bearings and the improved shoulder axes orientation lead to a tenfold drop of experience linkage impedance forces as compared to the Dampace. The Limpact elbow also uses push-pull rods instead of the cable in the Dampace, as rods are stiffer and require less maintenance.

10.5 EFFECTS OF WEIGHT SUPPORT ON RECOVERY

IV - Does weight support enhance recovery after stroke?

An explorative cross-sectional study with eight stroke patients (see Chap. 4) showed the Freebal instantly extends the range of motion of the affected arm. In other Freebal studies, we found muscle activity decreases during short point-to-point movements with weight support in cross-sectional experiments with both healthy elderly [163] and stroke patients [92]. The muscles maintaining arm posture against gravity are alleviated the most, yet for all muscles, the activation pattern stays roughly the same during movement acceleration, maintenance, and deceleration (to be published).

In a training study, the Freebal, assisted by a motivational computer game, improved the motor outcome scores of four stroke patients after six weeks of therapy (see Chap. 5). This is similar to results achieved by other dedicated weight support systems [180, 85, 5]. These dedicated devices achieve roughly equal improvement in motor control compared to complex rehabilitation robots. This shows that the optimal rehabilitation strategy with robots has not yet been found, and that simple device like the Freebal can have their place in the rehabilitation process

10.6 FUTURE DIRECTION OF REHABILITATION ROBOTIC RESEARCH

V - Is the full potential of rehabilitation robots used?

Most rehabilitation robots perform similar, conventional-therapy exercises. These robots can make these exercises more intensive and repetitive, while also offering additional motivation by coupling the performance to a gaming environment. This has been shown to improve therapy outcomes [219, 157, 162, 112].

But re-creating conventional exercises with robots only taps a subset of their possibilities. Robots can, for instance, also offer more complex guiding forces optimizing the experienced error for motor relearning [229, 151]. And they can easily change interaction forces, like the amount of support given, based on the patient's performance [206, 46]. Unfortunately, it is not clear which strategies offer the best outcome. This is partly because we do not yet fully understand the neurological implication of a stroke on motor control, where even motor control in healthy subjects is subject to ongoing research [218, 217, 89, 104, 203, 163, 188, 87, 102, 191].

Small steps in stroke research result in clearer strategies to improve robot-assisted therapy. For instance, a better understanding of the loss of independent joint control [11, 206] led to new robot-assisted therapies to tackle the loss [45, 46]. Understanding the coupling between spasticity and the loss of independent joint control [211, 131] may favor treating the second over the first, the other way around, or both at the same time. Robots may assist in quantification by systematically and repetitively triggering or perturbing the human motor control system [33, 188].

However, many clinical trials involving robots focus on proving the advantages of using robot-assisted therapy over conventional therapy. This lumps many therapy components together. For instance, a study on passive and active bimanual wrist movements showed a nice jump over conventional therapy [78]. But it did not pinpoint whether the benefits are due to the combination of passive and active movements, the bimanual aspects, or simply the increased intensity. Although necessary to justify investment in these new devices, studies like this do not add much to our understanding of motor relearning. Therefore, it can be argued that rehabilitation research is best aided by studies focusing on single components, while keeping other components, like the intensity received by different groups, constant.

Future drug development or stem cell research may yield major improvements in rehabilitation results, since the main causes of stroke impairments are still neurological. Robots, however, are excellent at providing controlled movement and forces, and are probably useful in combination with these therapies. The best current therapy probably consists of a combination of drugs, robots, and electrical stimulation. Drugs get the neural system in optimal learning mode, robots control the movements and interaction forces, and functional electrical stimulation triggers

the internal neurological system. However, such a combination while hoping for the best would conflict with the advice given above, to carefully work at improving rehabilitation strategies and focusing on single components.

10.7 CONCLUSIONS

The large differences among patients mean that therapists will need multiple devices to handle the range of needs. Current rehabilitation devices were compared on therapy performance, ability to handle different level of impairments in different stadia of rehabilitation, and the technical aspects of the designs. Although no difference in therapy performance was found in literature, analysis of the other aspects led to the conclusion that weight-supported training is best realized with dedicated cable devices. For full control with passive-resistance and active-assistance training, exoskeletons were found to be optimal.

Based on these results, three new rehabilitation devices were designed with several proposed improvements. The first device, the Freebal, was designed based on the analysis of weight support systems in current rehabilitation devices. Analysis of potential self-aligning exoskeleton joints and hydraulic disk brakes led to the design of the passive exoskeleton, the Dampace. For the active exoskeleton, the Limpact, the disk brakes were replaced with rotational hydroelastic actuation. It also features improved self-aligning mechanisms. In conclusion, by creating these three new devices, we succeeded in improving rehabilitation robots.

[1] L Ada, S Dorsch, and C Canning. Strengthening interventions increase strength and improve activity after stroke: a systematic review. *Aust J Physiother*, 52(4):241–248, 2006. (Cited on pages 103, 118, and 155.)

[2] ML Aisen, HI Krebs, N Hogan, F McDowell, and BT Volpe. The effect of robot-assisted therapy and rehabilitative training on motor recovery following stroke. *Arch Neurol-Chicago*, 54(4):443–446, 1997. (Cited on pages 28 and 43.)

[3] L Alibiglou, WZ Rymer, RL Harvey, and MM Mirbagheri. The relation between ashworth scores and neuromechanical measurements of spasticity following stroke. *J Neuroengineering Rehabil*, 5:18, 2008. (Cited on page 17.)

[4] F Amirabdollahian, WS Harwin, and RCV Loureiro. Analysis of the fugl-meyer outcome measures assessing the effectiveness of robot-mediated stroke therapy. In Driessen et al. [42]. (Cited on pages 47, 60, 61, and 73.)

[5] F Amirabdollahian, R Loureiro, E Gradwell, C Collin, W Harwin, and G Johnson. Multivariate analysis of the Fugl-Meyer outcome measures assessing the effectiveness of Gentle/s robot-mediated stroke therapy. *J Neuroengineering Rehabil*, 4:4, 2007. (Cited on pages 76, 84, and 159.)

[6] P Baraduc, E Guigon, and Y Burnod. Recoding arm position to learn visuomotor transformations. *Cereb Cortex*, 11(10):906–917, 2001. (Cited on page 41.)

[7] A Barbalace, A Luchetta, G Manduchi, M Moro, A Soppelsa, and C Taliercio. Performance comparison of VxWorks, Linux, RTAI, and Xenomai in a hard real-time application. *IEEE Trans Nucl Sci*, 55(1):435–439, 2008. (Cited on pages 108 and 128.)

[8] S Barreca, SL Wolf, S Fasoli, and R Bohannon. Treatment interventions for the paretic upper limb of stroke survivors: a critical review. *Neurorehabil Neural Repair*, 17(4):220–226, 2003. (Cited on pages 21, 28, 59, 103, 118, 135, and 151.)

[9] RF Beer, JD Given, and JP Dewald. Task-dependent weakness at the elbow in patients with hemiparesis. *Arch Phys Med Rehabil*, 80(7):766–72, 1999. (Cited on page 76.)

[10] RF Beer, JP Dewald, and WZ Rymer. Deficits in the coordination of multijoint arm movements in patients with hemiparesis: evidence for disturbed control of limb dynamics. *Exp Brain Res*, 131(3):305–319, 2000. (Cited on page 76.)

[11] RF Beer, JPA Dewald, ML Dawson, and WZ Rymer. Target-dependent differences between free and constrained arm movements in chronic hemiparesis. *Exp Brain Res*, 156(4):458–70, 2004. (Cited on pages 17, 23, 71, 76, 83, 103, 118, 131, and 159.)

[12] RF Beer, MD Ellis, BG Holubar, and JPA Dewald. Impact of gravity loading on post-stroke reaching and its relationship to weakness. *Muscle Nerve*, 36(2):242–250, 2007. (Cited on pages 84 and 118.)

[13] JS Bendat and AG Piersol. *Random Data: Analysis and Measurement Procedures*. Wiley, New York, USA, 1986. (Cited on pages 110, 126, and 142.)

[14] RW Bohannon. Muscle strength and muscle training after stroke. *J Rehabil Med*, 39 (1):14–20, 2007. (Cited on page 118.)

[15] B Boroojerdi, U Ziemann, R Chen, CM Butefisch, and LG Cohen. Mechanisms underlying human motor system plasticity. *Muscle Nerve*, 24(5):602–13, 2001. (Cited on pages 61 and 71.)

[16] TJ Bovend'Eerdt, M Newman, K Barker, H Dawes, C Minelli, and DT Wade. The effects of stretching in spasticity: a systematic review. *Arch Phys Med Rehabil*, 89(7): 1395–1406, 2008. (Cited on pages 21 and 119.)

[17] E Bressel and PJ McNair. The effect of prolonged static and cyclic stretching on ankle joint stiffness, torque relaxation, and gait in people with stroke. *Phys Ther*, 82 (9):880–887, 2002. (Cited on page 21.)

[18] S Brunnstrom. *Movement therapy in hemiplegia: a neurophysiological approach.* Harper and Row, New York, 1970. (Cited on pages 17, 18, 19, 71, 75, 103, and 118.)

[19] M Brus-Ramer, JB Carmel, S Chakrabarty, and JH Martin. Electrical stimulation of spared corticospinal axons augments connections with ipsilateral spinal motor circuits after injury. *J Neurosci*, 27(50):13793–13801, 2007. (Cited on page 15.)

[20] R Bucher and S Balemi. Rapid controller prototyping with Matlab/Simulink and Linux. *Control Eng Pract*, 14(2):185–192, 2006. (Cited on pages 108 and 128.)

[21] E Burdet, R Osu, DW Franklin, TE Milner, and M Kawato. The central nervous system stabilizes unstable dynamics by learning optimal impedance. *Nature*, 414 (6862):446–449, 2001. (Cited on page 40.)

[22] CG Burgar, PS Lum, PC Shor, and HFM van der Loos. Development of robots for rehabilitation therapy: The Palo Alto VA/Stanford experience. *J Rehabil Res Dev*, 37 (6):663–673, 2000. (Cited on pages 21, 51, 59, 89, 117, 118, and 152.)

[23] JH Buurke. *Walking after stroke: co-ordination patterns & functional recovery*. PhD thesis, University of Twente, Enschede, The Netherlands, 2005. (Cited on page 20.)

[24] LL Cai, AJ Fong, CK Otoshi, Y Liang, JW Burdick, RR Roy, and VR Edgerton. Implications of assist-as-needed robotic step training after a complete spinal cord injury on intrinsic strategies of motor learning. *J Neurosci*, 26(41):10564–8, 2006. (Cited on pages 23, 44, 104, 119, 133, and 155.)

[25] G Caithness, R Osu, P Bays, H Chase, J Klassen, M Kawato, DM Wolpert, and JR Flanagan. Failure to consolidate the consolidation theory of learning for sensorimotor adaptation tasks. *J Neurosci*, 24(40):8662–8671, 2004. (Cited on pages 29 and 40.)

[26] CG Canning, L Ada, R Adams, and NJ O'Dwyer. Loss of strength contributes more to physical disability after stroke than loss of dexterity. *Clin Rehabil*, 18(3):300–8, 2004. (Cited on page 103.)

[27] C Carignan, J Tang, S Roderick, and M Naylor. A configuration-space approach to controlling a rehabilitation arm exoskeleton. In Driessen et al. [42]. (Cited on pages 48, 51, 89, 90, 99, and 119.)

[28] JJ Chang, WL Tung, WL Wu, MH Huang, and FC Su. Effects of robot-aided bilateral force-induced isokinetic arm training combined with conventional rehabilitation on arm motor function in patients with chronic stroke. *Arch Phys Med Rehabil*, 88(10): 1332–1338, 2007. (Cited on page 103.)

[29] R Chen, LG Cohen, and M Hallett. Nervous system reorganization following injury. *Neuroscience*, 111(4):761–73, 2002. (Cited on pages 61 and 71.)

[30] G Colombo, M Joerg, R Schreier, and V Dietz. Treadmill training of paraplegic patients using a robotic orthosis. *J Rehabil Res Dev*, 37(6):693–700, 2000. (Cited on pages 15, 28, 90, and 151.)

[31] R Colombo, F Pisano, S Micera, A Mazzone, C Delconte, MC Carrozza, P Dario, and G Minuco. Robotic techniques for upper limb evaluation and rehabilitation of stroke patients. *IEEE Trans Neural Syst Rehabil Eng*, 13(3):311–324, 2005. (Cited on pages 23, 104, 119, 133, and 155.)

[32] R Colombo, F Pisano, S Micera, A Mazzone, C Delconte, MC Carrozza, P Dario, and G Minuco. Assessing mechanisms of recovery during robot-aided neurorehabilitation of the upper limb. *Neurorehabil Neural Repair*, 22(1):50–63, 2008. (Cited on page 19.)

[33] E de Vlugt, AC Schouten, and FCT van der Helm. Quantification of intrinsic and reflexive properties during multijoint arm posture. *J Neurosci Methods*, 155(2): 328–349, 2006. (Cited on page 159.)

[34] JP Desai, D Meldrum, and O Khatib, editors. *Proc Biorob'o8*, Scottsdale (AZ), USA, Oct 19-22 2008. (Cited on pages 170 and 174.)

[35] JP Dewald, PS Pope, JD Given, TS Buchanan, and WZ Rymer. Abnormal muscle coactivation patterns during isometric torque generation at the elbow and shoulder in hemiparetic subjects. *Brain*, 118(2):495–510, 1995. (Cited on pages 17 and 76.)

[36] JPA Dewald and RF Beer. Abnormal joint torque patterns in the paretic upper limb of subjects with hemiparesis. *Muscle Nerve*, 24(1):273–283, 2001. (Cited on pages 17, 71, 76, 83, and 84.)

[37] L Dipietro, HI Krebs, SE Fasoli, BT Volpe, J Stein, C Bever, and N Hogan. Changing motor synergies in chronic stroke. *J Neurophysiol*, 98(2):757–768, 2007. (Cited on pages 19, 76, 83, and 103.)

[38] L Dipietro, HI Krebs, SE Fasoli, BT Volpe, and N Hogan. Submovement changes characterize generalization of motor recovery after stroke. *Cortex*, 2008. (Cited on pages 19, 23, and 104.)

[39] BH Dobkin. Strategies for stroke rehabilitation. *Lancet Neurol*, 3(9):528–36, 2004. (Cited on pages 85 and 118.)

[40] O Donchin, JT Francis, and R Shadmehr. Quantifying generalization from trial-by-trial behavior of adaptive systems that learn with basis functions: theory and experiments in human motor control. *J Neurosci*, 23(27):9032–45, 2003. (Cited on page 29.)

[41] S Dong, KQ Lu, JQ Sun, and K Rudolph. A prototype rehabilitation device with variable resistance and joint motion control. *Med Eng Phys*, 28(4):348–355, 2006. (Cited on page 104.)

[42] B Driessen, JL Herder, and GJ Gelderblom, editors. *Proc 10th ICORR'07*, Noordwijk, the Netherlands, Jun 13-15 2007. (Cited on pages 161, 162, 163, 164, 166, 167, 169, 171, and 174.)

[43] R Ekkelenkamp, P Veltink, S Stramigioli, and H van der Kooij. Evaluation of a Virtual Model Control for the selective support of gait functions using an exoskeleton. In Driessen et al. [42], pages 693–699. (Cited on pages 125, 130, and 136.)

[44] M Ellis, A Acosta, J Yao, and J Dewald. Position-dependent torque coupling and associated muscle activation in the hemiparetic upper extremity. *Exp Brain Res*, 176 (4):594–602, 2007. (Cited on pages 118 and 119.)

[45] MD Ellis, BG Holubar, AM Acosta, RF Beer, and JPA Dewald. Modifiability of abnormal isometric elbow and shoulder joint torque coupling after stroke. *Muscle Nerve*, 32(2):170–178, 2005. (Cited on pages 23, 84, 103, 118, 119, 131, and 159.)

[46] MD Ellis, T Sukal, T DeMott, and JPA Dewald. ACT-3D exercise targets gravity-induced discoordination and improves reaching work area in individuals with stroke. In Driessen et al. [42]. (Cited on pages 17, 23, 47, 60, 61, 73, 76, 84, 103, 118, 131, and 159.)

[47] MD Ellis, T Sukal, T Demott, and JPA Dewald. Augmenting clinical evaluation of hemiparetic arm movement with a laboratory-based quantitative measurement of kinematics as a function of limb loading. *Neurorehabil Neural Repair*, 2008. (Cited on pages 17, 19, 83, 103, 118, 119, 155, and 157.)

[48] JL Emken and DJ Reinkensmeyer. Accelerating motor adaptation by influencing neural computations. In *Proc 26th EMBS'04*, volume 2, pages 4033–4036, San Francisco (CA), USA, Sep 1-5 2004. (Cited on page 28.)

[49] JL Emken and DJ Reinkensmeyer. Robot-enhanced motor learning: accelerating internal model formation during locomotion by transient dynamic amplification. *IEEE Trans Neural Syst Rehabil Eng*, 13(1):33–39, 2005. (Cited on page 40.)

[50] JL Emken, R Benitez, and DJ Reinkensmeyer. Human-robot cooperative movement training: learning a novel sensory motor transformation during walking with robotic assistance-as-needed. *J Neuroengineering Rehabil*, 4:8, 2007. (Cited on page 44.)

[51] JL Emken, R Benitez, A Sideris, JE Bobrow, and DJ Reinkensmeyer. Motor adaptation as a greedy optimization of error and effort. *J Neurophysiol*, 97(6):3997–4006, 2007. (Cited on pages 28 and 41.)

[52] JA Eyre. Development and plasticity of the corticospinal system in man. *Neural Plast*, 10(1-2):93–106, 2003. (Cited on page 15.)

[53] SE Fasoli, HI Krebs, J Stein, WR Frontera, and N Hogan. Effects of robotic therapy on motor impairment and recovery in chronic stroke. *Arch Phys Med Rehab*, 84(4): 477–482, 2003. (Cited on pages 103, 118, and 155.)

[54] M Ferraro, JJ Palazzolo, J Krol, HI Krebs, N Hogan, and BT Volpe. Robot-aided sensorimotor arm training improves outcome in patients with chronic stroke. *Neurology*, 61(11):1604–1607, 2003. (Cited on pages 28, 44, 151, and 152.)

[55] A Feydy, R Carlier, A Roby-Brami, B Bussel, F Cazalis, L Pierot, Y Burnod, and MA Maier. Longitudinal study of motor recovery after stroke: recruitment and focusing of brain activation. *Stroke*, 33(6):1610–7, 2002. (Cited on page 85.)

[56] H Feys, W De Weerdt, G Verbeke, GC Steck, C Capiau, C Kiekens, E Dejaeger, G Van Hoydonck, G Vermeersch, and P Cras. Early and repetitive stimulation of the arm can substantially improve the long-term outcome after stroke: a 5-year follow-up study of a randomized trial. *Stroke*, 35(4):924–929, 2004. (Cited on pages 21, 28, 59, 103, 118, 135, and 151.)

[57] M Flanders and U Herrmann. Two components of muscle activation: scaling with the speed of arm movement. *J Neurophysiol*, 67(4):931–943, 1992. (Cited on page 47.)

[58] DW Franklin, R Osu, E Burdet, M Kawato, and TE Milner. Adaptation to stable and unstable dynamics achieved by combined impedance control and inverse dynamics model. *J Neurophysiol*, 90(5):3270–82, 2003. (Cited on page 40.)

[59] M Frey, G Colombo, M Vaglio, R Bucher, M Jorg, and R Riener. A novel mechatronic body weight support system. *IEEE Trans Neural Syst Rehabil Eng*, 14(3):311–321, 2006. (Cited on pages 56 and 64.)

[60] KM Friel and JH Martin. Bilateral activity-dependent interactions in the developing corticospinal system. *J Neurosci*, 27(41):11083–11090, 2007. (Cited on page 15.)

[61] A Frisoli, F Rocchi, S Marcheschi, A Dettori, F Salsedo, and M Bergamasco. A new force-feedback arm exoskeleton for haptic interaction in virtual environments. In *Proc 1st WHC'05*, pages 195–201, Pisa, Italy, Mar 18-20 2005. (Cited on pages 51, 89, 90, 96, and 119.)

[62] AR Fugl-Meyer, L Jaasko, I Leyman, S Olsson, and S Steglind. The post-stroke hemiplegic patient. I. A method for evaluation of physical performance. *Scand J Rehabil Med*, 7(1):13–31, 1975. (Cited on pages 19, 68, 75, and 84.)

[63] J Furusho, K Koyanagi, K Nakanishi, Y Fujii, K Domen, K Miyakoshi, U Ryu, S Takenaka, and A Inoue. A 3-D exercise machine for upper-limb rehabilitation using ER actuators with high safety. In *Proc 11th AIM'05*, pages 455–460, Monterey (CA), USA, Jul 24-28 2005. (Cited on page 104.)

[64] C Ghez, JW Krakauer, RL Sainburg, and MF Ghilardi. Spatial representation and internal models of limb dynamics in motor learning. In MS Gazzaniga, editor, *The new cognitive neurosiences*, pages 501–514. MIT press, Cambridge, 2000. (Cited on page 29.)

[65] DJ Gladstone, CJ Danells, and SE Black. The Fugl-Meyer assessment of motor recovery after stroke: a critical review of its measurement properties. *Neurorehabil Neural Repair*, 16(3):232–240, 2002. (Cited on pages 81 and 84.)

[66] SJ Goodbody and DM Wolpert. Temporal and amplitude generalization in motor learning. *J Neurophysiol*, 79(4):1825–38, 1998. (Cited on page 29.)

[67] S Grange, F Conti, P Rouiller, P Helmer, and C Baur. The Delta haptic device. In *Proc 5th Mecatronics'01*, Besancon, France, Jul 7 2001. (Cited on pages 93 and 124.)

[68] A Griffin and J Bernhardt. Strapping the hemiplegic shoulder prevents development of pain during rehabilitation: a randomized controlled trial. *Clin Rehabil*, 20(4): 287–295, 2006. (Cited on pages 62 and 74.)

[69] DI Grow, M Wu, MJ Locastro, SK Arora, AJ Bastian, and AM Okamura. Haptic simulation of elbow joint spasticity. In *Proc 16th HAPTICS'08*, pages 475–476, Reno (NV), USA, Mar 13-14 2008. (Cited on page 104.)

[70] CE Hafer-Macko, AS Ryan, FM Ivey, and RF Macko. Skeletal muscle changes after hemiparetic stroke and potential beneficial effects of exercise intervention strategies. *J Rehabil Res Dev*, 45(2):261–272, 2008. (Cited on page 17.)

[71] DE Haines. *Neuroanatomy: An Atlas of Structures, Sections, and Systems*. Wolters Kluwer | Lippincott Williams & Wilkins, 2008. (Cited on page 16.)

[72] M Hallett. Cortical control of brainstem motor systems. *Mov Disord*, 17:S23–S26, 2002. (Cited on page 15.)

[73] JE Harris and JJ Eng. Paretic upper-limb strength best explains arm activity in people with stroke. *Phys Ther*, 87(1):88–97, 2007. (Cited on page 16.)

[74] JL Herder. *Energy-Free Systems. Theory, conception and design of statically balanced spring mechanisms*. PhD thesis, Delft University of Technology, Delft, The Netherlands, 2001. (Cited on pages 57, 62, 64, 65, 74, and 128.)

[75] JL Herder, N Vrijlandt, T Antonides, M Cloosterman, and PL Mastenbroek. Principle and design of a mobile arm support for people with muscular weakness. *J Rehabil Res Dev*, 43(5):591–604, 2006. (Cited on pages 51, 60, 63, 73, and 155.)

[76] H Herr and A Wilkenfeld. User-adaptive control of a magnetorheological prosthetic knee. *Ind Robot*, 30(1):42–55, 2003. (Cited on page 104.)

[77] S Hesse, G Schulte-Tigges, M Konrad, A Bardeleben, and C Werner. Robot-assisted arm trainer for the passive and active practice of bilateral forearm and wrist movements in hemiparetic subjects. *Arch Phys Med Rehab*, 84(6):915–920, 2003. (Cited on pages 28 and 43.)

[78] S Hesse, C Werner, M Pohl, S Rueckriem, J Mehrholz, and ML Lingnau. Computerized arm training improves the motor control of the severely affected arm after stroke: a single-blinded randomized trial in two centers. *Stroke*, 36(9):1960–1966, 2005. (Cited on page 159.)

[79] O Hikosaka, K Nakamura, K Sakai, and H Nakahara. Central mechanisms of motor skill learning. *Curr Opin Neurobiol*, 12(2):217–222, 2002. (Cited on page 43.)

[80] N Hogan and HI Krebs. Interactive robots for neuro-rehabilitation. *Restor Neurol Neurosci*, 22(3-5):349–358, 2004. (Cited on pages 23, 28, 43, and 151.)

[81] N Hogan, HI Krebs, J Charnnarong, P Srikrishna, and A Sharon. MIT-MANUS: a workstation for manual therapy and training. i. In *Proc 2th ROMAN'92*, pages 161–65, Tokyo, Japan, Sep 1-3 1992. (Cited on pages 15, 51, 89, and 118.)

[82] N Hogan, HI Krebs, A Sharon, and J Charnnarong. Interactive robotic therapist. Patent, 1995. US 5,466,213. (Cited on pages 21, 59, 117, and 152.)

[83] N Hogan, HI Krebs, B Rohrer, JJ Palazzolo, L Dipietro, SE Fasoli, J Stein, R Hughes, WR Frontera, D Lynch, and BT Volpe. Motions or muscles? some behavioral factors underlying robotic assistance of motor recovery. *J Rehabil Res Dev*, 43(5):605–18, 2006. (Cited on pages 43, 44, and 118.)

[84] T Hortobagyi, D Tunnel, J Moody, S Beam, and P DeVita. Low- or high-intensity strength training partially restores impaired quadriceps force accuracy and steadiness in aged adults. *J Gerontol A Biol Sci Med Sci*, 56(1):B38–B47, 2001. (Cited on pages 103, 118, and 155.)

[85] SJ Housman, V Le, T Rahman, RJ Sanchez, and DJ Reinkensmeyer. Arm-training with T-WREX after chronic stroke: Preliminary results of a randomized controlled trial. In Driessen et al. [42]. (Cited on pages 22, 47, 60, 61, 73, 76, 84, 85, 153, and 159.)

[86] JA Houtsma and FJAM Van Houten. Virtual reality and a haptic master-slave set-up in post-stroke upper-limb rehabilitation. *Proc Inst Mech Eng [H]*, 220(6):715–718, 2006. (Cited on page 155.)

[87] VS Huang, R Shadmehr, and J Diedrichsen. Active learning: learning a motor skill without a coach. *J Neurophysiol*, 100(2):879–887, 2008. (Cited on page 159.)

[88] JE Huber, NA Fleck, and MF Ashby. The selection of mechanical actuators based on performance indices. *Proc R Soc A*, 453(1965):2185–2205, 1997. (Cited on page 112.)

[89] EJ Hwang and R Shadmehr. Internal models of limb dynamics and the encoding of limb state. *J Neural Eng*, 2(3):S266–78, 2005. (Cited on page 159.)

[90] SH Jang. A review of motor recovery mechanisms in patients with stroke. *NeuroRehabilitation*, 22(4):253–259, 2007. (Cited on pages 15 and 76.)

[91] E Jankowska and SA Edgley. How can corticospinal tract neurons contribute to ipsilateral movements? A question with implications for recovery of motor functions. *Neuroscientist*, 12(1):67–79, 2006. (Cited on page 15.)

[92] MJA Jannink, GB Prange, AHA Stienen, H van der Kooij, J Kruitbosch, MJ IJzerman, and HJ Hermens. Reduction of muscle activity during repeated reach and retrieval with gravity compensation in stroke patients. In Driessen et al. [42]. (Cited on pages 47, 60, 73, 76, 118, 119, 135, and 158.)

[93] GM Jenkins and DG Watts. *Spectral Analysis and Its Applications*. Holden-Day, San Francisco (CA), USA, 1969. (Cited on pages 110, 126, and 142.)

[94] MJ Johnson. Recent trends in robot-assisted therapy environments to improve real-life functional performance after stroke. *J Neuroengineering Rehabil*, 3:29, 2006. (Cited on page 59.)

[95] MJ Johnson, HFM van der Loos, CG Burgar, and LJ Leifer. Driver's SEAT: Simulation environment for arm therapy. In van der Loos [220], pages 227–234. (Cited on page 59.)

[96] KE Jones, C Wessberg, and A Vallbo. Proprioceptive feedback is reduced during adaptation to a visuomotor transformation: preliminary findings. *Neuroreport*, 12 (18):4029–4033, 2001. (Cited on page 42.)

[97] JB Jonker and JP Meijaard. SPACAR-computer program for dynamic analysis of flexible spatial mechanisms and manipulators. In W Schiehlen, editor, *Multibody Systems Handbook*, pages 123–143. Springer-Verlag, Berlin, Germany, 1990. (Cited on page 94.)

[98] LE Kahn, M Averbuch, WZ Rymer, and DJ Reinkensmeyer. Comparison of robot-assisted reaching to free reaching in promoting recovery from chronic stroke. In *Proc 7th ICORR'01*, pages 39–44, Evry, France, Apr 25-27 2001. (Cited on page 119.)

[99] LE Kahn, ML Zygman, WZ Rymer, and DJ Reinkensmeyer. Effect of robot-assisted and unassisted exercise on functional reaching in chronic hemiparesis. In *Proc 23rd EMBC'01*, Istanbul, Turkey, Oct 25-28 2001. (Cited on page 85.)

[100] LE Kahn, PS Lum, WZ Rymer, and DJ Reinkensmeyer. Robot-assisted movement training for the stroke-impaired arm: Does it matter what the robot does? *J Rehabil Res Dev*, 43(5):619–630, 2006. (Cited on pages 27, 28, 43, 103, 118, 151, and 155.)

[101] R Katz. [reevaluation of physiological mechanisms generating the stretch reflex: new hypotheses on the physiopathology of spasticity]. *Ann Readapt Med Phys*, 44(5): 268–272, 2001. (Cited on page 17.)

[102] J Kluzik, J Diedrichsen, R Shadmehr, and AJ Bastian. Reach adaptation: what determines whether we learn an internal model of the tool or adapt the model of our arm? *J Neurophysiol*, 100(3):1455–1464, 2008. (Cited on page 159.)

[103] JW Krakauer. Motor learning: its relevance to stroke recovery and neurorehabilitation. *Curr Opin Neurol*, 19(1):84–90, 2006. (Cited on page 43.)

[104] JW Krakauer and . Shadmehr. Consolidation of motor memory. *Trends Neurosci*, 29 (1):58–64, 2006. (Cited on page 159.)

[105] JW Krakauer, MF Ghilardi, and C Ghez. Independent learning of internal models for kinematic and dynamic control of reaching. *Nat Neurosci*, 2(11):1026–31., 1999. (Cited on page 29.)

[106] JW Krakauer, ZM Pine, MF Ghilardi, and C Ghez. Learning of visuomotor transformations for vectorial planning of reaching trajectories. *J Neurosci*, 20(23):8916–24, 2000. (Cited on pages 33 and 40.)

[107] HI Krebs, JJ Palazzolo, L Dipietro, BT Volpe, and N Hogan. Rehabilitation robotics: Performance-based progressive robot-assisted therapy. *Auton Robot*, 15(1):7–20, 2003. (Cited on pages 23, 104, 117, 119, 133, and 155.)

[108] HI Krebs, S Mernoff, SE Fasoli, R Hughes, J Stein, and N Hogan. A comparison of functional and impairment-based robotic training in severe to moderate chronic stroke: a pilot study. *NeuroRehabilitation*, 23(1):81–87, 2008. (Cited on pages 23, 118, 152, 155, and 157.)

[109] G Kwakkel, RC Wagenaar, JWR Twisk, GJ Lankhorst, and JC Koetsier. Intensity of leg and arm training after primary middle-cerebral-artery stroke: a randomised trial. *Lancet*, 354(9174):191–196, 1999. (Cited on pages 21, 28, 43, 59, 103, 118, 135, and 151.)

[110] G Kwakkel, BJ Kollen, J van der Grond, and AJH Prevo. Probability of regaining dexterity in the flaccid upper limb - impact of severity of paresis and time since onset in acute stroke. *Stroke*, 34(9):2181–2186, 2003. (Cited on page 75.)

[111] G Kwakkel, R van Peppen, RC Wagenaar, S Wood-Dauphinee, C Richards, A Ashburn, K Miller, N Lincoln, C Partridge, I Wellwood, and P Langhorne. Effects of augmented exercise therapy time after stroke: a meta-analysis. *Stroke*, 35(11):2529–39, 2004. (Cited on page 28.)

[112] G Kwakkel, BJ Kollen, and HI Krebs. Effects of robot-assisted therapy on upper limb recovery after stroke: A systematic review. *Neurorehabil Neural Repair*, 22(2): 111–21, 2008. (Cited on pages 19, 23, 47, 59, 89, 103, 117, 135, 151, 152, and 159.)

[113] JW Lance. Symposium synopsis. In RG Feldmann, RR Young, and WP Koella, editors, *Spasticity: disordered motor control.*, pages 485–95. Chicago: Year Book Medical Publishers, 1980. (Cited on page 17.)

[114] JW Lance. What is spasticity? *Lancet*, 335(8689):606, 1990. (Cited on page 17.)

[115] ES Lawrence, C Coshall, R Dundas, J Stewart, AG Rudd, R Howard, and CD Wolfe. Estimates of the prevalence of acute stroke impairments and disability in a multiethnic population. *Stroke*, 32(6):1279–84, 2001. (Cited on pages 16 and 75.)

[116] RN Lemon. Descending pathways in motor control. *Annu Rev Neurosci*, 31:195–218, 2008. (Cited on pages 15 and 16.)

[117] J Lenarcic and M Stanisic. A humanoid shoulder complex and the humeral pointing kinematics. *IEEE Trans Robotic Autom*, 19(3):499–506, 2003. (Cited on pages 50, 63, 90, 99, and 120.)

[118] WH Li and H Du. Design and experimental evaluation of a magnetorheological brake. *Int J Adv Manuf Technol*, 21(7):508–15, 2003. (Cited on page 104.)

[119] J Liu, SC Cramer, and DJ Reinkensmeyer. Learning to perform a new movement with robotic assistance: comparison of haptic guidance and visual demonstration. *J Neuroengineering Rehabil*, 3:20, 2006. (Cited on pages 103, 118, and 135.)

[120] R Loureiro, F Amirabdollahian, M Topping, B Driessen, and WS Harwin. Upper limb robot mediated stroke therapy - Gentle/s approach. *Auton Robot*, 15(1):35–51, 2003. (Cited on pages 51, 59, 89, 118, and 119.)

[121] RCV Loureiro and WS Harwin. Reach & grasp therapy: Design and control of a 9-dof robotic neuro-rehabilitation system. In Driessen et al. [42]. (Cited on page 59.)

[122] PS Lum, CG Burgar, PC Shor, M Majmundar, and HFM van der Loos. Robot-assisted movement training compared with conventional therapy techniques for the rehabilitation of upper-limb motor function after stroke. *Arch Phys Med Rehab*, 83(7): 952–959, 2002. (Cited on pages 28, 44, and 151.)

[123] L Lunenburger, G Colombo, and R Riener. Biofeedback for robotic gait rehabilitation. *J Neuroengineering Rehabil*, 4(1):1, 2007. (Cited on pages 28 and 62.)

[124] D Lynch, M Ferraro, J Krol, CM Trudell, P Christos, and BT Volpe. Continuous passive motion improves shoulder joint integrity following stroke. *Clin Rehabil*, 19 (6):594–9, 2005. (Cited on pages 21, 28, and 43.)

[125] JH Martin. The corticospinal system: from development to motor control. *Neuroscientist*, 11(2):161–173, 2005. (Cited on page 15.)

[126] JH Martin. Chapter 3 development of the corticospinal system and spinal motor circuits. *Handb Clin Neurol*, 82:39–56, 2007. (Cited on page 15.)

[127] S Masiero, A Celia, M Armani, and G Rosati. A novel robot device in rehabilitation of post-stroke hemiplegic upper limbs. *Aging Clin Exp Res*, 18(6):531–535, 2006. (Cited on pages 22, 51, 59, 89, 119, and 153.)

[128] K Matsuyama, F Mori, K Nakajima, T Drew, M Aoki, and S Mori. Locomotor role of the corticoreticular-reticulospinal-spinal interneuronal system. *Prog Brain Res*, 143: 239–249, 2004. (Cited on pages 15 and 76.)

[129] D Mayhew, B Bachrach, WZ Rymer, and RF Beer. Development of the MACARM - a novel cable robot for upper limb neurorehabilitation. In Patton and Weir [148], pages 299–302. (Cited on pages 89, 119, and 153.)

[130] P Mazzoni and JW Krakauer. An implicit plan overrides an explicit strategy during visuomotor adaptation. *J Neurosci*, 26(14):3642–5, 2006. (Cited on page 42.)

[131] JG McPherson, MD Ellis, CJ Heckman, and JPA Dewald. Evidence for increased activation of persistent inward currents in individuals with chronic hemiparetic stroke. *J Neurophysiol*, 2008. epub. (Cited on pages 17 and 159.)

[132] J Mehrholz, K Wagner, D Meissner, K Grundmann, C Zange, R Koch, and M Pohl. Reliability of the modified tardieu scale and the modified ashworth scale in adult patients with severe brain injury: a comparison study. *Clin Rehabil*, 19(7):751–759, 2005. (Cited on page 19.)

[133] SM Michaelsen, R Dannenbaum, and MF Levin. Task-specific training with trunk restraint on arm recovery in stroke: randomized control trial. *Stroke*, 37(1):186–192, 2006. (Cited on page 20.)

[134] MM Mirbagheri and WZ Rymer. Time-course of changes in arm impairment after stroke: variables predicting motor recovery over 12 months. *Arch Phys Med Rehabil*, 89(8):1507–13, 2008. (Cited on pages 18, 20, 104, and 113.)

[135] MM Mirbagheri, K Settle, R Harvey, and WZ Rymer. Neuromuscular abnormalities associated with spasticity of upper extremity muscles in hemiparetic stroke. *J Neurophysiol*, 98(2):629–637, 2007. (Cited on page 17.)

[136] MM Mirbagheri, L Alibiglou, M Thajchayapong, and WZ Rymer. Muscle and reflex changes with varying joint angle in hemiparetic stroke. *J Neuroengineering Rehabil*, 5: 6, 2008. (Cited on page 17.)

[137] K Mitsuhashi, K Seki, C Akamatsu, and Y Handa. Modulation of excitability in the cerebral cortex projecting to upper extremity muscles by rotational positioning of the forearm. *Tohoku J Exp Med*, 212(3):221–228, 2007. (Cited on page 130.)

[138] SL Morris, KJ Dodd, and ME Morris. Outcomes of progressive resistance strength training following stroke: a systematic review. *Clin Rehabil*, 18(1):27–39, 2004. (Cited on pages 118 and 155.)

[139] K Nagai, I Nakanishi, and T Kishida. Design of robotic orthosis assisting human motion in production engineering and human care. In van der Loos [220], pages 270–275. (Cited on page 54.)

[140] A Nakai, T Ohashi, and H Hashimoto. 7 DOF arm type haptic interface for teleoperation and virtual reality systems. In *Proc IROS'98*, volume 2, pages 1266–1271 vol.2, Victoria (BC), Canada, Oct 13-17 1998. (Cited on pages 89 and 119.)

[141] T Nef and R Riener. ARMin - Design of a Novel Arm Rehabilitation Robot. In Patton and Weir [148], pages 57–60. (Cited on page 59.)

[142] T Nef and R Riener. Shoulder actuation mechanisms for arm rehabilitation exoskeletons. In Desai et al. [34]. (Cited on pages 50, 63, 120, and 154.)

[143] T Nef, M Mihelj, and R Riener. ARMin: a robot for patient-cooperative arm therapy. *Med Biol Eng Comput*, 45(9):887–900, 2007. (Cited on pages 22, 28, 47, 51, 60, 89, 90, 96, 99, 117, 119, 136, 151, and 155.)

[144] G Nelles, W Jentzen, M Jueptner, S Müller, and HC Diener. Arm training induced brain plasticity in stroke studied with serial positron emission tomography. *Neuroimage*, 13(6 Pt 1):1146–1154, 2001. (Cited on page 85.)

[145] MM Ouellette, NK LeBrasseur, JF Bean, W Phillips, J Stein, WR Frontera, and RA Fielding. High-intensity resistance training improves muscle strength, self-reported function, and disability in long-term stroke survivors. *Stroke*, 35(6):1404–1409, 2004. (Cited on pages 118 and 155.)

[146] C Patten, J Lexell, and HE Brown. Weakness and strength training in persons with poststroke hemiplegia: Rationale, method, and efficacy. *J Rehabil Res Dev*, 41(3A): 293–312, 2004. (Cited on page 103.)

[147] C Patten, J Dozono, S Schmidt, M Jue, and P Lum. Combined functional task practice and dynamic high intensity resistance training promotes recovery of upper-extremity motor function in post-stroke hemiparesis: a case study. *J Neurol Phys Ther*, 30(3):99–115, 2006. (Cited on pages 103 and 118.)

[148] J Patton and RF Weir, editors. *Proc 9th ICORR'05*, Chicago (IL), USA, Jun 28-Jul 1 2005. (Cited on pages 169, 170, 172, and 176.)

[149] JL Patton and FA Mussa-Ivaldi. Robot-assisted adaptive training: custom force fields for teaching movement patterns. *IEEE Trans Biomed Eng*, 51(4):636–46, 2004. (Cited on page 152.)

[150] JL Patton, M Kovic, and FA Mussa-Ivaldi. Custom-designed haptic training for restoring reaching ability to individuals with poststroke hemiparesis. *J Rehabil Res Dev*, 43(5):643–656, 2006. (Cited on page 28.)

[151] JL Patton, ME Stoykov, M Kovic, and FA Mussa-Ivaldi. Evaluation of robotic training forces that either enhance or reduce error in chronic hemiparetic stroke survivors. *Exp Brain Res*, 168(3):368–383, 2006. (Cited on pages 40, 118, 152, and 159.)

[152] JL Patton, SL Small, and WZ Rymer. Functional restoration for the stroke survivor: Informing the efforts of engineers. *Top Stroke Rehabil*, 2009. in press. (Cited on pages 23, 44, 119, and 152.)

[153] EJ Perreault, K Chen, RD Trumbower, and G Lewis. Interactions with compliant loads alter stretch reflex gains but not intermuscular coordination. *J Neurophysiol*, 99(5):2101–2113, 2008. (Cited on page 155.)

[154] JC Perry, J Rosen, and S Burns. Upper-limb powered exoskeleton design. *IEEE-ASME Trans Mech*, 12(4):408–417, 2007. (Cited on pages 51, 89, 90, 96, 99, and 119.)

[155] R Pintelon and J Schoukens. *System identification: a frequency domain approach*. IEEE Press, New York, USA, 2001. (Cited on pages 110 and 142.)

[156] K Pipereit, O Bock, and JL Vercher. The contribution of proprioceptive feedback to sensorimotor adaptation. *Exp Brain Res*, 174(1):45–52, 2006. (Cited on pages 42 and 151.)

[157] T Platz. Evidence-based arm rehabilitation - a systematic review of the literature. *Nervenartz*, 74(10):841–849, 2003. (Cited on pages 22, 47, 59, 89, 103, 117, 135, 151, 152, and 159.)

[158] VM Pomeroy, D Dean, L Sykes, EB Faragher, M Yates, PJ Tyrrell, S Moss, and RC Tallis. The unreliability of clinical measures of muscle tone: implications for stroke therapy. *Age Ageing*, 29(3):229–233, 2000. (Cited on page 17.)

[159] JL Poole. Application of motor learning principles in occupational therapy. *Am J Occup Ther*, 45(6):531–537, 1991. (Cited on page 118.)

[160] RK Powers, J Marder-Meyer, and WZ Rymer. Quantitative relations between hypertonia and stretch reflex threshold in spastic hemiparesis. *Ann Neurol*, 23(2):115–124, 1988. (Cited on page 17.)

[161] M Praagman, EKJ Chadwick, FCT van der Helm, and HEJ Veeger. The relationship between two different mechanical cost functions and muscle oxygen consumption. *J Biomech*, 39(4):758–765, 2006. (Cited on page 43.)

[162] GB Prange, MJA Jannink, CGM Groothuis-Oudshoorn, HJ Hermens, and MJ IJzerman. Systematic review of the effect of robot-aided therapy on recovery of the hemiparetic arm after stroke. *J Rehabil Res Dev*, 43(2):171–184, 2006. (Cited on pages 23, 44, 47, 59, 89, 103, 117, 135, 151, 152, and 159.)

[163] GB Prange, LAC Kallenberg, MJA Jannink, AHA Stienen, H van der Kooij, MJ IJzerman, and HJ Hermens. Influence of gravity compensation on muscle activity during reach and retrieval in healthy elderly. *J Electromyogr Kinesiol*, 2007. epub. (Cited on pages 47, 60, 73, 76, 118, 119, 135, 158, and 159.)

[164] GB Prange, AHA Stienen, MJA Jannink, H van der Kooij, MJ IJzerman, and HJ Hermens. Increased range of motion and decreased muscle activity during maximal reach with gravity compensation in stroke patients. In Driessen et al. [42]. (Cited on pages 61, 73, 76, 83, 118, 119, and 135.)

[165] GB Prange, T Krabben, BI Molier, H van der Kooij, and MJA Jannink. A low-tech virtual reality application for training of upper extremity motor function in neurorehabilitation. In *Proc Virt Rehab'08*, Vancouver, Canada, Aug 25-27 2008. (Cited on pages 73 and 78.)

[166] GA Pratt and MM Williamson. Series elastic actuators. In *Proc IROS'95*, pages 399–406, Aug 5-9 1995. (Cited on pages 105, 106, 113, 125, 136, and 138.)

[167] JE Pratt. *Virtual model control of a biped walking robot*. PhD thesis, MIT, Cambridge (MA), USA, 1995. (Cited on page 130.)

[168] DJ Reinkensmeyer, LE Kahn, M Averbuch, A McKenna-Cole, BD Schmit, and WZ Rymer. Understanding and treating arm movement impairment after chronic brain injury: Progress with the arm guide. *J Rehabil Res Dev*, 37(6):653–662, 2000. (Cited on pages 23, 104, 119, 133, and 155.)

[169] DJ Reinkensmeyer, CD Takahashi, WK Timoszyk, AN Reinkensmeyer, and LE Kahn. Design of robot assistance for arm movement therapy following stroke. *Adv Robotics*, 14(7):625–637, 2000. (Cited on pages 51, 89, and 118.)

[170] DJ Reinkensmeyer, JL Emken, and SC Cramer. Robotics, motor learning, and neurologic recovery. *Annu Rev Biomed Eng*, 6:497–525, 2004. (Cited on page 118.)

[171] DW Robinson. *Design and analysis of series elasticity in closed-loop actuator force control.* PhD thesis, MIT, Cambridge (MA), USA, 2000. (Cited on pages 105, 113, 125, and 136.)

[172] DW Robinson and GA Pratt. Force controllable hydro-elastic actuator. In *Proc ICRA'oo*, volume 2, pages 1321–1327, 2000. (Cited on pages 137, 138, 140, 141, 143, and 148.)

[173] B Rohrer, SE Fasoli, HI Krebs, R Hughes, BT Volpe, WR Frontera, J Stein, and N Hogan. Movement smoothness changes during stroke recovery. *J Neurosci*, 22(18): 8297–8304, 2002. (Cited on page 23.)

[174] B Rohrer, S Fasoli, HI Krebs, B Volpe, WR Frontera, J Stein, and N Hogan. Submovements grow larger, fewer, and more blended during stroke recovery. *Motor Control*, 8(4):472–483, 2004. (Cited on page 23.)

[175] DP Romilly, C Anglin, RG Gosine, C Hershler, and SU Raschke. A functional task analysis and motion simulation for the development of a powered upper-limb orthosis. *IEEE Trans Rehabil Eng*, 2(3):119–129, 1994. (Cited on page 90.)

[176] W Rosamond, K Flegal, K Furie, A Go, K Greenlund, N Haase, SM Hailpern, M Ho, V Howard, B Kissela, S Kittner, D Lloyd-Jones, M McDermott, J Meigs, C Moy, G Nichol, C O'Donnell, V Roger, P Sorlie, J Steinberger, T Thom, M Wilson, Y Hong, and AHA committees. Heart disease and stroke statistics–2008 update: a report from the American Heart Association Statistics Committee and Stroke Statistics Subcommittee. *Circulation*, 117(4):e25–146, 2008. (Cited on pages 15, 16, and 75.)

[177] OM Rutherford. Muscular coordination and strength training. implications for injury rehabilitation. *Sports Med*, 5(3):196–202, 1988. (Cited on pages 103, 118, and 155.)

[178] RL Sainburg and JS Wang. Interlimb transfer of visuomotor rotations: independence of direction and final position information. *Exp Brain Res*, 145(4):437–447, 2002. (Cited on pages 29 and 33.)

[179] RJ Sanchez, E Wolbrecht, R Smith, J Liu, S Rao, S Cramer, T Rahman, JE Bobrow, and DJ Reinkensmeyer. A pneumatic robot for re-training arm movement after stroke: rationale and mechanical design. In Patton and Weir [148], pages 500–504. (Cited on pages 51, 59, 89, 90, and 119.)

[180] RJ Sanchez, J Liu, S Rao, P Shah, R Smith, T Rahman, SC Cramer, JE Bobrow, and DJ Reinkensmeyer. Automating arm movement training following severe stroke: functional exercises with quantitative feedback in a gravity-reduced environment. *IEEE Trans Neural Syst Rehabil Eng*, 14(3):378–389, 2006. (Cited on pages 22, 47, 51, 59, 60, 61, 73, 76, 84, 85, 90, 153, 155, and 159.)

[181] JD Schaechter. Motor rehabilitation and brain plasticity after hemiparetic stroke. *Prog Neurobiol*, 73(1):61–72, 2004. (Cited on page 85.)

[182] RA Scheidt, DJ Reinkensmeyer, MA Conditt, WZ Rymer, and FA Mussa-Ivaldi. Persistence of motor adaptation during constrained, multi-joint, arm movements. *J Neurophysiol*, 84(2):853–862, 2000. (Cited on pages 28 and 41.)

[183] RA Scheidt, JB Dingwell, and FA Mussa-Ivaldi. Learning to move amid uncertainty. *J Neurophysiol*, 86(2):971–985, 2001. (Cited on pages 28 and 151.)

[184] RA Scheidt, MA Conditt, EL Secco, and FA Mussa-Ivaldi. Interaction of visual and proprioceptive feedback during adaptation of human reaching movements. *J Neurophysiol*, 93(6):3200–3213, 2005. (Cited on page 29.)

[185] A Schiele. An explicit model to predict and interpret constraint force creation in pHRI with exoskeletons. In *Proc ICRA'o8*, pages 1324–1330, 2008. (Cited on pages 99, 124, 132, and 154.)

[186] A Schiele and FCT van der Helm. Kinematic design to improve ergonomics in human machine interaction. *IEEE Trans Neural Syst Rehabil Eng*, 14(4):456–469, 2006. (Cited on pages 50, 63, 90, 99, 121, 132, and 154.)

[187] RA Schmidt and TD Lee. *Motor control and learning*. Human Kinetics Publishers, Champaign (IL), USA, 3rd edition, 1999. (Cited on pages 21, 103, 118, and 135.)

[188] AC Schouten, E de Vlugt, JJB van Hilten, and FCT van der Helm. Quantifying proprioceptive reflexes during position control of the human arm. *IEEE Trans Biomed Eng*, 55(1):311–321, 2008. (Cited on page 159.)

[189] JW Sensinger and RF Weir. Unconstrained impedance control using a compact series elastic actuator. In *Proc 2nd MESA'o6*, pages 1–6, Beijing, China, Aug 13-16 2006. (Cited on page 138.)

[190] JW Sensinger and RFF Weir. User-modulated impedance control of a prosthetic elbow in unconstrained, perturbed motion. *IEEE Trans Bio-Med Eng*, 55(3):1043–1055, 2008. (Cited on page 138.)

[191] R Shadmehr and JW Krakauer. A computational neuroanatomy for motor control. *Exp Brain Res*, 185(3):359–381, 2008. (Cited on pages 28 and 159.)

[192] R. Shadmehr and F. A. Mussa-Ivaldi. Adaptive representation of dynamics during learning of a motor task. *J Neurosci*, 14(5 Pt 2):3208–24, 1994. (Cited on page 29.)

[193] LR Sheffler and J Chae. Neuromuscular electrical stimulation in neurorehabilitation. *Muscle Nerve*, 35(5):562–590, 2007. (Cited on page 21.)

[194] EM Siekierka, K Eng, C Bassetti, A Blickenstorfer, MS Cameirao, V Dietz, A Duff, F Erol, T Ettlin, DM Hermann, T Keller, B Keisker, J Kesselring, R Kleiser, S Kollias, JP Kool, A Kurre, S Mangold, T Nef, P Pyk, R Riener, C Schuster, F Tosi, PFMJ Verschure, and L Zimmerli. New technologies and concepts for rehabilitation in the acute phase of stroke: a collaborative matrix. *Neurodegener Dis*, 4(1):57–69, 2007. (Cited on page 155.)

[195] AJ Simmonds. Electro-rheological valves in a hydraulic circuit. *IEE Proc D Control Theory Appl*, 138(4):400–404, 1991. (Cited on pages 104 and 127.)

[196] ND Sims, NJ Holmes, and R Stanway. A unified modelling and model updating procedure for electrorheological and magnetorheological vibration dampers. *Smart Mater Struct*, 13(1):100–121, 2004. (Cited on pages 104 and 127.)

[197] DI Slater, SA Curtin, JS Johns, Schmidt C, JL Tipton, and Newbury R. Middle cerebral artery stroke. eMedicine website, 2008. Available at: http://emedicine.medscape.com/article/323120-overview. Accessed Dec 10, 2008. (Cited on page 15.)

[198] BF Spencer, SJ Dyke, MK Sain, and JD Carlson. Phenomenological model for magnetorheological dampers. *Journal Eng Mech-ASCE*, 123(3):230–238, 1997. (Cited on pages 104 and 127.)

[199] J Stein, HI Krebs, WR Frontera, SE Fasoli, R Hughes, and N Hogan. Comparison of two techniques of robot-aided upper limb exercise training after stroke. *Am J Phys Med Rehabil*, 83(9):720–728, 2004. (Cited on page 103.)

[200] AHA Stienen, FCT van der Helm, GB Prange, MJA Jannink, and H van der Kooij. Effects of gravity compensation on the range-of-motion of the upper extremities in robotic rehabilitation after stroke. In *Proc ISG'06*, Chicago, Illinois, USA, Oct 9-10 2006. Included in Chap. 4 in this dissertation. (Cited on page 61.)

[201] AHA Stienen, EEG Hekman, FCT van der Helm, GB Prange, MJA Jannink, AMM Aalsma, and H van der Kooij. Freebal: dedicated gravity compensation for the upper extremities. In Driessen et al. [42]. Expanded upon in Chap. 8 in this dissertation. (Cited on pages 51, 53, 57, 61, 76, 77, 85, 89, 119, 127, 128, and 135.)

[202] AHA Stienen, EEG Hekman, FCT van der Helm, GB Prange, MJA Jannink, AMM Aalsma, and H van der Kooij. Dampace: dynamic force-coordination trainer for the upper extremities. In Driessen et al. [42]. Expanded upon in Chap. 8 in this dissertation. (Cited on pages 47, 50, 51, 59, 63, 78, 95, 97, 103, 115, 118, and 135.)

[203] AHA Stienen, AC Schouten, J Schuurmans, and FCT van der Helm. Analysis of reflex modulation with a biologically realistic neural network. *J Comput Neurosci*, online, 2007. (Cited on pages 17 and 159.)

[204] AHA Stienen, EEG Hekman, H ter Braak, AMM Aalsma, FCT van der Helm, and H van der Kooij. Rotational hydro elastic actuator for a torque driven exoskeleton for the upper-extremities. In Desai et al. [34]. Included as Chap. 9 in this dissertation. (Cited on pages 97 and 137.)

[205] S Stroeve. Learning combined feedback and feedforward control of a musculoskeletal system. *Biol Cybern*, 75(1):73–83, 1996. (Cited on page 28.)

[206] TM Sukal, MD Ellis, and JPA Dewald. Shoulder abduction-induced reductions in reaching work area following hemiparetic stroke: neuroscientific implications. *Exp Brain Res*, 183(2):215–223, 2007. (Cited on pages 17, 20, 21, 23, 51, 52, 59, 61, 62, 71, 76, 83, 84, 85, 89, 117, 118, 119, 152, 157, and 159.)

[207] R Teasell, J Bitensky, K Salter, and NA Bayona. The role of timing and intensity of rehabilitation therapies. *Top Stroke Rehabil*, 12(3):46–57, 2005. (Cited on page 28.)

[208] KA Thoroughman and R Shadmehr. Learning of action through adaptive combination of motor primitives. *Nature*, 407(6805):742–7, 2000. (Cited on pages 28 and 151.)

[209] E Todorov. Optimality principles in sensorimotor control. *Nat Neurosci*, 7(9):907–915, 2004. (Cited on page 28.)

[210] C Tong, DM Wolpert, and JR Flanagan. Kinematics and dynamics are not represented independently in motor working memory: evidence from an interference study. *J Neurosci*, 22(3):1108–13, 2002. (Cited on pages 29, 32, and 42.)

[211] RD Trumbower, VJ Ravichandran, MA Krutky, and EJ Perreault. Altered multijoint reflex coordination is indicative of motor impairment level following stroke. In *Proc. 30th EMBS 08*, pages 3558–3561, Vancouver (BC), Canada, Aug 20-24 2008. (Cited on page 159.)

[212] GJM Tuijthof and JL Herder. Design, actuation and control of an anthropomorphic robot arm. *Mech Mach Theory*, 35(7):945–962, 2000. (Cited on pages 56 and 57.)

[213] TE Twitchell. The restoration of motor function following hemiplegia in man. *Brain*, 74(4):443–80, 1951. (Cited on pages 18, 19, 75, and 118.)

[214] H Vallery, JF Veneman, EHF van Asseldonk, R Ekkelenkamp, and H M Buss van der Kooij. Compliant actuation of rehabilitation robots: Benefits and limitations of series elastic actuators. *IEEE Rob Autom Mag*, 15(3):60–69, 2008. (Cited on pages 105, 113, 125, 136, and 147.)

[215] CJ van Andel, N Wolterbeek, CAM Doorenbosch, DHEJ Veeger, and J Harlaar. Complete 3d kinematics of upper extremity functional tasks. *Gait Posture*, 27(1): 120–127, 2008. (Cited on page 120.)

[216] EHF van Asseldonk. *Restitution and compensation in the recovery of function in the lower extremities of stroke survivors: design of evaluation and training methods*. PhD thesis, University of Twente, Enschede, The Netherlands, 2008. (Cited on page 20.)

[217] FCT van der Helm, AC Schouten, E de Vlugt, and GG Brouwn. Identification of intrinsic and reflexive components of human arm dynamics during postural control. *J Neurosci Methods*, 119(1):1–14, 2002. (Cited on pages 110, 136, 142, 155, and 159.)

[218] H van der Kooij, R Jacobs, B Koopman, and H Grootenboer. A multisensory integration model of human stance control. *Biol Cybern*, 80(5):299–308, 1999. (Cited on pages 28 and 159.)

[219] JH van der Lee, IA Snels, H Beckerman, GJ Lankhorst, RC Wagenaar, and LM Bouter. Exercise therapy for arm function in stroke patients: a systematic review of randomized controlled trials. *Clin Rehabil*, 15(1):20–31, 2001. (Cited on pages 22, 47, 59, 89, 103, 117, 135, 151, 152, and 159.)

[220] HFM van der Loos, editor. *Proc 6th ICORR'99*, Stanforc (CA), USA, Jul 1-2 1999. (Cited on pages 167 and 170.)

[221] WJ Van Ouwerkerk, JA van der Sluijs, F Nollet, F Barkhof, and AC Slooff. Management of obstetric brachial plexus lesions: state of the art and future developments. *Childs Nerv Syst*, 16(10-11):638–644, 2000. (Cited on page 120.)

[222] RPS Van Peppen, G Kwakkel, S Wood-Dauphinee, HJM Hendriks, PJ van der Wees, and J Dekker. The impact of physical therapy on functional outcomes after stroke: what's the evidence? *Clin Rehabil*, 18(8):833–62, 2004. (Cited on pages 21, 43, and 151.)

[223] JF Veneman, R Ekkelenkamp, R Kruidhof, FCT van der Helm, and H van der Kooij. A series elastic- and bowden-cable-based actuation system for use as torque actuator in exoskeleton-type robots. *Int J Robot Res*, 25(3):261–281, 2006. (Cited on pages 105, 113, 125, and 136.)

[224] JF Veneman, R Kruidhof, EEG Hekman, R Ekkelenkamp, EHF van Asseldonk, and H van der Kooij. Design and evaluation of the lopes exoskeleton robot for interactive gait rehabilitation. *IEEE Trans Neural Syst Rehabil Eng*, 15(3):379–386, 2007. (Cited on pages 132, 136, and 137.)

[225] BT Volpe, HI Krebs, N Hogan, L Edelstein, CM Diels, and ML Aisen. Robot training enhanced motor outcome in patients with stroke maintained over 3 years. *Neurology*, 53(8):1874–1876, 1999. (Cited on page 44.)

[226] JS Wang and RL Sainburg. Adaptation to visuomotor rotations remaps movement vectors, not final positions. *J Neurosci*, 25(16):4024–4030, 2005. (Cited on page 29.)

[227] NS Ward. The neural substrates of motor recovery after focal damage to the central nervous system. *Arch Phys Med Rehabil*, 87(12 Suppl 2):S30–S35, 2006. (Cited on page 43.)

[228] NS Ward, MM Brown, AJ Thompson, and R S J Frackowiak. Neural correlates of motor recovery after stroke: a longitudinal fMRI study. *Brain*, 126(Pt 11):2476–96, 2003. (Cited on page 43.)

[229] Y Wei, P Bajaj, R Scheidt, and J Patton. Visual error augmentation for enhancing motor learning and rehabilitative relearning. In Patton and Weir [148], pages 505–510. (Cited on pages 28, 40, 41, 152, and 159.)

[230] A Weiss, T Suzuki, J Bean, and RA Fielding. High intensity strength training improves strength and functional performance after stroke. *Am J Phys Med Rehabil*, 79(4):369–76; quiz 391–4, 2000. (Cited on pages 118 and 155.)

[231] ET Wolbrecht, V Chan, DJ Reinkensmeyer, and JE Bobrow. Optimizing compliant, model-based robotic assistance to promote neurorehabilitation. *IEEE Trans Neural Syst Rehabil Eng*, 16(3):286–297, 2008. (Cited on pages 23, 44, 104, 119, 136, 152, and 155.)

[232] World Health Organization. *The Global Burden of Disease: 2004 Update*. WHO Press, Geneva, Switserland, 2008. (Cited on page 15.)

[233] G Wu, FCT van der Helm, HEJ Veeger, M Makhsous, P Van Roy, C Anglin, J Nagels, AR Karduna, K McQuade, X Wang, FW Werner, and B Buchholz. ISB recommendation on definitions of joint coordinate systems of various joints for the reporting of human joint motion–part II: shoulder, elbow, wrist and hand. *J Biomech*, 38(5): 981–992, 2005. (Cited on pages 31, 50, 68, 69, 79, 90, 98, and 120.)

[234] YR Yang, RY Wang, KH Lin, MY Chu, and RC Chan. Task-oriented progressive resistance strength training improves muscle strength and functional performance in individuals with stroke. *Clin Rehabil*, 20(10):860–870, 2006. (Cited on pages 118 and 155.)

[235] W Zhou, CM Chew, and GS Hong. Development of a compact double-disk magneto-rheological fluid brake. *Robotica*, 25(04):493–500, 2007. (Cited on pages 104 and 112.)

BIOGRAPHY

Arno Stienen was born on August 28th, 1976 in Delft (the Netherlands). He got his high school degree in 1994 at the Interconfessional Westland College in Naaldwijk (Netherlands). After a short spell with Electrical Engineering, he studied Mechanical Engineering at the Delft University of Technology. During his masters degree, he completed a five month project at the Technical University Berlin (Germany) in 2001 on an Erasmus scholarship. For this project, he recreated a 3D neurological computer model of the visual cortex. Back at the TU Delft, he used this knowledge to create a biologically realistic neural model of the spinal cord. The model interacted with a single degree of freedom musculoskeletal model through virtual muscle activation and proprioceptors. It nicely mimicked the behavior of the human musculoskeletal system when compared with both human measurements and measurements done on complex regional pain syndrome patients. He finished his Master of Science degree in Mechanical Engineering with a specialization in Biomechanical Engineering in 2003. Three days later, he started working as a research assistant at the University of Twente, Enschede (Netherlands), under the supervision of Prof.dr. Frans van der Helm and Dr.ir. Herman van der Kooij in the Biomechanical Engineering group. This dissertation on rehabilitation robots is the result of this project. From the Summer of 2008 onwards, he has been working at the Physical Therapy and Human Movement Sciences department at Northwestern University in Chicago (IL, USA). He is currently investigating the effects of abnormal multi-joint torque-couplings in stroke patients, for which he uses all kinds of rehabilitation robots.

LIST OF PUBLICATIONS

PEER-REVIEWED JOURNALS:

- AHA Stienen, EEG Hekman, H ter Braak, AMM Aalsma, FCT van der Helm, and H van der Kooij. Design of a Rotational Hydro-Elastic Actuator for an Active Upper-Extremity Rehabilitation Exoskeleton. *IEEE Trans Bio-Med Eng*, 2008 (accepted pending minor revisions).
- EHF van Asseldonk, M Wessels, AHA Stienen, FCT van der Helm, and H van der Kooij. Influence of haptic guidance in learning a novel visuomotor task. *J Physiol Paris*, 2008 (accepted pending minor revisions).
- GB Prange, MJA Jannink, AHA Stienen, H van der Kooij, MJ IJzerman, and HJ Hermens. Influence of gravity compensation on muscle activation patterns during different temporal phases of arm movements of stroke patients. *Neurorehab Neural Repair*, 2008 (epub).
- GB Prange, LAC Kallenberg, MJA Jannink, AHA Stienen, H van der Kooij, MJ IJzerman, and HJ Hermens. Influence of gravity compensation on muscle activity during reach and retrieval in healthy elderly. *J Electromyogr Kinesiol*, 2007 (epub).
- AHA Stienen, AC Schouten AC, J Schuurmans, and FCT van der Helm. Analysis of reflex modulation with a biologically realistic neural network. *J Comput Neurosci*, 23(3):333-48, 2007.

PEER-REVIEWED CONFERENCE PROCEEDINGS:

- AHA Stienen, EEG Hekman, H ter Braak, AMM Aalsma, FCT van der Helm, and H van der Kooij. Design of a Rotational Hydro-Elastic Actuator for an Active Upper-Extremity Rehabilitation Exoskeleton. *Proc Biorob'08*, Scottsdale (AZ), USA, Oct 20-22, 2008.
- AHA Stienen, EEG Hekman, FCT van der Helm, GB Prange, MJA Jannink, AMM Aalsma, and H van der Kooij. Dampace: dynamic force-coordination trainer for the upper extremities. *Proc ICORR'07*, Noordwijk, the Netherlands, Jun 13-15, 2007.
- MJA Jannink, GB Prange, AHA Stienen, H van der Kooij, Kruitbosch JM, MJ IJzerman, and HJ Hermens. Reduction of muscle activity during repeated reach and retrieval with gravity compensation in stroke patients. *Proc ICORR'07*, Noordwijk, the Netherlands, Jun 13-15, 2007.
- GB Prange, AHA Stienen, MJA Jannink, H van der Kooij, MJ IJzerman, and HJ Hermens. Increased range of motion and decreased muscle activity during maximal reach with gravity compensation in stroke patients. *Proc ICORR'07*, Noordwijk, the Netherlands, Jun 13-15, 2007.
- AHA Stienen, EEG Hekman, FCT van der Helm, GB Prange, MJA Jannink, AMM Aalsma, and H van der Kooij. Freebal: dedicated gravity compensation for the upper extremities. *Proc ICORR'07*, Noordwijk, the Netherlands, Jun 13-15, 2007

DANKBETUIGINGEN

VAN DE ENE PARANIMF ...

In de afgelopen jaren heb ik in Enschede een zeer plezierige tijd gehad. Allereerst wil ik "die lange met die baard" bedanken. Edsko, nooit eerder heb ik zo goed samengewerkt als aan de UT met jou; de meeste concepten uit dit proefschrift zijn echt gezamenlijk tot stand gekomen. Het was een waar genot om de meest waanzinnige ideeën bij je op 't bord te kladden, waarna uitgebreide—soms wekenlange—discussies volgden. Je hebt geloof ik nooit die sensor ontdekt waarmee ik vast kon stellen of je je bord had opgeschoond, zodat ik hem binnen een uurtje weer kon vullen. En monochroom maar verschillend kleurgebruik optimaliseerde de beschikbare ruimte door de verschillende tekeningen door elkaar te laten lopen. Je bent met recht co-auteur op alle ontwerphoofdstukken en ik ben je dankbaar dat je mijn paranimf wil zijn. (Mag ik nu op ook op jouw promotiefeestje komen?) Hopelijk vielen mijn vertragingsstrategieën om niet buiten adem te raken bij 't naar huis fietsen niet teveel op.

Had Edsko nog de mazzel om alleen over mijn whiteboard schetsen te hoeven discussiëren, Gert-Jan was diegene die het echte werk heeft gedaan. Evert, je wist mijn 'ontwerpsuggesties' realiseerbaar te maken en in elkaar te zetten. En vervolgens mocht je nog vele maanden lang kleine en grote verbeteringen aanbrengen in de minuscule ruimte die ik tussen onderdelen had gelaten. Dat de Dampace nu echt werkt, is toch voor een groot deel aan jou te danken. Wanneer je later in je schommelstoeltje zit met een pijp in de mond, kan je daar nog eens met voldoening aan terugdenken.

En dan Herman. Herman. Tja, wat valt er over Herman te zeggen. Herman, op de eerste plaats weet ik zeker dat domeinkapers die URLs kopen met een net afwijkende spelling van een merknaam zich volledig op mensen zoals jij gefocust hebben: Freeball, Freebel, Damspace, Limpace, etc. zijn nog de meest 'normale' spellingen die regelmatig langs zijn gekomen. Maar ik denk niet dat je mijn naam snel zal vergeten: de discussies waren mooi en diepgaand, hoewel we lang niet altijd tot dezelfde conclusies kwamen. (En even voor de duidelijkheid, jij had altijd ongelijk.) Ik ben je begeleiding meer en meer gaan waarderen. Eerlijk, zakelijk, to-the-point, maar met een humoristische kwinkslag. Hoewel een laagdoorlaatfilter in de interactie met je zeker verstandig is. (Voor de niet-ingenieurs onder ons, Edwin, is een laagdoorlaatfilter het filter waarmee je hoogfrequente fluctuaties wegneemt en het signaal stabiliseert.) Zeker de laatste jaren in de kroegen in Brazilië en Zwitserland hebben we een menig biertje op ons project en het leven gedronken. Hopelijk blijven we in de toekomst samenwerken.

Frans, misschien was je bij dit project minder dominant aanwezig dan eerder bij mijn afstuderen, maar wanneer je er was, was je ook gelijk een meerwaarde. Je verstaat echt de kunst om met minimale informatie precies tot de essentie van het geheel te komen. Discussies waarbij zowel jij als Herman aanwezig waren, zijn zeker de meest interessante. Hopelijk dwingt je betrokkenheid met Jules in Chicago je ook regelmatig deze kant op te komen.

In ons project had ik het plezier om samen te werken met de zeer ervaren ontwerpers van BAAT en wetenschappers van RRD. Gert en Arthur, dank voor al jullie grote en kleine bijdrages tijdens het ontwerpen. En Huub, ik vond het mooi de vorige winter met jou in de schuur en bij je familie in het mooie midden van nergens doorgebracht te hebben. Het artikel wat eruit voortgekomen is (H9), is waarschijnlijk 't beste onderdeel van mijn proefschrift. Jouw ervaringen met hydrauliek en je oplossend vermogen waren hiervoor essentieel.

Bij RRD wil ik met name Gerdienke, Michiel en Leendert bedanken. De zorgvuldige manier waarop jullie met patiënten en experimenten omgaan blijft voor mij een voorbeeld van hoe het moet. Ik heb misschien wel eens tegen wat muurtjes geschopt, maar altijd

met de beste intenties. Desondanks hebben jullie mij altijd warm ontvangen en mij ook bij RRD thuis laten voelen. Gerdienke, ik wens je veel succes in jouw laatste fase.

Dit werk was er niet gekomen zonder de wezenlijke bijdrages van vele afstudeerders. Ik heb het plezier gehad te mogen samenwerken met Jorn, Chris, Arjen, Astrid, Martijn, Lukke, Stijn, Thijs R., Marleen, Rolf, Ewoud, Frank, Sjors en Thijs K. Van ieder project is wel een stukje direct of indirect in dit proefschrift gekomen. Windel, je was dan wel geen afstudeerder, maar jij hebt wel essentieel werk verricht aan de computer interface van de Dampace. Ik wil jullie allemaal hartelijke bedanken voor deze bijdrages.

En ik moet het toegeven, zonder LOPES waren mijn ontwerpen nooit zover gekomen. Ik heb ontzettend veel geleerd van jullie vergissinkjes, maar nog veel meer van de talrijke succesverhalen. Jullie behielden een zeer goede onderlinge samenwerking, ondanks(/dankzij?) al mijn—vermeende—sabotagepogingen. En Heike was misschien het laatste beetje magie wat jullie nodig hadden. Ik ben blij dat jullie mij uitvoerig hebben bedankt dat ik haar overtuigd heb met jullie te gaan praten voor een goede voortgang van haar project. En Heike, het was altijd intessant met jou erbij!

Ik wil ook mijn andere collega's bedanken bij BW. Theo was de voorganger van Gert-Jan en in die rol de hoofdontwerper van de Freebal. Dank voor je werk hieraan, Theo, en voor de gewichtsondersteuning die je later nog voor de Dampace hebt ontworpen. Ook met Alfred heb ik op de valreep nog kunnen samenwerken. Dank voor je nachtelijke uren met de testopstelling terwijl je mijn telefonische instructies uitvoerde. Met vele andere BWers en BSSers ben ik ook regelmatig wezen stappen, eten, squashen en voetballen. Dank voor de mooie jaren.

Maar buiten deze fysiek aanwezige collega's, ben ik ook dank verschuldigd aan een aantal externe wetenschappers. Zonder adviezen over de realtime software van Paolo Mantegazza, Roberto Bucher en Marco Romagnoli, had ik het geheel niet aan de praat gekregen. En dit proefschrift maakt gebruik van het Classic-Thesis sjabloon ontworpen door Andre Miede. Mijn dank dus voor deze en alle overige kleine bijdrages uit de open-source gemeenschap.

Na al het echte werk in Twente is een groot deel van het uiteindelijke schrijfwerk ook in de nachtelijke uren in Chicago verricht, waarbij soms de nacht alweer overging in de dag. Maar niet alleen op deze manier heb ik van je tijd gesnoept, Jules, je hebt ook via enkele zorgvuldige reviews nog vele nuttige suggesties geleverd voor de klinische aspecten van dit proefschrift. Ook het stuiteren van wat ideeën tegen Mike en David resulteerde in goede verbeteringen. Allemaal bedankt daarvoor.

Ik denk dat dit ook de goede plek is om mijn familieleden en Marieke te bedanken. Dankzij de opvoeding van mijn ouders, en in het bijzondere van mijn moeder, heb ik de waarde van een goede onafhankelijkheid en grote zelfstandigheid kunnen inzien. Dit is met recht zeer nuttig voor een carièrre in de wetenschap. En Marieke, dank voor alle mooie jaren tot dusverre, en hopelijk kunnen we weer snel huisje, boompje, beestje spelen.

Tenslotte heb ik ook vele uren rondgebracht op de velden en in 't clubhuis van de hockeyclub PW. Daar ben ik vanaf het eerste begin fantastisch opgevangen en ik hoop dat ik ook mijn nuttige steentje bijgedragen heb. Specifiek wil ik Hein, Freek, Eelco, Gert-Jan, Malte, Jeroen, Renate, Frank en Menno bedanken, omdat zij ieder op hun manier uit hun weg zijn gegaan om mij thuis te laten voelen in Enschede. Maar daar doe ik eigenlijk de rest tekort mee, want ik heb met iedereen op de club een goede tijd gehad.

Maar de beste tijd met de hockeyers was denk toch wel met jou, Ewoud. Dank voor alle gedeelde biertjes, etentjes, verhalen en wedstrijden. Sorry dat ik je niet een keer heb kunnen laten winnen met RA2, maar bij een van die vijftien potjes had je best wel recht op wat meer. Ik ben blij dat ook jij mijn paranimf wilt zijn.

... NAAR DE ANDERE.

Allemaal bedankt!
Arno.

The support of these companies is gratefully acknowledged:

KUNST & VAN LEERDAM
MEDICAL TECHNOLOGY BV

MOOG

FCS

WWW.MOOGFCS.COM ● NIEUW VENNEP ● THE NETHERLANDS

HAPTICMASTER

The HapticMASTER is a 3 DOF force controlled haptic interface. It uses the so-called admittance control paradigm. This gives the device unprecedented stiffness, mechanical robustness and stability, including master-slave stability under delays. HapticMASTER is a perfect building block for your rehabilitation applications.

SIMODONT

SIMODONT is a high quality, high fidelity dental simulator allowing future dentists to be trained in operative dental procedures in a realistic dedicated virtual environment while receiving haptic, visual and audio sensory information. SIMODONT uses the same admittance control technology as HapticMASTER.

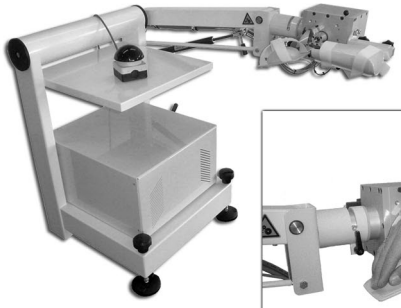

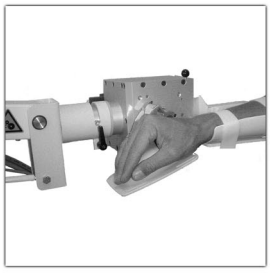

WRISTALYZER

Wristalyzer is a portable robotic device combining haptic technology with electromyographic assessment. It allows to assess wrist motion in physiological'and pathological conditions by applying loads and mechanical oscillations, taking into account the ergonomy and the angular positioning of the joints.

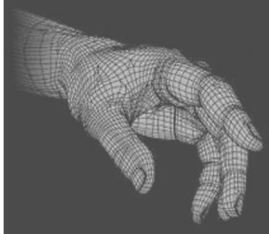

COME TO HAPTIST.COM

A USER COMMUNITY FOR HAPTICS RESEARCH

Haptics is the science of creating a realistic sense of touch to the user in a virtual environment. Haptic comes from the Greek word haptesthai, meaning to touch.

Share your haptics experiences and applications through this website!

DL REHAB

Science Based Rehabilitation

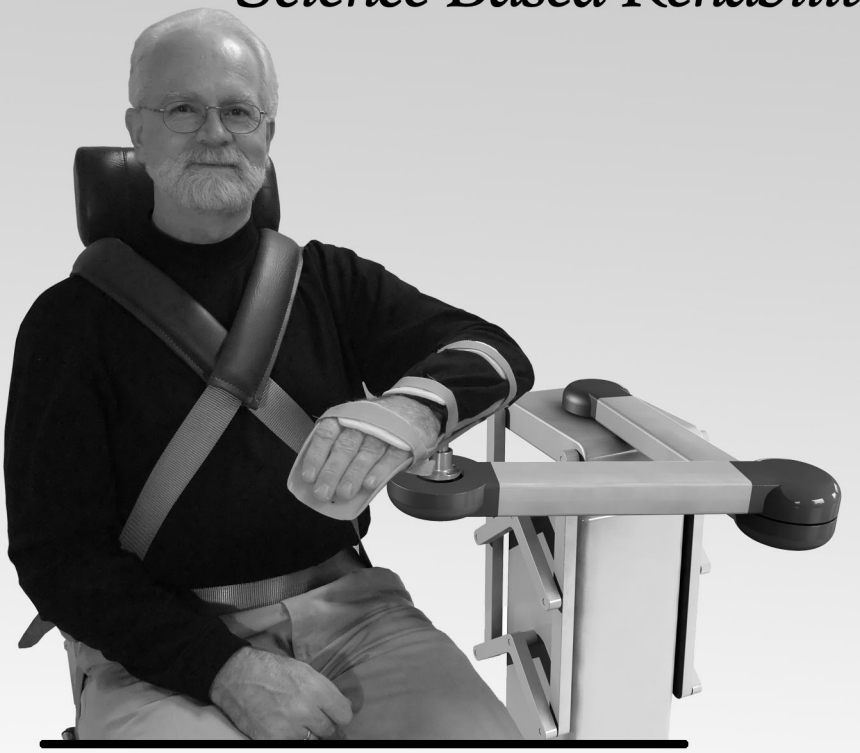

More information to follow soon at www.dlrehab.com

ACT^{3D} Rehabilitation Robot

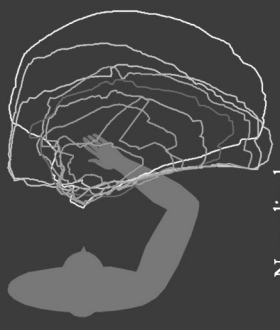

Implementation of the ACT^{3D} robot to measure workspace as a function of arm weight

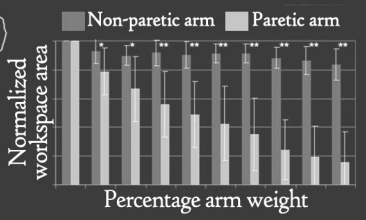

[Sukal et al. in Exp Brain Res (2007) & Ellis et al. in Neurorehabil Neural Repair (2008)]

"With our ACT^{3D} rehabilitation robot, we directly target the abnormal multi-joint torque coupling often found in indivuals with stroke. Our recently completed clinical trial demonstrated an increase of functional workspace of the paretic arm following a progressive limb-weight training protocol." [Ellis et al. in Neurorehabil Neural Repair (2009)]